

COMPUTATIONAL CIVIL ENGINEERING 2005

F. Paulet-Crainiceanu, C. Ionescu, H. Barbat

editors



EDITURA SOCIETĂȚII ACADEMICE "MATEI - TEIU BOTEZ"

Iasi, 2005

International Symposium

“Computational Civil Engineering 2005”

Iași, România, May 27, 2005



F. Paulet-Crainiceanu, C. Ionescu, H. Barbat
Editors



EDITURA SOCIETĂȚII ACADEMICE "MATEI-TEIU BOTEZ"
Iași, 2005

"Computational Civil Engineering. 2005", International Symposium
Iași, România, May 27, 2005
F. Paulet-Crainiceanu, C. Ionescu, H. Barbat
Editors

Descrierea CIP a Bibliotecii Naționale a României

**COMPUTATIONAL CIVIL ENGINEERING. INTERNATIONAL
SYMPOSIUM (2005 ; Iași)**

Computational civil engineering – 2005 Iași : 2005, 27 mai /
editors: Fidelio Păuleț-Crăiniceanu, Constantin Ionescu, Horia Barbat. -
Iași : Editura Societății Academice "Matei-Teiu Botez", 2005

Bibliogr.

ISBN 973-7962-65-6

I. Păuleț-Crăiniceanu, Fidelio (ed.)

II. Ionescu, Constantin (ed.)

III. Barbat, Horia (ed.)

004:624(063)

Table of Contents

1. Păuleț-Crăiniceanu, F., Ionescu, C., Barbat, H. Use of computers and computation in Civil Engineering	5
2. Anghel, C.V., Onchiș, D. Flexible algorithm for FFT parallel implementation	11
3. Popa, A.G., Cucu, H.L. Finite Element Analysis of Thin-walled Bars with U-shaped Section	15
4. Cucu, H.L., Popa, A.G. Considerations about the Hybrid-Strain Finite Element Analysis of Plates and Shells in the Theory of Thick Plates	23
5. Gobesz, F.Z. Some aspects of Computer-Based Education in Civil Engineering	33
6. Gobesz, F.Z., Turda, D.V. Knowledge in construction, from the perspective of communication	43
7. Alexa, P., Mociran, H., Mathe, A. Passive control of semirigid steel structures	51
8. Turda, D.V., Gobesz, F.Z. Python is a C++ made easy for Civil Engineers	59
9. Chiorean, C.G. Computer program for nonlinear inelastic analysis of 3D RC building frameworks	66
10. Oller, S., Barbat, Al.H., Miquel, J. Estudio del comportamiento de los hormigones reforzados con fibras cortas	76
11. Oller, S., Barbat, Al.H. Moment-curvature damage bridge piers subjected to horizontal loads	99
12. Barbuta, M., Nour, D.S. Mix optimization for high strength concrete	128
13. Nutiu, C. Notes on microtriangulation network types as applied to the study of construction displacements	138
14. Dima, Al., Răcănel, I.R. 3D modelling and calculation of the fixed platform PFS-U (PESCARUS)	146
15. Rotberg, R. Dynamic thermal behavior of building components. Calculation methods	157
16. Jantea, C., Varlam, F. Designing reticulated space systems	163
17. Diaconu, E., Răcănel, C. The study of geocomposite influence on wearing course asphalt mixture behavior at permanent deformation	174
18. Balcu, M., Lazăr, Șt.M.	

A viscoelastic-plastic prediction of rutting in asphalt mixtures	180
19. Petrina, M., Balc, R., Ciplea, C., Marchis, C. AutoLISP automated drawing programming under AutoCAD	192
20. Petrina, M., Balc, R., Static analysis of semi-rigid structures - Computation program	202
21. Nutiu, C. Considerations on the quality and importance of the existing high-accuracy levelling networks on the territory of Romania	210
22. Scînteie, R., Ionescu, C. Prediction of condition of structures using Markov chains	217
23. Comisu, C.C. Single exciter techniques for structural identification	224
24. Comisu, C.C. Multiple exciter techniques for structural identification	237
25. Paulet-Crainiceanu, F. Structures with active hinges, a step to Structural Robotics	246
26. Ionescu, C. Considerations concerning the optimization of reinforced concrete bridge design	257
27. Budescu, M., Ciongradi, I., Roşca, O. A new type of joint assemblage for the thin-walled steel profiles	262
28. Barsan, Em., Ignat, A. Optimization of Booster Disinfection in Water Distribution	272
29. Barsan, Em., Ignat, A. Impact of failures from water distribution networks on booster disinfection	283
30. Țepeş Onea, F. Finite element model for obtaining the structural response considering soil-structure interaction	293

Use of computers and computation in Civil Engineering

Fideliu Păuleț-Crăiniceanu¹, Constantin Ionescu¹, Horia Barbat²

¹"Gh. Asachi" Technical University of Iași, România

²Universitat Politècnica de Catalunya, Barcelona, Spain

Summary

This paper shows the diversity of the work in Civil Engineering that uses computers and computation, hoping that, by knowing more from the scientists and practitioners, improvements and developments can arise for all the Civil Engineering society.

Importance of computation and computers is revealed by analysis of achievements obtained in sub-domains and research in Civil Engineering as: Finite Element Method, analysis in frequency domain, education in Civil Engineering, active and passive control of structures, databases, meta-languages, inelastic analysis, damage assessment, fiber reinforced concrete structure, high concrete structures, surveying, offshore platforms, thermodynamics, special three-dimensional structures, composite materials, road engineering, computer drawing and graphics, analysis of semi-rigid structures, probabilistic analysis, structural identification, structural optimization, thin-walled steel profiles assembling and so on.

KEYWORDS: Civil Engineering, use of computer, computation, software, computer programming

1. INTRODUCTION

Civil Engineering is one of the engineering fields that uses computers and computation very intensively. This determines that the fast changes in Computer Science have implications also in Civil Engineering. Also the demands from Civil Engineering imply reactions from people involved in Computer Sciences.

As a matter of fact one can easily observe that inter-disciplinary civil – computer science engineers' teams already exist. However, especially because of economical condition, even in very famous universities and large companies, the duty to use and program computers is the task of civil engineers.

The implication of the above statement is that, sometimes, Civil Engineers are forced to concentrate a lot of energy in understanding pure computational means. Also, it could be observed that parallelism in making software for solving the same problems is very high.

This paper shows the diversity of the work in Civil Engineering that uses computers and computation, hoping that, by knowing more from the scientists and practitioners, improvements and developments can arise for all the Civil Engineering society.

2. COMPUTERS AND COMPUTATION, AT THE BASE OF RESEARCHES AND ACHIEVEMENTS IN CIVIL ENGINEERING

In [1], Anghel and Onchis propose an algorithm for parallel implementation of FFT, a tool to be used in Civil Engineering as in many other engineering fields. Estimation of this flexible algorithm is done in order to determine the performance of the computer program implemented on a Linux clusters system. Conclusions show that, the C program issued for the proposed FFT method is effective as the number of processors is higher.

Popa and Cucu, in [2] are performing a Finite Element Analysis on thin-walled cantilever bars with a U-shaped section. The elements used for this analysis are incompatible rectangular finite elements manipulated by an in-house computer program, HYFEM. Theoretical background is followed by numerical examples and comparisons are performed with commercial FEM program NASTRAN and analytical results. Good agreements of results are validating the in-house program especially for restrained torsion. Also, the three degrees of freedom per node assumption for the proposed elements is acceptable.

The theory of thick plates is at the core of the study done by Cucu and Popa in [3]. Hybrid-strain finite elements are used in analyzing orthotropic plates and shells. The in-house HYFEM computer program is employed. Theoretical background is explaining the finite element method and the used elements from this computer program. The application was done on flat plates, circular and ring-shaped plates, slabs punctually supported on columns and curved plates (shells). Analytical solutions and three commercial computer programs were used for validation of the in-house approach. Conclusions withdrawn are showing robustness of the proposed elements and their very good behavior.

In [4], Gobesz is dealing with the computer-based education of Civil Engineers. The importance of the matter is underlined. Concepts as knowledge and information are treated. The levels of the knowledge and the nowadays search of information needs are shown. Modern education, based on virtual reality is presented as the way the teaching process should follow. Other important aspects of new higher education are also revealed. The author points that the importance of humans in using software with a high degree of understanding of computations done by that software, especially when designing civil structures. A very impressive internet site was created in assisting civil engineers and architects into the information era.

Communication and knowledge that construction field is using are the main topics for [5]. The authors, Gobesz and Turda, are revealing tendencies created by the unified markets of EU. The Internet is proven to be a very important tool in manipulation of data. XML language and its version for building and construction, bcXML, is pointed as an important step in information handling. The AIC internet site design is analyzed and its importance for civil engineers and architects is presented.

In [6], Alexa, Mociran and Mathe are concerned with the passive control of semirigid steel structures. They started from showing the difficulties in repairing welded joints of steel structure. Therefore they performed analytical studies in elasto-plastic domain on a six stories steel frame structure. The situations taken into account were the four combinations of structure with or without rigid connections and with and without base isolation. The research is showing that, with proper choice of passive devices, very good structural behavior is achieved.

Turda and Gobesz, [7] are introducing the Python computer programming languages to Civil Engineers. After a short and critical history regarding the Fortran computer language, the authors are showing the need and importance of object oriented programming. Python is a wrapper of C++ object oriented language with a Pascal-like syntax that authors prove to be very helpful for Civil Engineering. A *Graphical User Interface* (GUI) for Fortran users was conceived with Python and shown in details. Its usefulness in teaching is revealed.

Chiorean, [8], built a computer program for nonlinear static analysis of three-dimensional concrete frame structure. The paper shows the main assumption taken into the algorithm and the theoretical background. The object-oriented computer program is then used in a computational example on a six floor structure. The computer program proved to be efficient, robust and fitted for nonlinear analysis (yielding, material nonlinearities, cross-section changes, geometrical nonlinearities and others).

In [9], Oller, Barbat and Miguel are using fiber concrete in rehabilitation of buildings. A very refined general analysis of composite materials is presented and then short fiber concrete composite materials are introduced. Many composition are explained. For these type of materials, mathematical modeling is exposed. An application example, with a simple supported concrete girder is shown. The experimental and analytical work proves significant increase in ductility for the element.

Damages to bridge piers is the topic of the paper [10]. The authors, Oller and Barbat, are analyzing the damages caused by horizontal actions (earthquakes) through the moment-curvature models. The main hypothesis is the flexible pier – rigid deck behavior. Dynamic model of the typical bridge is shown and discussed. Then the non-linear analysis of pier is presented and the damage of cross section due to skew bending is studied. The numerical example is performed on the model of the Warth Bridge, Austria and experimental data were also obtained from other researches. Results show very good agreement between the proposed model and experimental data.

In [11], Barbuta and Nour present the optimizing process for the mix of high strength concrete. An experimental program is applied by the author, using different cement dosages, aggregates and admixtures for different contents of silica fume. The results are tracking the workability, density and consistency of the experimental concrete mixtures. Also the strength of hardened concrete is shown and discussed. Optimal values are selected.

Nutiu, in [12], is dealing with new methodologies employed in studying the construction displacement based on micro-triangulation networks. The main goal is to study the behavior of constructions during their life. Measuring methods are then exposed (physical and geometrical). Also the types of supporting networks are listed and commented.

Dima and Racanel, [13], present their research on modeling and calculation of a fixed offshore platform. After a presentation of the structure, the three-dimensional finite element model is shown then the loads hypothesis and the check of stability are presented. Loads from wind and waves are taken into account. Dynamic model and eigenvalue analysis is performed together with resistance and stability analysis. Results show general good behavior, though in some parts of the structure, strengthening would be needed.

Calculation methods for dynamic thermal behavior of buildings are presented by Rotberg, [14]. The EU standard for the calculation of the thermal transfer matrix is shown and commented. Dynamic thermal characteristics of buildings components are revealed. An application presents the way to use this code regulations.

Jantea and Varlam, [15], are dealing with the design of spatial reticulated structures. With the help of a finite element computer program, two complex structures are analyzed: a power line pole for high games on a stadium and a brine pipe duct over a river. Structural details are presented together with loads. Computer results are shown and discussed.

The influence of geocomposition on wearing course of asphalt mixture behavior is researched by Diaconu and Racanel in [16]. The importance of octahedral shear stress ratio (OSSR) is shown and explained. The analysis is made on four types of asphalt mixtures. The laboratory results are presented and commented.

Prediction based on a viscoelastic-plastic behavior of asphalt mixtures on the rutting phenomenon is studied by Balcu and Lazar, [17]. Mechanical models for asphalt mixtures are presented and a solution algorithm is issued. Then a finite element procedure, named RAM (Rutting in Asphalt Mixtures), is shown. A way to choose the parameters in computation is proposed and a numerical application is performed.

Petrina, Balc, Ciplea and Marchis, [18], are showing the way to use AutoLISP under AutoCAA for automatic drawing. The main advantage of using AutoLISP is that the user can have total control on all routine of AutoCAD. The paper presents how reinforcement tables can be drawn through the use of three programs (one written in Fortran and two written in LISP). A description on the use of the procedure is also presented along with a work example.

A computer program for static analysis of semi-rigid structures is proposed by Petrina and Balc, [19]. The joints modeling is taking into account a linear moment-rotation relation, the rigid-plastic analysis is based on calculation of capable moment of the joint, and elastoplastic analysis based on non-linear moment-rotation characteristic. The algorithm of the proposed model is shown and examples of application are performed. Results are shown the appropriateness of the computer program.

In [20], Nutiu is concentrating on the importance and the quality of the existing high-accuracy leveling networks on the Romanian territory. The four level systems in Romania are presented and deeply commented. The results of the modernization of the Romanian geometrical leveling of grade I using high accuracy geometrical leveling are underlined. Details of the leveling database are revealed. The integration of Romanian networks into the European network is pointed out.

Scinteie and Ionescu deal with the use of Markov chains for predicting the structures condition, [21]. The proposed method, a part of modern management, is applied to obtaining highway bridges condition indices. A particular index, C1, is deeply analyzed. Conclusions show that prediction is issued through a probability transition matrix and propose further studies for comparing the behavior of old and new bridges.

In [22], Comisu is dealing with single exciter techniques for structural identification applied to bridge structures. An algorithm for qualifying modal parameters obtained through single exciter technique is shown. The dynamic analysis details and the technique involved are presented. The limitations of the peak amplitude method are underlined.

Also Comisu, [23], is analyzing the multiple exciter techniques for structural identification. The experimental procedure is described along with practical details and characteristic phase-lag modes.

Paulet-Crainiceanu, in [24], is developing the means for active hinges to be used in controlled structures. This study is a step forward for the analysis of such controlled structures, and also in the vision of robotic structures.

Optimization of reinforced concrete bridge design is in the views of Ionescu, in [25]. Optimization technique is described, in order to use some commercial finite element computer programs. The concept of optimal design of bridges is also presented. The iterative nature of designing process is underlined, but adequate methods could lead to limit the number of needed iterations.

A new type of joint assemblage for the thin-walled steel profiles is presented by Budescu, Ciongradi and Rosca, [26]. The KONTI type of element joints is taken into account. Because some common connections with HSFG bolt had proven lessening of bearing capacity during tests, a new type of joints is proposed. The philosophy of the new type of joint is presented and tests were carried out. Good behavior of the new joints compared to common type was observed.

Barsan and Ignat, in [27] and [28], are dealing with the optimization of boosters disinfection in water distribution systems and with the impact of failures in that can occur in this water distribution systems. Models an analytical work is completed experimental work. These papers show a tremendous interest on behalf of the social community using advanced computational techniques.

In [29], Tepes Onea is showing an analysis that takes into consideration the soil-structure interaction in obtaining the non-linear dynamic response. An application is showing the way to make such computation for a hotel structure. Comparisons are performed with the case of a common linear spectral analysis. Differences are underlined and commented.

3. CONCLUSIONS

Computational Civil Engineering is showing to be an important support layer of most Civil Engineering domain. Examples shown in this paper are covering large sub-domains from Civil Engineering and the interaction that arises between them and Computer Science domain. Studies and researches in Civil Engineering are developing and improving in part because of the use of computers and computation.

References

1. Anghel, C.V., Onchiş, D., Flexible algorithm for FFT parallel implementation, *Computational Civil Engineering 2005*, Editura Societăţii Academice "Matei-Teiu Botez", Iasi, 2005, ISBN 973-7962-65-6, pp.11-14
2. Popa, A.G., Cucu, H.L., Finite Element Analysis of Thin-walled Bars with U-shaped Section, *idem*, pp.15-22
3. Cucu, H.L., Popa, A.G., Considerations about the Hybrid-Strain Finite Element Analysis of Plates and Shells in the Theory of Thick Plates, *idem*, pp.23-33
4. Gobesz, F.Z., Some aspects of Computer-Based Education in Civil Engineering, *idem*, pp.33-43
5. Gobesz, F.Z., Turda, D.V., Knowledge in construction, from the perspective of communication, *idem*, pp.43-50

6. Alexa, P., Mociran, H., Mathe, A., Passive control of semirigid steel structures, *idem*, pp.51-58
7. Turda, D.V., Gobesz, F.Z., Python is a C++ made easy for Civil Engineers, *idem*, pp.59-65
8. Chiorean, C.G., Computer program for nonlinear inelastic analysis of 3D RC building frameworks, *idem*, pp.66-75
9. Oller, S., Barbat, Al.H., Miquel, J., Estudio del comportamiento de los hormigones reforzados con fibras cortas, *idem*, pp.76-98
10. Oller, S., Barbat, Al.H., Moment-curvature damage bridge piers subjected to horizontal loads, *idem*, pp.99-127
11. Barbuta, M., Nour, D.S., Mix optimization for high strength concrete, *idem*, pp.128-137
12. Nutiu, C., Notes on microtriangulation network types as applied to the study of construction displacements, *idem*, pp.138-145
13. Dima, Al., Răcănel, I.R., 3D modelling and calculation of the fixed platform PFS-U (PESCARUS), *idem*, pp.146-156
14. Rotberg, R., Dynamic thermal behavior of building components. Calculation methods, *idem*, pp.157-162
15. Jantea, C., Varlam, F., Designing reticulated space systems, *idem*, pp.163-173
16. Diaconu, E., Răcănel, C., The study of geocomposite influence on wearing course asphalt mixture behavior at permanent deformation, *idem*, pp.174-179
17. Balcu, M., Lazăr, Șt.M., A viscoelastic-plastic prediction of rutting in asphalt mixtures, *idem*, pp.180-191
18. Petrina, M., Balc, R., Ciplea, C., Marchis, C., AutoLISP automated drawing programming under AutoCAD, *idem*, pp.192-201
19. Petrina, M., Balc, R., Static analysis of semi-rigid structures - Computation program, *idem*, pp.202-210
20. Nutiu, C., Considerations on the quality and importance of the existing high-accuracy levelling networks on the territory of Romania, *idem*, pp.210-216
21. Scînteie, R., Ionescu, C., Prediction of condition of structures using Markov chains, *idem*, pp.217-223
22. Comisu, C.C., Single exciter techniques for structural identification, *idem*, pp.224-236
23. Comisu, C.C., Multiple exciter techniques for structural identification, *idem*, pp.237-245
24. Paulet-Crainiceanu, F., Structures with active hinges, a step to Structural Robotics, *idem*, pp.246-256
25. Ionescu, C., Considerations concerning the optimization of reinforced concrete bridge design, *idem*, pp.257-261
26. Budescu, M., Ciongradi, I., Roșca, O., A new type of joint assemblage for the thin-walled steel profiles, *idem*, pp.262-271
27. Barsan, Em., Ignat, A. Optimization of Booster Disinfection in Water Distribution, *idem*, pp.272-283
28. Barsan, Em., Ignat, A. Impact of failures from water distribution networks on booster disinfection, *idem*, pp.283-292
29. Țepeș Onea, F., Finite element model for obtaining the structural response considering soil-structure interaction *idem*, pp.293-297

Flexible algorithm for FFT parallel implementation

Cornelia Victoria Anghel¹, Darian Onchiș²

¹PhD, Computers Science Department, “Eftimie Murgu” University, Reșița, 1700, Romania

² Computers Science Department, “Eftimie Murgu” University, Reșița, 1700, Romania

Summary

For the parallel execution on distributed memory Linux clusters, the Fast Fourier Transform algorithm (FFT) is partitioned into a number of processes which concurrently run on the available processors of the system. The analysis of sequential algorithm points out different types of data dependencies that are removed by insertion of synchronization points between processes. For the parallel algorithm, an estimation of its runtime parameters is done in order to determine the performance of the parallel execution.

KEYWORDS: Fast Fourier Transform, implementation in parallel algorithm.

1. INTRODUCTION

The Fast Fourier Transform algorithm (FFT) is one of the most useful algorithm in digital signals processes applications: audio processing, images processing, statistic and scientific applications, and so on.

This paper presents an eloquent example of a parallel multiprocessor system, which is implemented by the flexible FFT algorithm.

So, a number of points are considered, like, $X = (X[0], X[1], \dots, X[n - 1])$, the Discrete Fourier Transform become a sequence $Y = (Y[0], Y[1], \dots, Y[n - 1])$, with same n dimension, in that the elements $Y[i]$, have the expression:

$$Y[i] = \sum_{k=0}^{n-1} X[k] \omega^{ik}, \quad 0 \leq i < n \quad (1)$$

where $\omega = e^{2\pi\sqrt{-1}/n}$ is the n solution from the complex plane. From relation (1) results that the evaluation for each element $Y[i]$, need n complex operations, so the execution time for all n points with Discrete Fourier Transform (DFT) is $O(n^2)$.

The FFT algorithm reduce this execution time at $O(n \log n)$.

To obtain this algorithm each element who has n DFT points is written like sum of two elements, with $n/2$ points DFT, each, relation (2):

$$\begin{aligned}
Y[i] &= \sum_{k=0}^{(n/2)-1} X[2k] \omega^{2ki} + \sum_{k=0}^{(n/2)-1} X[2k+1] \omega^{(2k+1)i} \\
&= \sum_{k=0}^{(n/2)-1} X[2k] e^{2(2\pi\sqrt{-1}/n)ki} + \sum_{k=0}^{(n/2)-1} X[2k+1] \omega^i e^{2(2\pi\sqrt{-1}/n)ki} \\
&= \sum_{k=0}^{(n/2)-1} X[2k] e^{2\pi\sqrt{-1}ki/(n/2)} + \omega^i \sum_{k=0}^{(n/2)-1} X[2k+1] e^{2\pi\sqrt{-1}ki/(n/2)}
\end{aligned} \tag{2}$$

In these expressions n is considered a power of 2.

Using the notations $\omega = e^{2\pi\sqrt{-1}/(n/2)} = \omega^2$, where ω is the $n/2$ of the unit. Equation (2) can be written:

$$Y[i] = \sum_{k=0}^{(n/2)-1} X[2k] \omega^{ki} + \omega^i \sum_{k=0}^{(n/2)-1} X[2k+1] \omega^{ki} \tag{3}$$

The multiprocessing system herein considered for parallelization of the FFT algorithm is a multiprocessor with shared memory, which may have up to P processors. The execution of the algorithm is partitioned into a number P of threads, which concurrently run on the available processors. In this multiprocessor system, the communication among threads is implemented as fast, shared access to global variables, which involves low parallel overhead, efficiency and scalability.

2. THE FFT ALGORITHM

Sequential FFT algorithm can be expressed in a recursive or iterative form. The simplest parallelization of FFT can be obtained based on iterative sequential algorithm. There are many parallelization methods of FFT algorithm. The proposed algorithm in this paper, permit an efficient communication to calculate the parallel Fourier Transform and use for each processor the known fast Fourier Transform algorithm, Cooley-Tukey. In multithreaded execution on shared memory multiprocessors, the Fast Fourier Transform algorithm (FFT) is partitioned into a number of P threads which concurrently run on the available N processors of the system.

The algorithm can be detailed in follows phases:

1. The initialization of sending message system (MPI_Init).
2. Shared date of the processors in N/P blocks. Use function MPI_Scatter.

3. Implementation in C software of FFT algorithm to calculate the local kernel.
4. Calculus for all receiving communications coefficients. We use the version non-blocking MPI_Wait.
5. Same steps for calculus of Inverse Fourier Transform. For collecting dates we use MPI_Gather.
6. Compile the program and correct the errors to finalize the algorithm (MPI_Finalize)

To prove the scalability of the algorithm, the parallel algorithm was implemented by a Linux cluster with Myrinet network, and we obtain the numerical results as follows.

3. NUMERICAL RESULTS

Number of samples - 2 power 16

For 10 processors

Time of parallel processing = 0.190443 ms

Estimation in MFLOPs = 34.353376

For 15 processors

Time of parallel processing = 0.18219 ms

Estimation in MFLOPs=35.299035

For 16 processors

Time of parallel processing = 0.17611 ms

Estimation in MFLOPs=35.454276

For 20 processors

Time of parallel processing = 0.16111 ms

Estimation in MFLOPs=35.774838

4. CONCLUSIONS

The FFT algorithm was implemented in C program language, and the parallelization was realized by message passing with MPI help.

The results obtained in a multithreaded implementation of FFT algorithm prove that the speed of computation increases by using a multiprocessor system. Even if the number of processors on such a system is, in general, small, the high-

performance processors and the short time consumed for communication via shared memory leads to a significant decrease of computational time reporting to a sequential system.

We use this methods because with the portability and generalized properties of the algorithm, can easy translate on other parallel system.

The implementation uses the MIMD (Multiple Instruction Multiple Data) procedures, who include a large scalability and flexibility for FFT parallel implementation.

References

1. Kumar, V., Grama, A., Gupta, A. and Karpis, G., **Introduction to Parallel Computing**, The Benjamin/Cummings Publishing Company, Inc., Redwood City, CA, 1994.
2. Quinn, M., **Parallel Computing- Theory and Practice**, 3. McGraw-Hill, New-York, 1994;
3. Hwang, K., **Advanced Computer Architecture: Parallelism, Scalabilily, Programmability**, McGraw-Hill, New-York, 1993;
4. IBM, AIX Version 4.3 General Programming Concepts, 1997.

Finite Element Analysis of Thin-walled Bars with U-shaped Section

Anca Gabriela Popa¹ and Hortensiu Liviu Cucu¹

¹Department of Structural Mechanics, Technical University of Cluj-Napoca, Cluj-Napoca, 400020,
Romania

Summary

The paper presents a finite element analysis of the behaviour of the U-shaped thin-walled elements subject simultaneously to bending and restrained torsion.

The principal aspects of the analysis regard the distribution of the strains and stresses. The problem is treated in a finite element approach, using plane stress incompatible finite elements and the program HYFEM, conceived at the Technical University of Cluj-Napoca by the authors and others.

There are presented numerical results concerning the distribution of the strains and stresses and comparisons with the results obtained with the commercial program NASTRAN and the theory of the thin-walled bars.

KEYWORDS: Thin-walled bars, finite element analysis.

1. INTRODUCTION

The paper presents numerical results obtained for the thin-walled bars with U-shaped cross section, considered as cantilevers fixed at the base (Figure 1).

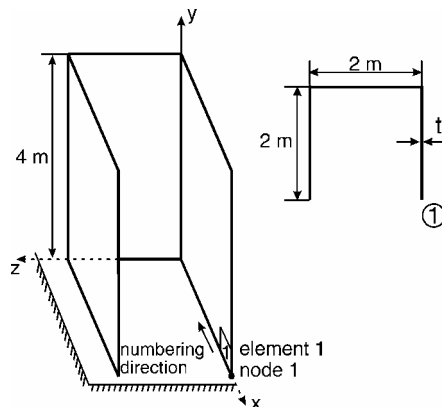


Figure 1. U-shaped structure – basic data

The finite element formulation is based on the 4-node isoparametric rectangular element with 2 degrees of freedom (dof) per node (Figure 2,a). For a higher accuracy in bending, shear is assumed to be constant over the finite element, equal to the value in the center.

For 3-D structures, an additional dof – representing the translation normal to the element's plane – is considered in each node, in order to describe the spatial state of displacements (Figure 2,b).

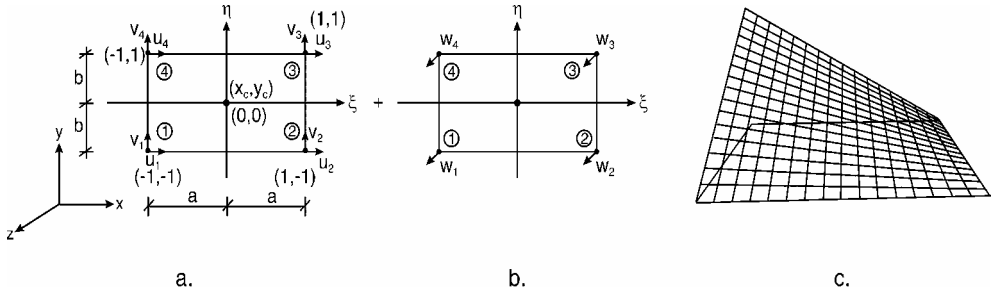


Figure 2. The finite element PLAN-12

The shape functions are assumed to be the bi-linear Lagrange polynomial

$$N_i = \frac{1}{4}(1 + \xi\xi_i) \cdot (1 + \eta\eta_i), \quad i = 1, 2, 3, 4, \quad (1)$$

furnishing linear displacements on the sides of the element (Figure 3,c).

The analysis was performed for three meshes:

- meshwork U_1 : 24 elements (1.0×1.0 m)
- meshwork U_2 : 96 elements (0.5×0.5 m)
- meshwork U_3 : 384 elements (0.25×0.25 m).

It is assumed that the numbering of the nodes and elements starts at the right corner of the section and it is left handed (Figure 1).

The three meshes were analyzed for the following loading cases (Figure 3):

- case (a): symmetrical uniform distributed forces;
- case (b): horizontal symmetrical concentrated forces;
- case (c): horizontal force acting on the direction of the web.

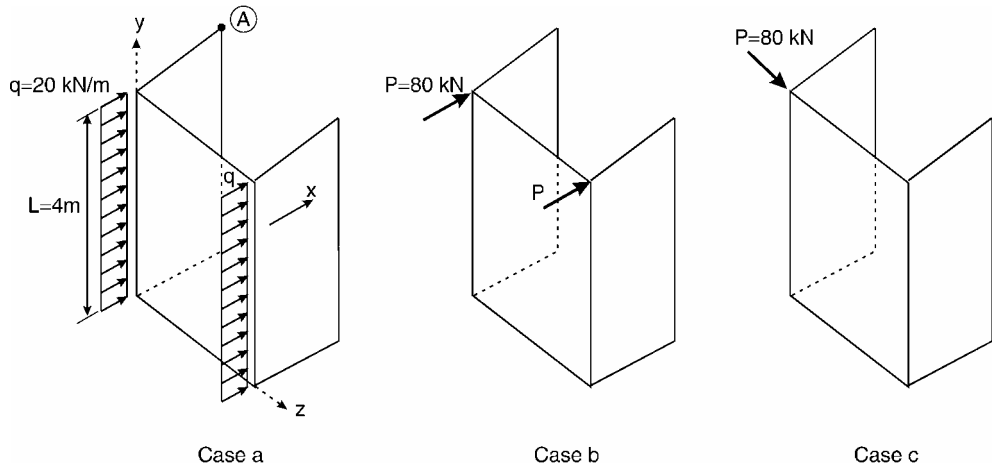


Figure 3. The loading cases

In the two first loading cases, the structure is subject to bending; the last case leads to restrained torsion with bending.

2. NUMERICAL RESULTS

It is assumed that the structure works in the elastic stage. The analysis was performed with the program HYFEM conceived at the Technical University of Cluj-Napoca. The results were compared to those obtained with the program MSC NASTRAN for Windows 4.5 or in the elastic bar / thin-walled bar theory.

It is to be mentioned that the program NASTRAN uses compatible plane stress finite elements.

2.1 Displacements

The displacements of the structure are represented in the Figures 4 and 5. For the loading case (b), the deformed structure is alike to the case (a).

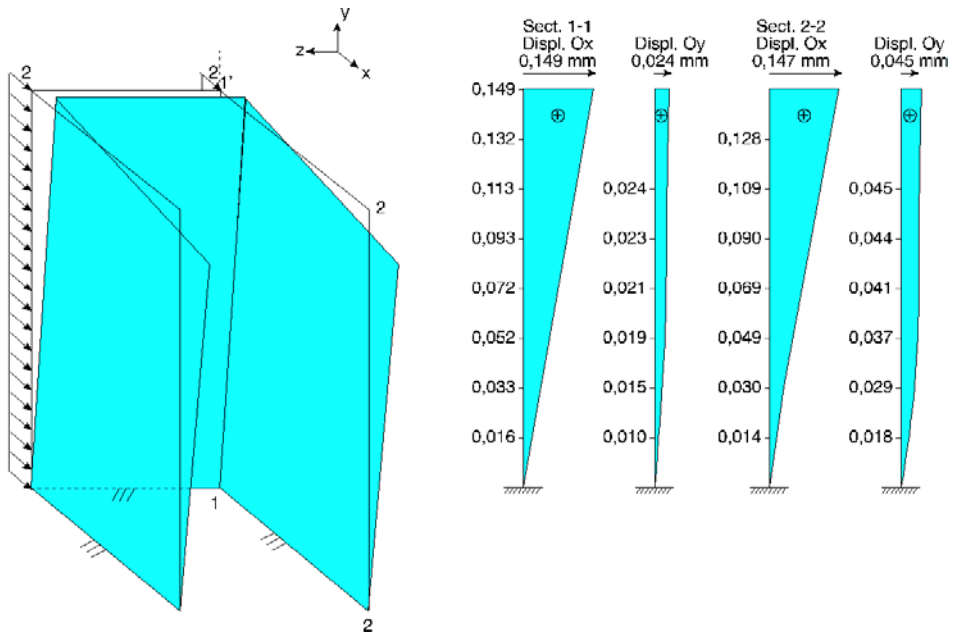


Figure 4. Displacements of the structure, meshwork U_2 , loading case (a)

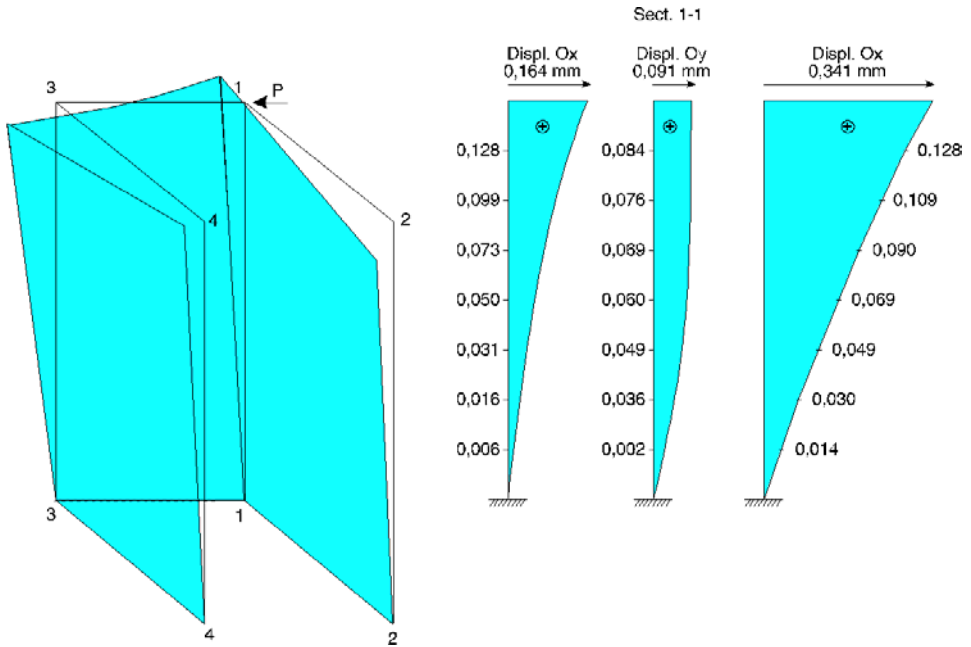


Figure 5. Displacements of the structure, meshwork U_2 , loading case (c)

The displacements obtained with the incompatible element PLAN-12 are close to those obtained in the bar theory, in the case of bending, or in the thin-walled bars theory, for the complex action of restrained torsion and bending. The differences between the results are less than 2%, the finite element approach generally overestimating the displacements.

It can be noticed (Figure 4) that the Bernoulli’s hypothesis of plane sections is respected for bending. For the restrained torsion (Figure 5), the warping of the cross section is obvious. A comparative study of the vertical displacements at the top of the structure (the warping effect) is given in Figure 6 and Table 1.

Table 1. Vertical displacements at the top level of the structure

HYFEM		NASTRAN		Deviation %
Node	Displacement [mm]	Node	Displacement [mm]	
34	- 3.6	29	- 3.5223	2.20
32	1.7	30	1.6567	2.61
29	8.3	31	8.0186	3.51
30	- 0.6	32	- 0.48	25
31	- 7.3	33	- 7.0585	3.42
33	- 1.7	34	- 1.646	3.28
35	+ 3.4	35	+ 3.3225	2.33
Mean deviation 6.05%				

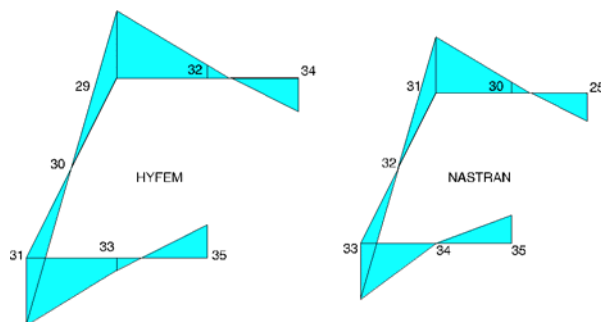


Figure 6. Vertical displacements at the top level of the structure, meshwork U₂, loading case (c)

The results suggest a good concordance of the two programs, the average gap being around 6.05%.

Also it is worth to mention that the incompatible finite element with 3 dof per node is able to overtake the out of plane displacements of the structure which represents an advantage especially in 3-D.

2.2 Stresses and internal actions

The normal stresses in simple bending, obtained with the finite element method, are plotted in Figure 7. The values are close to those obtained in the elastic bar theory and, generally, slightly overestimated. The same observation applies to the internal actions (bending moments) represented in Figure 8.

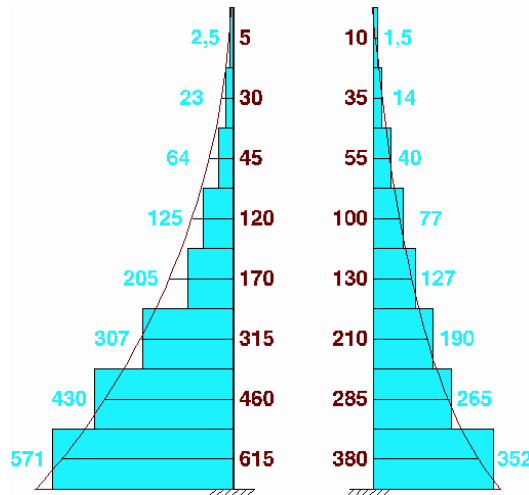


Figure 7. Normal stresses in simple bending [kN/m²], meshwork U₂, loading case (a)

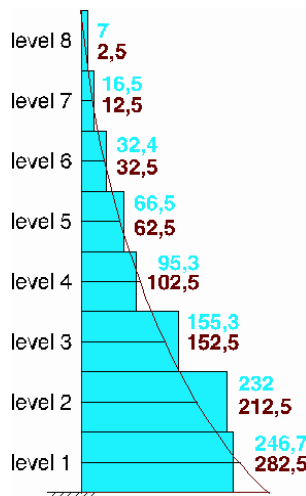


Figure 8. Bending moments [kNm], meshwork U₂, loading case (a)

In Figure 9 is represented the normal stress distribution at the base of the structure for restrained torsion and bending (loading case c). The analysis of these results reveal that the incompatible finite element PLAN-12 has a mean deviation of 9.685% with respect to the thin-walled bar theory, lower than the one obtained with the classical plane stress element use by NASTRAN.

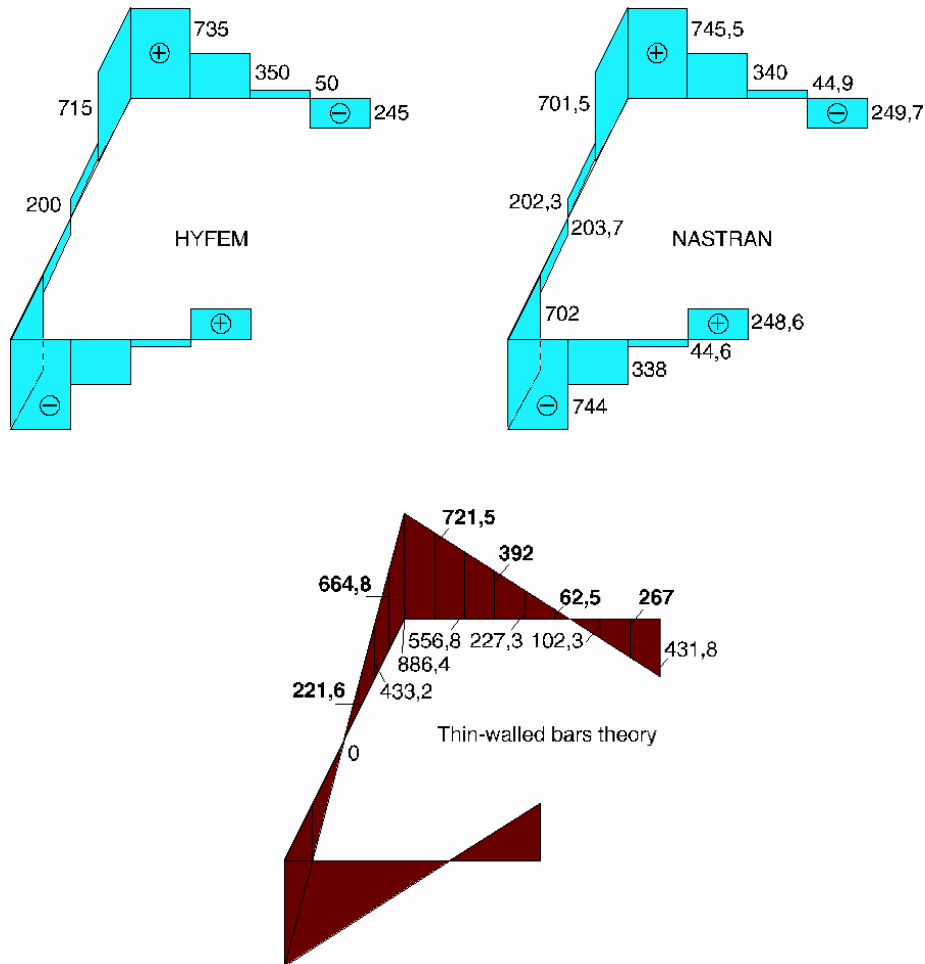


Figure 9. Normal stresses at the level 1 [kN/m^2], meshwork U_2 , loading case (c)

The internal actions (Figure 10) suggest a good correlation between the finite element analysis with the incompatible element PLAN-12 and the theory of thin-walled bars.

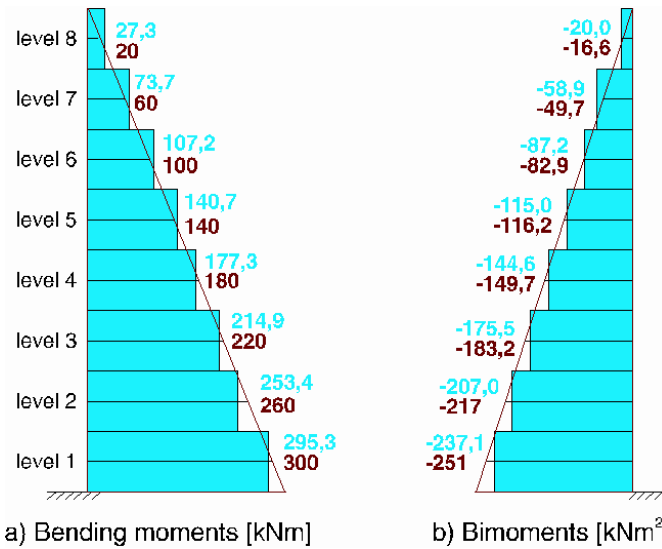


Figure 10. Normal stresses at level 1 [kN/m²], meshwork U₂, loading case (c)

3. CONCLUSIONS

Numerical tests performed with the incompatible plane element with three degrees of freedom per node PLAN-12 have revealed a good behavior in all the loading cases and especially for restrained torsion.

The mean deviation of the displacements is less than 2% with respect to the analytical solutions. For stresses and internal actions, the gap between the two solutions, analytical and numerical, is greater but still in technically accepted limits. It has been mentioned that finite elements used in the analysis have quite large dimensions and the solutions are improving with the refining of the meshes.

The above considerations lead to the conclusion that the plane incompatible finite element with three degrees of freedom per node is efficient in the analysis of the thin-walled bars with open section.

References

1. Kolbrunner, C.F. and Hajdiu N., *Dünnwändige Stäbe*, Springer Verlag, Berlin 1975.
2. Chen, B. and Hu, Y., *A Consistent Theory for Torsion of Thin-walled Bars*, Thin-walled Structures, nr.7, 1988.
3. El-Hammasi, A.S., *Numerical Method for Analysing Open Thin-walled Structures under Interaction of Bending and Torsion*, Computer & Structures, vol.37, 1990.
4. Marțian, I., *Teoria elasticității și plasticității pentru constructori*, Universitatea Tehnică din Cluj-Napoca, 1999, (in Romanian).
5. Roberts, T.M. and Achour, B., *Torsion and Bending of Braced Thin-walled Open Sections*, Journal of Structural Engineering, vol.116, 1990.

Considerations about the Hybrid-Strain Finite Element Analysis of Plates and Shells in the Theory of Thick Plates

Hortensiu-Liviu CUCU¹, Anca Gabriela POPA²

¹ “Structural Mechanics” Department, Technical University of Cluj-Napoca, 400.020, Cluj

² “Structural Mechanics” Department, Technical University of Cluj-Napoca, 400.020, Cluj

Summary

The paper is presenting two new hybrid-strain finite elements for the analysis of orthotropic plates and shells. The finite elements were implemented in the program for structural analysis “HYFEM” (program developed - since the year 2000 - by the Structural Mechanics Department from the Technical University of Cluj-Napoca, Faculty of Civil Engineering). The program offers extended possibilities for research by using advanced methods and procedures for the analysis and the optimization of bar structures, shear wall structures and structures with thick plates and/or shells.

The first section of the paper gives a brief description of the general methodology applied for the formulation of the hybrid-strain finite elements and their particularities. The next section is a synthetically presentation of the tests performed with the new hybrid-strain finite elements in order to appreciate their accuracy in modeling the plates and shells. Finally, based on the interpretation of the numerical results, are given some observations regarding the advantages offered by the new hybrid-strain finite elements in the analysis of plates and shells in the thick plate approach.

KEYWORDS: Finite Element Method; Hu-Washizu Principle; hybrid approach; orthotropic thick plates; orthotropic shells.

1. INTRODUCTION

The starting point for the development of the “hybrid” finite elements is represented by a particular form of the Hu-Washizu^[1] functional in which, beside the displacements, the stresses and the strains are considered as independent variables. The hybrid approach assumes that the two groups of variables (displacements and stresses/strains) are interpolated independently. The particularity of the hybrid-strain finite elements consist in the fact that the last group of variables (stresses/strains) is eliminated at the element level so that, in the global equations, only the displacements appear as unknowns. Depending on the

independent variables eliminated at the element level (stresses or strains), the finite elements obtained are named hybrid – stress or hybrid – strain.

Based on the proposals, observations and recommendations made along the years by great researchers in the field of the finite element structural analysis (T. H. H. Pian and P. Tong^{[2], [3]}, K. J. Bathe^[4], R. D. Cook^[5], O. C. Zienkiewicz^[6] and J. D. Chiesler and A. Ghali^[7]), the authors of the present paper have succeed in the development of hybrid-strain finite elements, applicable to plates and shells analysis in the theory of thick plates.

2. NEW HYBRID-STRAIN FINITE ELEMENTS

2.1 The Hybrid-strain Formulation of Finite Element Method

T. H. H. PIAN [8] is the one who modified the Hu-Washizu functional under the following form:

$$\Pi_{HW*} = \int_V \left[-\frac{1}{2} \{\varepsilon\}^T \cdot [D] \cdot \{\varepsilon\} + \{\varepsilon\}^T \cdot ([L] \cdot \{u\}) \right] \cdot dV - \int_V \{b\}^T \cdot \{u\} \cdot dV - \int_{S_i} \{t\}^T \cdot \{u\} \cdot ds \quad (1)$$

Introducing in this expression:

i) the interpolation of the displacement field over the finite element $\{u\}$ with respect to the nodal displacements $\{q\}$, through the isoparametric shape functions matrix $[N]$:

$$\{u\} = [N] \cdot \{q\} \quad (2)$$

ii) the interpolation of the strains on the finite element's domain $\{\varepsilon\}$ with respect to the generalized displacements parameters, through the strain interpolation matrix $[P]$:

$$\{\varepsilon\} = [P] \cdot \{\alpha\} \quad (3)$$

functional (1) becomes:

$$\begin{aligned} \Pi_{HW*} = \int_V \left[-\frac{1}{2} \{\alpha\}^T \cdot [P]^T \cdot [D] \cdot [P] \cdot \{\alpha\} + \{\alpha\}^T \cdot [P]^T \cdot [D] \cdot ([L] \cdot [N]) \cdot \{q\} \right] \cdot dV \\ - \int_V \{b\}^T \cdot [N] \cdot \{q\} \cdot dV - \int_{S_i} \{t\}^T \cdot [N] \cdot \{q\} \cdot ds \end{aligned} \quad (4)$$

With the following notations:

$$\text{the generalized stiffness matrix} = \int_V [P]^T \cdot [D] \cdot [P] \cdot dV = [K^*] \quad (5)$$

$$\text{the transformation matrix} = \int_V [P]^T \cdot [D] \cdot ([L] \cdot [N]) = [G] \quad (6)$$

$$\text{the load (nodal forces) vector} = \int_V [N]^T \cdot \{b\} \cdot dV + \int_{S_i} [N]^T \cdot \{t\} \cdot ds = \{F\} \quad (7)$$

the functional (4) may be written under the form:

$$\Pi_{HW*} = -\frac{1}{2} \cdot \{\alpha\}^T \cdot [K*] \cdot \{\alpha\} + \{\alpha\}^T \cdot [G] \cdot \{q\} - \{q\}^T \cdot \{F\} \quad (8)$$

By minimizing the functional (8) with respect to $\{q\}$ and $\{\alpha\}$, it is obtained the matrix equation:

$$\begin{bmatrix} 0 & G^T \\ G & -K^* \end{bmatrix} \begin{Bmatrix} q \\ \alpha \end{Bmatrix} = \begin{Bmatrix} F \\ 0 \end{Bmatrix} \quad (9)$$

Taking into account that $[K^*]$ has a defined nature, $\{\alpha\}$ may be eliminated through the Gauss technique (backwards), and it is obtained the stiffness matrix of the element, $[K]$:

$$[K] = [G]^T \cdot [K^*]^{-1} \cdot [G] \quad (10)$$

With the global solution for the nodal displacements $\{q\}$, the stresses are obtained with:

$$\{\sigma\} = [D] \cdot [P] \cdot ([G]^T \cdot [K^*]^{-1})^T \cdot \{q\} \quad (11)$$

Based on the technique described above were developed two finite elements, both with 24 degrees of freedom (dofs):

- i) the bi-dimensional element “HYBFLAT-24”, with 4 nodes and 6 dofs per node,
- ii) the three-dimensional element “HYBBRICK-24”, with 8 nodes and 3 dofs per node.

Details about the particularities of these developments are presented in the references [8], [9].

2.2 The Bi-dimensional Hybrid-Strain Finite Element “HYBFLAT” (Figure 1.a)

The main steps followed in order to formulate that finite element are:

- step 1) the choice of the shape functions; the option was for the type:

$$N_i = \frac{1}{4} \cdot (1 + \xi \xi_i) \cdot (1 + \eta \eta_i) \quad \text{with } \xi_i, \eta_i = \pm 1 \quad (12)$$

- step 2) the interpolation of the displacements on the finite element, through the isoparametric shape functions matrix $[N]$:

$$[N]_{(3 \times 24)} = \begin{bmatrix} N_1 & \cdot & \cdot & -A_1 \cdot l_2 & A_1 \cdot l_1 & A_1 \cdot l_3 & \cdots & N_4 & \cdot & \cdot & -A_4 \cdot l_2 & A_4 \cdot l_1 & A_4 \cdot l_3 & \cdots \\ \cdot & N_1 & \cdot & -A_1 \cdot m_2 & A_1 \cdot m_1 & A_1 \cdot m_3 & \cdots & \cdot & N_4 & \cdot & -A_4 \cdot m_2 & A_4 \cdot m_1 & A_4 \cdot m_3 & \cdots \\ \cdot & \cdot & N_1 & -A_1 \cdot n_2 & A_1 \cdot n_1 & A_1 \cdot n_3 & \cdots & \cdot & \cdot & N_4 & -A_4 \cdot n_2 & A_4 \cdot n_1 & A_4 \cdot n_3 & \cdots \end{bmatrix} \quad (13)$$

with: $A_1 = N_1 \cdot t \cdot \frac{\zeta}{2}; \quad A_2 = N_2 \cdot t \cdot \frac{\zeta}{2}; \quad A_3 = N_3 \cdot t \cdot \frac{\zeta}{2}; \quad A_4 = N_4 \cdot t \cdot \frac{\zeta}{2}$ (14)

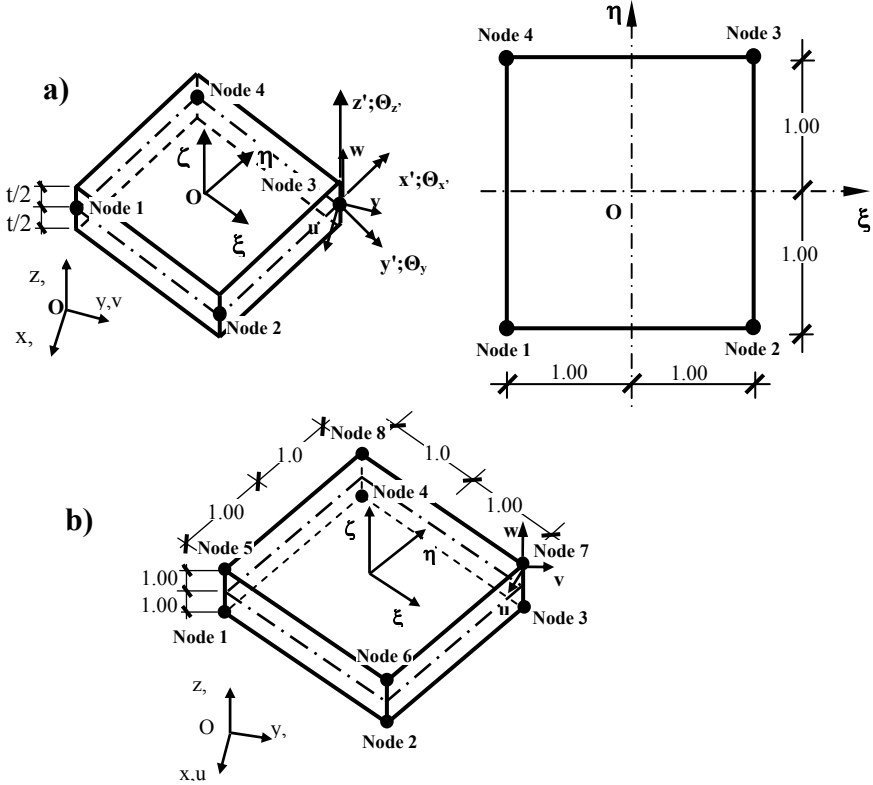


Figure 1. The two new hybrid-strain finite element proposed (a – the element “HYBFLAT”; b – the element “HYBBRICK”)

· step 3) the interpolation of the strains on the finite element, through the strain interpolation matrix $[P]$:

$$[P]_{(6 \times 18)} = \begin{bmatrix} 1 & \eta & \zeta & \eta \cdot \zeta & \cdot \\ \cdot & \cdot & \cdot & \cdot & 1 & \xi & \zeta & \xi \cdot \zeta & \cdot \\ \cdot & 1 & \xi & \eta & \xi \cdot \zeta & \cdot & \cdot & \cdot & \cdot & \cdot & \cdot \\ \cdot & 1 & \zeta & \cdot & \cdot & \cdot & \cdot \\ \cdot & 1 & \xi & \cdot & \cdot \\ \cdot & 1 & \eta \end{bmatrix} \quad (15)$$

· step 4) the transposition of the strains into the global system:

$$[\varepsilon] = [T_\sigma]^T \cdot [\varepsilon'] \quad (16)$$

$\begin{matrix} (6 \times 1) & & (6 \times 6) & & (6 \times 1) \end{matrix}$

with $[T_\sigma] =$ Cook's matrix [5].

· step 5) the selection of an orthotropic constitutive matrix for the material:

$$[D'] = \begin{bmatrix} e_{11} & e_{12} & e_{13} & 0 & 0 & 0 \\ e_{12} & e_{11} & e_{13} & 0 & 0 & 0 \\ e_{13} & e_{13} & e_{33} & 0 & 0 & 0 \\ 0 & 0 & 0 & g_{13} & 0 & 0 \\ 0 & 0 & 0 & 0 & g_{13} & 0 \\ 0 & 0 & 0 & 0 & 0 & g_{33} \end{bmatrix} \quad (17)$$

$\begin{matrix} (6 \times 6) \end{matrix}$

· step 6) the transposition of the constitutive matrix in global co-ordinates:

$$[D] = [T_\varepsilon]^T \cdot [D'] \cdot [T_\varepsilon] \quad (18)$$

$\begin{matrix} (6 \times 6) & & (6 \times 6) & & (6 \times 6) & & (6 \times 6) \end{matrix}$

with $[T_\varepsilon] =$ Cook's matrix [5].

· step 7) the application of the differential operator

$$[L] = \begin{bmatrix} \frac{\partial}{\partial x} & \cdot & \cdot \\ \cdot & \frac{\partial}{\partial y} & \cdot \\ \cdot & \cdot & \frac{\partial}{\partial z} \\ \frac{\partial}{\partial y} & \frac{\partial}{\partial x} & \cdot \\ \cdot & \frac{\partial}{\partial z} & \frac{\partial}{\partial y} \\ \frac{\partial}{\partial z} & \cdot & \frac{\partial}{\partial x} \end{bmatrix} \quad (19)$$

$\begin{matrix} (6 \times 1) \end{matrix}$

and the Gauss numerical integration of the following two matrices:

$$\text{the generalized stiffness matrix} = [K^*] = \int_V [P]^T \cdot [D] \cdot [P] \cdot dV \quad (20)$$

$\begin{matrix} (18 \times 18) & & (18 \times 6) & & (6 \times 6) & & (6 \times 18) \end{matrix}$

$$\text{the transformation matrix} = [G] = \int_V [P]^T \cdot [D] \cdot \left([L] \cdot [N] \right) \cdot dV \quad (21)$$

$\begin{matrix} (18 \times 24) & & (18 \times 6) & & (6 \times 6) & & \left(\begin{matrix} (6 \times 3) \\ (3 \times 24) \end{matrix} \right) \end{matrix}$

· step 8) the development of the stiffness matrix of the finite element:

$$[K] = [G]^T \cdot [K^*] \cdot [G] \quad (22)$$

$\begin{matrix} (24 \times 24) & & (24 \times 18) & & (18 \times 18) & & (18 \times 24) \end{matrix}$

· step 9) the development of the nodal forces (load) vector:

$$\{F\} = \int_V [N]^T \cdot \{b\} \cdot dV + \int_{S_i} [N]^T \cdot \{t\} \cdot ds \quad (23)$$

· step 10) the solution of the system of equations for a classical finite element approach:

$$[K] \cdot \{q\} = \{F\} \quad (24)$$

gives the nodal displacements vector $\{q\}$.

· step 11) the solution for the stresses vector:

$$\{\sigma\} = [D] \cdot [P] \cdot \left([G]^T \cdot [K^*]^{-1} \right)^T \cdot \{q\} \quad (25)$$

2.3 The Three-dimensional Hybrid-Strain Finite Element “HYBBRICK” (Figure 1.b)

This finite element was obtained by operating the following modifications on the finite element HYBFLAT, described in paragraph 2.2:

· 1) the addition of the third non-dimensional co-ordinate and the modification, accordingly, of the shape functions

$$N_i = \frac{1}{4} \cdot (1 + \xi \xi_i) \cdot (1 + \eta \eta_i) \cdot (1 + \zeta \zeta_i); \text{ with } \xi_i, \eta_i, \zeta_i = \pm 1 \quad (26)$$

· 2) the consideration of eight nodes (in each corner) and of three degrees of freedom per node, representing the translations on the global co-ordinate axes (u, v and w).

· 3) the interpolation of the displacements field on the finite element through the isoparametric shape functions matrix $[N]$ of the form:

$$[N]_{(3 \times 24)} = \begin{bmatrix} N_1 & \cdot & \cdot & N_2 & \cdot & \cdot & N_3 & \cdot & \cdot & \dots & N_7 & \cdot & \cdot & N_8 & \cdot & \cdot \\ \cdot & N_1 & \cdot & \cdot & N_2 & \cdot & \cdot & N_3 & \cdot & \dots & \cdot & N_7 & \cdot & \cdot & N_8 & \cdot \\ \cdot & \cdot & N_1 & \cdot & \cdot & N_2 & \cdot & \cdot & N_3 & \dots & \cdot & \cdot & N_7 & \cdot & \cdot & N_8 \end{bmatrix} \quad (27)$$

· 4) the introduction of the weights and numerical integration co-ordinates correspondent to the third direction.

Because the total number of DOFs on the finite element was kept to 24, as for the plane finite element „HYBFLAT”, the solution technique for the stiffness matrix of the element, the assembling of the global stiffness matrix (corresponding to the whole structure), the solution for the finite element equation system, the recover of the displacements and – finally – the calculation of the stresses and the internal actions, remain the same.

2.4 The Testing of the Two Proposed Hybrid-strain Finite Elements

The tests of the bi-dimensional hybrid-strain finite element “HYBFLAT”, meant to the calculation of thick plates, have been made on a great variety of models: rectangular flat plates (“a” in Figure 2), circular and ring-shaped plates (“b” in Figure 2), slabs punctually supported or supported on columns (“c” in Figure 2) and shells (curved plates) (Figure 3). For the three-dimensional hybrid-strain element “HYBBRICK”, supplementary tests were performed on 3-D elements, such blocks (Figure 4).

For the validation of the two hybrid-strain finite elements, the results were compared to the analytical or approximate known solutions and/or solutions delivered by some commercial programs well qualified for structural analysis: “MSC-Nastran”, “MSC-MARC” and “ROBOT Millennium”.

2.5 The Analysis of the Proposed Hybrid-Strain Finite Elements

The analysis of the results obtained for both categories of test-problems, plane as well as spatial, gave raise to the following conclusions:

1. The results obtained with the meshes based on the two proposed finite elements, based on the hybrid-strain finite element approach, are very close or even identical to those obtained with analytical methods, furnished by the technical literature, when the principles of the optimal discretisation are respected. For exemplification in Figure 5 is represented the relative error of the solution given by the element “HYBFLAT” for one of the plane test-problem, considering four uniform meshes with 2, 4, 8 and respectively 16 elements per edge.
2. The results supplied by the analysis program based on the two propose finite elements are comparable with those obtained with the reference commercial programs for structural analysis: “MSC-Nastran”, “MSC-MARC” and “ROBOT Millennium”.
3. The accuracy and the stability of the solutions is situated within the limits accepted in the engineering practice, even for the case of some deficient meshes which do not respect the classical principles of an optimal discretisation (quadratic form or close, the edges’ ratio $\leq 1.5 \div 2$, the absence of sharpened angles and intrusive angles, the gradual variation of the elements’ dimensions, the refining of the meshes in the proximity of the singularities etc.).
4. The proposed finite elements demonstrate a great robustness, being able to offer realistic solutions even in the case of a reduced number of nodes in which are imposed the limit conditions.
5. For the same degree of refinement of the meshes, the two new hybrid-strain finite elements offer improved solutions for the stresses and the internal actions as the structural analysis programs based on a classical displacement approach.

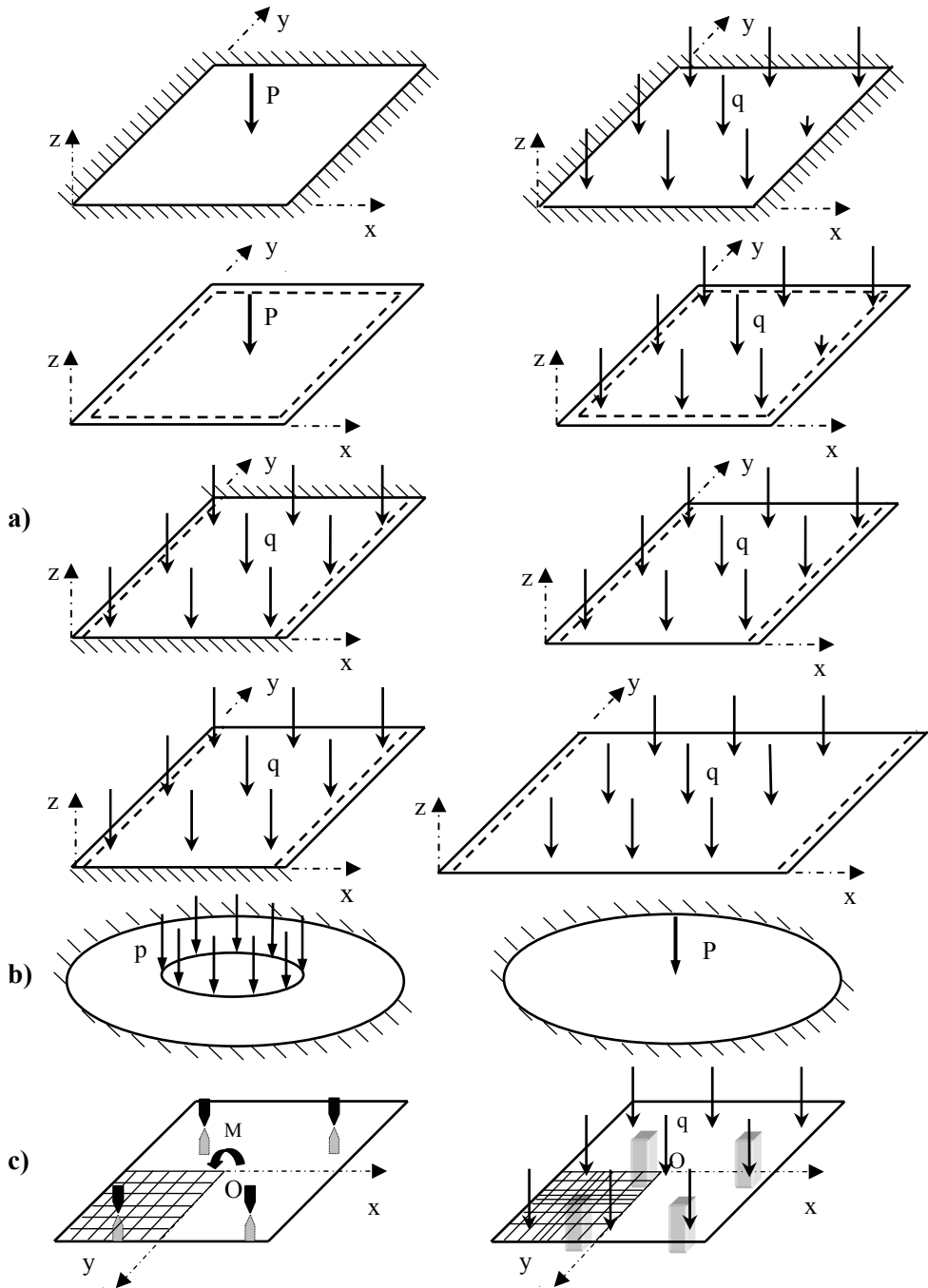


Figure 2. Some plate tests.

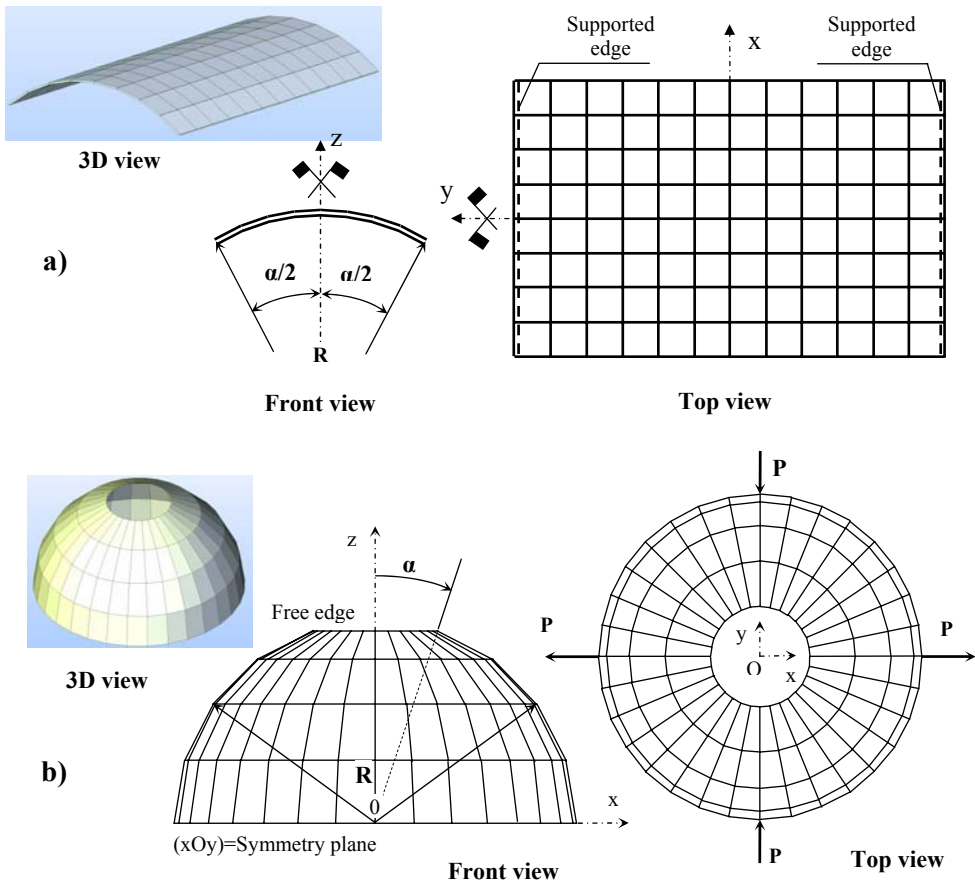


Figure 3. Two classical shell tests (a – Scordelis-Lo roof; b – MacNeal-Hardner hemispherical shell).

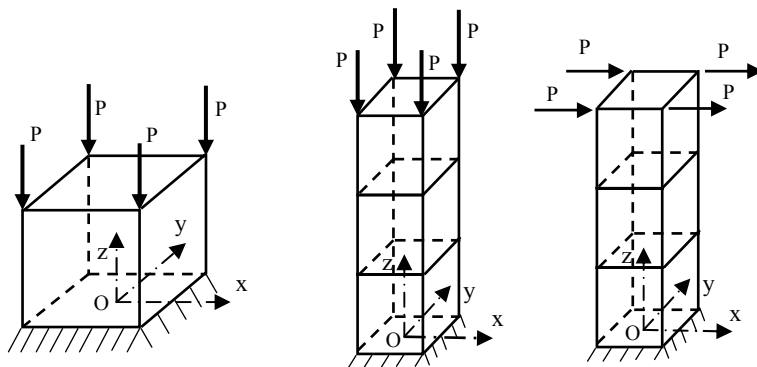


Figure 4. Some block tests.

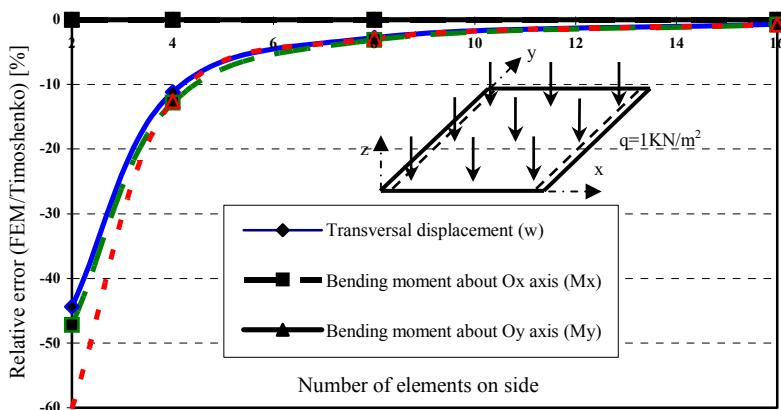


Figure 5 – Relative error (FEM/Timoshenko's solution) for a plane test-problem.

3. CONCLUSIONS

The two new finite elements proposed in this paper, based on the hybrid-strain finite element approach, represent a useful and powerful tool for the analysis of the plates and shells in the thick plate theory, offering spectacular results, with great accuracy.

References

1. Washizu, K. *Variational Methods in Elasticity and Plasticity*; 2nd Edn., Pergamon Press, New York, 1975.
2. Pian, T. H. H., Tong, P. Basis of Finite Element Methods for Solid Continua, *International Journal for Numerical Methods in Engineering*, vol. 1, no. 1, 1969.
3. Tong, P., Pian, T. H. H. A Variational Principle and the Convergence of a Finite Element Model Based on Assumed Stress Distributions, *International Journal of Solids and Structures*, vol. 5, no. 5, 1969.
4. Bathe, K. J. *Finite Element Procedures*, Prentice-Hall, New Jersey, 1996.
5. Cook, R. D. *Concepts and Applications of Finite Element Analysis*, John Wiley, New York, 1974.
6. Zienkiewicz, O. C. *The Finite Element Method*; Fourth Edn., McGraw-Hill, London, 1989.
7. Chieslar, J. D., Ghali, A. A Hybrid Strain Technique for Finite Element Analysis of Plates and Shells, *Computers and Structures*, vol. 24, no.5, 1986.
8. Cucu, H. L. *Analiza prin elemente finite hibride a plăcilor plane și curbe anizotrope.*, PhD Thesis, UTC-N, Cluj-Napoca, 2003.
9. Cucu, H. L., Góbesz, F. Z., Turda, D. V., Popa, A. G., Marțian, I. *Two new hybrid finite elements for thick plates and shells*. Proceedings of the International Conference « Construction 2003 », Cluj-Napoca, 16-17 mai 2003.
10. Turda, D. V., Cucu, H. L., Popa, A. G., Góbesz, F. Z. *A New Finite Element Analysis System*. Acta Technica Napocensis, 45/2002.

Some aspects of Computer-Based Education in Civil Engineering

Ferdinand-Zsongor Gobesz¹

¹*Department of Structural Mechanics, Technical University of Cluj-Napoca, Cluj-Napoca, 400020, Romania*

Summary

The use of computers in several educational activities within technical fields has already a consolidated tradition. Starting with the “initiation” of freshmen students, towards information and self-education of trained professionals, a lot of users become frustrated due to the inevitable evolution and changes of technologies. From this point of view, any “computer aided” activity (education, design, selling etc.) should be considered as a state of mind with adequate acting modes.

In this paper, I will try to discuss a few aspects concerning higher education, Internet based e-learning, and computer aided design, emphasizing the role of “aided” every-day education (almost unnoticed in most of the cases). As example, I will mention briefly the “AIC info” informational system, conceived at Cluj-Napoca (Romania). Starting from this experience we developed other applications too, taking advantage of the evolution of technologies and user mentality, but also as a link to other computer aided activities. The system offers free access to Romanian construction and building resources through the Internet and in the same time educational support through articles, discussion forums, etc. for people interested in building and construction.

KEYWORDS: education; computer; information system; engineering; Internet.

1. INTRODUCTION

The impact of information technology on the evolution of our society is broad and profound. The construction and building industry is undergoing significant changes due to the increasingly intensive use of networked computers and multimedia equipment. This fact changes not just ways and means of education in this field, but also the nature of many human activities. Most people will agree with the statement that we are going through a transition from an “industrial economy” towards a “knowledge economy”, because knowledge and information are playing an increasingly important role in all aspects of our lives. As academic mentors or scholars, practitioner engineers or architects, managers, but also as parents or just curious gapers, we have to deal with many facets of this broad process every day.

Higher education is in the unique position to act as a driver and it should remain an evolutionary environment fostering creativity, communication skills, and critical thinking.

2. KNOWLEDGE AND INFORMATION

Knowledge is understood to be a human, conceptual process. In the Merriam-Webster dictionary [9] this is defined as knowing something through experience or association; an understanding of technique; a fact or condition of being aware of something; a range of one's information or understanding. Knowledge applies to facts or ideas acquired by study, investigation, observation or experience, while learning applies to knowledge acquired especially through formal, often advanced, schooling. Information is the communication or reception of knowledge or intelligence; knowledge obtained from investigation, study or instruction; the attribute of sequences or arrangements of something producing specific effects; data representative. It is also something justifying a change in a construct that represents physical or mental experience or another construct. [9].

When dealing with knowledge we have to deal with various levels, going through and through these different stages repeatedly:

- creating knowledge;
- identifying knowledge;
- collecting knowledge;
- organizing knowledge;
- sharing knowledge;
- adapting knowledge;
- using knowledge.

Omitting a few will give us a headache. If we do not share knowledge, we will get less knowledge from others in return. If we do not adapt knowledge, it will be less useful [6].

In order to retrieve information, we tend to look in three places, walking through them in sequence until we find an answer:

- our own knowledge base, conditioned from personal experience and education;
- other knowledgeable people (relatives, friends, colleagues, experts etc.);
- proprietary or public sources and media (books, reviews, CDs, Internet etc.).

“In the past, you asked friends for an answer, now you ask google”. Apparently accessing computers can prove many times easier than accessing people. That’s just one of the endorsements asserting artificial intelligence research, more specifically knowledge bases and expert systems. But it’s also true that there is a lot of knowledge inside people, so finding people can prove as important as finding documents.

Searching for information can be done in many ways. There is a definitive scale from a structured search to an unstructured prowl. Restricting to computer aided activities, consulting a document management system, looking for a specific document, is a very structured way to search. Also structured is using search engines over the Internet, but among the results there may be other things that might make us wander away a bit from the structuredness of pursuit. Coining ideas, discussing in groups, paying attention to other’s can be mostly unstructured, but at least we will probably find many new, interesting ideas. Browsing through libraries, bibliographies, references and links, is even more unstructured. The most unstructured is probably the serendipity level, namely: making fortunate discoveries by accident.

3. EDUCATION AND INFORMATION

As technology rapidly changes, the importance of educating and training becomes more critical for the human society. Young people are more receptive to evolving means and resources due to their higher degree of susceptibility combined with the axiomatic curiosity of human nature. The first glimpse in sometime amazingly evolving technology conformance is often made in family environment or school. The adequate use of changing technologies is considered a trivially requirement in higher education and mostly professional activities.

In academic education the traditional teaching format of having an individual lecture to an audience has been supplemented, in some cases even replaced by the development and implementation of new learning methods, due to the evolution of information technology and multimedia equipment. Conventional lecture format teaching methods sometimes fall short of conveying the complex analysis and design principles that need to be mastered in engineering and structural design. However when the theories are exemplified in a virtual environment with multimedia presentation, animation, interaction, and manipulated image visualization techniques, the conceptual understanding is expected to be enhanced.

The important advantages of virtual reality environments over other computer-based design tools are that they enable the user to interact through simulation in order to conceptualize relations that may not be apparent from a less dynamic representation, and to visualize models that are difficult to understand in

other ways. The interactive nature of virtual environments can enable students and professionals to visualize real life structures before actually building them. Certainly, technology cannot be regarded as a substitute for talent. Mediocrity does not necessarily evolve to excellence due to the availability of sophisticated software.

Another aspect is the development of distance learning, due to the evolution of the World Wide Web, which led to an unprecedented growth of accessibility to information over the Internet. The web-based learning environment offers many advantages including tolerable ease of use, quick access, low cost, available (at least theoretically) without the limitations of time or location, independently from computer platform, and flexible in allowing students to control their learning pace. The current information technology allows us to develop student-centered virtual environments that can be reached to a large student population via the web. The student-centered distance learning archetype include dynamic demonstration of theoretical engineering models allowing students to manipulate, experiment, and translate theories into real-world applications.

By allowing users to control the sequence and the pacing of the materials, multimedia packages facilitate greater individualization in learning, allowing students to proceed at their own pace in a tailored learning environment. Furthermore, interactive multimedia can be a powerful learning and teaching tool because it engages multiple senses. Students using multimedia are reading, seeing, hearing, and actively manipulating materials. Quoting from Menn [5]:

“As humans, we seem hard-wired for multiple input. Consider that we remember only about 10% of what we read; 20%, if we hear it; %30, if we can see visuals related to what we're hearing; %50, if we watch someone do something while explaining it; but almost 90%, if we do the job ourselves – if only as a simulation. In other words, interactive multimedia – properly developed and properly implemented – could revolutionize education.”

In other words, guided tutoring and computer simulations, through studios or lab works, that are properly designed and implemented could rampantly change technological education. Computer-based simulation software can enable students and professionals to experiment interactively with the fundamental theories and to apply them using modern technologies, getting instant and reliable feedback. According to Gokhale [2], in situations where the objective of instruction is to learn the facts without application or transfer, method of instruction is not a significant factor. However, if the educational goal is for students to transfer and apply the knowledge to real-world problems, then simulation integration into the class structure is an effective learning strategy.

The conventional teacher-centered classroom denies the student the opportunity to be more self-directed, autonomous, enterprising and creative. The distance-learning archetype can be best described as a dynamic creative autonomous learning

environment. Advisable a virtual educational delivery system should be used to facilitate distance learning, rather than the age-old method of correspondence course curriculum. Such virtual delivery systems hold student autonomy and creativity as essential attributes.

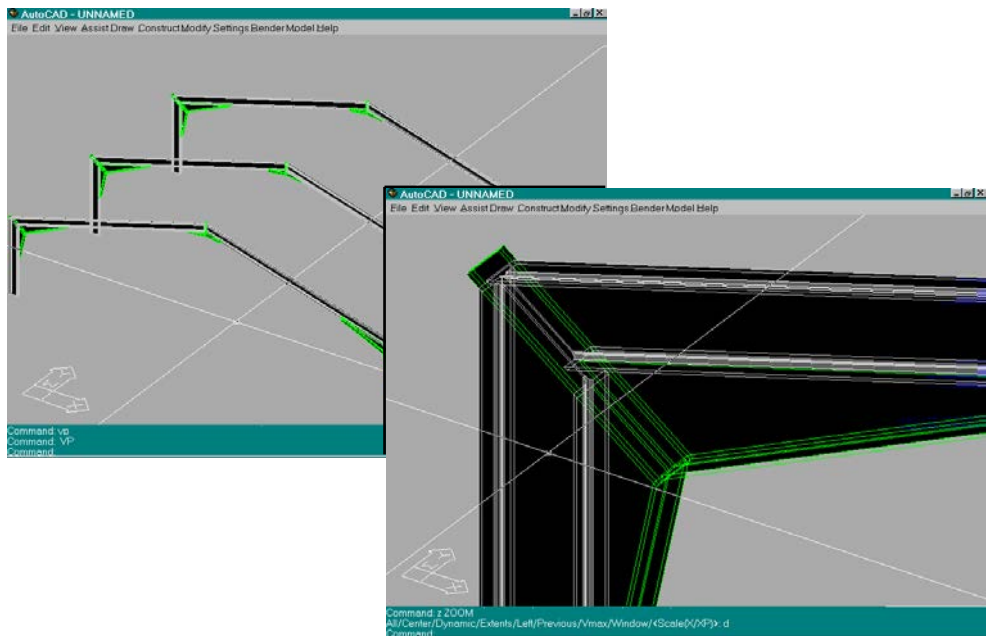


Figure 1. Virtual design in the classroom.

Structural design concept visualization whether in reinforced concrete, steel or wooden structure depends mostly on geometric and physical perception, and every educator should made efforts to enhance such abilities. This is a quite interesting challenge in an exciting area, requiring creativity and imagination as well as knowledge and systematic thinking. Although the classroom environment in Engineering and Construction Science is highly structured by the instructor, teaching students to be critical thinkers is also essential. The workplace is not always systematic and concise, real life postures are generally filled with ambiguous situations, so enterprise and exercise should be constantly developed even among practicing professionals.

4. DESIGN AND INFORMATION

Whilst design, as a conceptual process can be defined as the solving of ill-defined problems with multiple objectives and sub-optimal solutions, many AEC professionals still rely on other non-model means, sketching and using

metaphorical associations in order to develop understanding and knowledge of a design solution. Operationally, construction is a complex sequence of actions and responsibilities linked to the explicit communication of information. This process is derived from information resulting from both model and non-model means of knowledge-construction. Knowledge in turn is used to inform which models are made that adequately represents form, utility, behavior and relations amongst primary elements and functional parts or systems.

Many friends have asked me which software to use in order to achieve best results in architectural and structural design. Well-known software packages are usually not cheap and using them on racy systems can prove even too costly. Many people are thinking that a higher investment in equipment can enable working with fewer personnel or lower qualified staff in order to achieve a desired productivity.

In my experience, people can prove more important than technology. It is true, that using computers allows us to solve a greater amount of projects and details, but nevertheless it is true, that all of those should be properly mastered and checked. Without proper understanding of structural behavior and design results there is no guarantee for the output, just feeding computers with data can in no way be considered engineering. Evolving standards and implementing newer theories are just “cherry on the cake” beside technological changes in the development of design, presuming a constant training, learning and upskilling for competitiveness.

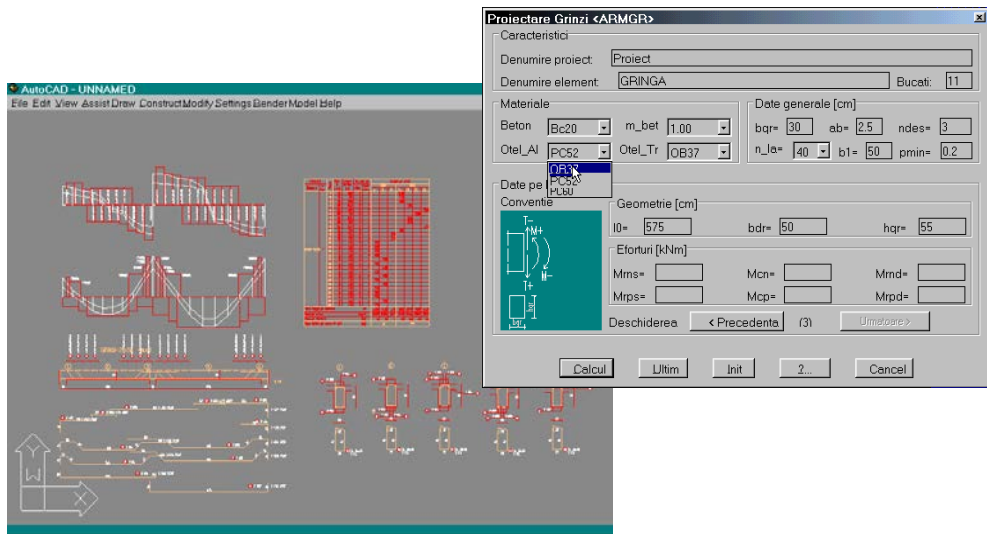


Figure 2. Reinforcement drawing generated through automated design in 1998 [1].

“With the technology and connections finally in place, we now face the truly difficult part of the virtual equation – the people element. Real groups are notoriously complicated. Anything that goes wrong face-to-face also goes wrong

online, only faster and less gracefully. Going virtual is for most people a wrenching experience, both in adapting to new technologies and in adopting new behaviors and working relationships... The steps that teams take to cope with their network nature – using collaborative technologies and designing flexible organizations – not only compensate for capabilities lost, but also establish the basis for extraordinary performance” [4].

5. AEC INFORMATION

The evolution of IT has brought numerous changes to the AEC industry. The predominant approach to design and the construction process as a whole has undergone a radical shift to a synthesis, overlapping professional expertise with technological advancements.

IT was regarded as the main source of information in the Industrial Economy. The predominant approach to handling information was through its manipulation, analysis and ultimate utilization. In the Knowledge Economy information goes through the evolutionary process of becoming knowledge. “When working in this distributed, networked environment, we evolve this new world and our lives become inextricably enmeshed in the survival of our nets with all intended and unintended consequences of its evolution” [3]. In this context, the biggest challenge becomes the effective utilization of this knowledge. Its impact on technology is profound and so powerful that it has fundamentally changed the way we act and live. The market dynamics and the realities of our entire industry impose additional challenges that need to be well managed, this is redounding upon education to. “Creating a competitive advantage and staying successfully in the race means working in environments replete with elements of unpredictability, increased tension and stress and a constant need to adapt” [3].

Electronic information systems are prevalent in many fields and increasingly accessible due to the outspread of web-based communication. Aside many national and professional organizations, several building and construction portals are offering product data catalogues, information about services and specific resources nowadays. In order to increase global and local market efficiency, there are more and more initiatives involved in the development of data modeling and communication standards, enfolding many construction activities, from individual conception and fabrication to cooperative e-building and e-commerce.

The advantages of electronic documents and data management systems over traditional ones mostly based on paper support, as well as the efficiency of electronic specifications over textual ones are already well known, but it’s still offering new business opportunities. Finding and retrieving information through the Internet is considered almost a common sense today. This is why among so

many information systems “AIC Info” (<http://www.aic.info.ro/>) succeeded to impose itself on the market, holding today a honorable fifth place in the traffic ranking statistics of Romanian science and technology sites according to the number of daily visitors (<http://www.trafic.ro/top/stiintatehnologie/pagina1.html>).

My colleague Dan Turda from the Technical University of Cluj-Napoca started the system in 1997, in a time when the Internet was considered a strange novelty in Romania. Due to my research interests in knowledge base systems at that time I joined his project, contributing to the transformation and development of it. The AIC Info system grants free access for browsing not just for students and professionals, but for anyone interested in AEC (Architecture, Engineering and Construction) resources, bearing a denotative editorial accent. The main goal behind its development is the wide dissemination of building and construction concepts, services and products available on the Romanian market, not just for pertinent and current information, but also for education and promotion. The system is intended also to be a virtual meeting place for students and alumni, professionals and tradesman, people interested in construction.

The screenshot shows the AIC Info website interface. The address bar displays <http://www.aic.info.ro>. The main content area is titled "Anunturi / cereri (ultimele)" and contains a table of recent posts:

Subiect	Raspunsuri	Citari	Autor	Data
➔D Avantajele / Dezavan...	(29)	(1959)	de Visitator	la 03. Mai
➔D Caut ARHITECT astept...	(0)	(12)	de Visitator	la 30. Apr
➔D demersuri pt. autori...	(3)	(127)	de Visitator	la 30. Apr
➔D casa in Delta Dunarii...	(38)	(1489)	de Visitator	la 30. Apr
➔D Ochi pe un proiect.....	(4)	(90)	de Visitator	la 29. Apr

Below the table is a link: [\[Anunta / cere aici \]](#). The main article, "Din nou ecologie", is dated April 30, 2005. It includes a photograph of a house interior and discusses the use of straw bales in construction. The article text is as follows:

Am avut o tema mai veche in legatura cu chirpicul, denumirea in limba romana a unui compozit primitiv. Daca ingredientele ar fi tratate corespunzator, chirpicul ar primi o denumire comerciala, sa-i spunem "Kyrpcech" - oare s-ar vinde?

A fost, mai demult, o emisiune TV in legatura cu balotii de paie folositi la constructia de case parter. Tot in SUA, probabil din cauza ca stau mai bine cu banii. Asa ca o cautare dupa subiect a dat rezultate interesante.

Rezultate interesante dar si foarte multe. De aceea o sa va lasam pe Dvs. sa descoperiti cat de mult se poate face cu o materie prima pe care o ardem cand este prea multa.

Sau pe care o lasam sa se deprecieze (i.e. sa putrezeasca), chiar daca Soarele a pompat caldura pentru a o dezvolta. Ne referim la fibrele celulozice, dar daca aveti rabdare, veti descoperi mult mai multe teme. Deci, daca subiectul constructiilor ecologice durabile va intereseaza, noi va recomandam ca punct de plecare <http://www.ecoact.org/>.

Fotografia ilustreaza interiorul unei case din California pe structura (osatura) din lemni iar peretii impluti cu baloti de paie. A fost preluata de la <http://www.one-world-design.com/>.

In rest, numai bine si Sarbatori fericite (si sa fiti cuminti!).

comentarii?

Other sections visible include "Biblioteca tehnica", "Colectivitati", "Login", "Ultimele situri adaugate", and "Cabina de vot".

Figure 3. AIC Info [7] on the Web.

Alternatively, aside structured up to day information about Romanian construction and building resources there is also a dictionary under development.

Upon the experience with AIC Info, we managed to develop several other electronic information systems, from product catalogues on CDs and web to rule-based decision systems.



Figure 4. Electronic information systems distributed on CDs.

6. CONCLUSIONS

Building and construction bears a very important role all over the globe, due to the creation of long term use objects which increasingly impinge upon every branch of human economy, social life, habitat as well as upon the surrounding nature. The interdisciplinary and multidisciplinary conspicuousness of construction activity presumes a waste knowledge through a dynamic perpetual updating process. Life has fully demonstrated that information signifies power, that documentation denotes the key to progress in every activity field.

Developing a continually high performing academic institution requires changes of many old habits, practices and thought patterns that people feel comfortable with.

Losing a safe and familiar situation and moving into strange and unknown environments might mean a possible loss of values that are currently meaningful to the institution. As change is an ongoing process, managers, teachers and students should get used to the attitude that things are never perfect and can be improved.

The evolution of IT, network-based computing and multimedia equipment established the background for the development of electronic information systems, virtual environments and the widespread of computer-based education. In order to capitalize the fruits of this new revolutionary transformation, we have to know the directions and forms of achievement, a very important role re-emerging to higher education. Academic institutions must have more time and resources to experiment, taking advantage while they are not at the mercy of the vendors' vision regarding how technology can or should be used.

As Michael Korda (Publisher and Author, 1919-1973) stated: "To succeed, it is necessary to accept the world as it is and then rise above it" [8].

References

1. Gobesz, F.Zs. *Contribuții la dezvoltarea sistemelor expert în domeniul construcțiilor*, Ph.D. Thesis, Technical University of Cluj-Napoca, 1999. (in Romanian)
2. Gokhale, A.A. Effectiveness of computer simulation for enhancing higher order thinking, *Journal of Industrial Teacher Education*, vol.33, no.4, (<http://scholar.lib.vt.edu/ejournals/JITE/v33n4/jite-v33n4.gokhale.html>), 1996.
3. Kiroff, L., Ostrowski, P. IT and E-Architecture – A technological breakthrough, a technology race or a new paradigm in business, *CIB-W78 International Conference. IT in Construction in Africa 2001*, CSIR, Division of Building and Construction Technology, Mpumalanga, South Africa (<http://buildnet.csir.co.za/constructafrica/authors/Papers/w78-017.pdf>), 2001.
4. Lipnack, J., Stamps, J. *Virtual Teams*, John Wiley & Sons Inc., USA, 2000.
5. Menn, D. Multimedia in Education: Arming Our Kids for the Future, *PC World*, No.11 (October), 1993.
6. <http://vanrees.org/research/>
7. <http://www.aic.info.ro/>
8. <http://www.brainyquote.com/quotes/quotes/m/michaelkor153486.html>
9. <http://www.m-w.com/>

Knowledge in construction, from the perspective of communication

Ferdinand-Zsongor Gobesz¹, Dan V. Turda¹

¹*Department of Structural Mechanics, Technical University of Cluj-Napoca, Cluj-Napoca, 400020,
Romania*

Summary

Some tendencies towards unified markets, due to the development of the European Union, had led inherently to initiatives in the field of construction too, in order to increase efficiency and cut losses. From this point of view, communication and modeling has a leading role.

There are significant differences between data structures offered by various Internet portals, also national languages and specific structural concepts are inducing difficulties in this area. Some joint European projects tried to surpass these obstacles, but their restrained resources let local initiatives to play a significant role, although not always in a clear context.

If at the beginning there were problems regarding the representation of various information items from the domain of construction (images: pictures/drawings/models/animations; text: descriptions/instructions/standards/Q&A; values: quantities/prices/deadlines etc.), later the priorities were shifted over the meaning (semantics) and security of data.

Back in 1977, the development and start of a computer-based informational system (“AIC info” – the first of its kind in Romania) was a pioneer task. Nowadays, the maintenance and continuous development of this system is made with respect to present tendencies regarding efficiency and technological evolution. At this time the system is functioning with a knowledge-base from which, upon the formulated queries, user pages are generated for viewing, based on existing web technologies using low-cost instruments with a very high degree of compatibility (in order to avoid as much as possible conflicts between different hardware and software platforms).

KEYWORDS: knowledge; modeling, construction; communication.

1. INTRODUCTION

Computers and networks are playing an increasing role in the field of AEC (Architecture, Engineering & Construction) and building industry. The number of

companies advertising through web pages, offering services, materials, technologies, even publishing product catalogues, is growing every day. Moreover, consumers are searching for information over the Internet, using so-called “portals”, commercial intermediaries that bring suppliers together and provide improved access to supplier information.

Though institutions and organizations that may provide lists of web addresses of suppliers and portals often support professionals in AEC, it is still quite difficult to find what is needed. From international point of view, significant differences in data structures, classifications, specifically industrial fragmentation (sometimes due to national characteristics and social traditions) are making hard to find and sell construction products and services over the national borders. Although there were some international (also European) initiatives addressing this issue, there is still need for a viable solution.

2. INFORMATION THROUGH THE WEB

One of the most impressive European initiatives was the development of XML applications for building and construction. XML (eXtended Mark-up Language) is very suitable to structure data, to create and handle taxonomies. Data processing, browsing, viewing can be done in many ways, almost independently from the source files, in accordance to the needs.

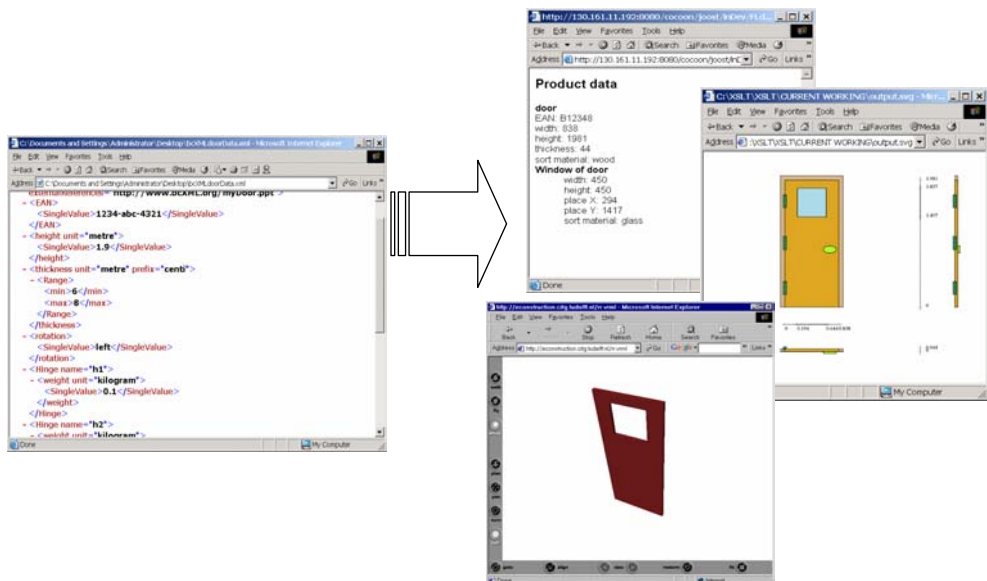


Figure 1. XML content visualization as HTML, 2D-SVG, 3D-VRM.

The source files are based on text, emphasizing rather semantics than syntax with a high degree of definition possibilities. As such, they are also a better alternative versus proprietary binary files, considering portability, handling and security against data corruption.

The development of bcXML (Building and Construction XML – <http://www.bcxml.net/>) based on the EU IST-10303 “eConstruct” initiative from 1999, was an important stepping stone in this direction beyond other international projects like aecXML (Architecture, Engineering and Construction XML – started by Bentley, <http://www.aecXML.org/>), gbXML (Green Building XML – developed by GeoPraxis, <http://www.geopraxis.com/>), LandXML (Land Development and Transportation XML, <http://www.landxml.org/>), eBIS_XML (Electronic Business Interchange Standard XML, <http://www.ebis-xml.net/>) etc. For data modeling the IFC (Industrial Foundation Classes) developed through IAI (International Alliance of Interoperability, <http://www.iai-international.org/>) offered a strong support [3].

“The goal of eConstruct (<http://www.econstruct.org/>) was to harness the possibilities of the Internet for the building industry, concentrating on the communication in the buying and selling phase. Conceptually, three things are needed for communication: a vocabulary, a grammar and a communication medium” [4]. As vocabulary of terms, taxonomy was used (with specialization hierarchy, property definitions and multilinguality) upon the ISO/DIS 12006-3 developments. The resulting grammar (data format) was bcXML and the communication medium was the Internet.

The moment “eConstruct” finished, another project called “E-cognos” (<http://www.e-cognos.org/>) started and took the development into the direction of knowledge management: “Harnessing the existing and available, but not well-findable, knowledge contained in documents and in people” [5]. In this project the term ontology was used instead of taxonomy, defining a formal way of describing the set of concepts used in a certain field, from a certain viewpoint.

The goal was to create multiple cooperating ontologies in order to provide multiple cooperative ways to access, find and classify information. As data format XML and RDF/OWL (Resource Description Framework/Ontology Web Language – an XML format for ontologies and ontology-based data) was used, and like in eConstruct, the Internet was the communication medium. The main innovation of this project was the proof of the possibility of superimposing ontological richness onto existing document management systems and databases. In terms of communication, ontologies and the information that uses them can be accessed and exchanged in the familiar open and standardized way using the Internet. “This semantic web allows you to make explicit statements and explicit links about (and in) Internet-accessible resources using ontologies as loosely-coupled, expandable vocabularies. This greatly enhances the semantic richness of Internet-based information exchange” [5].

Upon the achieved results, the authors made the following suggestions as best practice: using the internet as basic communication medium, XML (or the more specific RDF) is to be used as data format for information exchange, while definitions of terms, vocabularies, etc. should be stored in widely accessible ontologies. “This way, the terminology used is made explicit. Explicit is better than implicit” [5].

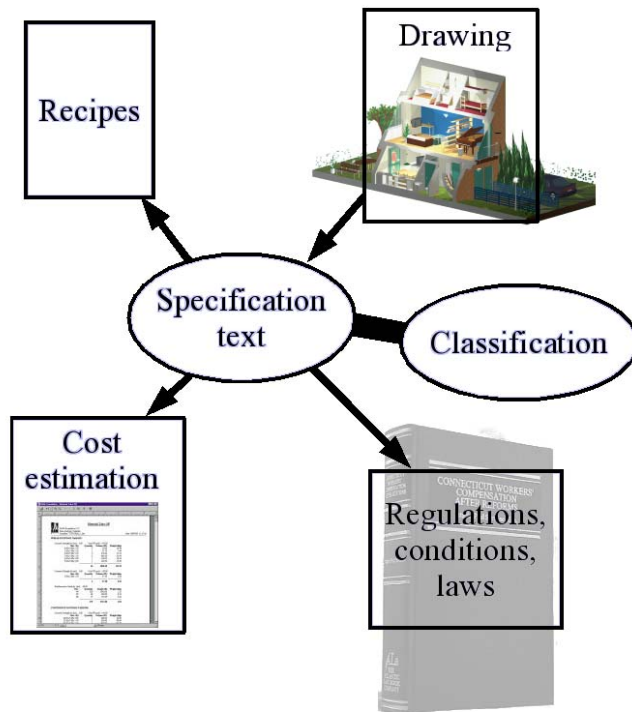


Figure 2. Specification text connected (Recipes and Cost estimation are just example applications), one reason more to become “eSpecs” through a semantic web [5].

Thus, the semantic web can provide the means by which the building specification can gain real semantic links to other documents and programs, and vice versa. The research showed that open source software is well suited to this kind of task. The semantic web helps building specifications to become “eSpecs” and to re-assert their role as a central building document.

Mainly, to be able to create and apply eSpecs, it is of course necessary to use the Internet as the communication medium. Secondly, the definitions of terms, vocabularies, etc. have to be made explicit in accessible ontologies. Multiple cooperating ontologies can form an ontology web. These ontologies and the data that uses them ideally should be communicated using XML and RDF/OWL over the Internet, creating thus a semantic web.

3. THE AIC INFO INFORMATION SYSTEM

Back in 1997, Dan Turda had the idea to make a first step by creating an electronic information system in Romania, available not just for AEC professionals but also for the public. He named it “AIC info” (<http://www.aic.info.ro/>) upon AEC (Architecture, Engineering and Construction) + information. It was, basically, an electronic catalogue of construction products and services, accessible through the Internet but published also on CDs (due to the lack of Internet connection for many users at that time). The main idea behind this project was the large dissemination of building and construction concepts, services and products, not just for accurate and efficient information, but also for education and promotion.

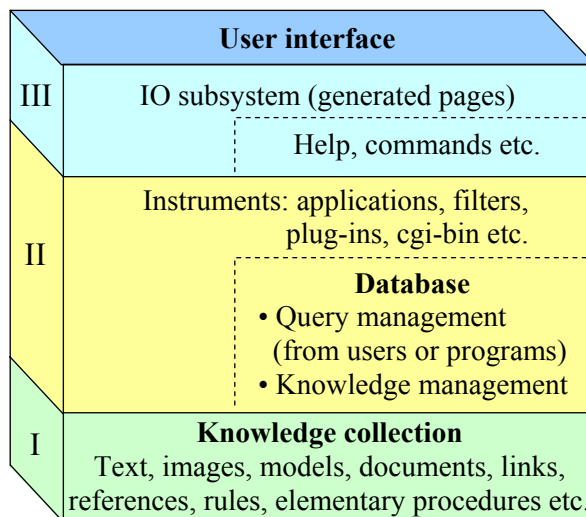


Figure 3. The initial layers of “AIC info” [2].

The available resources were classified considering the life cycle of a construction, from conception to demolition, also according to the instant and complexity of a product or technology. Normally, at the beginning, every new building object goes through conception, certification etc., so we named the first category “Services”. In the next category, we included the tools, devices, machinery etc. needed for building activities. The material part of a construction is already subordinated to the complexity level of entities, thus after “Raw and basic materials” the more compounded entities were grouped under “Building parts, units and assemblies”. Networks, plants, building equipment were divided in two categories: internal and external ones, such a differentiation being necessary also according to their importance and complexity. The most complex category was “Buildings” (integral constructions). According to the life cycle, the next category was “Repair and maintenance” while the last one “Demolition, recovery and recycling”.

The top view of this classification is illustrated by the following screen captures, as it was in past (Figure 4) and as it appears today (Figure 5), after some considerable evolution into a hierarchy.



Figure 4. The “AIC info” categories, as they were in 1999.

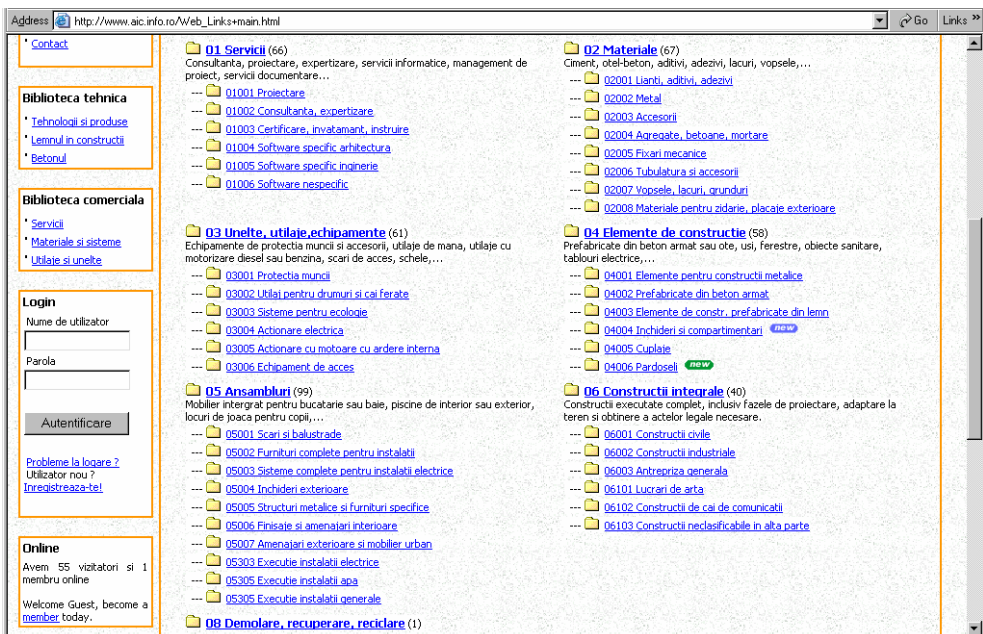


Figure 5. The top view of the hierarchy for building products and services.

The system was imagined from start as a knowledge base, considering that we had to deal with a lot of information and many data formats. The generated output is still in HTML (including frames, style-sheets and scripts), considering the prevalence and nearly compatibility of most browsers on various hardware and software platforms, and the processing speed. Due to that reason, the best-suited communication medium was and remains the increasingly accessible Internet.

The knowledge server is in fact a database server (Postgres, on Linux of course) and the meta-knowledge was formulated using mainly JavaScript and cgi (common gateway interface – a facility through which the Apache server launches local applications), exploiting most of the possibilities offered by HTML. The interrogation of the database goes through SQL, via PERL. The search is done by Postgres, the query being transmitted via psql (PostgreSQL) front-end. The search results are buffered and processed afterwards by a set of applications into a showy graphical arrangement. After a while, we started to use Apache ASP (Active Server Pages) which gave us the feasibility to separate the logic of the content from the logic of the visualization. Although we are still not using XML, the inclusion of CIFS (Common Internet File System) type referring and relational (ANSI SQL) ones offered us opening and scalability in the same time.

From editorial point of view, we are still using ANSI text editors, but we are considering to step toward LATEX because, besides typographical preprocessing, it offers replication possibilities in DVI, PS and PDF formats, aside HTML.



Figure 6. User interface of the “AIC info” dictionary.

4. CONCLUSIONS

The construction and building industry is undergoing significant changes due to the evolution of information technology, involving more and more intensive use of networked computers and communication devices. In this transition period from an “industrial economy” to a “knowledge economy”, knowledge plays an increasingly important role in all aspects of our lives.

In this evolutionary process, a very important role emerges for local initiatives in a global context. There are increasingly more possibilities for data structuring and information processing, thus leading to a more colorful world, but also towards economic and industrial fragmentation. Ultimately, beyond the market, our inventiveness and our way of handling resources will decide which way to go or follow.

The use of Internet as communication medium is almost innate nowadays, and businesses as much as people do need information, communication. Open source software and accessible technologies can be efficiently used in order to give forth and raise the quality of the web, enhancing the semantic richness of Internet-based information exchange.

References

1. Gobesz, F.Zs., Turda, D.V. AIC Info, *EPKO'99 – International Conference of Civil Engineering and Architecture (Odorheiu Secuiesc)*, Hungarian Technical Sciences Society of Transylvania (EMT), Cluj-Napoca, 1999. (in Hungarian)
2. Gobesz, F.Zs. *Contribuții la dezvoltarea sistemelor expert în domeniul construcțiilor*, Ph.D. Thesis, Technical University of Cluj-Napoca, 1999. (in Romanian)
3. Gobesz, F.Zs., Turda, D.V. bcXML kívülállónak, *EPKO 2004 – International Conference of Civil Engineering and Architecture (Șumuleu Ciuc)*, Hungarian Technical Sciences Society of Transylvania (EMT), Cluj-Napoca, 2004. (in Hungarian)
4. Tolman, F., Van Rees, R., Böhms, M. Building and Construction Extensible Mark-Up Language (bcXML): The C2B/B2C Scenario, *CIB-W78 International Conference. IT in Construction in Africa 2001*, (<http://buildnet.csir.co.za/constructafrica/authors/Papers/w78-067.pdf>) CSIR, Division of Building and Construction Technology, Mpumalanga, South Africa, 2001.
5. Van Rees, R., Tolman, F. Semantic Web Technologies Applied to Building Specifications, *Proceedings of the 2004 CIB w78 conference*, Section T6S7 Information technology in Construction, Toronto (Ontario), Canada, 2004.
6. <http://aic.info.ro/>
7. <http://vanrees.org/research/>

Passive control of semirigid steel structures

Pavel Alexa¹, Horatiu Mociran² and Aliz Mathe³

¹Faculty of Civ. Eng., Technical University, Cluj Napoca, 3400, Romania

²Faculty of Civ. Eng., Technical University, Cluj Napoca, 3400, Romania

³Faculty of Civ. Eng., Technical University, Cluj Napoca, 3400, Romania

Summary

The present contribution refers to the possibility and efficiency of applying passive control to the seismic behavior of steel skeletal structures with semirigid beam – column connections. The semirigidity is a way on its own to introduce a certain level of ductility into the steel structures of the frame type. Nevertheless, the semirigidity accounts for other beneficial effects during seismic action on this type of structures. The Northridge 1994 earthquake emphasized the difficult and, even, impossible technical approach to the rehabilitation of seismically damaged steel welded beam – column connections. It proved the advantage of using bolted (replacable) beam – column connections

The study presents in a comparative manner several sets of numerical results regarding the kinematic and static parameters that govern the seismic behaviour of steel frames. A six story one bay steel frame rigidly connected is considered in both situation: without base isolation and with base isolation. The same structure is, then, taken with semirigidly beam – column connections. The mechanical semirigid model of the beam - column connections are of the usual types: web angles, top and seat angles and top and seat and web angles. Also, several analytical bending moment – relative rotation $M - \theta_r$ have been considered. The semirigid connected structure is then analyzed in both situations, without base isolators and with base isolators. The analysis is of the time history type conducted in the elasto – plastic domain. The dead load is taken into the analysis when the accelerogram is applied. The parameters that are considered relevant for the seismic behaviour of the frames are: the natural periods of vibration, the acceleration and displacements induced into the top floor nodes, the lateral displacements variation, the base shear variation, the elasto – plastic mechanisms, (location and history of plastic hinges formation), the ductility levels.

The conclusions inferred from the numerical results are focused on the role of the passive seismic control via base isolators. The base isolators used into the analysis are of the elastomeric type chosen from FIP INDUSTRIALE catalog.

Keywords: steel frames, semirigidity, passive control, base isolators, time history analysis, elasto – plastic mechanism, ductility.

1. INTRODUCTION

Since Northridge 1994 earthquake, the semirigid connectivity of steel skeletal structures has been more and more focused on, as an instrument of avoiding seismic induced damages into welded beam – column connections and, in the same time, as a more economical way of dealing with the the post - seism rehabilitaion of these vulnerable zones of steel frame type structures.

By their locations and their ultimate bending moment capacities, the semirigid connections offer, also, up to a certain extent, the possibility of controlling the seismic behaviour of steel frames by directing the plastic hinges to the beam connecting cross sections as the most seismic codes require [1].

Nevertheless, the semirigidity of beam – column connections can not be “lowered” very much as it will trigger a lowering of the global structural capacity. The bending moment capacity of a semirigid connection should be lower, but comparable to the bending moment capacity of the connected beam, otherwise, the columns and the middle – span zone of the beams will be overloaded. This is why the semirigidity only offers a limited level of seismic behaviour control, though, it does not lose its advantage of an easy post – seism intervention on possible damaged connecting zones.

By selecting the ultimate bending capacity of the beam – column semirigid connecting section, the control of the seismic behaviour can, also, be approached and dealt with from another point of view: that of ductility (at the global, joint, sectional levels) [2], [3], [4]. The ductility is becoming the today commandment besides the classical requirements of strength and stiffness a structure has to provide. The quasi – general recognition of seismic performances of steel skeletal structures comes from the fulfilment of the ductility demands by these structures. The ductility is revealed by the capacity of the structure to dissipate the kinetic energy induced into the structure during seismic action. The ductility demands can be satisfactory provided for by a moment resisting (rigidly connected) steel structure via directing the plastic hinges (the energy absorbing zones) to the end sections of the beams. This control approach can be achieved either by providing sufficient strength for the beam – column connection so that the plasticity is developed in the beam section or by directing the plasticity to the connecting elements (connecting the beam to the column) that has to be able to absorb and dissipate kinetic energy and ensure rotational capacity during the seismic cyclic loading. Whatever the approach is used, the role of the connecting zones in the global seismic behaviour of steel skeletal structures is highly important.

The status of the semirigid connectivity evolved from that of unavoidable structural imperfection to that of a recommended connection equal to the two classical categories of rigid and pinned connectivity [5]. Now this third (semirigid) category of connectivity proves to be more than a connecting type: it is an efficient way of

controlling the overall structural behaviour, of avoiding overstrengthening of beam – column welded connections and making possible the post - seism rehabilitation of damaged connecting zones.

In the context of rapid development of other technologies of controlling the seismic behaviour of skeletal structures, mainly through seismic base isolation, it could be of relevance to study the behaviour of base isolated semirigidly connected steel structures. A comparative study is able to provide relevant conclusions regarding the fulfilment of design requirements by these structures and the level of their seismic performances.

The passive control of structural behaviour via base isolation is increasingly used in seismic protection of new and existing buildings. Combining the seismically efficient technology of base isolation with technically affordable semirigid connectivity could lead to an higher seismic performances of steel skeletal structures.

The present contribution is dealing with numerical studies carried out on base isolated semirigid steel frames under cyclic (time history) loading in the presence of associated gravitational loads. The studies consist of geometrical nonlinear analyses in elasto – plastic domain taking into account the P - Δ effects. The presented results refer to a six story one bay planar steel frame considered in four “equipping” situations:

- * Rigid connectivity, no base isolation;
- * Rigid connectivity and base isolation;
- * Semirigid connectivity, no base isolation;
- * Semirigid connectivity and base isolation.

2. THE STRUCTURE, CONNECTIONS, LOADS, BASE ISOLATORS

The geometry, the mechanical properties of the structural elements the loadings, the locations of rigid and semirigid beam – column connections, the location of possible plastic hinges and the base isolation system are presented for each of the above four study cases.

The theoretical geometrical axes of beam – column connections in both cases, rigid and semirigid, is considered as tangent to the column interior flange and not adjacent to the column geometrical axis. The locations of plastic hinges are: beam – column connections, the middle sections of the beams and both ends of the columns.

The base isolators have been chosen from FIP INDUSTRIALE catalog [6] such as to satisfy the vertical reactions requirements.

2.1 The structure

Subchapter title uses “Subchapter” style, Times New Roman font, 11 points, line space single, alignment left, italic, 12 points before and 6 points after.

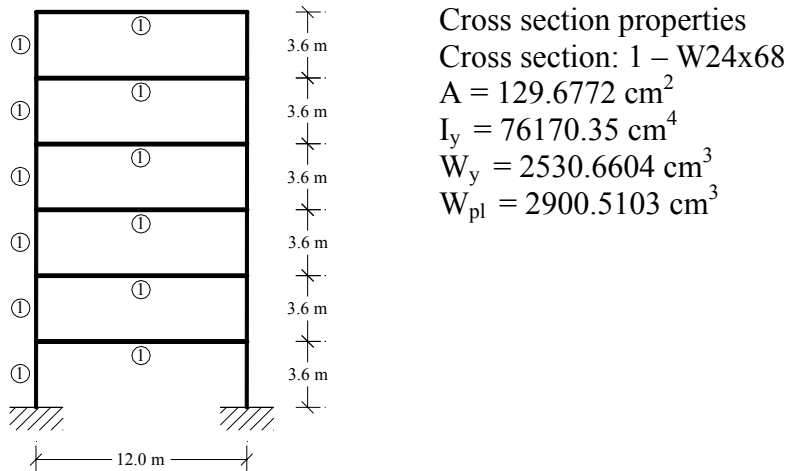


Figure 1. General geometry

2.2 The connections

Tables should be numbered and centered written with Times New Roman font, 10 points, without vertical lines (if possible). Use the next example (“Table Simple 1” in Word).

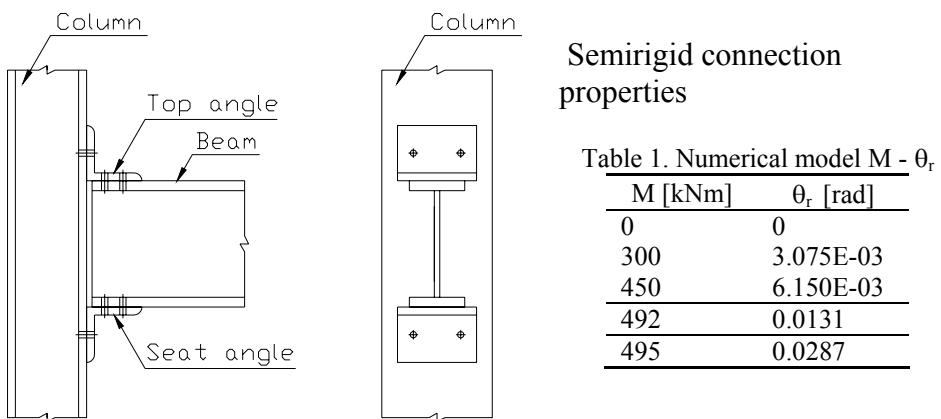


Figure 2. Semirigid beam – column connection

2.3 The loads

Tables should be numbered and centered written with Times New Roman font, 10 points, without vertical lines

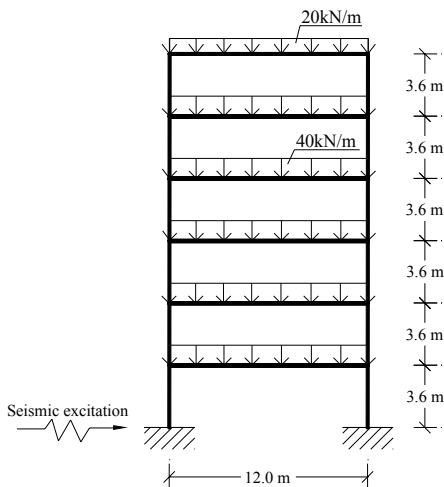


Figure 3. Loading

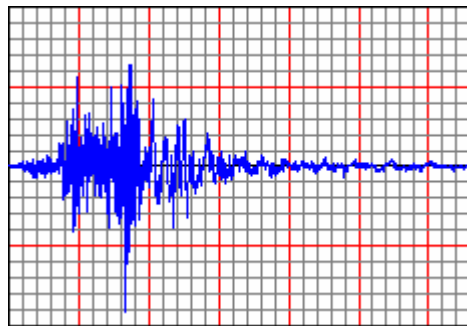
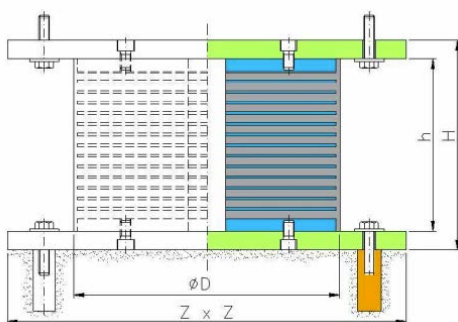


Figure 4. Santa Monica accelerogram

2.4 The base isolators

Use the “Table name” style (Times New Roman font, 10 points, centered, 12 points before, 6 points after).



SI – S 500/54 base isolator
 Mechanical properties
 Vertical load $V = 1660.0 \text{ kN}$
 Horizontal stiffness $k_e = 2.01 \text{ kN/mm}$
 Geometrical characteristics
 $D = 600 \text{ mm}$; $t_e = 56 \text{ mm}$;
 $H = 164 \text{ mm}$; $h = 114 \text{ mm}$;
 $Z = 650 \text{ mm}$

Figure 5. FIP INDUSTRIALE base isolator

The isolators are of elastomeric type and have been chosen from FIP INDUSTRIALE catalog according to the vertical reactions requirements [6].

3. NUMERICAL RESULTS

3.1 Case 1. Non-isolated rigid structure

Plastic hinges form only at beams ends and column bottoms (Fig.6), while top lateral displacement (Fig.7) reaches 13.63 cm.

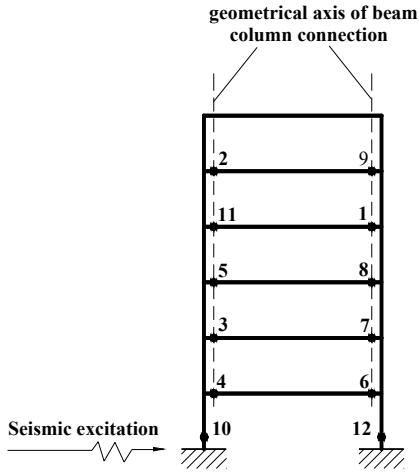


Figure 6. Plastic hinge formation

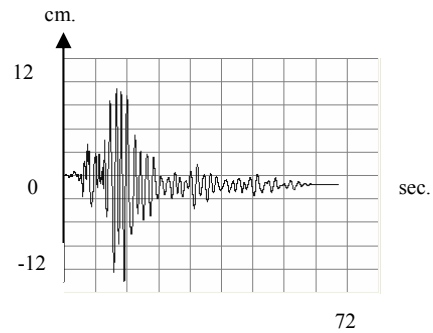


Figure 7. Top lateral displacement

3.2 Case 2. Isolated rigid structure

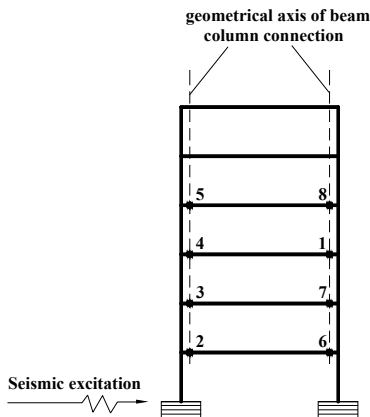


Figure 8. Plastic hinge formation

Smaller number of hinges (Fig.8) and larger displacements (Fig.9) appear.

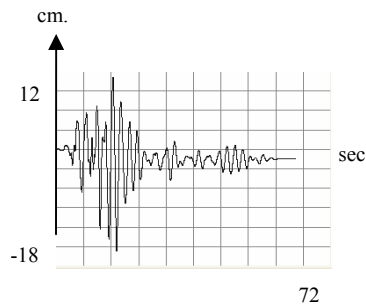


Figure 9. Top lateral displacement

3.3 Case 3. Non-isolated semirigid structure

Semirigidity lead to middle span plastic hinges formation (Fig.10) and smaller lateral displacements (Fig.11).

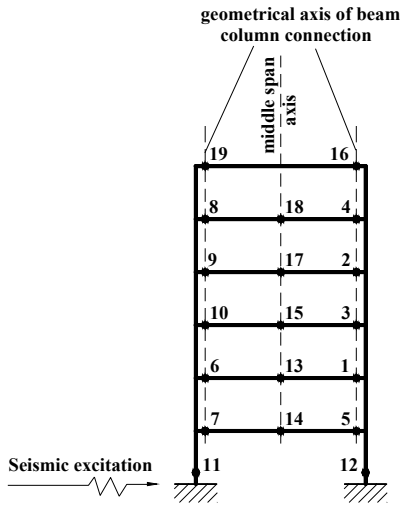


Figure 11. Top lateral displacement

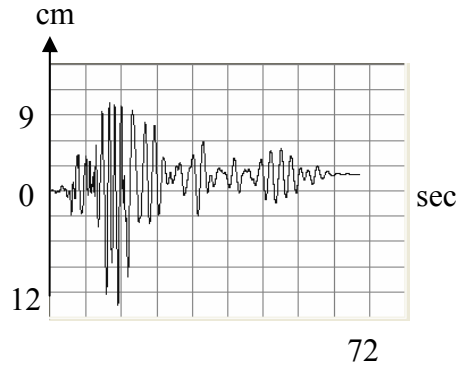


Figure 10. Plastic hinge formation

3.4 Case 4. Isolated semirigid structure

Plastic hinges, appear, exclusively, in the semirigid beam column connection (Fig.12), while top lateral displacement reaches 21.03 cm (Fig. 13).

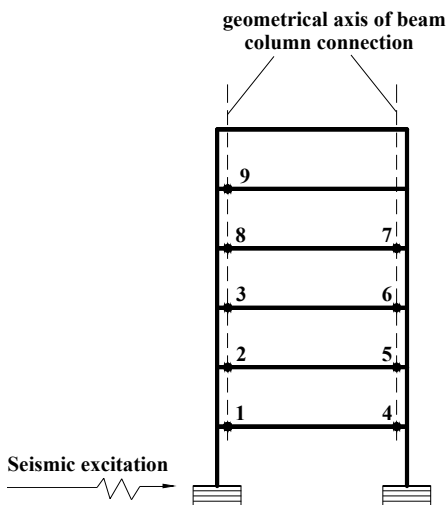


Figure 12. Plastic hinge formation

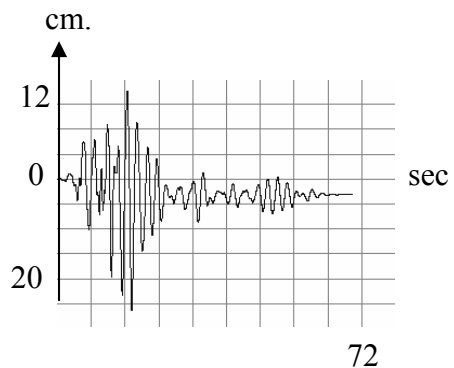


Figure 13. Top lateral displacement

4. CONCLUSIONS

The above numerical results – presented for the six story one bay frame – can not be generalized. Nevertheless, the associated results are in line with other numerical results obtained from other case studies. The main aspect that can be emphasized is the beneficial effect of base isolators in all cases. This is – in fact – the general expectation. Whatever comparison is inferred from the numerical results, it has to be mentioned that the ultimate bending capacity of the semirigid connection is about 80% of the bending capacity of the connected beam. A reduction of 20% in the bending capacity of the connecting section proves to be too much, since the semirigid structure (Case 3 – Non-isolated semirigid structure) leads to the formation of plastic hinges in the middle span sections of the beams (Fig. 10). This fact has to be viewed correctly: the semirigid connecting sections are placed in the immediate vicinity of the column flange (not in the vicinity of the column axis). This real model leads to a “delay” in the loading of the semirigid connections due to smaller values of the (bending) moments at column flanges.

Another feature of the non-isolated semirigid structure (Fig. 10) versus the non-isolated rigid case (Fig. 6) is the higher number of plastic hinges (19 versus 12) developed over approximately the same duration – about 16 seconds) which leads to a higher quantity of dissipated (through plastic hinges) of induced kinetic energy.

The two cases of base isolated structures (Case 2 and, respectively, Case 4) emphasize the higher benefit obtained in the case of isolating semirigid structure than in the case of rigid structure: no plastic hinges in the middle span sections of the beams. This benefit has to be assessed together that obtained from the possibility of post – seism rehabilitation.

References

1. Gioncu, V. Influence of strain – rate on the behaviour of steel members, *Proceedings of the 3rd International Conference STESSA 2000*, A. A. Balkema, Rotterdam, 2000, pp. 19 – 26.
2. De Martino, A. State of the art report on the basic problems of seismic behaviour of steel structures: General Report, *Behaviour of Steel Structures in Seismic Areas*, Aug. 1997, Kyoto, Edizioni 10/17, 1997, pp. 3-20.
3. Akiyama, H. An overview of global ductility, *Proceedings of the International Workshop STESSA, Timisoara, 1994*, E & FN Spon, London, 1995, pp. 519 - 534.
4. Alexa, P. et al. Ductility via semirigidity, *Proceedings of the 9th Conference on Metal Structures, Timisoara 200*, edited by M. Ivan, Orizonturi Universitare, Timisoara 2000, pp. 361 – 366.
5. Georgescu, D. *Semirigidity: General report*, *Proceedings of the International Workshop STESSA, Timisoara, 1994*, E & FN Spon, London, 1995, pp. 519 - 534.
6. www.fip-group.it/

Python is a C++ made easy for Civil Engineers

Dan V. Turda¹, F.-Zsongor Gobesz²

¹Ph.D., Chair of Structural Mechanics, Technical University of Cluj, Cluj-Napoca, 400020, Romania

²Ph.D., Chair of Structural Mechanics, Technical University of Cluj, Cluj-Napoca, 400020, Romania

Summary

There is an issue on the teaching of the programming, when non-programmers are the subject. It is, in our opinion, the "appeal to programming" which should be the "corner stone" a teacher should find.

Python is a very modern programming language, interpreted, very fast, built as a C++ wrapper having a Pascal-like syntax. When it is used with specific libraries, like wxPython, SciPy or vtkPython, it becomes a very powerful tool in developing even professional engineering applications.

Not only there is the ease of programming, but also it transforms programming in a pleasure. Moreover, py2exe can transform any interpreted Python code in a MS-Windows .exe, by translating in C++ code and doing native compilation. We like FORTRAN, but we really love Python. Here is our motivation, along with examples.

KEYWORDS: teaching, programming, Civil Engineering, Python, C++.

1. INTRODUCTION

Civil Engineers are often put in situations when hand-calculus is too complicated, even if a pocket calculator would be available. From on-site situations up to designing in short term, making its own program could solve the problem.

While we recognize the tradition of *FORTRAN*, we have to advocate our conviction that we are talking about a *lost tradition*. The original *FORTRAN* was conceived under the concept of "*structure of procedures*". It was added a support for "*structure of data*", but the separation between data and statements was rigorously respected. One can remark the position of *COMMON* or *EQUIVALENT* blocks in a *FORTRAN* program.

We have to remark that at the time when *FORTRAN* was *the only* scientific programming language, a compiler had to fight hard restrictions. Beyond the processor's speed, it was the amount of *RAM (Random Access Memory)* available for a program. Some of us remember how the passing from *FELIX-256* to *FELIX-1024* was seen as a "*big step forward*". Yes, upgrading from 256kb of *RAM* to 1Mb *RAM* was an important step. We do not realize now, when a single no-name *PC* can have 512Mb, how our "*ancestors*" could solve heavy problems. *FORTRAN* was the answer of the time. However, this language remains the fastest under any comparisons and uses the smallest memory spot.

While recognizing the merits of *the old FORTRAN (up to FORTRAN77)*, we have the right to state that the new versions of *FORTRAN (from FORTRAN90)* denaturizes the principles of the original concept. One cannot say that *a new language is born*, and that *should have another name! We have no more FORTRAN*. We get compilers with a paid license for which the learning curve is very long.

The learning process excludes block-diagrams as the starting point in teaching *Logic Mathematics* and *Boolean Algebra*. This exclusion make many students to put an innocent question: "*What for we have to learn that?*". And this question is an ultimate one for a teacher.

2. OBJECTS

2.1 *The object paradigm*

With the advent of modern computers, including network facilities, there is no more need of such data and statement structures as in the original *FORTRAN*. Data

and statements are contained (*encapsulated*) in *objects*. As a result an object can be *created* or *deleted*, but the gain is that an object can *communicate* inside the program (or outside of it) as the object includes statements. It appeared also the *Application Interface Programming (API)* concept, which allows a programmer to address or to link to objects already compiled and tested.

The advent of *objects* is surely not the final point in the evolution of computer programming, but it was a major "*step forward*". From *a list of hierarchical structures of data and statements*, as in FORTRAN, the new techniques approach an *n-dimensional graph*. It is not a philosophy here; it is just about changing a point of view. With care for the inheritance, we have to mention that *Python* can inherit *FORTRAN* programs or libraries.

Guido van Rossum has had a marvelous idea to make a C++ wrapper using a *Pascal-like* syntax. Using *strong-typed* **and** *objectual* approaches, he wrote a new language. This new language got the name *Python*, as *Guido* like very much the *Monty Python* film series. The intention, from the very start, was to make a language very easy to learn, very powerful, and to be in the position to declare: *Do you see how easy is to program a computer?* And he had a great success. He was hired at the main education center in the United States.

2.2 About the Graphical User Interface (GUI)

The evolution of the personal computers, but also of other devices like the mobile phones is going in (at least) two directions, namely computation power and a mix of text and image information.

We, as teachers, know that an image could "worth a thousand of words". We know that, because any time when it is necessary, we drop a sketch on the blackboard. However, we are not still able to make dynamic representations. Moreover, once the blackboard is wiped, we are not able to make back comparison, unless we redraw the sketch.

From now on, we will call *FORTRAN* as any version up to *FORTRAN77*. *FORTRAN* is not able to carry *GUI* programming or to have access at *XML* parsing, as examples. Graphics are necessary but they are not taught. Our proposal was to use *FORTRAN* for heavy computation (*it is unbeatable!*) and to use *Python* for *GUI* programming and for small computation (*it is unbeatable!*). As *Python* can wrap *FORTRAN*, we could get a *swiss tool* instead a *single* one.

2.3 What we did

We created an experimental tool for teaching some matters in *Python*. We gave the name *aicSimpleSol* to the program, and there is a free download, use and distribution at <http://www.aic.info.ro/> in the "Software" section.

It consists of a main panel which contains a tree, from any particular application can be launched (Figure 1).

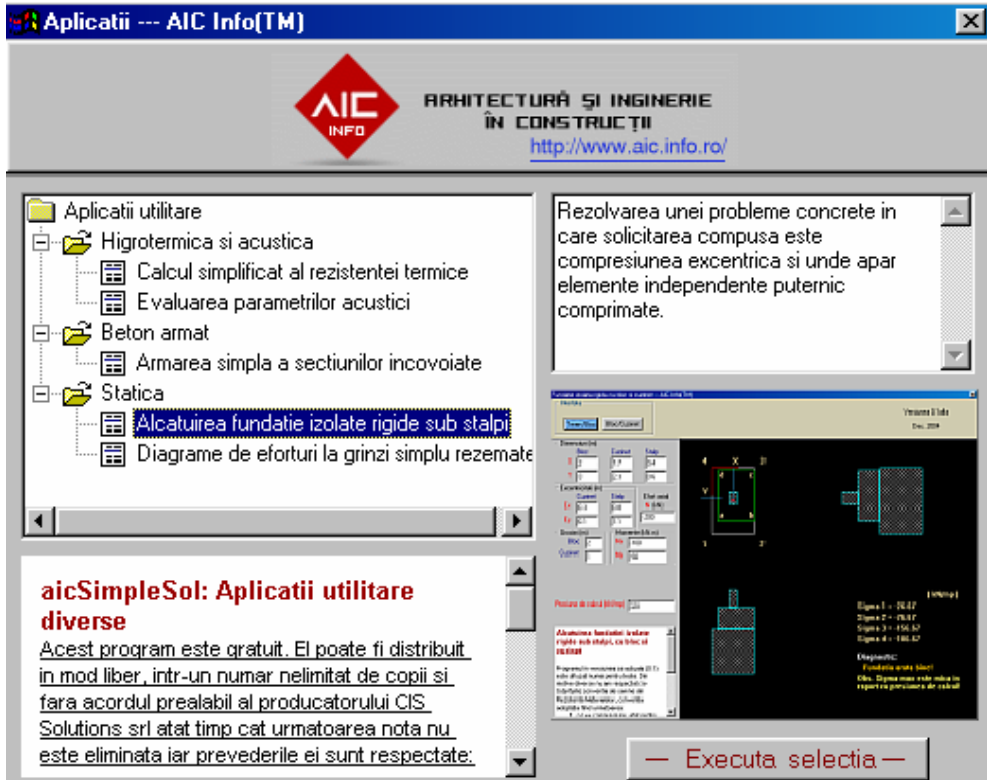


Figure 1. *aicSimpleSol*'s main panel

Once launched, each new window has three areas, namely the data area, the graphic area and the help area. The help area use a *wxPython* widget which allowed us to right the help text in HTML format (Figure 2).

There is an important feature we had in mind when we designed the program, and that is the link between data and graphics. That is, any time data change, the graphic window is updated. At this time, the graphics window is insensitive, i.e. no data can be changed using pointing devices (e.g. the mouse). It is not a disadvantage, as we have to focus on data, and to give the mean to see how a change in data affects the stress distribution, as an example.

The entire task was possible by using *PYTHON* in combination with *wxPython* and *Boa Constructor*. *wxPython* stands for a port of *wxWidgets* to Python, i.e. the implementation of windows, buttons, scrollbars, etc., as elements of a *GUI*, for their direct use under *PYTHON*. *Boa Constructor* is a powerful tool for editing *PYTHON* files and arranges *GUI* elements on a frame.

So, we did a mix. It is the programming, on one hand, and elements of Civil Engineering disciplines, on the other. Using a laptop and a big screen projector we can now better explain the matter issues. But this is a point of view. Seeing the fact from another point of view, we succeeded in new concepts and language appraisals. We know now how to integrate a perfect heavy computation tool (*FORTRAN*) with a *GUI*, with network facilities, with database server access, and with *XML* facilities, all platform independent.

After all these gains, we put ourselves, rhetorically, a single question: Why not developing ourselves the tools we need for teaching, just by teaching new programming languages and not a single one?

For anyone curious about how a *PYTHON* script is looking, we give in Figure 3 a fragment of the code for the application shown in Figure 2. One can observe that the syntax is close to the *C* and *C++* programming languages, even if it has a very interesting particularity: *the white space is important*. That means that the programmer is obliged to take care of the source layout, as the statements that are more in-depth are subordinated to the one which is less nested. One can observe how an *if* statement is looking like, in the Figure 3.

We underline that all the tools we used are free of charge, and can be downloaded from *INTERNET*. This aspect is very important in teaching, as most of the students have computers at home, or have access to a colleague's one. This mean that we had been used commercial software, the students could do their homework using only commercial software. As most of them do not have enough financial support, we would encourage them to use pirated software. But our mission is to teach for the good behaviour, not for a bad one. Or this is not a part of our mission?

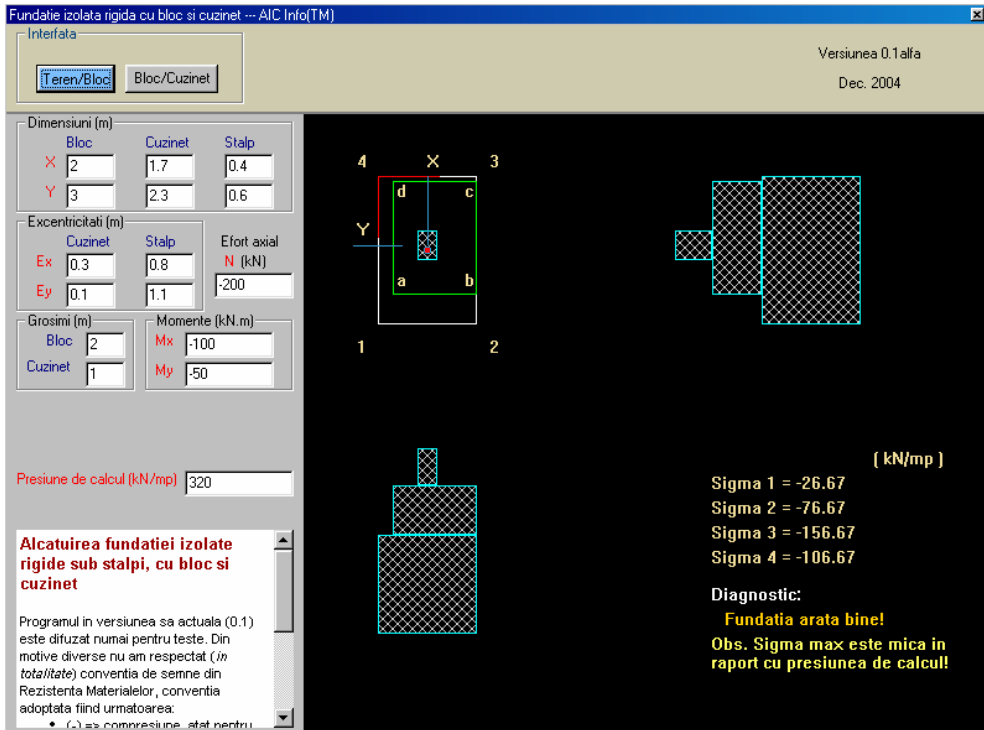


Figure 2. A launched application.

3. CONCLUSIONS

The teaching process is a very complex one. The modern technology offers a wide range of tools, and we should learn how to use them. We should do so, because the technological advance is very fast, and there remain only two years or so until Romania will be part of the European Union. And from than on, will not be a surprise to hear phrases as "Learning in another EU country is better than in Romania, even if it is a bit more expensive". For that we are preparing!

```

dc0.DrawText("Sigma 1 = "+str(s1),369,290)
dc0.DrawText("Sigma 2 = "+str(s2),369,310)
dc0.DrawText("Sigma 3 = "+str(s3),369,330)
dc0.DrawText("Sigma 4 = "+str(s4),369,350)
dc0.SetTextForeground("#ffffff")
dc0.DrawText("Diagnostic:",369,380)
dc0.SetTextForeground("#ff0000")
if abs(s1) > abs(PC) or abs(s3) > abs(PC):
    dc0.DrawText("Presiunea suportata de", 380,400)
    dc0.DrawText("teren este depasita!", 380,415)
    return
if s3 > 0 or s1 > 0 or s4 > 0 or s2 > 0:
    dc0.DrawText("Presiune pozitiva (intindere)", 380,400)
    dc0.DrawText("la baza fundatiei!", 380,415)
    return
dc0.SetTextForeground("#ffcc00")
dc0.DrawText("Fundatia arata bine!",380,400)

```

Figure 3. Code fragment in *PYTHON*

References

1. PYTHON, <http://www.python.org/>.
2. wxWidgets, <http://www.wxwindows.org/>.
3. Boa Constructor, <http://www.boa.sourceforge.net/>.

Computer program for nonlinear inelastic analysis of 3D RC building frameworks

Cosmin G. Chiorean¹

¹Faculty of Civil Engineering, Technical University of Cluj-Napoca, Cluj-Napoca, 400020, Romania

Summary

This paper presents an efficient computer-based analysis method for practical advanced analysis of three-dimensional reinforced concrete frameworks. The proposed formulation is intended to model the geometrically nonlinear inelastic behavior of RC frame elements using only one element per member. The behaviour model accounts for material inelasticity due to combined bi-axial bending and axial force, and provides the ability to monitor progressive plastification across the cross-sections of frame elements and structural system under increasing intensity of external loads.

Using an updated Lagrangian formulation (UL) the nonlinear geometrical effects are considered updating the element forces and geometry configurations at each load increment. The natural deformation approach (NDA) in conjunction with the geometrical “rigid body qualified” stiffness matrix is adopted for the element force recovery and the web plane vector approach is effectively used to update the frame element coordinates.

The analytical method described in this paper can be used to analyze 3D frameworks with or without a rigid floor diaphragm. The multi-freedom constraints, required by the rigid body floor model, are imposed by augmenting the finite element model with the penalty elements.

The proposed nonlinear analysis formulation has been implemented in a general - nonlinear static purpose computer program NEFCAD. A computational example is given to validate the effectiveness of the proposed method and the reliability of the code.

KEYWORDS: nonlinear analysis; three-dimensional RC frames; large deflections; spread of plasticity; rigid body diaphragm.

1. INTRODUCTION

In recent years, have witnessed significant advances in nonlinear inelastic analysis methods for steel and reinforced concrete framed structures [5,6,7]. There currently exist several methods and computer programs concerning the nonlinear inelastic

analysis that calculate strength limit states of reinforced concrete frame structures. At one extreme, two- and three- dimensional finite elements, enhanced with advanced material constitutive laws [7] were used to investigate the nonlinear response of RC frame members. At the other extreme, the *line elements* approach, in conjunction with either distributed or concentrated plasticity models, have been devoted to the development of nonlinear analysis tools for frames that provide a desirable balance between accuracy and efficiency [5,6]. In spite of the availability of such FEM algorithms and powerful computer programs, the nonlinear inelastic analysis of real large-scale frame structures still poses huge demands on the most powerful of available computers and still represents unpractical tasks to most designers. Currently the available tools for such analysis are research programs lacking convenient user-interfaces, or are general purpose FE programs that require very fine-grained modeling that is often impractical to the structural engineer. The approach presented in this paper is intended to overcome these inconveniences and represents an efficient computer method for large displacement elasto-plastic analysis of 3D-RC frames fulfilling the practical and advanced analysis requirements. Essentially, advanced analysis proposed herein uses the accuracy of the *fiber elements* approach for inelastic frame analysis and address its efficiency and modeling shortcomings both to element level, through the use of only one element to model each physical member of the frame, and to cross-sectional level through the use of path integral approach to numerical integration of the concrete in compression. The proposed nonlinear analysis formulation has been implemented in a general-nonlinear static purpose computer program NEFCAD-3D. The analytical method described in this paper can be used to analyze 3D frameworks with or without a rigid floor diaphragm. A computational example is given to validate the effectiveness of the proposed method and the reliability of the code.

2. FORMULATION

In this paper the following assumptions are adopted in the formulation of analytical model: (1) plane section remain plane after flexural deformation; (2) full strain compatibility exists between concrete and steel reinforcement; (3) reinforcement steel bars cannot buckle under compression; (4) mechanical properties of concrete may vary according to confinement levels. The first two assumptions allow the formulation details to be considered on two distinct levels, namely, the cross-sectional level and the member longitudinal axis level. In this way, the nonlinear response of a beam-column element can be computed as a weighted sum of the response of a discrete number of cross-sections. Gradual plastification through the cross-section subjected to combined action of axial force and biaxial bending moments is described through basic equilibrium, compatibility and material nonlinear constitutive equations of concrete and reinforcement steel in any section

by an iterative process. In this way, the arbitrary cross-sectional shape and reinforcement layout, the effect of concrete tensile cracking, the nonlinear compressive response of concrete with different levels of confinement are accurately included in the analysis.

2.1 Cross-section analysis

Consider the cross-section subjected to the action of the external bending moments about each global axes and axial force as shown in Fig. 1. Under the above assumptions the resultant strain distribution corresponding to the curvatures about global axes $\Phi = [\Phi_z \ \Phi_y]$ and the axial compressive strain u can be expressed in point $\mathbf{r} = [z \ y]$ in a linear form as:

$$\varepsilon = u + \Phi_z y + \Phi_y z = u + \Phi \mathbf{r}^T \quad (1)$$

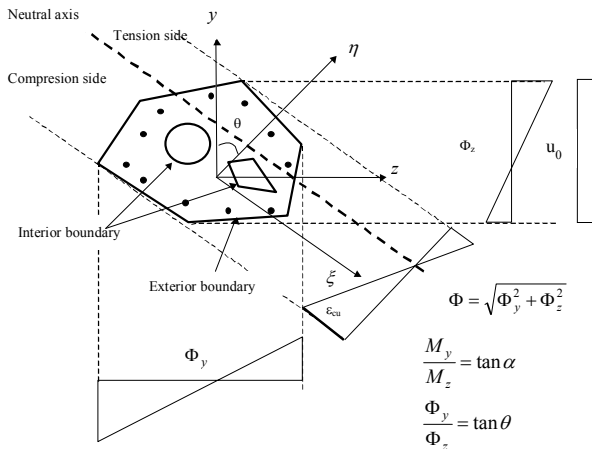


Fig.1. Cross-section analysis

Equilibrium is satisfied when the external forces are equal to the internal forces. The basic equations of equilibrium for the axial load N and the biaxial bending moments $M_{z,ext}$, $M_{y,ext}$ are given in terms of the stress resultants as:

$$\int_A \sigma(\varepsilon_0, \Phi_y, \Phi_z) \cdot \begin{bmatrix} 1 \\ \mathbf{r}^T \end{bmatrix} dA - \mathbf{S}_{ext}^T = 0 \quad (2)$$

where the vector $\mathbf{S}_{ext} = [N \ M_{y,ext} \ M_{z,ext}]$. The Eqs. (2) are solved numerically using the Newton-Raphson method, and results in three recurrence relationships to obtain the unknowns u and Φ and then flexural EI and axial EA rigidity modulus

can be computed [2]. A particularly important feature of the present method is based on Green’s integration formula according to which the domain integrals appearing in the evaluation of internal resultant efforts and tangent stiffness matrix coefficients of the section can be evaluated in terms of boundary integral [2]. Then the boundary integrals can be evaluated numerically using the Gauss-Lobatto integration rule.

This approach is extremely rapid because stress integrals need only be evaluated at a small number of points on the section boundary. In addition rapid convergence is assured by the inclusion of exactly determined tangent stiffnesses and, of great importance, it is assure convergence for any load case [2]. In this way, the states of strain, stress and yield stress are monitored explicitly during each step of the analysis and the arbitrary cross-sectional shape and reinforcement layout, the effect of concrete tensile cracking, the nonlinear compressive response and strain softening of concrete in compression with different levels of confinement, are accurately included in the analysis.

2.2 Elasto-plastic tangent stiffness matrix

Flexibility-based method is used to formulate the distributed plasticity model of a 3D frame element (12 DOF) under the above assumptions. An element is represented by several cross sections (i.e. stations) that are located at the numerical integration scheme points (Fig.2). The bending moments in these stations are computed through a second order transfer matrix as functions of the nodal element forces following a detailed procedure given in [1].

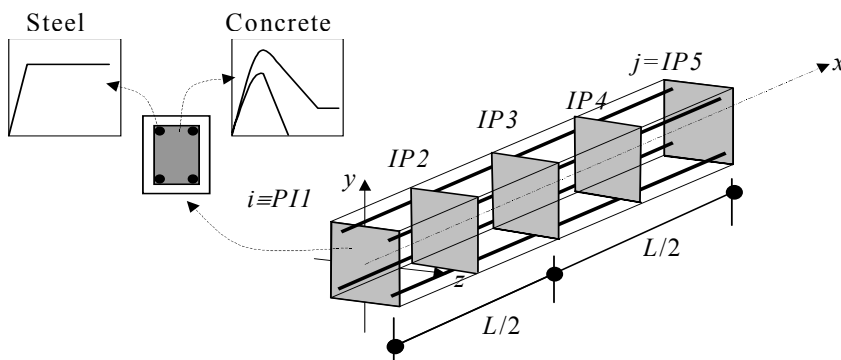


Fig.2. 3-D fiber beam-column element

The spread of inelastic zones within an element is captured considering the variable section flexural EI_y and EI_z and axial EA rigidity along the member length, depending on the bending moments and axial force level, concrete cracking and nonlinear mechanical properties of the concrete in compression and variation of reinforcement bars in size and location along the member length. The tangent

flexural rigidities for major and minor axis bending under conditions of constant axial load are evaluated by inverting the cross-section tangent stiffness matrix (1), imposing the condition of constant axial load to obtain a flexural flexibility matrix and inverting this to find the tangent flexural rigidities at constant axial load [2]. As aforementioned, the cross-section stiffness is modeled by explicit integration of stresses and strains over the cross-section area and then tangent stiffness properties of the cross sections are integrated along the member length to yield member stiffness coefficients [1].

2.3 The second-order effects on tangent stiffness matrix

The geometrical nonlinear effects for each element are taken into account in the present analysis, in a beam column approach, by the use of the inelastic stability stiffness functions and updating at each load increment the length, axial force and the flexural rigidity about of each principal axes of the element. This way minimizes modelling and solution time, generally only one or two elements are needed per member.

2.4 Member lateral loads

To perform the nonlinear analysis of frame structures, in the majority of previous publications, the loads are assumed to apply only at the nodes. In the present investigation, the loading due to the member lateral loads and transferred to the nodes are allowed and included automatically in the analysis. This leads to a significant saving in imputing the member loads, without the need to divide a member into several elements for simulation of these loads. The elasto-plastic equivalent nodal forces transferred to the nodes, from the member loads, will not be constant during the analysis, and will be dependent on the variable flexural rigidity along the member according with the process of gradual formation of plastic zones [1].

2.5 Diaphragm action

For normal building frameworks, a floor slab may be modelled as a rigid diaphragm, which is assumed to provide infinite in-plane stiffness and without any out of plane stiffness. The lateral response of the floor slab is characterized by two translational and one rotational degrees of freedom located at the floor master node. The multi-freedom constraints, required by the rigid body floor model, are imposed by augmenting the finite element model just described, with the penalty elements. The main advantages of this technique with respect to the traditional master-slave elimination technique is its lack of sensitivity with respect to whether constraints are linearly dependent and its straightforward computer implementation. Considering the homogenous constraints $\mathbf{A}\mathbf{u}=0$ the penalty augmented system can be written compactly as:

$$\left(\mathbf{K}_T + \mathbf{A}^T \mathbf{W} \mathbf{A}\right) \Delta \mathbf{U} = \Delta \mathbf{F} \quad (3)$$

where \mathbf{W} is a diagonal matrix of penalty weights, \mathbf{A} is the unscaled matrix of the penalty elements, \mathbf{K}_T is the global tangent stiffness matrix, $\Delta \mathbf{U}$ and $\Delta \mathbf{F}$ are the incremental displacement and force vector, respectively.

2.6 Geometry updating and force recovery

Using an updated Lagrangian formulation (UL) the nonlinear geometrical effects are considered updating the element forces and geometry configurations at each load increment. The natural deformation approach (NDA) in conjunction with the geometrical “rigid body qualified” stiffness matrix [8] is adopted for the element force recovery and the web plane vector approach is effectively used to update the frame element coordinates [1].

The element incremental displacements can be conceptually decomposed into two parts: the rigid body displacements and the natural deformations. The rigid body displacements serve to rotate the initial forces acting on the element from the previous configuration to the current configuration, whereas the natural deformations constitute the only source for generating the incremental forces. The element forces at the current configuration can be calculated as the summation of the incremental forces and the forces at the previous configuration.

3. ANALYSIS ALGORITHM AND COMPUTER PROGRAM

In order to trace the equilibrium path, for proportionally and non-proportionally applied loads, the proposed model has been implemented in a simple incremental and incremental- iterative matrix structural-analysis program. In the simple incremental method, the simple Euler stepping algorithm is used in conjunction with constant work-load increments, whereas in the incremental-iterative approach, at each load increment a modified constant arc-length method is applied to compute the complete nonlinear load-deformation path [1]. Convergence of the iterative process is said to have occurred when within certain tolerances the internal actions are in equilibrium with the applied external loads.

Based on the analysis algorithm just described, an object-oriented computer program, NEFCAD 3D, has been developed to study the combined effects of material, geometric and semi-rigid connection nonlinear behaviour on the load-versus-deflection response for spatial framed structures. It combines the structural analysis routine with a graphic routine to display the final results [4]. The graphical interface allows for easy generation of data files, graphical representation of the data, and plotting of the deflected shape, bending moments, shear force and axial force diagrams, load-deflection curves for selected nodes, area of uncracked, cracked and yielded parts of the elements as shown in Fig. 3.

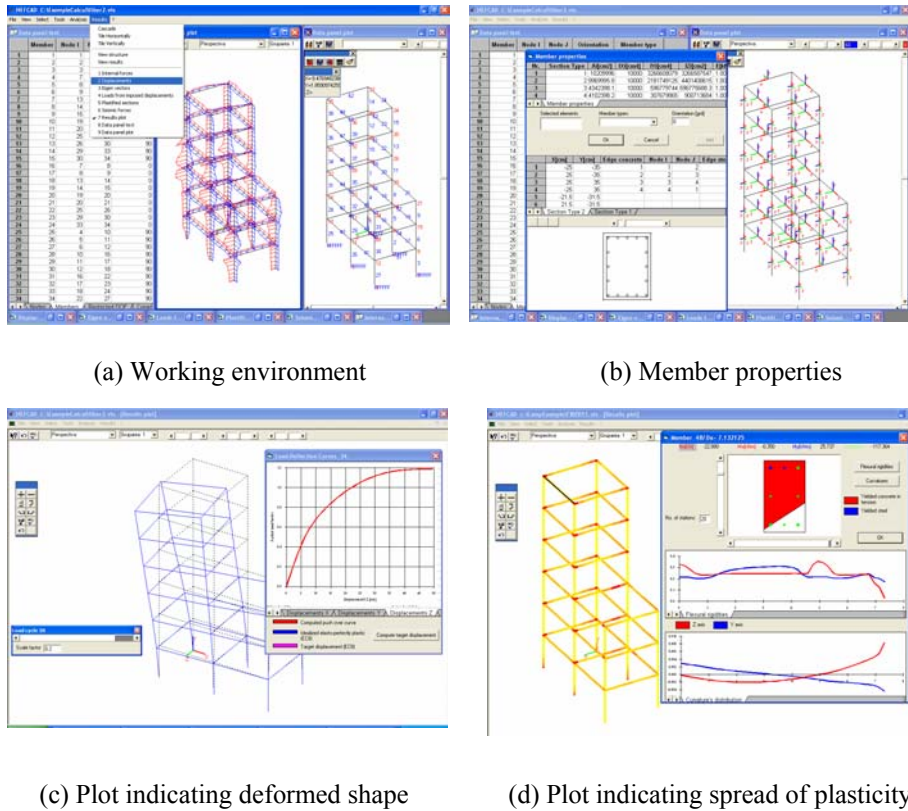


Fig.3. NEFCAD screen-shots

4. COMPUTATIONAL EXAMPLE

The effectiveness of the analytic procedure presented here has been evaluated using a six story RC space frame whose nonlinear response is dominated by the spreading plasticity effects in individual members and nonlinear geometrical effects. The frame is subjected to the non-proportional action of gravity loads and lateral seismic loads. Uniform floor pressure is 4.48 kN/m^2 and represents the first sequence of loading. The seismic loads are simulated by point loads in the Y and Z directions at every beam-column joints using the 3D modal load pattern (Fig.4). The frame column dimensions are the same from ground to upper story ($60 \times 60 \text{ cm}$) with the same reinforcement layout ($16\Phi 25$). All the longitudinal and transversal beams are the same dimensions ($30 \times 50 \text{ cm}$) and reinforcement layout ($8\Phi 20$). The stress-strain curve of the concrete under compression is represented by a combination of a second-degree parabola (for ascending part) and a straight line

(for descending part) [3]. The concrete tensile strength is neglected. A bi-linear elasto-plastic stress-strain relationship for the reinforcement bars, both in tension and in compression is assumed. The frame constituent materials include concrete with crushing strength $f_c=24\text{N/mm}^2$, crushing strain $\epsilon_0=0.002$, and ultimate strain $\epsilon_u=0.0035$, and strain softening factor $\gamma=0.15$, reinforcement steel with yield stress of $f_y=350\text{N/mm}^2$ and Young modulus $E_s=200 \times 10^3 \text{ N/mm}^2$. The nonlinear analysis of this frame was carried out using the proposed fiber beam-column element and the $M-N-\Phi$ approach developed in [3]. In both cases one element with eleven integration points has been used to model each column and beam.

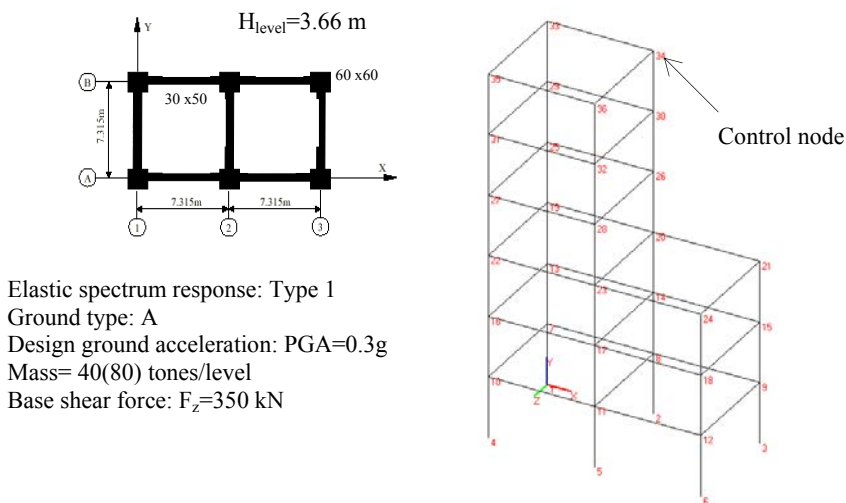
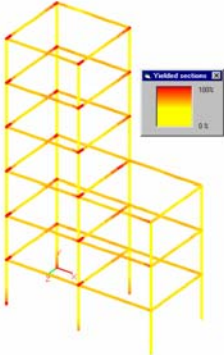
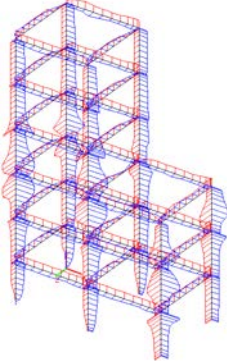
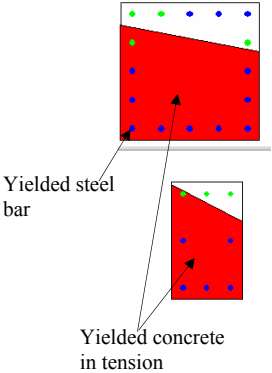


Fig. 4. Case study

In the $M-N-\Phi$ approach flexural and axial stiffness of the beam and columns are based on the cracked section using moment-curvature ($M-\Phi$) curve. To accurately determine beam and column moment-curvature relationships, separate computer analyses, using a cross-sectional fiber model, were conducted [2]. The plastic moments are evaluated approximately using a cubic polynomial interpolation curve based on exact interaction curves obtained through an accurate fiber model and then the interaction surface equation given in [3] were used to evaluation the biaxial strength capacity of cross-sections. Elastic-perfectly plastic behavior of cross-section was assumed in the $M-N-\Phi$ approach. The load-deflection curves of node A at the top of the frame are shown in Fig. 5. As it can be seen, when the rigid floor diaphragm effect is ignored, both analyses gives practically the same ultimate load factor; the limiting strength of the frame is reached at load ratio of 1.186 in $M-N-\Phi$ approach, whereas a load ratio of 1.184 is obtained by the proposed fiber beam-column analysis. However, a significant difference in load-deflection history can be observed during the loading process. This is attributed to the fact that higher

external actions causes considerable cracking in reinforced concrete elements, the concrete in compression becomes less stiff and hence the frame response becomes more flexible. When the rigid floor diaphragm effect is assumed, the analyses carried out indicate more significant difference in load-deflection traces. As it can be seen in Fig. 5, the inelastic limit point obtained in the simplified $M-N-\Phi$ approach is 1.37, whereas, a load ratio of 1.28 is obtained by the proposed fiber element approach. Table 1 summarize different parameters used in this study for nonlinear evaluation: distribution of plastic zones along the member length with percentage of sections area yielded, distribution of flexural rigidities, deflected shapes and plastic status for most critical sections. Running on a Pentium III personal computer at 733 MHz the proposed fiber analysis was performed in approximately 10 minutes.

Table 1. Summarized outputs of nonlinear fiber beam-column analysis.

Distribution of plastic zones at collapse	Distribution of flexural rigidities at collapse	Plastic status for sections 1-1 and 2-2
		

5. CONCLUSIONS

A reliable and robust nonlinear inelastic analysis tool has been presented for advanced analysis of 3D-RC frame structures. The proposed formulation is intended to model the geometrically nonlinear inelastic behavior of RC beam-columns using only-one element per member. This is an essential requirement to approach real large spatial frame structures, combining modeling benefits, computational efficiency and reasonable accuracy. In summery the following effects can be considered in analysis: gradual yielding associated with biaxial bending and axial force, each material behavior-modeled with predefined stress-strain relationships, inclusive time-dependent effects like shrinkage and creep, continuous change of cross-section, arbitrary cross-sectional shape, local and

global nonlinear geometrical effects, distributed loads and rigid floor diaphragm action. The computational example presented in this paper is available for download from <https://users.utcluj.ro/~ccosmin/>

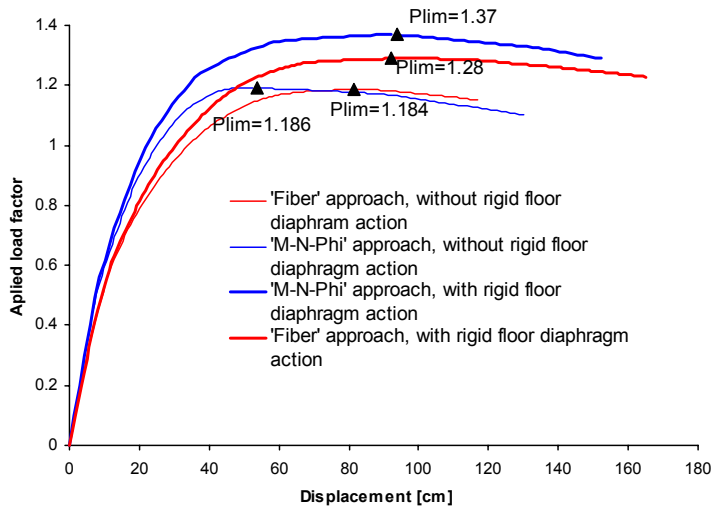


Fig. 5. Load-displacement traces

References

- Chiorean C.G., Bârsan, G.M., Large deflection distributed plasticity analysis of 3D steel frameworks, *Int. J. Computers & Structures*, Elsevier Science, vol. 83, 2005.
- Chiorean, C.G., A fast incremental-iterative procedure for inelastic analysis of RC sections of arbitrary shape, *Acta Technica Napocensis-Civil Engineering*, vol. 47, 2004.
- Chiorean, C.G., Application of pushover analysis for seismic performance evaluation of 3D RC frame structures, *Research report, POCTI-36019, UNL/FCT-DEC*, Lisbon, Portugal, 2003.
- Chiorean, C.G., NEFCAD-Computer program for nonlinear inelastic analysis of framed structures, Online documentation, <https://users.utcluj.ro/~ccosmin/>
- Izzudin, B.A., Siyam, A.A.F.M, Lloyd Smith, D., An efficient beam-column formulation for 3D RC frames, *Int. J. Computers & Structures*, Elsevier Science, vol. 80, 2002.
- Sivaselvan, M.V., Reinhorn, A.M., Collapse analysis: Large inelastic deformations analysis of planar frames, *J. Structural Engineering, ASCE*, vol. 128, 2002.
- Vidosa, F.G., Kostovos, M.D., Pavlovic, M.N., Nonlinear finite element analysis of concrete structures: performance of fully three-dimensional brittle model, *Int. J. Computers & Structures*, Elsevier Science, vol. 40, 1991.
- Yang, Y.B., Yau, J.D., Leu, L.J., Recent developments in geometrically nonlinear and postbuckling analysis of framed structures, *Applied Mechanics Review, ASME*, vol. 56, 2003

Estudio del comportamiento de los hormigones reforzados con fibras cortas

Sergio Oller, Alex H. Barbat, Juan Miquel

Departamento de Resistencia de Materiales, ETSECCPB, Universidad Politécnica de Cataluña

Resumen

En este trabajo se presenta un acercamiento al estudio del comportamiento de los hormigones reforzados con fibras cortas. Se establece una formulación basada en una modificación de la teoría de mezclas clásica para determinar sus parámetros mecánicos a partir de las características de los materiales componentes (hormigón-fibras cortas). También se muestran resultados numéricos obtenidos mediante el método de los elementos finitos y se comentan las posibilidades de un método analítico simplificado para el estudio de su comportamiento.

El desarrollo del trabajo trata sobre el comportamiento del hormigón reforzado con fibras y las características que justifican su utilización. Se estudia el equilibrio interno y mecanismo de transmisión de tensiones entre el hormigón y las fibras cortas y la formulación general del problema e inserción dentro de la técnica de los elementos finitos. Se hace un breve comentario sobre el tratamiento simplificado del comportamiento de los hormigones reforzados con fibras cortas y se presenta un ejemplo de comprobación.

Summary

An approach for the short fibers reinforced concrete behavior is presented in this work. A formulation based on a modification of the classical mixing theory to obtain the composite mechanical properties starting from the single compounding characteristics (concrete-short fibers) is developed. Numerical results obtained by means of the finite element method are also shown and the possibilities of using a simplified analytical method in the study of the short fibers reinforced concrete are commented.

The development of the work studies the behavior of the concrete reinforced with short fibers and the characteristics that justify its use. It studies the internal balance and the stress transmission mechanism between the concrete and the short fibers as well as the general formulation of the problem and its insertion within the frame of the finite element technique. A brief comment is made on the simplified treatment of the behavior of the concrete reinforced with short fibers and a validation example is presented.

1. CLASIFICACIÓN DE LOS MATERIALES COMPUESTOS

Es muy difícil definir un material compuesto dada sus cualidades, composición, propiedades, forma de fabricación, etc. Por esta razón hay distintas maneras de clasificar los materiales compuestos y con seguridad cada uno de ella acertaría en la forma de hacerlo. En este caso, y para ser coherente con el posterior desarrollo del trabajo, se presenta la siguiente clasificación:

1.1 Clasificación según su topología

Entre las posibles clasificaciones, está aquella que se basa en su configuración topológica, es decir en como son y como se distribuyen los componentes: materiales de matriz compuesta (hormigón), materiales de matriz compuesta con fibras cortas y/o largas (hormigón reforzado con fibras), materiales laminados y también una combinación de cada uno de estos tipos enunciados.

1.2 Clasificación según sus componentes

Los materiales compuestos pueden también clasificarse según el tipo y forma en que están constituidos:

- **Fibrosos:** Compuestos por fibras continuas cortas o largas, en una dos o tres direcciones, o bien distribuidas en forma aleatoria aglutinados por una matriz. A su vez esta matriz puede estar formada por dos o más materiales (caso de hormigones reforzados con fibras).
- **Particulados:** Formados por partículas que puntualmente trabajan aglutinadas por una matriz.
- **Laminares:** Compuestos por capas o constituyentes laminares con características de resistencia en magnitud y dirección diferentes.
- **Hojuelados:** Compuestos por hojuelas planas inmersas en una matriz.
- **Relleno esqueleto:** formado por un esqueleto relleno por otro material.

Los más utilizados son los fibrosos, en los cuales las fibras asumen el papel de resistir las acciones mecánicas y la matriz sirve como aglutinante y protector del medio ambiente. La resistencia mecánica de las fibras es del orden de 25 a 50 veces mayor que la matriz. En el caso del hormigón a tracción esta relación es del orden de 100 veces. Esto provoca un comportamiento fuertemente anisótropo.

Al aplicar una carga en un material compuesto se producen en su interior esfuerzos y para lograr una buena transmisión de estos entre fibra y matriz se estudia la longitud y adherencia de este refuerzo.

La función de la matriz (hormigón) es la de repartir y transmitir las cargas a las fibras. En el caso de laminados compuestos las propiedades de resistencia al corte son muy importantes. La matriz cumple la función de asegurar la continuidad de

desplazamientos entre láminas en todo el espesor de la estratificación e influye en el modo de rotura.

1.3 Clasificación estructural

Desde el punto de vista del estudio del comportamiento mecánico, los materiales compuestos pueden clasificarse según su

- **Estructura básica.** En este caso se considera en la clasificación la estructura a nivel de las simples moléculas o mallas cristalinas,
- **Estructura microscópica.** Se tiene en cuenta para la clasificación la interacción fibra-matriz, su influencia en la distribución de tensiones y la aparición de fallas, discontinuidades o fisuras bajo condiciones de cargas elementales,
- **Estructura macroscópica.** Se considera en la clasificación al material compuesto desde un punto de vista macroscópico, como una combinación de sustancias diferentes, que contribuyen al estado de equilibrio del conjunto.

En este trabajo se presentará un estudio estructural desde el punto de vista macroscópico, considerando las siguientes hipótesis:

- Las fibras se distribuyen uniformemente en la matriz,
- Existe perfecta adherencia entre la matriz y el refuerzo, pudiéndose considerar el deslizamiento relativo entre ambos mediante la incorporación de la teoría de la plasticidad en la interface de la matriz-fibra,
- La matriz no contiene vacíos ni defectos,
- No existen tensiones residuales en el material compuesto provenientes de posibles defectos en la fabricación. Sin embargo, es posible incluirlos como condiciones iniciales.

Una extensa descripción sobre los tipos de materiales compuestos y de componentes, formas de fabricación y aplicaciones industriales, puede consultarse en Miravete (2000) [1] y Car (2000) [2].

2. INTRODUCCIÓN LOS COMPUESTOS REFORZADOS CON FIBRAS

La utilización de nuevos materiales compuestos en el diseño de las estructuras se ha visto incrementada notablemente en los últimos años. Esta tendencia se debe a la posibilidad de diseñar el material con ciertas propiedades especiales que mejoren las cualidades de comportamiento de las estructuras.

Las mayores dificultades que se encuentran en la utilización de estos nuevos materiales radican en la falta de tecnología apropiada para garantizar su correcto funcionamiento. Esta situación ocurre en los materiales con fibras largas de matrices de hormigón o epoxy. Hay también una cierta incertidumbre en cuanto a la durabilidad de los refuerzos cortos y largos y sobre todo, actualmente hay un problema serio en conseguir una evaluación estructural fiable, pues son materiales cuya no linealidad se manifiesta desde que comienzan los micro-movimientos entre fibra y matriz, situación que ocurre a cargas bajas.

Particularmente, se define el hormigón con fibras como aquel material compuesto por cemento árido y agua, más la adición de fibras cortas discontinuas y/o fibras largas continuas.

La distribución de estas fibras en el hormigón es aleatoria, pero se busca una homogeneidad que confiera una cierta isotropía al conjunto. Para conseguir esto se debe realizar una mezcla evitando tanto la segregación de los áridos como la concentración o preservando una dada orientación dominante en las fibras.

Las fibras para hormigones pueden ser de acero, de vidrio, de asbesto, cerámicas o de algún material plástico. Las fibras confieren al hormigón propiedades muy diversas, pero entre las cualidades mecánicas más importante que aporta al comportamiento del material compuesto se puede sintetizar en:

- a. Las fibras cortas dan al material compuesto mayor ductilidad, aunque no aumenta la resistencia del conjunto,
- b. Las fibras largas dan al material compuesto mayor resistencia, sin muestras de aumento de ductilidad.

De estas dos ideas surge que el hormigón con fibras cortas y largas se transforma en un buen material estructural, transformándose en un material de cualidades destacables frente a otros materiales tradicionales.

Entre las fibras más utilizadas en hormigones puede citarse:

- a. **Fibras de asbesto:** Se han utilizado en la década de los '60 y '70, desarrollándose patentes comerciales como “Uralita”. Proporcionan gran ductilidad al conjunto y mejoran sus propiedades mecánicas, pero en los últimos años se ha dejado de utilizar porque su manipulación produce alteraciones fisiológicas en el cuerpo humano. Este material es muy dúctil, tiene una resistencia a tracción entre 500 y 1000 MPa y su módulo de elasticidad es similar al del acero. Su utilización dentro del hormigón es muy buena, porque suelen acomodarse en forma paralela una a otra fibra dejándose envolver por la pasta de cemento, evitando enmarañarse y así perder efectividad.
- b. **Fibras de Vidrio:** Resultan de un filtrado del vidrio a través de una malla metálica. El diámetro depende de esta malla, de la temperatura del vidrio y de la velocidad de estiramiento. La colocación en el

hormigón puede realizarse luego de constituir un tejido uni, bi o tridimensional. Hay fibras con buenas propiedades mecánicas y aislantes de bajo medio y alto costo y suelen ser muy resistentes a los medios agresivos. Su primera incorporación en el mundo de los materiales compuestos data del 1950, cuando se intentó sustituir el acero mediante tendones de fibra de vidrio, puesto que su resistencia es del orden de los 2000 MPa y el módulo de elasticidad de 70 GPa. El mayor problema en la utilización de las fibras de vidrio surgió a nivel tecnológico por las dificultades de anclaje que estas tienen (Paez (1979) [3]).

- c. **Fibras Plásticas:** Se caracteriza por su bajo peso específico y bajo coste. Sus características mecánicas son más modesta que las del grupo anterior, pues su resistencia alcanza escasamente los 500 MPa con un módulo de elasticidad de 10 GPa. Este tipo de fibras admite endurecimientos y aumento de resistencia por plasticidad en frío, mediante retorcido y/o estirado. Entre sus cualidades está su inalterabilidad frente a agentes agresivos junto a su bajo coste y peso. También puede tratarse como ventaja su trabajabilidad durante la fabricación del hormigón.
- d. **Fibras Cerámicas:** Un grupo de materiales que ha comenzado a ser muy atractivo en la conformación de compuestos, son los denominados cerámicos de altas prestaciones o también cerámicas finas o nuevas cerámicas. Estos materiales se componen principalmente de Óxidos de Aluminio, Zirconio, Silicio, Berilio, Titanio, Magnesio, etc.; de Nitruros de Silicio, Boro, Aluminio, etc.; y de Carburos de Silicio (fibra de carbono) y Boro. Estos nuevos materiales tienen una gran potencialidad para ser utilizados en distintas formas, solos o formando parte de un compuesto. Tiene cualidades como alta tenacidad a la fractura, alta resistencia mecánica, la capacidad de soportar altas temperaturas y resistir la oxidación.

Tabla 1. Valor orientativo de la resistencia a tracción de algunos materiales.

Tipo de Material	Material	Resistencia [MPa]	Tenacidad [MPa m ^{1/2}]
Metálico	Aluminio LM27	153	–
Metálico	Hierro Fundido	265	15-50
Metálico	Acero Templado EN32	590	30-100
Cerámico Puro	Al ₂ O ₃ (Alúmina)	200-2000	5
Cerámico Puro	SiC (Carburo de Silicio – Fibras de Carbono)	300-3000	3
Cerámico Puro	Si ₃ N ₄ (Nitruro de Silicio)	350-3500	6
Cerámico Puro	ZrO ₂ (Oxido de Zirconio – Zirconia)	500-5000	9

- e. **Fibras Metálicas:** Es un tipo de fibras cortas muy utilizado en el hormigón. Su resistencia es del orden de 2 a 3 GPa y su modulo elástico de 210 GPa. Uno de los problemas más serios es su falta de adherencia con el hormigón, situación que se pone de manifiesto en ensayos a tracción y flexión. Esta situación, que en menor medida ocurre en otras fibras, hace que su capacidad de participación en el material compuesto está limitado a su posibilidad de transferir esfuerzos, más que a su resistencia nominal. En algunos casos se suele dar a las fibras cortas forma de grapas, ayudando así al anclaje de las mismas en el hormigón.

3. REPRESENTACIÓN DEL COMPORTAMIENTO DE UN COMPUESTO REFORZADO CON FIBRAS CORTAS

3.1. Introducción

Los materiales compuestos están formados por diferentes tipos de sustancias inorgánicas u orgánicas. Su estado de equilibrio atómico depende de distintos tipos de ligaduras interatómicas, dando lugar a materiales amorfos o cristalinos.

Las características mecánicas de los materiales compuestos dependen de sus propiedades intrínsecas: estructura macroscópica, tipo de ligadura, estructura cristalina, etc. También influyen en el comportamiento de estos materiales sus propiedades extrínsecas: características del proceso de fabricación, tamaño de micro-poros y defectos y distribución de los mismos, microfisuras, estados tensionales iniciales, etc. Desde el punto de vista de la simulación del comportamiento constitutivo sólo se puede aportar una contribución en estudios que conduzcan a mejorar las propiedades extrínsecas del compuesto.

Cada una de las sustancias componentes que integran el compuesto condicionan con su propia ley constitutiva el comportamiento del conjunto en función de la proporción del volumen en que participan y de su distribución morfológica dentro del compuesto.

Existen diversas teorías que permiten simular el comportamiento constitutivo de los materiales compuestos (ver una síntesis de ellos en Car (2000) [4], Zalamea (2000) [5]), una de ellas es la “Teoría de Mezclas” (Trusdell y Toupin (1960)[6]), que se considera adecuada para la simulación del comportamiento de materiales compuestos en régimen lineal y con ciertas modificaciones permite representar el comportamiento no lineal del material. Por otro lado, esta teoría, en su forma clásica, establece que los materiales componentes, que coexisten en un punto del sólido deben tener la misma deformación (componentes participando en paralelo). Esta hipótesis plantea una fuerte limitación en la utilización de esta teoría para la

predicción del comportamiento de los materiales compuestos. Para solucionar este problema, se debe reformular la teoría clásica a partir de una ecuación de compatibilidad que se adapte al comportamiento del compuesto (componentes participando en serie-paralelo).

El tratamiento de la anisotropía de los materiales componentes (Oller *et al.* (1995) [7] Car *et al.* (2001) [8]), abre de una manera muy amplia la posibilidad de tratamiento de distintos materiales compuestos de matriz reforzada con fibras.

La teoría de mezclas clásica fue estudiada inicialmente por Trusdell y Toupin (1960) [6] en el año 1960 y a su vez estos estudios establecieron las bases de otros trabajos posteriores (Green y Naghdi (1965) [9], Ortiz y Popov (1982) [10,11], Oller *et al.* (1996) [12], Oller y Oñate (1996) [13]). La teoría que aquí se presenta es más general que la clásica y representa el comportamiento constitutivo de un material compuesto por “*n-fases*” altamente anisótropas y sin la limitación exigida por la clásica ecuación de compatibilidad de la teoría original, permitiendo que la relación de comportamiento entre las sustancias componentes pueda ser en serie o en paralelo.

La teoría de mezclas podría entenderse como un “gestor de los modelos constitutivos” de cada componente del compuesto, permitiendo considerar la interacción entre las distintas leyes de comportamiento de las diversas fases de un compuesto. Esta técnica de combinación de comportamientos, o de sustancias en este caso particular, permite que cada una de ellas conserve su ley constitutiva original, isótropa o anisótropa, lineal o no-lineal, y a la vez condicione el comportamiento global del conjunto o compuesto.

Como ya se ha mencionado, la forma clásica de la teoría de mezclas es sólo adecuada para simular el comportamiento mecánico de ciertos materiales compuestos, cuyos componentes responden en paralelo (con igual deformación y sin movimientos relativos entre ellos). Materiales que responden a este perfil son aquellos constituidos de matrices con refuerzo de fibras largas alineadas con la acción de la carga. Para otra orientación de la carga u otros tipos de materiales compuestos, como son los tejidos cuyas fibras tienen diversas orientaciones entre sí, es necesario realizar modificaciones en la teoría clásica.

3.2 Teoría de mezclas clásica

La teoría de mezclas clásica de sustancias básicas se basa en la mecánica del sólido continuo local y se considera adecuada para explicar el comportamiento de un punto de un sólido compuesto. Se basa en el principio de interacción de entre las sustancias que componen el material compuesto, suponiendo las siguientes hipótesis básicas:

- i. En cada volumen infinitesimal de un compuesto participan un conjunto de sustancias componentes;

- ii. Cada componente contribuye en el comportamiento del compuesto en la misma proporción que su participación volumétrica;
- iii. Todos los componentes poseen la misma deformación –ecuación de cierre o compatibilidad–;
- iv. El volumen ocupado por cada componente es mucho menor que el volumen total del compuesto.

La segunda de las hipótesis implica una distribución homogénea de todas las sustancias en cada punto del compuesto. La interacción entre las diferentes sustancias componentes, cada una con su respectiva ley constitutiva, determina el comportamiento del material compuesto y depende básicamente del porcentaje en volumen ocupado por cada componente y de su distribución en el compuesto. Esto permite combinar materiales con comportamientos diferenciados (elástico, elasto-plástico, etc.), donde cada uno de ellos presenta un comportamiento evolutivo gobernado por su propia ley.

La tercera hipótesis establece que en ausencia de difusión atómica* se cumple la siguiente condición de compatibilidad bajo la hipótesis de pequeñas deformaciones para cada una de las fases del material compuesto:

$$\varepsilon_{ij} = (\varepsilon_{ij})_1 = (\varepsilon_{ij})_2 = \dots = (\varepsilon_{ij})_n \quad (1)$$

donde ε_{ij} y $(\varepsilon_{ij})_n$ representan respectivamente las deformaciones del material compuesto y de la componente *i-ésima* de dicho material compuesto.

El factor de ponderación o coeficiente de participación volumétrica k_c permite considerar la contribución de cada fase y se obtiene considerando la participación volumétrica de cada una de los materiales componentes respecto del volumen total

$$k_c = \frac{dV_c}{dV_0} \Rightarrow \sum_{c=1}^n k_c = 1 \quad (2)$$

donde V_c representa el volumen del componente *c-ésimo* del material y V_0 es el volumen total del material compuesto.

* **Nota:** Los fenómenos de difusión atómica se producen a temperaturas cercanas al punto de fusión. En los análisis se considera una temperatura inferior a la correspondiente al punto de fusión.

La ecuación constitutiva deriva de un planteo termodinámico consistente y tiene la siguiente forma

$$\sigma_{ij} = \mathbf{C}_{ijkl}^S \varepsilon_{kl}^e = \sum_{c=1}^n k_c (\sigma_{ij})_c = \sum_{c=1}^n k_c (\mathbf{C}_{ijkl}^S)_c (\varepsilon_{kl}^e)_c \quad (3)$$

Siendo σ_{ij} la tensión en el material compuesto, $(\sigma_{ij})_c$ la tensión en cada componente (fibra/matriz) \mathbf{C}_{ijkl}^S el tensor constitutivo del compuesto, $(\mathbf{C}_{ijkl}^S)_c$ el tensor constitutivo de cada material componente y $(\varepsilon_{kl}^e)_c = \varepsilon_{kl} - (\varepsilon_{kl}^p)_c - (\varepsilon_{kl}^\theta)_c$ la deformación elástica de cada material componente. En esta última $(\varepsilon_{kl}^e)_c$, $(\varepsilon_{kl}^p)_c$ y $(\varepsilon_{kl}^\theta)_c$ representan las cuotas de deformación elástica, plástica y de origen térmico.

De las ecuaciones anteriores surge que el tensor constitutivo del compuesto adquiere la forma

$$\mathbf{C}_{ijkl}^\sigma = \sum_{c=1}^n k_c (\mathbf{C}_{ijkl}^\sigma)_c \quad (4)$$

La teoría de mezclas clásica, la cual se parte de la hipótesis de que el campo de deformaciones es el mismo para todos los componentes del compuesto, es rigurosamente válida sólo si se aplica a materiales cuyos componentes trabajan en paralelo. Estos materiales se caracterizan por que su estado tensional resulta ser la suma de las tensiones de cada componente, ponderadas de forma proporcional al volumen que ocupa cada fase respecto del total –ejemplo: matriz con fibras largas, hormigón armado, etc.–. En el caso de matrices con refuerzo de corta longitud no resulta válida la hipótesis de igualdad entre las deformaciones de todos los componentes. Para solucionar este inconveniente existen dos alternativas: definir otra ecuación de cierre (ecuación (1)), que permita simular adecuadamente los fenómenos que se producen en el material, o realizar una corrección en las propiedades de cada componente y mantener la hipótesis de igualdad deformaciones en cada uno de los componentes del compuesto, expresión que se utilizará en este trabajo y se explicará más adelante.

3.3 Teoría de mezclas para refuerzo de poca longitud

La formulación de la teoría de mezclas clásica está orientada a un material de matriz reforzada con fibras largas, y a medida que la relación de aspecto* de la fibra disminuye, la condición de compatibilidad fibra-matriz deja de cumplirse.

*NOTA: Se define como relación de aspecto al cociente $l/2r$ donde l y r son la longitud y el radio de una fibra corta respectivamente.

Así, al acortarse la longitud de la fibra el efecto de deslizamiento se hace más significativo y disminuye la capacidad de transmisión de esfuerzos entre fibra y matriz y la “eficacia” de la contribución de las fibras en la rigidez del material compuesto disminuye.

La Figura 1 muestra la deformación de la matriz circundante a una fibra discontinua embebida en la misma y sometida a una carga de tracción paralela a la fibra.

En un material compuesto con refuerzo de fibras largas, se tiene el mismo estado de deformaciones para la matriz y las fibras. Por otro lado, la tensión a lo largo del refuerzo no varía salvo en la zona de los extremos, donde se verifica que la deformación de la misma es menor respecto a la de la matriz. En el caso de refuerzos de corta longitud embebidos en una matriz este fenómeno juega un papel fundamental en la determinación de las propiedades mecánicas del compuesto.

Este fenómeno puede explicarse teniendo en cuenta la Figura 1. En la misma, en la sección *AA* la deformación del conjunto se debe sólo a la deformación de la matriz. En la sección *BB*, justo en el extremo de la fibra, evidencias experimentales muestran que la transferencia de esfuerzos de la matriz hacia la fibra es gradual, con esfuerzo nulo en la punta y con un aumento gradual de la tensión a lo largo de la fibra hasta el punto en el cual las deformaciones de matriz y fibra son iguales. De acuerdo con esto, la zona central de una fibra presenta el máximo valor de tensión axial. Se define como *longitud de transferencia* l_c a la longitud de refuerzo necesaria para garantizar la compatibilidad fibra-matriz y la transferencia de los esfuerzos desde la matriz hacia la fibra. Cualquier refuerzo cuya longitud sea inferior a esta magnitud, no participa plenamente en los mecanismos de transferencia de esfuerzo (Jayatilaka (1969) [14]).

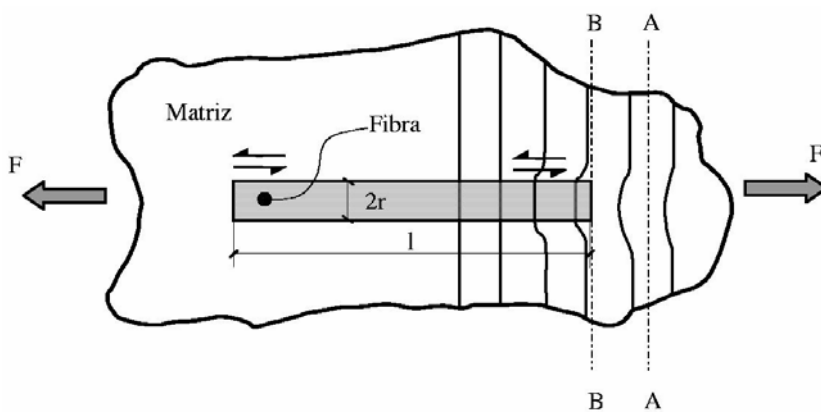


Figura 1 – Deformación alrededor de una fibra discontinua embebida en una matriz sometida a tracción.

En la Figura 2 se muestra la distribución de esfuerzos en una fibra de refuerzo. La tensión tangencial es máxima en los extremos de las fibras y resulta casi nulo en la zona central. En la misma Figura se observa que en los extremos de las fibras la tensión axial cae a cero, resultando un esfuerzo medio en la fibra de longitud l menor que en una fibra continua sometida a las mismas cargas externas. La “eficacia” del refuerzo disminuye en la medida en que lo hace la longitud de la fibra debido a que no toda la fibra puede trabajar a la máxima tensión. Por lo tanto, en los materiales compuestos reforzados con fibras cortas es necesario que la longitud l de la fibra sea superior a la longitud crítica de transferencia l_c con el objetivo de que las mismas sean aprovechadas a su máxima capacidad.

Debido a estos fenómenos locales, los materiales compuestos reforzados con fibras cortas no cumplen exactamente con la condición de compatibilidad expresada en la (1), debido a las diferentes deformaciones que se presentan entre la matriz y las fibras. Por ello, a los fines de representar el comportamiento constitutivo de estos materiales, es necesario el planteo de otra ecuación de cierre de deformaciones (Oller *et. al.* (1995) [11]), o mantener la clásica teoría de mezclas, manteniendo la hipótesis de igualdad de deformaciones en todos los componentes, y realizar una corrección en las propiedades de cada componente (Car *et al.* (1997) [15]).

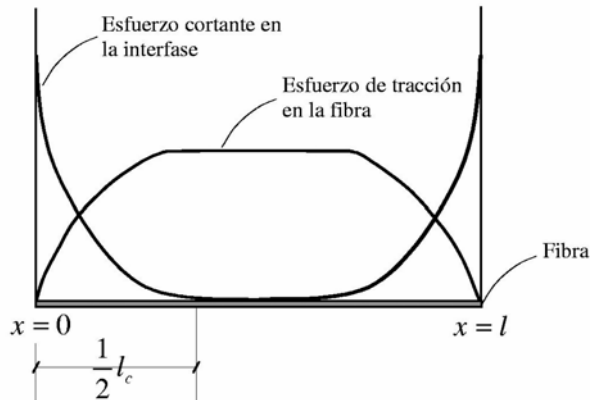


Figura 2 – Distribución de esfuerzos axiales en la fibra y cortantes en la interfaces fibra-matriz.

Distribución de tensión axial en la fibra

A los fines de determinar una expresión analítica de la distribución de tensiones en una fibra es necesario considerar el equilibrio en la zona de transferencia de tensiones (ver Figura 3). El equilibrio de la fibra en la dirección longitudinal x está dado por la siguiente ecuación

$$\sigma_f \pi r^2 + 2 \tau \pi r dx = (\sigma_f + d\sigma_f) \pi r^2 \Rightarrow \frac{\partial \sigma_f}{\partial x} = \frac{2 \tau}{r} \quad (5)$$

O en términos de fuerzas,

$$\frac{\partial P_f}{\partial x} = 2 \tau \pi r \quad (6)$$

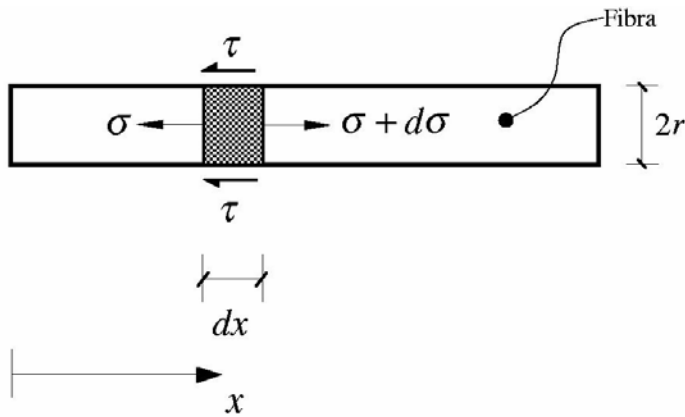


Figura 3 – Esfuerzos en los extremos de fibras.

donde σ_f es la tensión en la fibra en la dirección x , $d\sigma_f$ es el incremento de la tensión en la fibra en $x + dx$ y τ es la tensión tangencial en la interface fibra-matriz. La tensión tangencial τ se produce debido a las deformaciones diferenciadas entre fibra y matriz y por lo tanto depende de la diferencia entre los campos de desplazamientos de fibra y matriz. El equilibrio entre matriz y fibra corta puede describirse mediante la siguiente ecuación diferencial sobre el eje longitudinal de la fibra resulta (Jayatilaka, (1979) [14]).

$$\frac{\partial^2 P_f}{\partial x^2} = H \left[\frac{P_f}{C_f^\sigma A_f} - E_m \right] \quad (7)$$

donde P_f es la fuerza máxima de interacción entre el refuerzo y la matriz, H una constante que depende de la distribución topológica de las fibras, C_f^σ el módulo de Young del refuerzo, A_f la sección transversal media del refuerzo y E_m es la deformación longitudinal en la matriz. La solución de la ecuación diferencial (7) permite obtener la siguiente fuerza en la fibra,

$$P_f = C_1 \operatorname{senh}(\beta x) + C_2 \operatorname{cosh}(\beta x) + C_f^\sigma A_f E_m \quad (8)$$

siendo C_1 y C_2 las constantes que resultan de las condiciones de contorno $P_f = 0$ en $x = 0$ y $x = l$; β es un coeficiente dado por la siguiente expresión

$$\beta = \sqrt{\frac{H}{C_f A_f}} = \sqrt{\frac{G_c}{C_f^\sigma A_f} \frac{2\pi}{\ln\left(\frac{r'}{r}\right)}} \quad (9)$$

En la cual G_c es el módulo elástico transversal del compuesto y r' la distancia media entre las fibras de refuerzo (ver Figura 4).

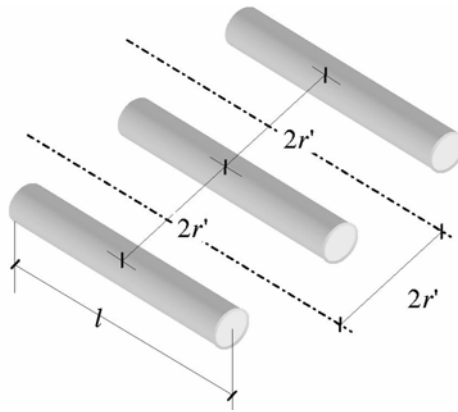


Figura 4 – Relación de aspecto que se considera en el refuerzo.

Una vez obtenidas las constantes de integración, la ecuación de la tensión resulta

$$\sigma_f(x) = C_f^\sigma E_m \left[1 - \frac{\cosh\left(\beta\left(\frac{l}{2} - x\right)\right)}{\cosh\left(\beta\frac{l}{2}\right)} \right] \quad \forall 0 \leq x \leq \frac{l}{2} \quad (10)$$

Esta ecuación establece la distribución de tensiones axiales a lo largo de la fibra. Esta distribución se muestra esquemáticamente en la Figura 2. En la zona central del refuerzo no existe un valor de tensión constante, pero si el refuerzo es lo suficientemente largo se puede admitir la hipótesis de que $\sigma_f \cong C_f^\sigma E_m$. El valor de tensión máximo se produce en $x = l/2$ y está dado por

$$(\sigma_f)_{\max} = \sigma_f(x = \frac{l}{2}) = C_f^\sigma E_m \left[1 - \frac{1}{\cosh\left(\beta\frac{l}{2}\right)} \right] \quad (11)$$

Distribución de tensión tangencial en la interface

La distribución de tensión tangencial en la zona de interface se obtiene haciendo el equilibrio en la fibra entre tensiones axiales y adherencia con la matriz. Para ello, teniendo en cuenta la ecuación (5) y (10), resulta

$$\tau_f(x) = \frac{C_f E r \beta}{2} \frac{\sinh\left(\beta\left(\frac{l}{2} - x\right)\right)}{\cosh\left(\beta\frac{l}{2}\right)} \quad (12)$$

Esta última ecuación establece la función de distribución de tensiones tangenciales en la interface fibra-matriz. Esta distribución se muestra esquemáticamente en la figura 2. El valor de la tensión cortante es nulo en la zona central de la fibra y coincidente con el máximo de la tensión axial. En esta zona no existen deformaciones diferenciadas entre fibra y matriz lo cual explica el valor nulo de las tensiones tangenciales. La máxima tensión tangencial se verifica en el extremo de la fibra y está dada por:

$$(\tau_f)_{\max} = \tau_f\left(x = \frac{l}{2}\right) = \frac{C_f^\sigma E r \beta}{2} \tanh\left(\frac{\beta l}{2}\right) \quad (13)$$

Una forma de incorporar la contribución del refuerzo en fibras cortas a la teoría de mezclas es a través de la tensión media a lo largo de la fibra, esto es

$$\bar{\sigma}_f = \frac{1}{l} \int_0^l \sigma_f(x) dx = C_f^\sigma \left[1 - \frac{\tanh\left(\beta\frac{l}{2}\right)}{\left(\beta\frac{l}{2}\right)} \right] E_m = \tilde{C}_f^\sigma E_m \quad (14)$$

siendo \tilde{C}_f^σ el módulo de Young medio del refuerzo o módulo homogeneizado. La ecuación (14), muestra que el módulo de Young de un refuerzo de fibras es función de la longitud de las mismas y de otros parámetros geométricos. En el caso de fibras largas el módulo elástico promedio tiende al valor del módulo de Young del refuerzo, en tanto en este caso se ve fuertemente afectado por las cualidades para transferir las tensiones que tiene la interface matriz-refuerzo.

La definición de un módulo de Young promedio del refuerzo, de magnitud inferior al real, explica que la participación de este aporta unas características mecánicas al compuesto que no sólo dependen de las propiedades intrínsecas del mismo, sino también de las propiedades del conjunto matriz-refuerzo. En esta situación las propiedades de la interface entre los componentes son determinantes en la forma de participación de los mismos. Esto significa que las propiedades mecánicas de un punto del sólido no sólo dependen de si mismas, sino del conjunto matriz-refuerzo.

Modelo constitutivo para fibras cortas

La matriz de un material compuesto reforzado con fibras de corta longitud suele estar sometido a tensiones superiores a aquellas constituidas con fibras largas. En general, las propiedades mecánicas del material compuesto con fibras cortas son inferiores que los compuestos con refuerzo continuo*.

El concepto de homogeneización que se describe en la sección anterior puede extenderse a "3-D" mediante la simplificación de admitir una distribución isótropa del cambio de propiedades, resultando el siguiente tensor constitutivo aproximado para la fibra corta,

$$\tilde{\mathbf{C}}_f^S = \mathbf{C}_f^S \left[1 - \frac{\tanh(\beta \frac{l}{2})}{(\beta \frac{l}{2})} \right] \quad (15)$$

donde el tensor constitutivo del refuerzo en la configuraciones referencial \mathbf{C}_f^S es ortótropo. De esta manera la formulación que se presenta permite tener en cuenta la pérdida de efectividad del refuerzo en la respuesta debido a su escasa longitud que impide una total transferencia de los esfuerzos desde la matriz.

Considerando el tensor constitutivo de la fibra corta, definido en la ecuación (15), se obtiene la ley constitutiva de la fibra, afectada de sus condiciones de contorno,

$$\boldsymbol{\sigma} = \underbrace{\left[1 - \frac{\tanh(\beta \frac{l}{2})}{(\beta \frac{l}{2})} \right]}_{\zeta} \cdot \mathbf{C}_f^S : \boldsymbol{\varepsilon}^e = \tilde{\mathbf{C}}_f^S : \boldsymbol{\varepsilon}^e \quad (16)$$

El factor ζ representa la corrección de las propiedades mecánicas del material debido a la presencia de un refuerzo de corta longitud dentro del material compuesto.

3.4 Ecuación del compuesto – Propiedades de conjunto del material compuesto

En el caso de materiales compuestos reforzados con fibras cortas se debe modificar la ecuación de compatibilidad (1) o hacer una corrección en las propiedades de cada componente manteniendo la ecuación de cierre de la teoría de mezclas clásica (Car *et al.* (1998) [16]). Este último método conduce a una formulación más simple que es la que se mostrará a continuación.

* NOTA: Se entiende por refuerzo continuo a aquel que presenta una longitud mayor a la necesaria para transmitir los esfuerzos desde la matriz hacia el refuerzo

La eficacia de la participación del refuerzo de fibras cortas es menor que la del de fibras largas, por lo tanto se deduce que las propiedades mecánicas de los materiales compuestos reforzados con fibras cortas no son mejores que aquellos reforzados con fibras largas. La expresión del tensor constitutivo del material compuesto dado en la ecuación (4) en pequeñas deformaciones se generaliza en la siguiente forma para el caso de refuerzos de cortas longitud.

$$\mathbf{C}_{ijkl}^S = \underbrace{\sum_{c_m=1}^{n_m} k_{c_m} (\mathbf{C}_{ijkl}^S)_{c_m}}_{\text{Componentes de la matriz}} + \underbrace{\sum_{c_r=1}^{n_r} k_{c_r} \zeta_{c_r} (\mathbf{C}_{ijkl}^S)_{c_r}}_{\text{Componentes del refuerzo}} \quad (17)$$

En las definiciones anteriores n_m es el número de materiales componentes que constituyen la matriz del compuesto y n_r es el número de materiales componentes que constituyen la fase del refuerzo. En el caso de refuerzos continuos el factor ζ_{c_r} tiende a la unidad y hace que la expresión para fibras cortas coincida con la de fibras largas.

La ecuación de la tensión en el material compuesto queda definida como

$$\sigma_{ij} = \underbrace{\sum_{c_m=1}^{n_m} k_{c_m} (\mathbf{C}_{ijkl}^S)_{c_m} (\varepsilon_{kl}^e)_{c_m}}_{\text{Componentes de la matriz}} + \underbrace{\sum_{c_r=1}^{n_r} k_{c_r} \zeta_{c_r} (\mathbf{C}_{ijkl}^S)_{c_r} (\varepsilon_{kl}^e)_{c_r}}_{\text{Componentes del refuerzo}} \quad (18)$$

3.5 Deslizamiento fibra-matriz

Entre las causas del comportamiento no-lineal de los materiales compuestos reforzados con fibras largas y más aun aquellos con fibras cortas, está el fenómeno de formación de grietas en la matriz, acompañada del deslizamiento o movimiento relativo entre fibra y matriz. Este fenómeno se conoce en la literatura en inglés como "*debonding*" y se caracteriza porque el agrietamiento de la matriz y el deslizamiento relativo entre fibra y matriz. Esta pérdida de adherencia se manifiesta como una pérdida de rigidez del material compuesto e induce a movimientos que pueden representarse en forma de deformaciones inelásticas, o no-recuperables, entre la fibra y la matriz. El fenómeno antes mencionado se designará en este trabajo con las siglas "DFM" (Deslizamiento Fibra-Matriz).

El proceso de apertura de fisuras en la matriz ocurre a niveles de tensiones que resultan significativamente menores que el nivel tensional necesario para producir la rotura de las fibras. La rotura de la matriz ocurre a valores bajos de tensión y está usualmente alineado con la dirección de las tensiones principales, produciendo una disminución en la rigidez e induciendo deformaciones inelásticas y ciclos de histéresis (Beyerley *et al.* (1992) [17]), (Preyce y Smith, (1992) [18]).

Los materiales compuestos sometidos a estados tensionales en los cuales se ha producido el fenómeno “DFM” no cumplen con la condición cinemática impuesta por la teoría de mezclas de sustancias básicas. Este fenómeno tiene como consecuencia directa la limitación de la matriz, para transferir esfuerzos a la fibra. Esto es, la fibra no es capaz de aumentar su estado tensional por causas atribuibles a la adherencia limitada que existe en la zona de interface fibra-matriz.

La incorporación de éste fenómeno en el modelo constitutivo mencionado en los apartados previos se basa en la idea de que el proceso de transferencia de cargas de matriz a fibra varía en el momento en que la matriz sufre deformaciones plásticas. El movimiento relativo entre fibra y matriz puede representarse en mecánica de medios continuos a través de una deformación inelástica irrecuperable en la fibra. La determinación del inicio de este fenómeno se realiza mediante una condición umbral máxima de resistencia que compara la tensión efectiva en un punto con la resistencia de la fibra. Dada la forma en que participa la fibra dentro del compuesto y el mecanismo de transmisión de tensiones entre fibra y matriz, la determinación de su máxima resistencia o resistencia real y su capacidad de colaboración depende de su propia resistencia nominal $(f^\sigma)_{\text{fib}}^N$, o resistencia de la fibra en condiciones aisladas, de la resistencia nominal de la matriz $(f^\sigma)_{\text{mat}}^N$ y de la resistencia nominal de la interface fibra-matriz $(f^\tau)_{\text{fib-mat}}^N$, o capacidad de transferencia de tensiones desde la matriz a la fibra. Desde otro punto de vista, se puede decir que la fibra participa dentro del compuesto en función de su propia resistencia y de la capacidad de transferencia de esfuerzo de la interfaz fibra-matriz, por lo tanto su resistencia está influenciada por el medio que la contiene y podría decirse que su tratamiento constitutivo implica una formulación no-local. Se define entonces la resistencia de una fibra contenida en una matriz como:

$$(f^\sigma)_{\text{fib}} = \min \left\{ (f^\sigma)_{\text{fib}}^N, (f^\sigma)_{\text{mat}}^N, \left[\frac{(f^\tau)_{\text{fib-mat}}^N \cdot 2\pi r_f}{A_f} \right] \right\} \quad (19)$$

en la que r_f representa el radio de la fibra y A_f es el área de la sección transversal del la fibra. A partir de la ecuación (19) se deducen los siguientes casos límites:

- Si la matriz es más resistente que la fibra y la adherencia fibra-matriz es perfecta, la capacidad de participación de la fibra queda limitada por su propia resistencia nominal $(f^\sigma)_{\text{fib}} \equiv (f^\sigma)_{\text{fib}}^N$.
- Si se produce un fallo en la matriz por microfisuras, etc., en tanto la fibra se mantiene en régimen lineal, la resistencia de la fibra queda limitada por la resistencia de la matriz, pues se rompe el “mecanismo” de transferencia de tensión entre fibra y matriz y no se podría transferir

más tensión que la permitida por el medio que contiene la fibra

$$(f^\sigma)_{\text{fib}} \equiv (f^\sigma)_{\text{mat}}^N .$$

- Si el fallo se produce en la interface fibra-matriz, la resistencia de la fibra queda limitada por la de la interface

$$(f^\sigma)_{\text{fib}} \equiv \frac{2 \cdot (f^\tau)_{\text{fib-mat}}^N \cdot 2 \pi r_f}{A_f} = \frac{2 \cdot (f^\tau)_{\text{fib-mat}}^N}{r_f} .$$

En la mayoría de los materiales compuestos se verifica que el agrietamiento por tensiones tangenciales en la interfaz se produce antes que la rotura de las fibras y se observa una separación masiva entre fibra y matriz y por lo tanto la resistencia de la fibra queda limitada por la capacidad de la interfaz de transmitir esfuerzos. La aparición de fenómenos plásticos en la matriz de un material compuesto sometido a un estado de cargas monótono creciente impide la transferencia de los esfuerzos desde la matriz hacia las fibras dando lugar a la aparición de deformaciones irreversibles por deslizamiento de la fase de refuerzo respecto de la matriz. A partir de este momento la transferencia de cargas de fibras a matriz no es nula debido a la presencia de fenómenos de fricción entre ambas fases del material compuesto. Por lo tanto, las fibras aumentan su estado tensional según un módulo elástico diferente del inicial.

4. EJEMPLO DE APLICACIÓN

A continuación se realiza una comparación de los resultados obtenidos en laboratorio [19] de una viga constituida de hormigón reforzado con fibras cortas de acero –DRAMIX–, con los que resultan de aplicar el modelo mencionado en este artículo a una discretización por elementos finitos de dicha viga.

4.1. Detalles del ensayo y la viga

El material compuesto utilizado en el ensayo de laboratorio es un hormigón de alta resistencia con humo de sílice reforzado con fibras cortas de acero en diferentes fracciones de volumen (0.0%, 0.5% y 1.0%).

Los materiales componentes del hormigón fueron cemento I 55-A (ASTM tipo III, CEN clase I 52.5), arena silícea (0-5 mm), arcilla (5-12 mm) y humo de sílice (ELKEM grado 920D). También se añadió súper plastificante GRACE Darcem 195 en la proporción de 25.4 litros/m³ de hormigón (súper plastificante seco/cemento = 1.5% en peso). Los valores medio de la resistencia a compresión $f_c = 86.4 \text{ MPa} (\pm 2.76\%)$, $f_c = 88.3 \text{ MPa} (\pm 2.82\%)$ y $f_c = 92.47 \text{ MPa} (\pm 5.39\%)$ para el 0.0%, 0.5% y 1.0% en volumen de fibra, respectivamente. Las fibras cortas fueron de acero tipo DRAMIX ZC30, con un límite elástico de 1150 MPa, 30 mm de longitud y 0.5 mm de diámetro.

Las vigas se construyeron en moldes de madera laminada, con el plano de carga vertical, echando el hormigón en dos capas compactadas por vibración.

Los ensayos se realizaron aplicando una carga de 1MN en un Instron 8505, bajo control de desplazamiento en el punto de aplicación de la carga Figura 5.

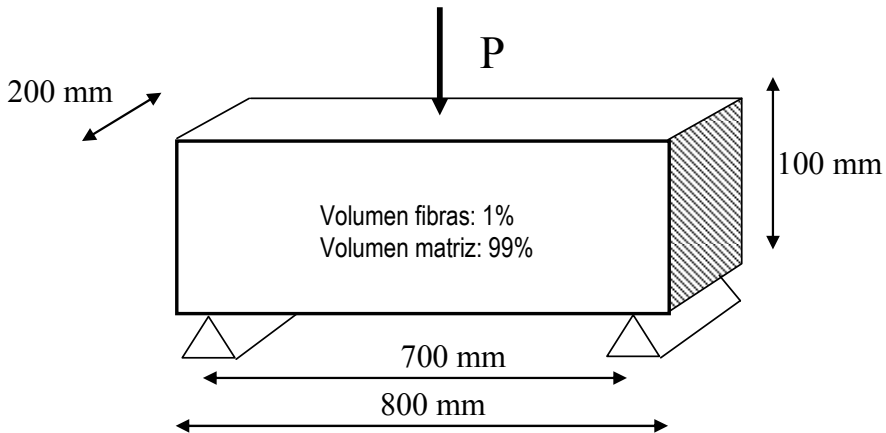


Figura 5 – Características geométricas de la viga del ensayo.

Tabla 2. Características mecánicas de los materiales componentes.

Propiedad	Matriz	Fibras (real)	Fibras (modificado)
Módulo de Young	50000 MPa	210000 MPa	190000 Mpa
Coefficiente de Poisson	0,17	0,25	0,25
Resistencia umbral a tracción	8,27 Mpa	1150 Mpa	277 Mpa
Resistencia umbral a compresión	82,7 Mpa	1150 Mpa	277 Mpa
Módulo de endurecimiento	Ablandamiento	0	0
Material simulado	Mohr-Coulomb, $\phi=30^\circ$	von-Mises	von.Mises
Energía de fractura	25 KN/m	3×10^6 KN/m	7.2×10^5
Energía de aplastamiento	2500 KN/m	3×10^6 KN/m	7.2×10^5

El problema por elementos finitos ha sido resuelto con 80 elementos de tensión plana con 4 nodos y dos grados de libertad por nodo, bajo la hipótesis de tensión cuasi-estática. A este modelo numérico se le ha incorporado el modelo constitutivo mencionado en apartados previos, considerando los siguientes tres casos:

- a- Hormigón 100%,

- b- Hormigón 99% + Fibras cortas metálicas 0.5% orientadas a 0° + Fibras cortas metálicas 0.5% orientadas a 90°,
- c- Hormigón 99% + Fibras cortas metálicas 0.3% orientadas a 0° + Fibras cortas metálicas 0.7% orientadas a 90°.

En las figuras que a continuación se muestran, puede verse la influencia de la ductilidad que añaden estas fibras cortas al hormigón simple. También puede verse la comparación de estos resultados numéricos con los experimentales.

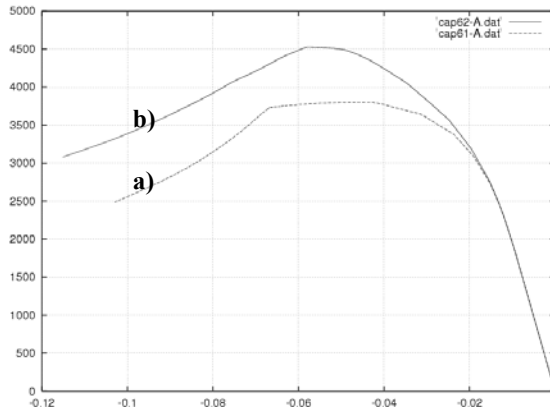


Figura 6 – Respuesta numérica Carga [$\times 10^6 \text{ N}$]– Desplazamiento [$\times 10^{-3} \text{ mm}$]: a) Hormigón (100%). b) Hormigón (99%)+ Fibra corta (0,5%-00)+ Fibra corta (0,5%-900)

En la Figura 6 puede verse la comparación entre la respuesta numérica de un hormigón simple y un hormigón con un 1% de fibras cortas, de las cuales la mitad de ellas está orientada según el eje longitudinal de las fibras (0°) y la otra mitad transversal a dicho eje (90°).

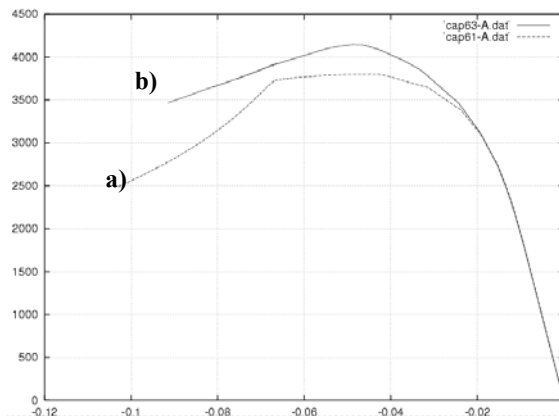


Figura 7 – Respuesta numérica Carga [$\times 10^6 \text{ N}$]– Desplazamiento [$\times 10^{-3} \text{ mm}$]: a) Hormigón (100%). b) Hormigón (99%)+ Fibra corta (0,3%-00)+ Fibra corta (0,7%-900)

Como puede verse en la Figura 7, la sola disminución de la proporción de fibras en la dirección longitudinal a 0° (de 0,5% a 0,3%), se produce una disminución de la carga máxima o carga de pico de 4500 N a 4200 N. Esta situación el material sea muy sensible a la orientación de dichas fibras.

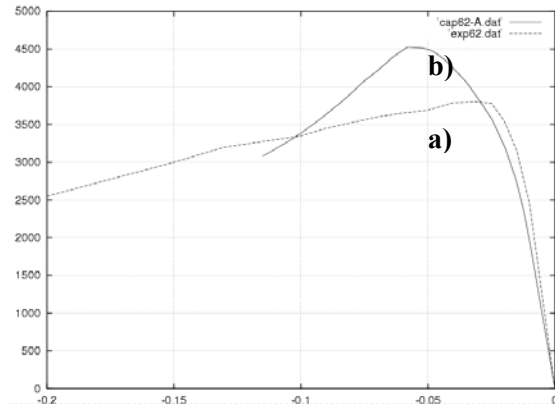


Figura 8 – Respuesta numérica Carga [$\times 10^5$ N]– Desplazamiento [$\times 10^{-2}$ mm]: a) Experimental. b) Hormigón (99%)+ Fibra corta (0,5%-00)+ Fibra corta (0,5%-900)

La Figura 8, muestra la comparación entre la respuesta numérica y experimental. En ella puede verse una diferencia en el nivel de la carga de pico que puede soportar la viga y se considera que esto se debe al problema de deslizamiento fibra matriz, del que no hay datos suficientes para ajustar el modelo.

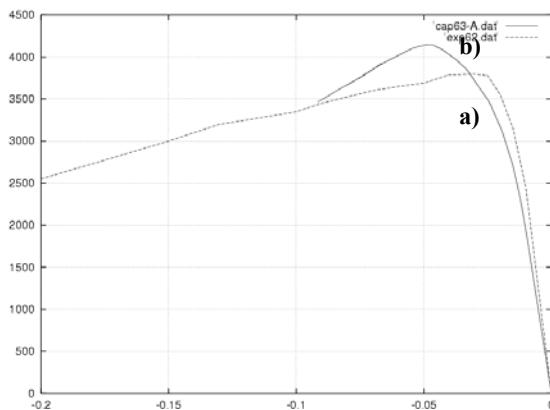


Figura 9 – Respuesta numérica Carga [$\times 10^5$ N]– Desplazamiento [$\times 10^{-2}$ mm]: a) Experimental. b) Hormigón (99%)+ Fibra corta (0,3%-00)+ Fibra corta (0,7%-900)

La Figura 9, muestra también la comparación entre la respuesta numérica y experimental. En ella nuevamente puede verse una diferencia en el nivel de la carga de pico que puede soportar la viga y se considera que esto se debe al

problema de deslizamiento fibra matriz, del que no hay datos suficientes para ajustar el modelo. A diferencia de la Figura 8, aquí puede verse que la diferencia entre la carga de pico entre la respuesta experimental y numérica es menor.

5. CONCLUSIONES

De todo esto surge como conclusión que la incorporación de fibras cortas en el hormigón mejora notablemente su ductilidad y por lo tanto se convierte en un material con mejores cualidades para su utilización estructural. Además, el cálculo y diseño de estructuras con este material es posible tratarlo en forma simplificada si se admite el cambio de las propiedades reales del material por otras que serían las denominadas propiedades efectivas. Esto permitiría utilizar estas nuevas propiedades dentro del esquema de cálculo simplificado tradicional que se realiza en el hormigón. No obstante esta simplificación, cabe decir que si se quiere estudiar el material en rotura es necesario incursionar la solución del mismo a través de las también denominadas propiedades equivalentes, pero prestando especial atención a los efectos no lineales del deslizamiento fibra matriz mediante la utilización del modelo constitutivo previamente presentado, dentro de la técnica de los elementos finitos.

Agradecimientos

Los autores agradecen a la DGICYT por la financiación concedida a través del contrato MAT2000-0741-C02-02 y al Ministerio de Fomento por el proyecto de investigación concedido en el área de la construcción civil.

Referencias

1. Miravete A. (2000). *Materiales Compuestos. Vol. 1 y Vol. 2*. Director de la obra: Antonio Miravete.
2. Car E. (2000). *Modelo constitutivo continuo para el estudio del comportamiento mecánico de los materiales compuestos*. Tesis Doctoral, Universidad Politécnica de Cataluña.
3. Paez A. (1979). *Hormigones fibrosos*. Universidad de Santander, Escuela de Ingenieros de Caminos Canales y Puertos.
4. Car E. (2000). *Modelo constitutivo continuo para el estudio del comportamiento mecánico de los materiales compuestos*. PhD thesis, Universidad Politécnica de Cataluña. Barcelona, España.
5. Zalamea F. (2000). *Tratamiento numérico de materiales compuestos mediante la teoría de homogeneización*. PhD thesis, Universidad Politécnica de Cataluña. Barcelona, España.
6. Trusdell, C. y Toupin, R. (1960). *The classical Field Theories*. Handbuch der Physik III/I. Springer Verlag, Berlin.
7. Oller S., Botello S., Miquel J. y Oñate E. (1995). “An anisotropic elastoplastic model based on an isotropic formulation”. *Engineering Computation*, 12 (3), pp. 245-262.

8. Car E., Oller S., Oñate E. (2001). "A large strain plasticity model for anisotropic materials – Composite material application". *International Journal of Plasticity*, 17, pp. 1437-1463.
9. Green A. and Naghdi P. (1965). "A dynamical theory of interacting continua". *Journal of Engineering Science*, 3 3-231.
10. Ortiz M. and Popov E. (1982). "A physical model for the inelasticity of concrete". *Proc. Roy. Soc. London*, A383, 101-125.
11. Ortiz M. and Popov E. (1982). "Plain concrete as a composite material". *Mechanics of Materials*, 1, 139-150.
12. Oller S., Oñate E., Miquel J., and Botello S. (1996). "A plastic damage constitutive model for composite materials". *Int. J. Solids and Structures*, 33 (17), 2501-2518.
13. Oller S., Oñate E. (1996). "A Hygro-Thermo-Mechanical constitutive model for multiphase composite materials". *Int. J. Solids and Structures*. Vol.33, (20-22), 3179-3186.
14. Jayatilaka, A. (1979). *Fracture of engineering brittle materials*. Applied Science Publishers
15. Car, E., Oller, S., & Oñate, E. (1997). "Un modelo constitutivo elasto-plástico acoplado con daño mecánico e higrométrico. Aplicación a pavimentos flexibles". U. de Brasilia (Ed.), *XVIII CILAMCE Congresso Ibero Latino-Americano de Métodos Computacionais Em Engenharia* (pp. 2100 - 2108). Brasilia.
16. Car, E., Oller, S., & Oñate, E. (1998). "Un modelo constitutivo elasto plástico acoplado con daño mecánico e higrométrico. Aplicación a pavimentos flexibles". *Rev. Int. de Ingeniería de Estructuras*, 3(1), 19 - 37
17. Beyerley D. and Spearing S. M. and Zok F. W. and Evans A. G. (1992). "Damage, degradation and failure in a unidirectional ceramic-matrix composite". *J. Am. Ceram. Soc.*, 75, pp. 2719-2725.
18. Pryce A. W. and Smith P. A. (1992). "Modelling of the stress/strain behavior of unidirectional ceramic matrix composite laminates". *J. Mater. Sci.*, 27, pp. 2695-2704.
19. Miravete A. (2000). *Materiales Compuestos. Vol. 1 y Vol. 2*. Director de la obra: Antonio Miravete.

Moment-curvature damage bridge piers subjected to horizontal loads

Sergio Oller and Alex H. Barbat

Escuela de Ingenieros de Caminos Canales y Puertos, Universidad Politécnica de Cataluña, Jordi Girona 1-3, CI, 08034 Barcelona, Spain.

ABSTRACT

The evaluation of the damage caused by horizontal loads, such as seismic action, to existing bridges has received an important attention in recent years, because it is the first step towards reducing casualties and economic losses. In damage detection and evaluation, the application of simple and reliable models has been prioritized, because they are necessary in further multi-analyses required by Monte Carlo simulations. A simplified moment-curvature damage model, capable of evaluating the expected seismic behaviour of RC highway bridges is proposed in this paper. The damage evaluation model is based on the mechanical modification of the cross sectional inertia of the bridge piers. The model was validated using experimental results obtained at the JRC Ispra for the Warth Bridge of Austria and also FEM analyses performed by other authors for the same bridge.

KEYWORDS: Damage estimation, continuum damage mechanics, damage constitutive model and moment curvature model.

INTRODUCTION

Nowadays, the evaluation of the damage caused by earthquakes in existing bridges received great attention. Numerous researches devoted to the structural damage evaluation have been performed, most of them considering the seismic behavior of buildings. The structural damage in the bridges can be characterized in two ways:

1. In the first way, the structural damage is evaluated at given points of the structure by means of local constitutive models describing the damage accumulation caused by a local micro-structural damage [13, 19, 21, 28].
2. In the second way, the local damage is used for the evaluation of global damage indices, which are scalars depending on some variables (or damage parameters) that characterize the dynamic response of the whole system [1, 2, 24].

This paper proposes a damage evaluation based on structural analysis for RC highway bridges with simple pier bents. This typology of bridges was very used all

over Europe during the 1960-1980 periods. The proposed structural model is based on the hypothesis of the *flexible pier-rigid deck* behaviour of the structure subjected to seismic loads. A flexible pier-rigid deck simplified model was therefore developed, which could be extending after some modification to other typologies of bridges. This model has been chosen after studying the responses correlation between the proposed model and the real structure [9]. Accordingly, the overall seismic behaviour of this bridge typology is decisively influenced by the damage of the piers. Therefore, the study of the damage produced by horizontal loads has been centered on the piers of the bridge [9], while the structural study of the deck has been performed after the structural analysis of the piers, in an uncoupled way. Thus, the maximum damage of the piers under horizontal loads is the principal aim of the proposed structural damage evaluation procedure.

A local damage index, which describes the state of the material at each point of the structure, is the starting point of the proposed method and is based on a constitutive damage law. Details on this constitutive law are given in the Annex of the paper. The global damage of each pier is obtained from the inertia reduction of the cross sections due to the material degradation. The validation of the proposed model was carried out by using the experimental tests on scale models of the piers of the Warth Bridge, Austria, carried out at the Joint Research Center of Ispra, Italy [25] and a FE model developed by R. Faria [8].

The proposed model permits a simple, reliable and efficient structural analysis. Therefore, it is suitable for considering uncertainties in its parameters and for using Monte Carlo simulations with the aim of evaluating the seismic vulnerability of bridges.

STRUCTURAL DESCRIPTION OF THE DYNAMIC MODEL

Reinforced concrete highway bridges with simple pier bents have greater redundancy and higher strength in their longitudinal direction; therefore they will undergo greater damage when subjected to transversal seismic actions. The proposed model aims studying the bridge response to horizontal loads acting transversally to the direction of the bridge axis. Experimental studies confirm that the structural system can be modeled simply by piers loaded transversally to the axis of the bridge interconnected at the deck level by means of box girders [9, 23]. Due to the high stiffness of the bridge in longitudinal direction, the structural analysis in this direction is out of the purposes of this work, focusing on the structural study of the pier in transversal direction.

The model has continuous elements with distributed mass for the piers and concentrated mass for the girders. The motion of the n_p piers in transversal direction to the bridge axis is partially restricted by the adjacent girders that are

supported by laminated neoprene bearings. Thus, the displacement of piers causes the distortion of the bearings and the consequent rotation of the adjacent girders. The simplified model shown in Figure 1 is based on the following general hypotheses:

1. The piers are continuous elements with distributed mass and infinite axial stiffness.
2. The girders are perfectly stiff elements concentrating the mass at the top of the piers.
3. The bearings of the girders are equivalent short elements that work to shear, having circular cross section and real dimensions.
4. The soil-structure interaction effect on piers and abutments is considered by means of linear springs that represent the rotational stiffness of the soil.
5. The abutments are perfectly stiff.

Accordingly, the model has as many degrees of freedom as transversal displacements at the top of the piers, that is, n_p degrees of freedom.

In following sections, the traverse stiffness of an isolated pier under non lineal damage effects produced by a horizontal load applied at the deck level will be studied.

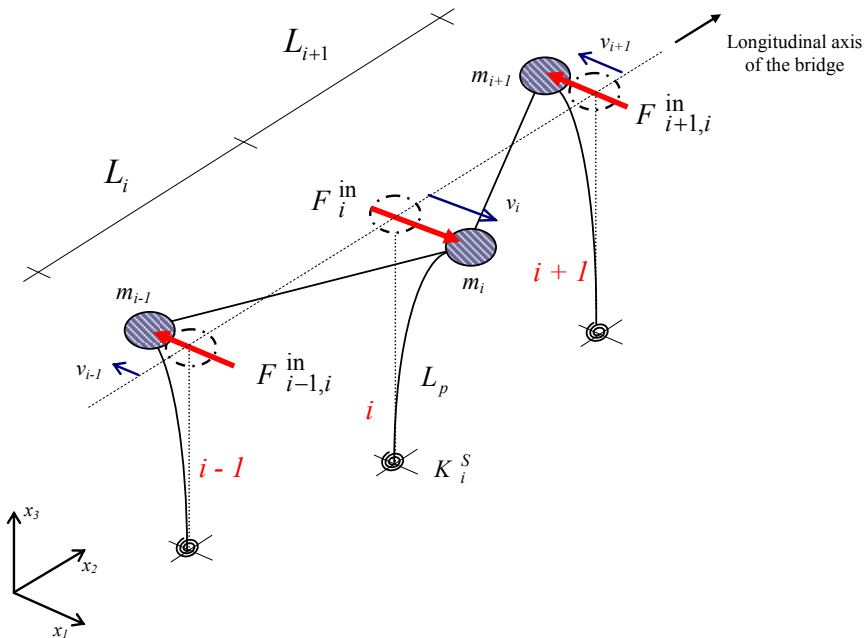


Figure 1. Model for the seismic analysis of the bridge

Transversal behaviour of a single pier

According to the general hypotheses and to Figure 2, the maximum displacement at the top of a pier is

$$v_i = v_\theta^i + v_p^i \quad (1)$$

where

$$v_\theta^i = \theta^i L_p^i = \frac{M_i^{\max}}{K_i^S} \quad (2)$$

is the elastic displacement produced by a rotation at the base of the pier, and

$$v_p^i = \frac{[11(q_i^{\text{in}})^{\max} + 4(q_i^{\text{in}})^{\min}](L_p^i)^4}{120 E_{c_i} I_i} + \frac{F_i^{\text{in}}(L_p^i)^3}{3 E_{c_i} I_i} \quad (3)$$

is the elastic displacement produced by external actions [9]. In equations (2) and (3), θ^i is the rotation due to the soil-structure interaction effect, M_i^{\max} is the maximum bending moment at the base of the pier, K_i^S is the equivalent stiffness of the soil, $(q_i^{\text{in}})^{\max}$ and $(q_i^{\text{in}})^{\min}$ are the maximum and minimum inertial loads by unit length produced by the horizontal acceleration, F_i^{in} is the total inertial force due to the bridge deck and L_p^i , E_{c_i} and I_i are the length, Young's modulus and the inertia of the reinforced concrete cross section of the pier, respectively.

For the maximum displacement of the pier (for $x_3 = 0$), the bending moment equation is [9]

$$M_i(x_3 = 0) = M_i^{\max} = \frac{[2(q_i^{\text{in}})^{\max} + (q_i^{\text{in}})^{\min}](L_p^i)^2}{6} + (F_i^{\text{in}} L_p^i) \quad (4)$$

Substituting equations (2), (3) and (4) into Equation (1), the equivalent internal force at the top of the pier is obtained in function of the maximum displacement v_i of the pier [9]

$$F_i^{\text{in}} = \frac{I}{\left[\frac{L_p^i}{K_i^S} + \frac{(L_p^i)^3}{3 E_{c_i} I_i} \right]} \left[v_i - \frac{[2(q_i^{\text{in}})^{\max} + (q_i^{\text{in}})^{\min}](L_p^i)^2}{6 K_i^S} - \frac{[11(q_i^{\text{in}})^{\max} + 4(q_i^{\text{in}})^{\min}](L_p^i)^4}{120 E_{c_i} I_i} \right] \quad (5)$$

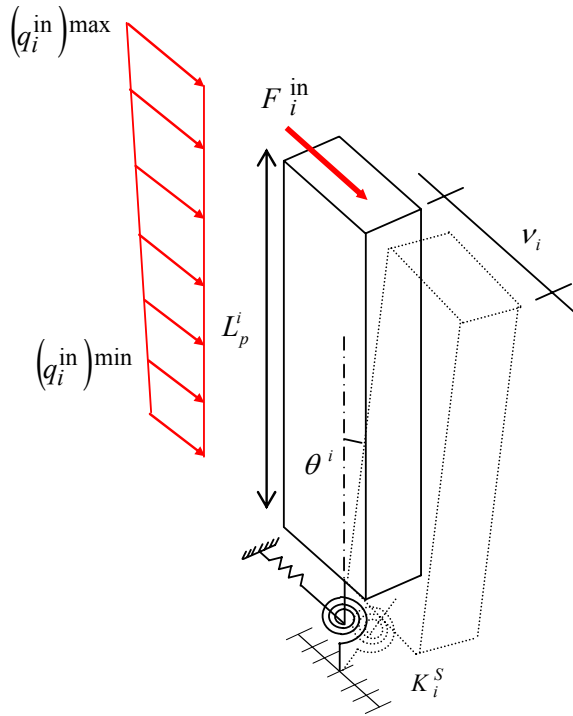


Figure 2. Transversal displacements of pier *I* considering the soil effect

NON-LINEAR ANALYSIS OF THE PIER

When the non-linear behavior of the structural materials is taken into account, the undamped equation of motion for each pier is written as

$$m_i a_i + F_i^{\text{in}} - \Delta F_i^R = 0 \quad (6)$$

where ΔF_i^R is the residual or out-of-balance force. This unbalanced force is due to the fact that the cross-section inertia and Young modulus are not constant during the non linear process and consequently the solution of Equation (6) should be obtained throughout an iterative process using a non-linear Newmark approach [3, 7].

The changes of the pier stiffness and of the internal cross sectional force depend on the damage level reached at each point of the pier whose numerical evaluation is carried out by means of the continuum damage model (see the Annex). In this work, the damage model [19] is used to calculate the local damage index at each

point of the structure. Then, by means of a numerical integration of the local damage indices on the cross-section at the base of the piers, the area and the inertia of the damaged cross section are obtained. Obviously, it is possible to obtain the damage evolution at each cross section of the pier, but the moment-curvature model requires the evaluation of damage only at the most loaded section (base cross section).

To obtain the response and the maximum damage of all the bridge piers using the proposed model, Newmark's non-linear algorithm, summarized in Box 1, is used to solve the equilibrium equation at each time of the process. In this analysis the balance force condition is achieved by eliminating $\Delta \mathbf{F}_i^R$ using a Newton-Raphson process. Indirectly, this process also eliminates the residual bending moment $\Delta \mathbf{M} = \mathbf{M}^0 - \mathbf{M}^{\text{int}}$ included in the residual force array, which is the difference between the maximum elastic external moment, \mathbf{M}^0 , and the pier internal strength capacity moment, \mathbf{M}^{int} . For each step of the non-linear analysis the properties of the system are updated, considering the local degradation of the material caused by the seismic action.

Box 1. Solution of the non-linear equilibrium equation applied for the bridge using Newmark's method.

1. **Displacement and velocity prediction at "t + Δt", starting from null initial conditions**

$$\begin{aligned}\ddot{\tilde{\mathbf{U}}}^{t+\Delta t} &= 0 ; \dot{\tilde{\mathbf{U}}}^{t+\Delta t} = \dot{\mathbf{U}}^t + (1-\gamma) \ddot{\mathbf{U}}^t \Delta t ; \\ \tilde{\mathbf{U}}^{t+\Delta t} &= \mathbf{U}^t + \dot{\mathbf{U}}^t \Delta t + \left(\frac{1}{2}-\beta\right) \ddot{\mathbf{U}}^t \Delta t^2 ; \quad {}^i \Delta \mathbf{F}^{t+\Delta t} = \mathbf{F}_i^q\end{aligned}$$

2. **Computation of displacement increment $\Delta \mathbf{U}^{t+\Delta t}$ at instant t + Δt, starting from the linearized balance equation**

$${}^i \Delta \mathbf{F}^{t+\Delta t} = {}^i \mathbf{J}^{t+\Delta t} {}^{i+1} \Delta \ddot{\mathbf{U}}^{t+\Delta t} \quad ; \quad {}^i \mathbf{J}^{t+\Delta t} = \left[\mathbf{M} \cdot \left(\frac{1}{\beta \Delta t^2} \right) + \mathbf{K} \right]^{t+\Delta t}$$

3. **Displacement and velocity correction**

$${}^{i+1} \ddot{\mathbf{U}}^{t+\Delta t} = \left(\frac{1}{\beta \Delta t^2} \right) {}^{i+1} \Delta \ddot{\mathbf{U}}^{t+\Delta t} ; \quad {}^{i+1} \dot{\mathbf{U}}^{t+\Delta t} = \dot{\tilde{\mathbf{U}}}^{t+\Delta t} + \left(\frac{\gamma}{\beta \Delta t} \right) {}^{i+1} \Delta \mathbf{U}^{t+\Delta t} ; \quad {}^{i+1} \mathbf{U}^{t+\Delta t} = \tilde{\mathbf{U}}^{t+\Delta t} + {}^{i+1} \Delta \mathbf{U}^{t+\Delta t}$$

4. **Loop over k bridge piers.** The damage constitutive equation are computed at each pier k and at each cross section (see next section and Box 2 for more details)

4a. **Computation of the generalized forces (predictor) and the elastic curvatures and axial strain** at each cross section x_3 , using the displacement ${}^{i+1} \mathbf{U}^{t+\Delta t}$ at the top of pier k

$$M_1^0(x_3) = \frac{(L_p^k - x_3)}{\frac{(L_p^k)^2}{K_k^S} + \frac{(L_p^k)^3}{3E_{ck}^0(I_k(0))_{11}}} {}^{i+1} [v_2(L_p^k)]_k^{t+\Delta t} ; M_2^0(x_3) = \frac{(L_p^k - x_3)}{\frac{(L_p^k)^2}{K_k^S} + \frac{(L_p^k)^3}{3E_{ck}^0(I_k(0))_{22}}} {}^{i+1} [v_1(L_p^k)]_k^{t+\Delta t}$$

$$N^0(x_3) = N^{ap} ; [\hat{\sigma}^0(x_3)]_k = \begin{cases} N^0(x_3) \\ M_1^0(x_3) \\ M_2^0(x_3) \end{cases} ; [{}^{i+1} \mathbf{U}^{t+\Delta t}(x_3)]_k = \begin{cases} [u(x_3)]_k \\ [v_1(x_3)]_k \\ [v_2(x_3)]_k \end{cases} {}^{i+1}$$

4b. Computation of the residual flexural moment

For the first load step : $[J(x_3)]_k \equiv [J^0(x_3)]_k ; [\hat{\sigma}^{int}(x_3)]_k = \mathbf{0}$

$$[\Delta \hat{\sigma}(x_3)]_k = [\hat{\sigma}^0(x_3) - \hat{\sigma}^{int}(x_3)]_k \stackrel{\text{Unbalanced equivalent force}}{=} [{}^{i+1} \Delta \mathbf{f}^{t+\Delta t}(x_3)]_k = \begin{cases} {}^{i+1} \Delta N^{t+\Delta t}(x_3) \\ {}^{i+1} \Delta M_1^{t+\Delta t}(x_3) / L_p^k \\ {}^{i+1} \Delta M_2^{t+\Delta t}(x_3) / L_p^k \end{cases} {}^{i+1}$$

4c. Balance equation verification on the clamped cross section

$$\|\Delta \hat{\sigma}(0)\| = \begin{cases} ? & \Rightarrow \text{go to EXIT} \\ \neq 0 & \Rightarrow \text{Continue} \end{cases}$$

4d. Computation of the incremental generalized strains and their current value

$$\begin{aligned} [{}^{n+1} \Delta \hat{\epsilon}^{t+\Delta t}(0)]_k &= -[{}^n \mathbf{J}^{n+1}(0)]_k^{-1} [{}^n \Delta \hat{\sigma}^{t+\Delta t}(0)]_k \\ [{}^{n+1} \hat{\epsilon}^{t+\Delta t}(0)]_k &= [{}^n \hat{\epsilon}^{t+\Delta t}(0)]_k + [{}^{n+1} \Delta \hat{\epsilon}^{t+\Delta t}(0)]_k \end{aligned}$$

4e. Damaged inertia computation at the base cross section of pier k (see Box 2)

5. **Back to point 4b** followed by the minimization of generalized unbalanced force equation.

6. **Calculate the displacement at each point x_3 of the pier and EXIT.**

$$\begin{aligned} [{}^{i+1} \mathbf{U}^{t+\Delta t}(x_3)]_k &= \begin{Bmatrix} [u(x_3)]_k \\ [v_1(x_3)]_k \\ [v_2(x_3)]_k \end{Bmatrix} {}^{i+1} = \begin{Bmatrix} [u(x_3 - \Delta x_3)]_k \\ [v_1(x_3 - \Delta x_3)]_k \\ [v_2(x_3 - \Delta x_3)]_k \end{Bmatrix} {}^{i+1} - \begin{Bmatrix} [\epsilon^N(x_3 - \Delta x_3)]_k \cdot \Delta x_3 \\ [\varphi_2(x_3 - \Delta x_3)]_k \cdot \Delta x_3 \\ [\varphi_1(x_3 - \Delta x_3)]_k \cdot \Delta x_3 \end{Bmatrix} {}^{i+1} \\ &+ \begin{Bmatrix} 0 \\ \frac{[\chi_2(x_3 - \Delta x_3)]_k}{2} \cdot \Delta x_3^2 \\ \frac{[\chi_1(x_3 - \Delta x_3)]_k}{2} \cdot \Delta x_3^2 \end{Bmatrix} {}^{i+1} \\ [{}^{i+1} [\varphi_1(x_3)]_k] &= [{}^{i+1} [\varphi_1(x_3 - \Delta x_3)]_k] + [{}^{i+1} [\chi_1(x_3 - \Delta x_3)]_k \cdot \Delta x_3] \\ [{}^{i+1} [\varphi_2(x_3)]_k] &= [{}^{i+1} [\varphi_2(x_3 - \Delta x_3)]_k] + [{}^{i+1} [\chi_2(x_3 - \Delta x_3)]_k \cdot \Delta x_3] \end{aligned}$$

7. **Back to point 2** after the damage evaluation over all the piers and balance equation over the complete bridge $\|{}^i \Delta \mathbf{f}^{t+\Delta t}\| \rightarrow 0$ verification.

8. **New time increment and dynamic load application over all the bridge.** Back to point 1.

Solution of the dynamic equation of equilibrium

The steps to define the damage in any pier of the bridge are described in boxes 1 and 2. The maximum global damage index of the structure is obtained starting from the cross-sectional damage calculated at the base of the piers for transversal seismic actions. Box 1 shows the numerical procedure to solve the dynamic balance equation (6) using Newmark's non-linear method. As shown previously, the type of bridge under study is modeled by means the piers that behaves like cantilever beams, for which the numerical integration of the damage on the cross section can be simplified, considering in the analysis only the cross-section at the pier base, that is, for $x_3 = 0$. Nevertheless, the procedure could be generalized including when necessary other cross-sections at levels x_3 in the damage integration procedure.

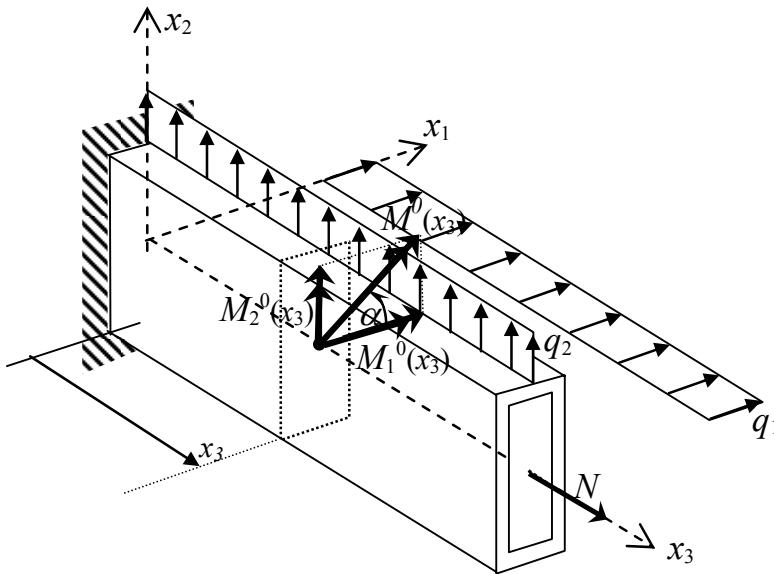


Figure 3. Bridge pier represented as a cantilever Bernoulli beam

STUDY OF THE DAMAGED CROSS SECTION FOR SKEW BENDING

Theoretical aspects

In order to define the inertia and the bending moment of the damaged base cross section of a pier required by the solution of the non linear equation (6) –see Box 1–, the isotropic damage model [19] has been applied (see Annex). In this section, the way of computing the local damage and its contribution to the cross sectional

damage of a pier is described for Bernoulli beams subjected to skew bending. For this purpose, the damaged cantilever beam under skew bending of Figure 3 is considered.

The external loads produce the following generalized forces in a cross section located at a distance x_3

$$\hat{\mathbf{\sigma}}^0(x_3) = \begin{Bmatrix} N^0(x_3) \\ M_1^0(x_3) \\ M_2^0(x_3) \end{Bmatrix} = \begin{Bmatrix} N^0(x_3) \\ M^0(x_3) \cdot \cos \alpha \\ M^0(x_3) \cdot \sin \alpha \end{Bmatrix} \quad (7)$$

The following strain and curvature of the Bernoulli beam, due to the elastic bending moment of Equation (7), will be taken as the predictor variables of the algorithm

$$\begin{aligned} \varepsilon^N(x_3) &= \frac{du(x_3)}{dx_3} = \frac{N(x_3)}{E^0 A^0} \\ \chi_1(x_3) &= -\frac{d^2 v_2(x_3)}{dx_3^2} = \frac{M_1^0(x_3)}{E^0 I_{11}^0} \\ \chi_2(x_3) &= -\frac{d^2 v_1(x_3)}{dx_3^2} = \frac{M_2^0(x_3)}{E^0 I_{22}^0} \end{aligned} \quad (8)$$

being E^0 the initial undamaged elasticity module, A^0 the initial area of the undamaged cross section and I_{ii}^0 the initial inertia of the undamaged of cross section regarding the principal reference system for $x_i \quad \forall i = 1,2$.

Considering the Bernoulli beam basic hypotheses, the expressions (9) for the strain and stress fields are obtained.

All the previous descriptions have been made for a linear elastic skew axial-bending problem. Thus, the material has limitless capacity to resist the applied loads as expressed in Equation (9). This threshold is not possible to be reached for a real material, because its strength is limited to c^{\max} , as it can be seen in Equation (A.8) of the Annex. Therefore, the initial generalized internal forces $\hat{\mathbf{\sigma}}^0(x_3)$ produced by the external loads $\mathbf{F}^0(x_3)$ are initially unbalanced with the generalized internal stresses $\hat{\mathbf{\sigma}}(x_3)$, producing unbalanced residual generalized internal forces $\Delta \hat{\mathbf{\sigma}}(x_3)$. These residual stresses should be zero due to the equilibrium condition and this

state is reached by increasing the curvature $\Delta\chi(x_3)$ and axial strain $\Delta\varepsilon^N(x_3)$ of the beam.

$$\left\{ \begin{array}{l}
 \varepsilon(x_1, x_2, x_3) = \varepsilon^N(x_3) + \chi_1(x_3) \cdot x_2 + \chi_2(x_3) \cdot x_1 = \frac{N^0(x_3)}{E^0 A^0} + \frac{M_1^0(x_3)}{E^0 I_{11}^0} x_2 + \frac{M_2^0(x_3)}{E^0 I_{22}^0} x_1 \\
 = \{1 \quad x_2 \quad x_1\} \cdot \begin{bmatrix} E^0 A^0 & 0 & 0 \\ 0 & E^0 I_{11}^0 & 0 \\ 0 & 0 & E^0 I_{22}^0 \end{bmatrix}^{-1} \cdot \begin{Bmatrix} N^0(x_3) \\ M_1^0(x_3) \\ M_2^0(x_3) \end{Bmatrix} \\
 \sigma(x_1, x_2, x_3) = E^0 \cdot \varepsilon(x_1, x_2, x_3) = \frac{N^0(x_3)}{A^0} + \frac{M_1^0(x_3)}{I_{11}^0} x_2 + \frac{M_2^0(x_3)}{I_{22}^0} x_1 \\
 = \{1 \quad x_2 \quad x_1\} \cdot \begin{bmatrix} A^0 & 0 & 0 \\ 0 & I_{11}^0 & 0 \\ 0 & 0 & I_{22}^0 \end{bmatrix}^{-1} \cdot \begin{Bmatrix} N^0(x_3) \\ M_1^0(x_3) \\ M_2^0(x_3) \end{Bmatrix} \\
 = \mathbf{x}^T \cdot [\mathbf{J}^0]^{-1} \cdot \hat{\boldsymbol{\sigma}}^0(x_3)
 \end{array} \right. \quad (9)$$

This procedure is iterative and starts with the linearization of the following unbalanced equilibrium equation at each cross section of the beam:

$$\Delta\hat{\boldsymbol{\sigma}}(x_3) = [\hat{\boldsymbol{\sigma}}^0(x_3) - \hat{\boldsymbol{\sigma}}^{\text{int}}(x_3)] \rightarrow \mathbf{0}$$

$$\left\{ \begin{array}{l} \Delta N(x_3) \\ \Delta M_1(x_3) \\ \Delta M_2(x_3) \end{array} \right\} = \left\{ \begin{array}{l} N^0(x_3) \\ M_1^0(x_3) \\ M_2^0(x_3) \end{array} \right\} - \left\{ \begin{array}{l} \int_A \sigma(x_1, x_2, x_3) \cdot dA \\ \int_A \sigma(x_1, x_2, x_3) \cdot x_2 dA \\ \int_A \sigma(x_1, x_2, x_3) \cdot x_1 dA \end{array} \right\} \rightarrow \mathbf{0} \quad (10)$$

where the stress at each point of the cross section is obtained by using the constitutive damage model briefly described by the following equations:

$$\sigma(x_1, x_2, x_3) = E(x_1, x_2, x_3) \cdot \varepsilon(x_1, x_2, x_3) = E(x_1, x_2, x_3) \cdot [\varepsilon^N(x_3) + \chi_1(x_3) \cdot x_2 + \chi_2(x_3) \cdot x_1] \quad (11)$$

with: $E(x_1, x_2, x_3) = f(x_1, x_2, x_3) \cdot E^0$

According to the Annex, the evolution of the local damage internal variable at each point of each cross section of the Bernoulli beam, obtained from the local damage

constitutive model, is $f(x_1, x_2, x_3) = (1 - d(x_1, x_2, x_3)) = \frac{c^{\max}}{c} e^{A(1 - \frac{c(d)}{c^{\max}})}$, with

$0 \leq c^{\max} \leq c$. The values c^{\max} and c are the maximum and current tension strength at each point of the solid, A is a parameter depending of the fracture energy and

$E(x_1, x_2, x_3) = f(x_1, x_2, x_3) \cdot E^0$ is the damaged elastic module. Substituting this expression in Equation (10), the residual forces become

$$\begin{aligned} \left\{ \begin{array}{l} \Delta N(x_3) \\ \Delta M_1(x_3) \\ \Delta M_2(x_3) \end{array} \right\} &= \left\{ \begin{array}{l} N^0(x_3) \\ M_1^0(x_3) \\ M_2^0(x_3) \end{array} \right\} - \left\{ \begin{array}{l} E^0 \cdot \int_A f(x_1, x_2, x_3) \cdot (\varepsilon^N(x_3) + \chi_1(x_3) \cdot x_2 + \chi_2(x_3) \cdot x_1) dA \\ E^0 \cdot \int_A f(x_1, x_2, x_3) \cdot (\varepsilon^N(x_3) \cdot x_2 + \chi_1(x_3) \cdot x_2^2 + \chi_2(x_3) \cdot x_1 \cdot x_2) dA \\ E^0 \cdot \int_A f(x_1, x_2, x_3) \cdot (\varepsilon^N(x_3) \cdot x_1 + \chi_1(x_3) \cdot x_2 \cdot x_1 + \chi_2(x_3) \cdot x_1^2) dA \end{array} \right\} \\ \left\{ \begin{array}{l} \Delta N(x_3) \\ \Delta M_1(x_3) \\ \Delta M_2(x_3) \end{array} \right\} &= \left\{ \begin{array}{l} N^0(x_3) \\ M_1^0(x_3) \\ M_2^0(x_3) \end{array} \right\} - \left\{ \begin{array}{l} E^0 \cdot (\varepsilon^N(x_3) \cdot A(x_3) + \chi_1(x_3) \cdot m_1(x_3) + \chi_2(x_3) \cdot m_2(x_3)) \\ E^0 \cdot (\varepsilon^N(x_3) \cdot m_1(x_3) + \chi_1(x_3) \cdot I_{11}(x_3) + \chi_2(x_3) \cdot I_{12}(x_3)) \\ E^0 \cdot (\varepsilon^N(x_3) \cdot m_2(x_3) + \chi_1(x_3) \cdot I_{21}(x_3) + \chi_2(x_3) \cdot I_{22}(x_3)) \end{array} \right\} \\ \left\{ \begin{array}{l} \Delta N(x_3) \\ \Delta M_1(x_3) \\ \Delta M_2(x_3) \end{array} \right\} &= \left\{ \begin{array}{l} N^0(x_3) \\ M_1^0(x_3) \\ M_2^0(x_3) \end{array} \right\} - E^0 \cdot \begin{bmatrix} A(x_3) & m_1(x_3) & m_2(x_3) \\ m_1(x_3) & I_{11}(x_3) & I_{12}(x_3) \\ m_2(x_3) & I_{21}(x_3) & I_{22}(x_3) \end{bmatrix} \left\{ \begin{array}{l} \varepsilon^N(x_3) \\ \chi_1(x_3) \\ \chi_2(x_3) \end{array} \right\} \end{aligned} \quad (12)$$

$$\Delta \hat{\sigma}(x_3) = \hat{\sigma}^0(x_3) - E^0 \cdot [\mathbf{J}] \cdot \hat{\varepsilon}(x_3)$$

In this equation, $A(x_3) = \int_A f(x_1, x_2, x_3) \cdot dA$ is the damaged cross section, $m_i(x_3) = \int_A f(x_1, x_2, x_3) \cdot x_j dA$ are the moment of the damaged area respecting the x_i centroidal principal axes (initially, for undamaged cross section, it is equal to zero), $I_{ii}(x_3) = \int_A f(x_1, x_2, x_3) \cdot x_j^2 dA$ are the damaged inertia corresponding to the same principal axes x_i and $I_{ij}(x_3) = \int_A f(x_1, x_2, x_3) \cdot (x_j \cdot x_i) dA$ are the damaged inertia products regarding to the same principal axes ($x_i \ x_j$). Notice that the principal inertia axes at certain time instant of the process can change their position in a next instant due to the damage of the cross section of the beam; consequently the damaged inertia products related to the changed axes can be not equal to zero.

Numerical evaluation of the inertia of the damaged cross-section

Due to the difficulties in performing a closed integration of the nonlinear equation (12) using the non-linear damage function defined by Equation (11), the inertia tensor and the area of the damaged cross section is calculated by means of a numerical algorithm (see Box 2). It is important to note that the selected integration algorithm requires to consider that one of the points at which the function to be integrated is located is on the border of the cross section, allowing to capture appropriately the evolution of the damage.

When the cross section of the pier to be analyzed has a rectangular shape, the described procedure is applied directly. However, if the piers have a box shape, the inertia of the damaged cross section is obtained by dividing the element into four

subsections, as shown in Figure 4. For each subsection, the damaged area, $A(x_3)_{(j)}$, is

$$A(x_3)_{(j)} = \int_{A_{(j)}} f(x_1, x_2, x_3) dA \quad (13)$$

and the distance between the neutral axes of each sub cross section and the global neutral axis of the complete cross section is calculated. The global inertia of the damaged cross section, $\mathbf{I}_T(x_3)_{(j)}$, is then defined by

$$\begin{aligned} \mathbf{I}_T(x_3)_{(j)} &= \sum_{j=1}^4 \mathbf{I}_{(j)} + A(x_3)_{(j)} \cdot \mathbf{X}^2_{(j)} = \\ &= \sum_{j=1}^4 \left\{ \begin{aligned} &\left[\begin{array}{cc} \int_{A_{(j)}} f(x_1, x_2, x_3) \cdot x_2^2 dA & \int_{A_{(j)}} f(x_1, x_2, x_3) \cdot x_2 \cdot x_1 dA \\ \int_{A_{(j)}} f(x_1, x_2, x_3) \cdot x_1 \cdot x_2 dA & \int_{A_{(j)}} f(x_1, x_2, x_3) \cdot x_1^2 dA \end{array} \right] + \\ &+ \left[\int_{A_{(j)}} f(x_1, x_2, x_3) dA \right] \cdot \begin{bmatrix} X_{2(j)}^2 & X_{2(j)} X_{1(j)} \\ X_{1(j)} X_{2(j)} & X_{1(j)}^2 \end{bmatrix} \end{aligned} \right\} \end{aligned} \quad (14)$$

where $\mathbf{I}_{(j)}$ is the damaged inertia of subsection j , evaluated by means of Equation (14), $A_{(j)}$ is the damaged area of the subsection j and $\mathbf{X}^2_{(j)}$ are the distances between the neutral axis of the subsections and the global neutral axis of the whole cross-section, which depend on the damage at the cross section. In the equations (13) and (14), the numerical integration has been carried out following its classical form

$$\begin{aligned} A(x_3)_{(j)} &= \int_{A_{(j)}} f(x_1, x_2, x_3) \cdot dA = J_{acob} \cdot \left[\sum_{p=1}^n \sum_{q=1}^n w_p \cdot w_q [f(\xi_1, \xi_2, x_3)] \right]_{(j)} \\ m_i(x_3)_{(j)} &= \int_{A_{(j)}} f(x_1, x_2, x_3) \cdot x_j dA = J_{acob} \cdot \left[\sum_{p=1}^n \sum_{q=1}^n w_p \cdot w_q [f(\xi_1, \xi_2, x_3) \cdot \xi_j] \right]_{(j)} \\ I_{ii}(x_3)_{(j)} &= \int_{A_{(j)}} f(x_1, x_2, x_3) \cdot x_j^2 dA = J_{acob} \cdot \left[\sum_{p=1}^n \sum_{q=1}^n w_p \cdot w_q [f(\xi_1, \xi_2, x_3) \cdot \xi_j^2] \right]_{(j)} \\ I_{ij}(x_3)_{(j)} &= \int_{A_{(j)}} f(x_1, x_2, x_3) \cdot x_j \cdot x_i dA = J_{acob} \cdot \left[\sum_{p=1}^n \sum_{q=1}^n w_p \cdot w_q [f(\xi_1, \xi_2, x_3) \cdot \xi_j \cdot \xi_i] \right]_{(j)} \end{aligned} \quad (15)$$

where J_{acob} is the determinant of the gradient of the strains, w_p and w_q are the numerical weight coefficients, ξ_1 and ξ_2 are the isoparametric normalized coordinates and n is the order of the quadrature of the numerical integration (see Zienkiewicz and Taylor [28]). Particularly, when damage occurs due to the external load, the position of the neutral axis of each subsection is modified according to the area of the subsection that is damaged. This modification must be reflected in the calculation of the distances to the global neutral axis of each subsection. Thus, to obtain each $\mathbf{X}^2_{(j)}$, it is necessary to know the coordinates $X_{1(j)}$ and $X_{2(j)}$ for each subsection, which are evaluated in a general form by means of the following equations:

$$X_{1(j)} = \left[\frac{\int_{A(j)} x_1 f(x_1, x_2, x_3) dA}{\int_{A(j)} f(x_1, x_2, x_3) dA} \right]; X_{2(j)} = \left[\frac{\int_{A(j)} x_2 f(x_1, x_2, x_3) dA}{\int_{A(j)} f(x_1, x_2, x_3) dA} \right] \quad (16)$$

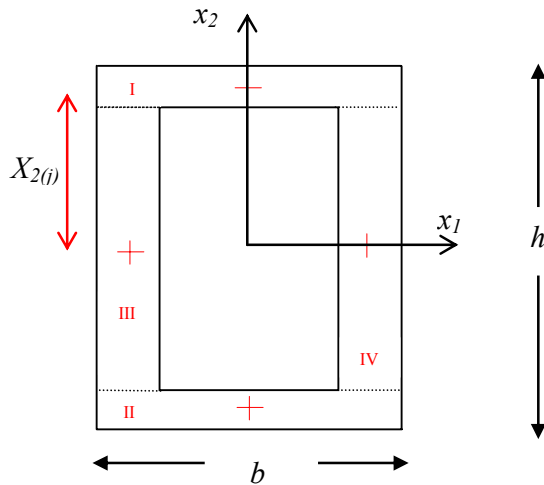


Figure 4. Subsections of a box cross section.

Linearization of the unbalanced equilibrium equation

Linearizing Equation (10) and using the Newton-Raphson procedure, the cross section equilibrium equation is solved by successive iterations, increasing the curvature and axial strain of the pier in the corresponding cross section. For this purpose, the generalized strains (axial strain and bending moment) at increment $(n+1)$ and instant $(t + \Delta t)$ is written by means of Taylor series, truncated at its first term, and then forced to zero

$$\begin{aligned}
\mathbf{0} &= {}^{n+1}\Delta\hat{\boldsymbol{\sigma}}^{t+\Delta t}(x_3) \cong {}^n\Delta\hat{\boldsymbol{\sigma}}^{t+\Delta t}(x_3) + \frac{\partial[{}^n\Delta\hat{\boldsymbol{\sigma}}^{t+\Delta t}(x_3)]}{\partial\hat{\boldsymbol{\varepsilon}}}. {}^{n+1}\Delta\hat{\boldsymbol{\varepsilon}}^{t+\Delta t}(x_3) + \dots \\
\Rightarrow {}^{n+1}\Delta\hat{\boldsymbol{\varepsilon}}^{t+\Delta t}(x_3) &= -[{}^n\mathbf{J}^{n+1}]^{-1} {}^n\Delta\hat{\boldsymbol{\sigma}}^{t+\Delta t}(x_3) \Rightarrow {}^{n+1}\hat{\boldsymbol{\varepsilon}}^{t+\Delta t}(x_3) = {}^n\hat{\boldsymbol{\varepsilon}}^{t+\Delta t}(x_3) + {}^{n+1}\Delta\hat{\boldsymbol{\varepsilon}}^{t+\Delta t}(x_3) \quad (17) \\
{}^{n+1}\Delta\hat{\boldsymbol{\sigma}}^{t+\Delta t}(x_1, x_2, x_3) &= E^0(x_1, x_2, x_3) \cdot {}^{n+1}\mathbf{x}^T \cdot \Delta\hat{\boldsymbol{\varepsilon}}^{t+\Delta t}(x_3) \Rightarrow {}^{n+1}\boldsymbol{\sigma}^{t+\Delta t} = {}^n\boldsymbol{\sigma}^{t+\Delta t} + {}^{n+1}\Delta\boldsymbol{\sigma}^{t+\Delta t}
\end{aligned}$$

being

$${}^n\mathbf{J}^{n+1} = \frac{\partial[{}^n\Delta\hat{\boldsymbol{\sigma}}^{t+\Delta t}(x_3)]}{\partial\hat{\boldsymbol{\varepsilon}}} = E^0 \cdot \begin{bmatrix} A(x_3) & m_1(x_3) & m_2(x_3) \\ m_1(x_3) & I_{11}(x_3) & I_{12}(x_3) \\ m_2(x_3) & I_{21}(x_3) & I_{22}(x_3) \end{bmatrix}$$

the Jacobian matrix.

For each time increment in which the predictor moment produces an unbalanced load increment greater than an adopted tolerance (equations 17 and 18), the procedure considers an increment of the curvature in order to obtain a corrector of generalized stresses which permits to reach the equilibrium state. The used convergence criterion states that the stable response is obtained for the cross section if

$$\sqrt{\frac{\sum_i \Delta\hat{\boldsymbol{\sigma}}_i^2}{\sum_i (\hat{\boldsymbol{\sigma}}_i^0)^2}} \leq TOL \quad (18)$$

where TOL is the tolerance adopted ($TOL \rightarrow 0$).

Box 2. Algorithm for the cross sectional damage integration.

1. Loop over the time $t + \Delta t$
2. Loop over the cross section position x_3
3. Compute the elastic generalized stresses –predictor– for each cross section.
4. Compute the residual generalized internal stresses
For the first load step : $\mathbf{J}(x_3) \equiv \mathbf{J}^0(x_3)$; $\hat{\boldsymbol{\sigma}}^{\text{int}}(x_3) = \mathbf{0}$
 $\Delta\hat{\boldsymbol{\sigma}}(x_3) = [\hat{\boldsymbol{\sigma}}^0(x_3) - \hat{\boldsymbol{\sigma}}^{\text{int}}(x_3)]$
5. Balance equation verification on x_3 cross section :

$$\|\Delta\hat{\boldsymbol{\sigma}}(x_3)\| = \begin{cases} 0 & \Rightarrow \text{go to EXIT} \\ \neq 0 & \Rightarrow \text{Continue} \end{cases}$$
6. Starting loop over Newton-Raphson $n^{\text{iteration}}$ process. Incremental generalized strain computation and obtaining of its current value:

$${}^{n+1}\Delta\hat{\boldsymbol{\varepsilon}}^{t+\Delta t}(x_3) = -[{}^n\mathbf{J}^{n+1}(x_3)]^{-1} {}^n\Delta\hat{\boldsymbol{\sigma}}^{t+\Delta t}(x_3)$$

$${}^{n+1}\hat{\boldsymbol{\varepsilon}}^{t+\Delta t}(x_3) = {}^n\hat{\boldsymbol{\varepsilon}}^{t+\Delta t}(x_3) + {}^{n+1}\Delta\hat{\boldsymbol{\varepsilon}}^{t+\Delta t}(x_3)$$
7. Damaged inertia computation at each x_3 cross section of pier k , using the continuum damage model showed in Box A-1 of the Annex:

$$\begin{aligned} {}^{n+1}[\sigma^0]^{t+\Delta t}(x_1, x_2, x_3) &= E^0 \cdot {}^{n+1} \mathbf{x}^T \cdot {}^n \hat{\boldsymbol{\epsilon}}^{t+\Delta t}(x_3) \\ \mathbf{f}(\sigma^0) - {}^n [c(f)]^{t+\Delta t} &\begin{cases} \leq 0 & \text{Maintain the inertia value and go to (**)} \\ > & \text{The process of damage continues (*)} \end{cases} \\ (*) \quad {}^{n+1} [f(x_1, x_2, x_3)]^{t+\Delta t} &= \frac{c^{\max}}{c} e^{A \left(1 - \frac{c(d)}{c^{\max}}\right)} \quad \text{with } 0 \leq c^{\max} \leq c \\ {}^n \mathbf{J}^{t+\Delta t}(x_3) &= \begin{bmatrix} \int_A f(x_1, x_2, x_3) \cdot dA & \int_A f(x_1, x_2, x_3) \cdot (x_2) dA & \int_A f(x_1, x_2, x_3) \cdot (x_1) dA \\ \int_A f(x_1, x_2, x_3) \cdot (x_2) dA & \int_A f(x_1, x_2, x_3) \cdot x_2^2 dA & \int_A f(x_1, x_2, x_3) \cdot (x_2 \cdot x_1) dA \\ \int_A f(x_1, x_2, x_3) \cdot (x_1) dA & \int_A f(x_1, x_2, x_3) \cdot (x_1 \cdot x_2) dA & \int_A f(x_1, x_2, x_3) \cdot x_1^2 dA \end{bmatrix}^{t+\Delta t} \\ (**) \quad \hat{\boldsymbol{\sigma}}^{\text{int}}(x_3) &= E^0 \cdot {}^n \mathbf{J}^{t+\Delta t}(x_3) \cdot {}^{n+1} \hat{\boldsymbol{\epsilon}}^{t+\Delta t}(x_3) \\ {}^{n+1} \sigma^{t+\Delta t}(x_1, x_2, x_3) &= E^0(x_1, x_2, x_3) \cdot {}^{n+1} \mathbf{x}^T \cdot {}^n \hat{\boldsymbol{\epsilon}}^{t+\Delta t}(x_3) \end{aligned}$$

8. Back to point 4
9. EXIT

NUMERICAL EXAMPLE FOR THE WARTH BRIDGE, AUSTRIA

General description of Warth Bridge

The Warth Bridge is located 63 km far from Vienna, Austria, was built 30 years ago and has two spans of the deck of 62.0 m and five of 67.0 m, with a total length of 459.0 m. The seven spans of the bridge give rise to six piers with heights of 31.0 m, 39.0 m, 37.0 m, 36.0 m, 30.0 m and 17.5 m, as it can be observed in Figure 5.

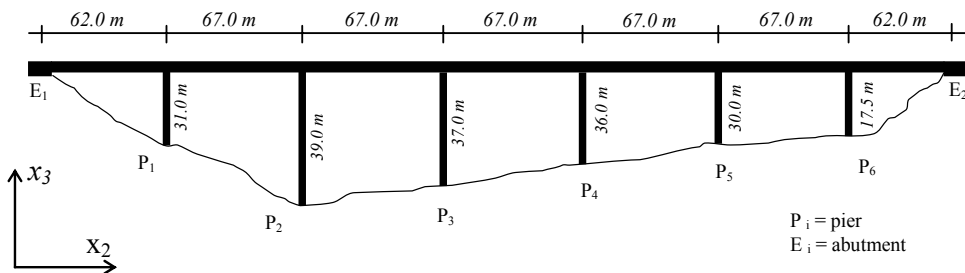


Figure 5. Elevation of the Warth Bridge, Austria

The geometrical and mechanical properties of the Warth bridge structure were obtained from the original design drawings [25]. Thus, the simple compression strength of the concrete is $f_{cu}^- = 45.0$ MPa for girders and $f_{cu}^- = 43.0$ MPa for piers. The weight density and Poisson modulus of the concrete are

$\gamma = 24.0 \text{ kN/m}^3$ and $\nu = 0.2$, respectively. In order to consider the weight of the non-structural components, the value of the weight density of the girders was increased to a value of $\gamma = 28.0 \text{ kN/m}^3$. For the reinforcement bars, $\gamma = 78.5 \text{ kN/m}^3$, $\nu = 0.3$ and $E_s = 2.0 \times 10^5 \text{ MPa}$ were considered. The elastic modulus of the reinforced concrete, E_c , was obtained using the Mixing Theory [10, 23] which allows calculating the properties of the elements composed of more than one material.

Quasi static pier response of the Warth Bridge

In this work, the numerical simulation of the quasi static structural behavior of shorter pier of the Warth Bridge is given (identified as P6 in the Figure 5). This pier was studied experimentally in the JCR Ispra Laboratory, Italy [25] and numerically, using a finite elements approach, by Faria et al. [8]. The top of this 5.75 m high pier has been subjected to a horizontal quasi static load. The seismic behavior of the pier has been evaluated using the described Bernoulli beam formulation extended to the non linear case of Kachanov damage [18, 12]. That is, without using the finite element approach, it has been introduced within the frame of the classical theory of Bernoulli a non linear continuum damage model. This formulation allows the evaluation of the structural behavior in the non linear field with a very low computational cost and results comparable with those obtained experimentally and also by means of the finite elements approach are obtained. This model leads to a good, low computational cost, non linear solution required by the evaluation of the seismic vulnerability of the bridge, what implies multiple structural dynamic response calculations. The objective of the structural solution developed in this paper is not only a good prediction of the load-displacement relationship, but also a good evaluation of the cross-sectional damage.

Properties of the materials

The mechanical properties of the reinforced concrete bridge pier are calculated using the mixing theory [4, 23], which combines the mechanical behavior of the concrete and steel. The behavior of the concrete is represented by means of a damage model described in the Annex and the behavior of the steel is represented by means of an anisotropic perfect elasto-plastic model [20]. This combination of the concrete and steel behaviors given by the mixing theory, permits considering a plastic-degradable behavior without softening at each point of the composite material

$$\boldsymbol{\sigma}(d, \boldsymbol{\varepsilon}^p) = k_c \boldsymbol{\sigma}_c(d) + k_s \boldsymbol{\sigma}_s(\boldsymbol{\varepsilon}^p) = k_c [(1-d)(\mathbf{C}_0)_c : \boldsymbol{\varepsilon}] + k_s [(\mathbf{C}_0)_s : (\boldsymbol{\varepsilon} - \boldsymbol{\varepsilon}_s^p)] \quad (19)$$

being: $\sigma, \sigma_c(d), \sigma_s(\epsilon^p)$, the stresses in the composite material, in the damaged concrete and in the plastic steel, respectively. $(C_0)_c$ and $(C_0)_s$ are, respectively, the initial constitutive tensors in the concrete and steel while $k_c = A_c(d)/[A_c(d) + A_s]$ and $k_s = A_s/[A_c(d) + A_s]$ are the relative areas corresponding to each material of the cross section of the pier. The characteristics of the used materials are given in Table 1.

Table1. Properties of the materials compounding the reinforced concrete.

Mechanical properties	Steel	Concrete
Young's modulus	$E_s = 200,00 \text{ GPa}$	$E_c = 33,50 \text{ GPa}$
Compression strength at the elastic limit	$f_{sy}^- = 545,00 \text{ MPa}$	$f_{cy}^- = 20,00 \text{ MPa}$
Maximum compression strength	$f_{su}^- = 600,00 \text{ MPa}$	$f_{cu}^- = 43,00 \text{ MPa}$
Tension strength at the elastic limit	$f_{sy}^+ = 545,00 \text{ MPa}$	$f_{cy}^+ = 3,10 \text{ MPa}$
Maximum tension strength	$f_{su}^+ = 600,00 \text{ MPa}$	$f_{cy}^+ = 3,10 \text{ MPa}$
Fracture energy	$(G_f)_s = 12.000,00 \text{ MN} / m$	$(G_f)_c = 1,20 \text{ MN} / m$

The initial values at the clamped cross section, corresponding to the initial, non damaged state, are the following:

$$\begin{aligned}
 (A_c)_0 = 0,6579 \text{ m}^2, (A_s)_0 = 76,77 \times 10^{-4} \text{ m}^2 &\Rightarrow \begin{cases} (k_c)_0 = 0,9884 \\ (k_s)_0 = 0,011533 \end{cases} \\
 (E)_0 = (k_c)_0(E_c)_0 + (k_s)_0 E_s = 35,418 \text{ MPa} & \quad (20) \\
 \left. \begin{aligned} (f_y^+)_0 &= (k_c)_0(f_{cy}^+)_0 + (k_s)_0(f_{sy}^+)_0 = 9,984 \text{ MPa} \\ (f_y^-)_0 &= (k_c)_0(f_{cy}^-)_0 + (k_s)_0(f_{sy}^-)_0 = 49,421 \text{ MPa} \end{aligned} \right\} n_r = \frac{(f_y^-)_0}{(f_y^+)_0} = 4,95
 \end{aligned}$$

Geometry and boundary conditions

Figure 6 shows the geometric characteristics and boundary condition for pier P6.

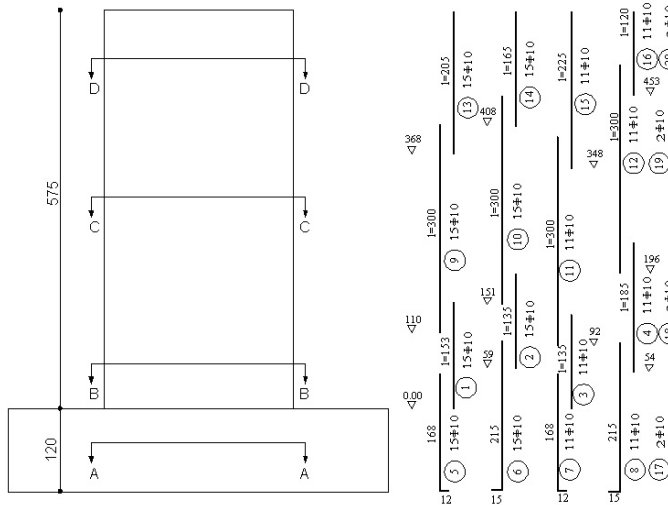


Fig.6. Geometry and reinforcement description of pier P6 belonging to Warth Bridge [25]

The pier is considered perfectly clamped to the foundation and the following sequence of loads is applied at its upper end:

1. A compressional axial load of 3820,00 kN
2. Once applied this load, three horizontal displacements are applied sequentially
 - 1) $-0,026\text{ m} \leq u_h \leq +0,026\text{ m}$
 - 2) $-0,055\text{ m} \leq u_h \leq +0,055\text{ m}$
 - 3) $-0,1\text{ m} \leq u_h \leq +0,1\text{ m}$

These cycles of displacements introduce degradation on the clamped cross section of the pier and the numerical results obtained in this paper (Figure 7.b.) are compared with those obtained by Faria et al. [8] and in the JCR Ispra laboratory [25] (see Figure 7.a).

From the results obtained in the present work by using the damage model and the described structural approach, a good solution is obtained in many cases. In spite of the simplicity of the model, the results, in their general features, reach similar values than those obtained experimentally and numerically through FEM models with two internal damage variables (damage variable for compression and tension). Nevertheless, the most important aspect is the very low computational cost that encourages to its application in solving multiple analysis problems like Monte Carlo simulations [11]. The most important differences between the two graphics of Figure 7 can be observed in the unloading branch, because in this case the

recovery of the material properties during the change of the sign of the load is evaluated using a simple constitutive model with a single damage index. In Figure 8 the top pier displacement is represented at the end of the load sequence 1 and then, in the same figure, the deformed pier is drawn at the end of the last load sequence 3. In this last case the damaged cross section is localized near the foundation of the pier, while the rest of cross-sections of the pier turns to its initial un-damaged state (rotation of rigid solid around the kneecap (Figure 8)).

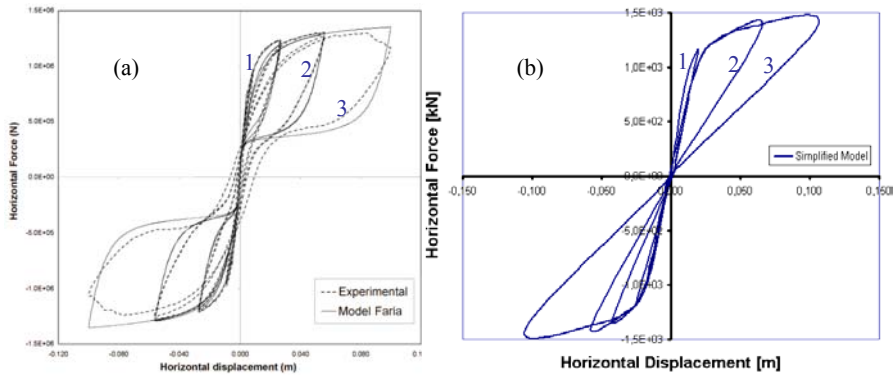


Figure 7. Load-displacement behavior in the pier for the load sequences 1, 2 and 3. a) Experimental results [25] and numeric results [8]. b) Results obtained in the present work

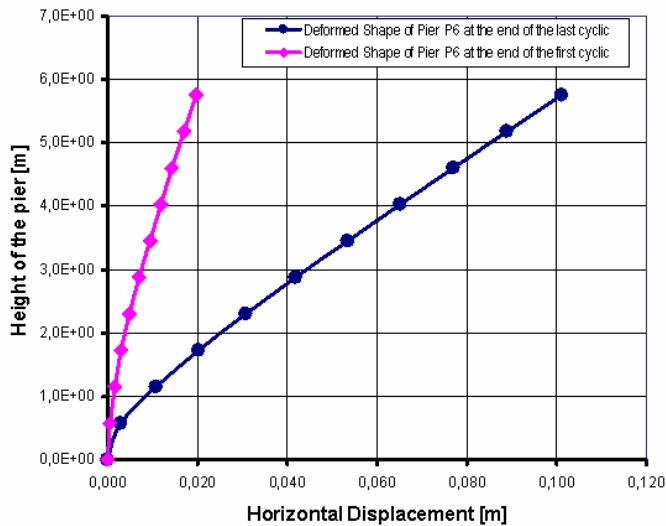


Figure 8. Displacement of the pier P6 at the end of the first load cycle and at the end of the last load cycle

The degradation of the cross-section is shown in Figure 9. Figure 9a shows the moment-curvature evolution, and Figure 9b shows the evolution of the damage index in function of the curvature. It can be seen in this figure that the level of damage at the end of the process is near to one.

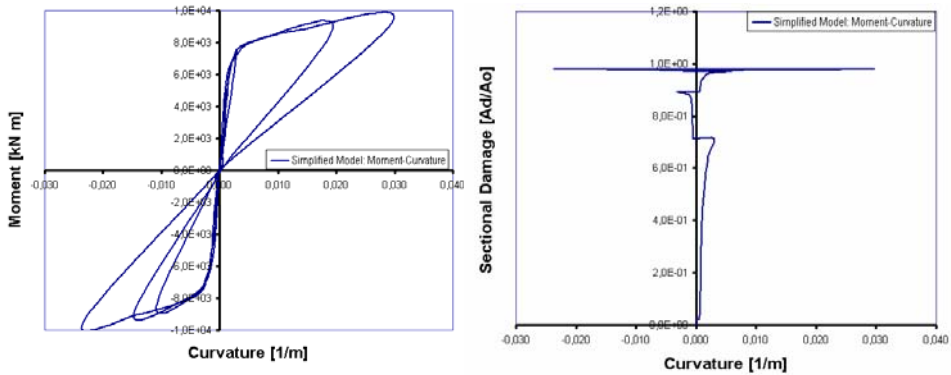


Figure 9. a) Moment-curvature evolution. b) Evolution of the cross-sectional damage depending on the curvature level.

SUMMARY AND CONCLUSIONS

A model of evaluation of the damage caused by a horizontal action in the piers of RC bridges with single pier bents is developed in this work. For this structure, the proposed model considers only one degree of freedom for each pier, namely the transversal displacements at their top.

The damage in a pier due to the seismic action is defined by using an isotropic damage model based on the Continuum Damage Mechanics. The damage is obtained in terms of the inertia of the damaged cross section at the base of each bridge pier is obtained. The proposed simplified model was verified using experimental and FEM results.

The simplified non-linear analysis performed with the proposed model gives satisfactory results similar to those of the laboratory test and the FEM results. On the basis of these results it is concluded that the proposed model suitably describes the maximum damages of the piers of RC bridges, and that it is a low-cost computer tool, ideal for the multi-analysis processes required by the evaluation of seismic vulnerability.

A future research objective is to develop a model for the complete bridge, using the developed pier model as an element of the structural model.

Acknowledgments

This research was partially supported by European Commission Environmental program RTD Project ENV4-CT-97-0574 “Advanced Methods for Assessing the Seismic Vulnerability of Bridges (VAB)”, by the Spanish Government (Ministerio de Educación y Ciencia), project REN2002-03365/RIES “Development and application of advanced approaches for the evaluation of the seismic vulnerability and risk of structures (EVASIS)” and project BIA2003-08700-C03-02 “Numerical simulation of the seismic behaviour of structures with energy dissipation devices”. This support is gratefully acknowledged.

ANNEX: CONTINUUM CONSTITUTIVE DAMAGE LAW

Introduction to isotropic damage model

This annex contains a brief review of the isotropic continuum damage model at a point of a structure [19], which is used in the paper to formulate the damage of the cross section of a bridge pier. The damage at a point of a continuous solid is defined as the degradation of the stiffness and strength due to the decrease of the effective area [11]. The continuum theory of the damage was formulated by Kachanov [12] in the creep behavior context, but later on it has been reformulated and accepted as a valid alternative to simulate the rate independent behavior of several materials [4-6, 14-17, 26, 27].

Formulation of isotropic damage model

Degradation of the material properties happens due to the presence and growth of small cracks and voids inside the structure of the material. This phenomenon can be simulated by means of the continuum mechanics taking into account a scalar or tensorial internal damage variable. This internal variable of damage measures the level of degradation of the material in a point and its evaluation is based on the transformation of the real stresses in other effective stresses. For the simple isotropic damage used here, the relationship between the real and the effective stress is described using an isotropic damage variable d

$$\boldsymbol{\sigma}_0 = \frac{\boldsymbol{\sigma}}{(1-d)} \quad (\text{A.1})$$

In this equation, d is the internal variable of damage; $\boldsymbol{\sigma}$ it is the Cauchy stress tensor and $\boldsymbol{\sigma}_0$ is the effective stress tensor, evaluated in the “no-damaged” space. This internal variable represents the loss of stiffness level in a point of the material and its upper and lower limits are given by

$$0 \leq d \leq 1 \quad (\text{A.2})$$

The upper limit ($d=1$) represents the maximum damage in a point and the lower limit ($d=0$) represents a non damaged point.

Helmholtz free energy and constitutive equation

The Helmholtz [18] free energy for the isotropic damage model is given by the expression

$$\begin{aligned}\Psi &= \Psi(\boldsymbol{\epsilon}; p_i) \quad \text{with } p_i = \{d\} \\ \Psi &= \Psi(\boldsymbol{\epsilon}; d) = (1-d)\Psi_0(\boldsymbol{\epsilon})\end{aligned}\tag{A.3}$$

The elastic part of the free energy, in the small strain case, can be written in the following quadratic form:

$$\Psi_0(\boldsymbol{\epsilon}) = \frac{1}{2} \boldsymbol{\epsilon} : \mathbf{C}_0 : \boldsymbol{\epsilon}\tag{A.4}$$

where \mathbf{C}_0 is the elastic undamaged constitutive tensor. The mechanical part of the dissipation, for uncoupled thermal problem, can be written by using the Clausius-Planck inequality [18]

$$\Xi = \left(\boldsymbol{\sigma} - \frac{\partial \Psi}{\partial \boldsymbol{\epsilon}} \right) : \dot{\boldsymbol{\epsilon}} - \frac{\partial \Psi}{\partial d} \dot{d} \geq 0\tag{A.5}$$

Applying the Coleman method (see Maugin [18]) to the dissipative power (Equation A.5) the following constitutive equation and dissipative inequality are obtained for each point of the material

$$\boldsymbol{\sigma} = \frac{\partial \Psi}{\partial \boldsymbol{\epsilon}} = (1-d) \frac{\partial \Psi_0}{\partial \boldsymbol{\epsilon}} = (1-d) \mathbf{C}_0 : \boldsymbol{\epsilon}\tag{A.6}$$

$$\Xi = \Psi_0 \dot{d} \geq 0\tag{A.7}$$

Fundamentals of the constitutive damage model

Damage threshold criterion

This approach defines the beginning of the non linear behavior in each point of the solid and it can be defined using the Plasticity Theory

$$F(\boldsymbol{\sigma}_0; \mathbf{q}) = f(\boldsymbol{\sigma}_0) - c(d) \leq 0, \quad \text{with } \mathbf{q} \equiv \{d\}\tag{A.8}$$

where $f(\boldsymbol{\sigma}_0)$ is a scalar function of the stress tensor $\boldsymbol{\sigma}_0 = \mathbf{C}_0 : \boldsymbol{\epsilon}$ and $c(d)$ is the strength threshold of damage. The initial value of damage is set up on $c(d^0) = c^{max} = \sigma^{max}$ and represents the uniaxial strength at crushing state. The damage process begins when $f(\boldsymbol{\sigma}_0)$ is greater than $c^{max} = \sigma^{max}$. Equation (A.8) can be written in a more general form throughout the following equivalent expression:

$$\bar{F}(\boldsymbol{\sigma}_0; \mathbf{q}) = G[f(\boldsymbol{\sigma}_0)] - G[c(d)] \leq 0, \quad \text{with} \quad \mathbf{q} \equiv \{d\} \quad (\text{A.9})$$

where $G[\chi]$ is a monotonic scalar function, invertible and positive with positives derivative.

Evolution law for the internal damage variable

The evolution law for the internal damage variable can be written in the following general form:

$$\dot{d} = \dot{\mu} \frac{\partial \bar{F}(\boldsymbol{\sigma}_0; \mathbf{q})}{\partial [f(\boldsymbol{\sigma}_0)]} \equiv \dot{\mu} \frac{\partial G[f(\boldsymbol{\sigma}_0)]}{\partial [f(\boldsymbol{\sigma}_0)]} \quad (\text{A.10})$$

where μ is a non negative scalar value named damage consistency parameter, whose definition is close to the plastic consistency parameter λ . As in the Plasticity Theory, the evaluation of this parameter is made using the Ilyushin [18] consistency condition. From this condition, and from the properties of $G[\chi]$, the following function is obtained:

$$\bar{F}(\boldsymbol{\sigma}_0; \mathbf{q}) = 0 \Rightarrow G[f(\boldsymbol{\sigma}_0)] = G[c(d)] \Rightarrow f(\boldsymbol{\sigma}_0) = c(d) \Rightarrow \frac{\partial G[f(\boldsymbol{\sigma}_0)]}{\partial f(\boldsymbol{\sigma}_0)} = \frac{\partial G[c(d)]}{\partial c(d)} \quad (\text{A.11})$$

and, from here, the permanency condition is deduced

$$\dot{\bar{F}}(\boldsymbol{\sigma}_0; \mathbf{q}) = 0 \Rightarrow \frac{\partial G[f(\boldsymbol{\sigma}_0)]}{\partial f(\boldsymbol{\sigma}_0)} \dot{f}(\boldsymbol{\sigma}_0) - \frac{\partial G[c(d)]}{\partial c(d)} \dot{c}(d) = 0 \Rightarrow \dot{f}(\boldsymbol{\sigma}_0) = \dot{c}(d) \quad (\text{A.12})$$

Observing the rate of the threshold damage function $\partial G[f(\boldsymbol{\sigma}_0)] / \partial t = \dot{G}[f(\boldsymbol{\sigma}_0)]$ (Equation A.12) and comparing with the evolution law of the internal variable \dot{d} (Equation A.10), the following expression for the damage consistency parameter is obtained:

$$\left. \begin{aligned} \dot{G}[f(\boldsymbol{\sigma}_0)] &= \frac{\partial G[f(\boldsymbol{\sigma}_0)]}{\partial f(\boldsymbol{\sigma}_0)} \dot{f}(\boldsymbol{\sigma}_0) \\ \dot{d} &= \dot{\mu} \frac{\partial G[f(\boldsymbol{\sigma}_0)]}{\partial [f(\boldsymbol{\sigma}_0)]} \end{aligned} \right\} \Rightarrow \begin{aligned} \dot{d} &\equiv \dot{G}[f(\boldsymbol{\sigma}_0)] \Rightarrow \dot{\mu} \equiv \dot{f}(\boldsymbol{\sigma}_0) = \dot{c}(d) = \\ &= \frac{\partial f(\boldsymbol{\sigma}_0)}{\partial \boldsymbol{\sigma}_0} : \dot{\boldsymbol{\sigma}}_0 = \frac{\partial f(\boldsymbol{\sigma}_0)}{\partial \boldsymbol{\sigma}_0} : \mathbf{C}_0 : \dot{\boldsymbol{\varepsilon}} \end{aligned} \quad (\text{A.13})$$

Time integration over the rate of internal damage variable (Equation A.13) gives the following explicit expression for the damage evaluation in each point of the solid:

$$d = \int_t \dot{d} dt = \int_t \dot{G}[f(\boldsymbol{\sigma}_0)] dt = G[f(\boldsymbol{\sigma}_0)] \quad (\text{A.14})$$

Substituting Equation (A.14) in (A.5), the following expression for the rate of the mechanical dissipation at each damaged point is established

$$\Xi = \Psi_0 \dot{G}[f(\boldsymbol{\sigma}_0)] = \Psi_0 \frac{\partial G[f(\boldsymbol{\sigma}_0)]}{\partial f(\boldsymbol{\sigma}_0)} \frac{\partial f(\boldsymbol{\sigma}_0)}{\partial \boldsymbol{\sigma}_0} : \mathbf{C}_0 : \dot{\boldsymbol{\epsilon}} \quad (\text{A.15})$$

The current value for the damage threshold c can be written, at time $s = t$, as

$$c = \max \left\{ c^{\max}, \max \left\{ f(\boldsymbol{\sigma}_0) \Big|_s \right\} \right\} \quad \forall \quad 0 \leq s \leq t \quad (\text{A.16})$$

Particular expression used for the damage threshold criterion

There are several ways to define the damage threshold criterion. In this work, the exponential of reference [19] for concrete structures is used. The scalar function $G[\chi]$ (Equation A.11) is here defined in function of the *unit normalized dissipation variable* κ as [15]

$$\dot{\kappa} = K(\boldsymbol{\sigma}_0) \cdot \Xi_m = \left[\frac{r(\boldsymbol{\sigma}_0)}{g_f} + \frac{1-r(\boldsymbol{\sigma}_0)}{g_c} \right] \cdot \Xi_m \Rightarrow 0 \leq \left[\kappa = \int_t \dot{\kappa} dt \right] \leq 1 \quad (\text{A.17})$$

where $\Xi_m = \Psi_0 \dot{d}$ is the damage dissipation and $r(\boldsymbol{\sigma}) = \sum_{\mathbf{I}=1}^3 \langle \sigma_{\mathbf{I}} \rangle / \sum_{\mathbf{I}=1}^3 |\sigma_{\mathbf{I}}|$ a scalar function to define the sign of the stress state at each point and at each time instant of the damage process, being $\langle x \rangle = 0,5 [x + |x|]$ the McAully function. The variables g_f and g_c are the maximum values for the tension-compression dissipation at each point, respectively [15]. By this way, the damage dissipation will be always normalized to the maximum consumed energy during the mechanical process.

Using κ as an auxiliary variable, it is now possible to evaluate the damage function $G[\chi]$ in the following form [19]:

$$d = G[c(\kappa)] = 1 - \frac{c^{\max}}{c(\kappa)} e^{A \left(1 - \frac{c(\kappa)}{c^{\max}} \right)} \quad \text{with} \quad 0 \leq c^{\max} \leq c(d) \quad (\text{A.18})$$

but, under the damage condition $f(\boldsymbol{\sigma}_0) \equiv c(\kappa)$. This equation can be also written as

$$G[f(\boldsymbol{\sigma}_0)] = 1 - \frac{f^0(\boldsymbol{\sigma}_0)}{f(\boldsymbol{\sigma}_0)} e^{A \left(1 - \frac{f(\boldsymbol{\sigma}_0)}{f^0(\boldsymbol{\sigma}_0)} \right)} \quad \text{with } f^0(\boldsymbol{\sigma}_0) = c^{\max}$$

where $A = \left[g_f / (f^0(\boldsymbol{\sigma}_0))^2 - 0.5 \right]^{-1}$ is a parameter depending on the fracture energy dissipation g_f [19]. The value $f^0(\boldsymbol{\sigma}_0) = c^{\max}$ is obtained from the agreement with the first damage threshold, when the condition $G[f^0(\boldsymbol{\sigma}_0)] - G[c^{\max}] = 0$ is reached and $G[f^0(\boldsymbol{\sigma}_0)] = G[c^{\max}] \equiv 0$ shows the damage integration algorithm for each single point of the structure.

Box A1. Integration of the continuum damage equation at each structural point with exponential softening

1. Compute the elastic prediction stress and the internal variable at current time " $t + \Delta t$ ", and equilibrium iteration " i ", ,

$$[\boldsymbol{\sigma}_0]^{t+\Delta t} = \mathbf{C}_0 : [\boldsymbol{\varepsilon}]^{t+\Delta t}$$

$${}^i [d]^{t+\Delta t} ; \tau = {}^i [G[f(\boldsymbol{\sigma}_0)]]^{t+\Delta t}$$

$$\tau^0 = {}^i [G[f^0(\boldsymbol{\sigma}_0)]]^{t+\Delta t}$$

2. Damage threshold checking:

- a. If: $\tau - \tau^{\max} \leq 0$

$$\text{Then } \left\{ \begin{array}{l} {}^i [\boldsymbol{\sigma}]^{t+\Delta t} = [\boldsymbol{\sigma}_0]^{t+\Delta t} \\ {}^i [d]^{t+\Delta t} ; \tau^{\max} = \tau \end{array} \right\} \text{ and go to the EXIT}$$

- b. If: $\tau - \tau^{\max} > 0$

Then start with the damage constitutive integration

3. Integration of the damage constitutive equation,

$$\tau^{\max} = \tau$$

$${}^i [d]^{t+\Delta t} = 1 - \left[\frac{\tau^0}{\tau} e^{A \left(1 - \frac{\tau}{\tau^0} \right)} \right]^{t+\Delta t}$$

4. Stress and tangent constitutive tensor actualization.

$${}^i [\boldsymbol{\sigma}]^{t+\Delta t} = (1 - {}^i [d]^{t+\Delta t}) [\boldsymbol{\sigma}_0]^{t+\Delta t}$$

$${}^i [\mathbf{C}^T]^{t+\Delta t} = \left[(1 - d) \mathbf{C}_0 - \frac{\partial G[f(\boldsymbol{\sigma}_0)]}{\partial [f(\boldsymbol{\sigma}_0)]} [\mathbf{C}_0 : \boldsymbol{\varepsilon}] \otimes \left[\frac{\partial f(\mathbf{C}_0 : \boldsymbol{\varepsilon})}{\partial \boldsymbol{\varepsilon}} \right] \right]^{t+\Delta t}$$

5. EXIT

Stress function particularization

Simo and Ju stress function [26, 27] is used in the paper

$$\tau = f(\boldsymbol{\sigma}_0) = \sqrt{2\Psi_0(\boldsymbol{\epsilon})} = \sqrt{\boldsymbol{\epsilon} : \mathbf{C}_0 : \boldsymbol{\epsilon}} \quad (\text{A.19})$$

Taking into account this function, parameter A used in Equation (A.18) can be written as

$$A = \frac{1}{\frac{g_f}{(f^0(\boldsymbol{\sigma}_0))^2} - \frac{1}{2}} \quad (\text{A.20})$$

where g_f represents the maximum of the fracture energy to be dissipated at each point of the solid and $f^0(\boldsymbol{\sigma}_0)$ is the value given by the threshold equation for the first damage threshold.

References

- [1] R. Aguiar and A. H. Barbat, “*Daño sísmico en estructuras de hormigón armado*”. Universidad Politécnica del Ejército, Quito, Ecuador., 1997.
- [2] S. Arman and M. Grigoriu, *Markov model for local and global damage indexes in seismic analysis*, **NCEER-94-0003**, National Center for Earthquake Engineering Research, 1994.
- [3] A. H. Barbat, S. Oller, E. Oñate and A. Hanganu, “Viscous Damage Model for Timoshenko Beam Structures”. *International Journal of Solids and Structures*, Vol.34, No.30, pp. 3953-3976. 1997.
- [4] E. Car, S. Oller and E. Oñate, “An anisotropic elastoplastic constitutive model for large strain analysis of fiber reinforced composite materials”. *Computer Methods in Applied Mechanics and Engineering*, Vol. 185, No. 2-4, 245-277, 2000.
- [5] J. Chaboche, “Continuum damage mechanics part I. General Concepts”. *Journal of Applied Mechanics*, 55, 59-64, 1988.
- [6] J. Chaboche, “Continuum damage mechanics part II. Damage Growth”. *Journal of Applied Mechanics*, 55, 65-72, 1988.
- [7] R. W. Clough and J. Penzien, *Dynamics of Structures*. McGraw-Hill, 1992.
- [8] R. Faria, N. Vila Pouca and R. Delgado, “Simulation of the cyclic behaviour of π/c rectangular hollow section bridge piers via a detailed numerical model”. *Journal of Earthquake Engineering*, Vol. 8, No. 5, 725-748, 2004.
- [9] C. Gómez-Soberón, S. Oller and A. Barbat, *Seismic vulnerability of bridges using simple models*. *Monographs of Seismic Engineering*, Monograph series in Earthquake Engineering, **CIMNE IS-47**, International Center of Numerical Methods in Engineering, Barcelona, Spain, 2002.
- [10] D. Hull, “*Materiales compuestos*”, Reverté Editorial, Spain, 1987.
- [11] J. E. Hurtado and A. H. Barbat, “Monte Carlo techniques in computational stochastic mechanics”. *Archives of Computational Methods in Engineering*, Vol. 5, No.1, 3-30, 1998.
- [12] L. M. Kachanov, “Time of rupture process under creep conditions”. *Izvestia Akademii Nauk; Otd Tech Nauk*, 8 26-31, 1958, .
- [13] J. Lemaitre “*A course on damage mechanics*”, 2nd edition, Springer, 1992.
- [14] J. Lemaitre and J. L. Chaboche “Aspects phénoménologiques de la rupture par endommagement”. *Journal of Applied Mechanics*, 2, 317-365, 1978.
- [15] J. Lubliner, J. Oliver, S. Oller and E. Oñate, “A plastic damage model for non linear analysis of concrete”. *Int. Solids and Structures*, Vol. 25, No. 3, pp. 299-326, 1989.
- [16] B. Luccioni and S. Oller, “A directional damage model”, *Computer Methods in Applied Mechanics and Engineering*. Vol. 192, No. 9-10, 1119-1145, 2003.
- [17] B. Luccioni, S. Oller and R. Danesi, “*Coupled plastic-damaged model*”. *Computer Methods in Applied Mechanics and Engineering*, Vol. 129, No. 1-2, 81-89, 1996.
- [18] G. A. Maugin, *The thermomechanics of plasticity and fracture*. Cambridge University Press, 1992.
- [19] J. Oliver, M. Cervera, S. Oller and J. Lubliner, “Isotropic damage models and smeared crack analysis of concrete”. *Second International Conference on Computer Aided Analysis and Design of Concrete Structures*, 2, 945-958, Austria, 1990.
- [20] S. Oller, E. Car and J. Lubliner, “Definition of a general implicit orthotropic yield criterion”. *Computer Methods in Applied Mechanics and Engineering*, Vol. 192, No. 7-8, 895-912, 2003.
- [21] S. Oller, B. Luccioni and A. Barbat, “Un método de evaluación del daño sísmico de estructuras de hormigón armado”. *Revista Internacional de Métodos Numéricos para el Cálculo y Diseño en Ingeniería*, **12(2)**, 215-238, 1996.

- [22] S. Oller, A. H. Barbat, E. Oñate and A. Hanganu, “A damage model for the seismic analysis of buildings structures”. *10th World Conference on Earthquake Engineering*. 2593-2598, 1992.
- [23] S. Oller, E. Oñate, J. Miquel and S. Botello, “A plastic damage constitutive model for composite material”. *International Journal of Solids and Structures*, Vol.33, No.17, pp. 2501-2518, 1996.
- [24] Y. J. Park and A. H. Ang, “Mechanistic seismic damage model for reinforced concrete”. *Journal of Structural Engineering*, **111(4)**, 722-739, 1985.
- [25] A. Pinto, J. Molina and G. Tsionis, *Cyclic Test on a Large Scale Model of an Existing Short Bridge Pier (Warth Bridge-Pier A70)*. EUR Report, Joint Research Centre, ISIS, Ispra, Italy.
- [26] J. Simo and J. Ju, “Strain and stress based continuum damage models – I Formulation”. *Int. J. Solids Structures*, 23, 821-840, 1987.
- [27] J. Simo and J. Ju, “Strain and stress based continuum damage models – II Computational aspects”. *Int. J. Solids Structures*, 23, 841-869, 1987.
- [28] O. Zienkiewicz and R. Taylor, *The Finite Element Method*. Fourth edition, Volume 1 and 2, McGraw-Hill, 1988.

Mix optimization for high strength concrete

Marinela Barbuta¹, Doina Smaranda Nour¹

¹Civil Engineering Faculty, “Gh. Asachi” University Iasi Romania

Summary

High strength concrete mixes are analysed for different cement dosages, different types of aggregates and admixtures, and for different contents of silica fume. Properties of fresh and hardened concrete were analysed for establishing the best mixture with best results of strengths. It appears that the best mixture of high strength concrete is realized in the case of crushed stone aggregate, superplasticizer type sulfonate-polymer and silica fume addition of 10%. Also, a combination of coarse aggregates and crushed stone aggregates result in a mixture with high properties even in the case of a 15% replacement of cement with silica fume.

KEYWORDS: High strength concrete, Silica fume, Aggregate, Admixture

1. INTRODUCTION

Concretes of high strength and high performance are replacing today the normal strength concrete being used in a large domain because the advantages that they offer (referring to their properties, even the initials costs are bigger).

For realizing high strength concretes are implied many factors (aggregate, cement, admixture and addition) and their mixture must be carefully analysed having in view the local possibilities and needs. Mix design involves studies of optimisation of all components (types, dosages), including also the addition, that in this case is silica fume (SUF).

This paper reports the results of a study conducted to investigate the optimum mixture of components for high strength concrete realized with local materials and the influence of each component on the properties of the mixture.

2. EXPERIMENTAL PROGRAM

2.1 Materials

The aggregates were of two types: river coarse aggregate and crushed stone, the sorts being 3-7 mm and 7-16 mm.

Five commercial superplasticizer have been used: type 1 –sulfonate polymer; type 2 –calcium sulfonate; type 3- naphthalene-sulfonate polymer; type 4-lignosulfonate additive and type 5-amonium lignosulfonate. They were used at the dose level as recommended by the manufactures.

The cement was type CEM I-42.5 R (SREN 197-1), with compressive strength at 28 days of 42.5 N/mm^2 . In two dosages were studied: 550 kg/m^3 and 650 kg/m^3 .

In the first phase, using the data given in [1], the concrete composition was determined for a grade Bc 70/80, with silica fume (SUF) addition of 10% from cement weight.

In Table 1 the mix of concrete for grade 70/80 is presented, were samples type **I** are with coarse aggregate, type **A** are with coarse aggregate sorte 3-7 mm, and crushed stone sorte 8-16 mm and type **B** are with crushed stone sorte 3-8 and 8-16 mm.

The second phase included the analyse of the best concretes to which a part of cement (10% and 15% by weight) was replaced with silica fume; the cement dosage was then increased to 650 kg/m^3 and the silica fume was used as replacement of 10% by weight of cement.

2.2 Test Sample

For each composition were realized cubes of 141 mm size for determining the compressive strength; for determining split tensile strength and tensile strength by bending were realized prism of $100 \times 100 \times 550 \text{ mm}$ size, according to romanian standard. The samples were kept at a constant temperature of $20 \pm 2^\circ\text{C}$ and demoulded after 24 hours; then were cured for 28 days under water stored at a constant temperature.

The properties of fresh concrete were analyzed: densities, workability, consistency, compaction degree; for hardened concrete were determined the tensile strength by bending, split tensile strength and compressive strength.

3. RESULTS AND DISCUSSION

3.1 Fresh Concrete

On fresh concrete there were determined the consistency, compaction degree, workability.

The values of slumps and densities are presented in Table 2.

In Fig. 1 the variation of densities is given function of the additive type.

Table 1. Experimental mixture

Sample	Cement dosage kg/mc	Aggregate			Water	w/c	Additive l/mc	Silica fume kg/mc
		0-3	3-7 (3-8)*	7-16 (8-16)**	l/mc	w/c + SUF		
I.Additive type 1	550	457	359	815	153,3	0,30 0,273	11	55
II.Additive type 2	550	457	359	815	153,3	0,30 0,273	11	55
III.Additive type 3	550	457	359	815	159,5	0,29 0,264	6,6	55
IV.Additive type 4	550	457	359	815	162,4	0,295 0,268	3,08	55
V.Additive type 5	550	457	359	815	162,4	0,295 0,268	3,3	55
AI** Additive type 1	550	457	359	815	153,3	0,30 0,273	11	55
AII** Additive type 2	550	457	359	815	153,3	0,30 0,273	11	55
AIII** Additive type 3	550	457	359	815	159,5	0,295 0,264	6,6	55
AIV** Additive type 4	550	457	359	815	162,4	0,295 0,268	3,08	55
AV** Additive type 5	550	457	359	815	162,4	0,295 0,273	3,3	55
BI*** Additive type 1	550	457	359	815	153,3	0,30 0,264	11	55
BII*** Additive type 2	550	457	359	815	153,3	0,30 0,264	11	55
BIII*** Additive type 3	550	457	359	815	159,5	0,295 0,264	6,6	55
BIV*** Additive type 4	550	457	359	815	162,4	0,295 0,264	3,08	55
BV*** Additive type 5	550	457	359	815	162,4	0,295 0,273	3,3	55

From Fig.1, it results that the biggest densities are for concrete realized with crushed aggregate (concrete type **B**), were with admixtures type 1, type 3 and type 4 result the biggest values of densities, and for admixture type 5 is the smallest value.

Table 2. Fresh concrete properties

Sample	Slump(cm)/workability	Density kg/mc
I	12,8/T4	2414
II	3,8/T2	2338
III	4,5/T2	2390
IV	0/T0	2277
V	0/T0	2340
AI	0/T0	2550
AII	0/T0	2497
AIII	0/T0	2345
AIV	0/T0	2479
AV	0/T0	2479
BI	0/T0	2568
BII	0/T0	2568
BIII	0/T0	2542
BIV	0/T0	2569
BV	0/T0	2506

Table 3. Concrete consistency

Sample	Time VE-BE (s)	Consistency
I	2,3	Plastic
II	4	Plastic
III	3,3	Plastic
IV	6,5	Low plastic
V	8,1	Low plastic
AI	5,3	Low plastic
AII	4,9	Plastic
AIII	10	Low plastic
AIV	9	Low plastic
AV	10,7	Low plastic
BI	5,4	Low plastic
BII	12,4	viscous
BIII	8,7	Low plastic
BIV	16,8	viscous
BV	12,2	viscous

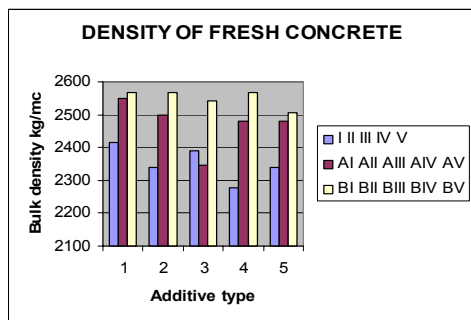


Figure 1. Density of fresh concrete

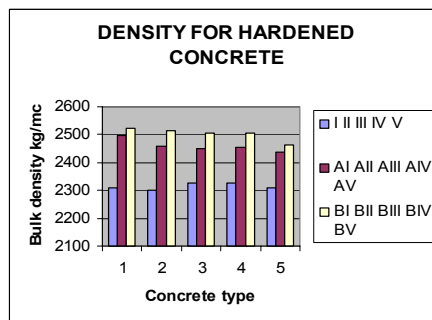


Figure 2. Density for hardened concrete

Reduced values of densities were obtained for concrete type **A**, to which for additive type 1 is the biggest density, and for additive type 2 is the smallest value.

The smallest values of densities are for concrete type **I**, for which the best results are obtained for admixture type 1.

In Table 3 are presented the data for concrete consistency determined by VE-BE method.

It results that for type **I** of concrete the superplasticizers results in plastic concrete, for type **A** only for additive type 2 there is plastic concrete and the other are low plastic. For concretes type **B** the consistency are from low plastic to viscous.

3.2 Hardened Concrete

For hardened concrete there were measured: density, porosity, compressive strength, split tensile strength, tensile strength by bending.

From Table 4 and Fig.2 it results that the biggest value for densities are obtained for concretes realized with crushed stone and additive type 1.

In Table 4 also are presented the values of concrete strengths determined at 28 days.

Table 4. Experimental results for hardened concrete

Sample	Bulk density N/m ³	R _c N/mm ²	R _{ti} N/mm ²	R _{td} N/mm ²
I	2310	69,3	3,99	4,8
II	2301	66,1	4,08	5,81
III	2328	70,45	4,15	5,49
IV	2328	66,8	4,18	4,45
V	2310	61,2	3,95	4,1
AI	2497	89,6	5,54	5,1
AII	2461	77,1	5,7	6,8
AIII	2453	77,2	4,8	6,3
AIV	2456	71,55	4,77	6,05
AV	2439	70,1	4,69	5,86
BI	2524	85,5	5,35	5,79
BII	2515	87,5	5,6	5,57
BIII	2506	90,3	5,53	4,01
BIV	2506	75,8	5,35	5,45
BV	2462	72,1	5,15	6,88

In Fig. 3,4 and 5 are presented the strengths of concrete function the additive type.

From Fig.3, we observe that for additive type 1 the best results for compressive strength were obtained. For concrete **type I**, the biggest values are for additive type 1. For concrete **type A** the biggest values are obtained for additive type 1 and for concrete **type B**, the maximum values are obtained for additive type 3.

According to [1], the minimum values of compressive strengths to 28 days for grade 70/80 are 84/94 N/mm². It can be observed that only to concretes type AI, BI, BII and BIII have accomplished this condition; the concretes type AII, AIII and BIV are 60/70 grade and the others are 60/70 grade [1].

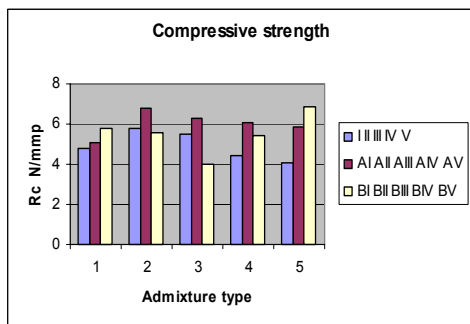


Figure 3. Compressive strength versus admixture type

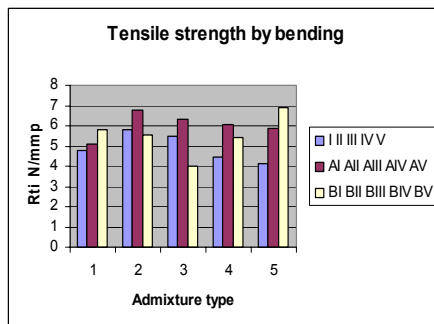


Figure 4. Tensile strength versus admixture type

From Fig. 4 it results that the best result for tensile strength by bending is for concrete type AII, followed by concrete type BII; big and homogeneous values are obtained for all concretes type B, followed by type A and at last concretes type I.

In Fig.5 it can analyse the results for split tensile strength: the maximum value is obtained for concrete type BV, then AII and II; more compact values are obtained for concretes type A than for type B.

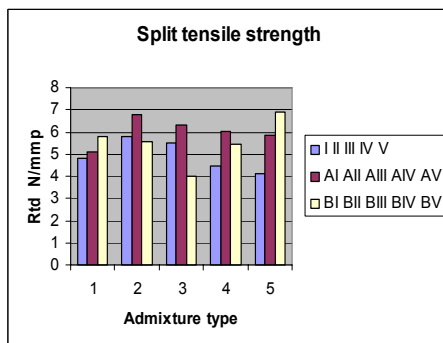


Figure 5. Split tensile strength versus admixture type

In the next stage from each type of concrete only one was analysed for replacements of cement with silica fume (10% and 15%): type II concrete with additive type 2, for second type: concrete with additive type 1 and for type B: with additive type 3.

In the last stage, the cement dosage was increased to 650 Kg/m³ and then cement was replaced with 10% silica fume for the upper types of concretes.

For the fresh concrete, there are almost the same characteristics: concrete plastic-viscous.

The results on test samples are given in Table 5.

In Fig. 6, 7 and 8 are presented the variations of strengths function the cement replacements for the initial mixture.

From Fig.6 it results that for all type of concrete with the increasing of the silica fume replacement the compressive strength also increase. The biggest value is for concrete type BIII (with crushed stone).

From Fig.7 it results that only for the concrete type AI (sort 3-7 of gravel and sort 7-16 mm of crushed stone) the increasing of silica fume content will result in an increasing of the tensile strength by bending.

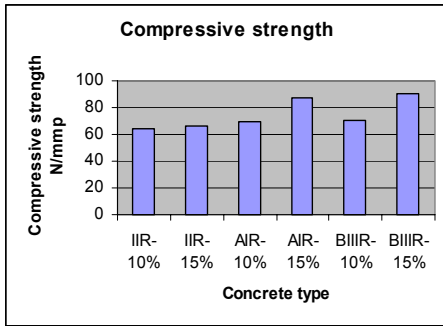


Figure 6. Compressive strength versus cement replacement with SUF

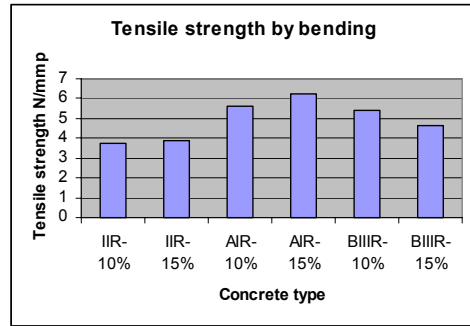


Figure 7. Tensile strength versus cement replacement with SUF

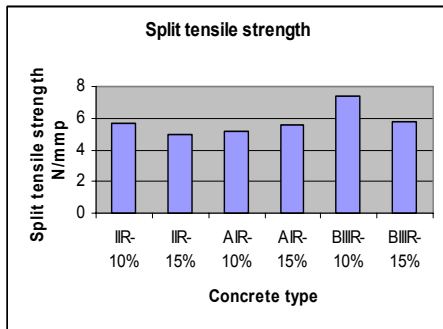


Figure 8. Tensile strength versus cement replacement with SUF

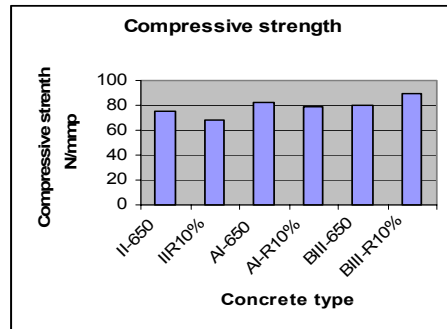


Figure 9. Compressive strength for high cement dosage

For concrete type I the increasing is reduced and for type BIII we observe a reduction of the tensile strength by bending.

From Fig.8 we can observe that only for type AII concrete we have an increasing of the strength, but for other types, we observe a reduction of the split tensile strength.

In Fig.9 we can see that the replacement of cement with silica fume 10% results in an increasing of the compressive strength only for the concrete type BIII; for other types the strength decreases.

From the graph of Fig.10 we can observe that for a bigger dosage of cement, the replacement of cement with silica fume 10% will result in a reduction of the tensile strength by bending in the case of concretes with river coarse aggregate and concretes with mix of aggregate and an increase of the strength in the case of crushed stone.

In the Fig.11 we can observe that a small increase of the split tensile strength in the case of concrete with river coarse aggregate when the replacement of cement with silica fume is 10%; in other cases the strength is reduced by the silica fume replacement.

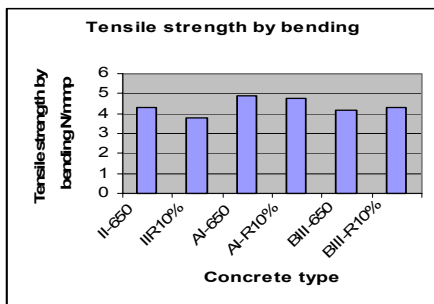


Figure 10. Tensile strength for high cement dosage

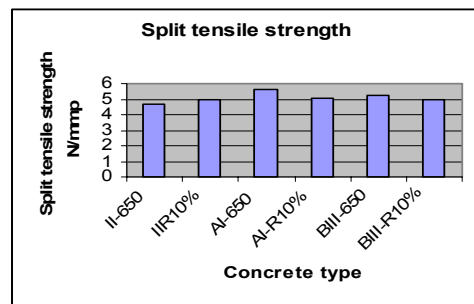


Figure 11. Split tensile strength for high cement dosage

If we are analysing the influence of the cement dosage, Fig.12 we observe that in the case of concrete type I the increasing of the cement dosage results in an increasing of the compressive strength, but an replacement of cement with 10 % silica fume results in a reduction of the strength.

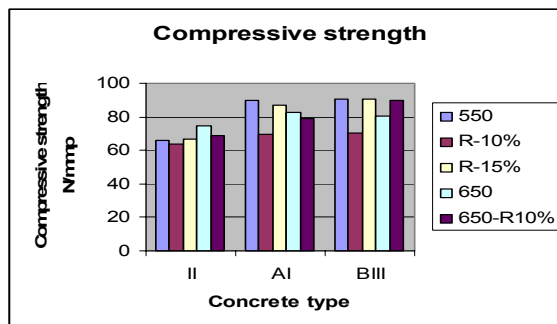


Figure 12. Compressive strength versus concrete type

For other types of concrete we observe that a bigger cement dosage results in a decrease of the strength; also, in the case of concrete type AII we observe that the replacement of cement with 15% silica fume in initial mixture results in an increase of the strength, bigger than that obtained with a dosage of 650 kg/m^3 . In the case of concrete type BIII, we observe that a bigger dosage will result in a decrease of the compressive strength and for replacements of cement with silica fume we obtain a bigger strength than in a case of a bigger cement dosage.

4. CONCLUSIONS

In the case of high strength concrete, that was analyzed in the article the optimization of mixture is reflected in the following conclusions:

- **Aggregates:** for fresh concrete we observe that a plastic behaviour has the concrete realized with river coarse aggregate (first type), then concrete type A and for concrete with crushed stone (type B) we obtain a viscous concrete.

The mechanical strengths are influenced by the aggregates type and we observe that for *compressive strength* are recommended crushed stone aggregate. For *tensile strength by bending* are recommended the river coarse and crushed stone aggregate and for *split tensile strength* are recommended crushed stone aggregate.

- **Cement:** in the case of cement 42.5 N/mm^2 that was used in the researches, the dosage given in [1] is good for crushed stone aggregate, but for river coarse aggregate it must be bigger or it must use a higher strength cement. An increase in cement dosage results in smaller strengths in the case of crushed stone.
- **Silica fume:** replacement with silica fume results in an increase of the compressive strength for all concretes in the case of smaller cement dosage; for bigger cement dosage, an increase of compressive strength is obtained only for concretes with crushed stone aggregate; to other types of concrete the replacement with silica fume results in an increase of compressive strength.
- **Admixtures:** In the case of compressive strength, the additive type 3 gave the best results for concretes with river coarse aggregate and with crushed stone. In the case of tensile strength by bending the additive type 2 gave the biggest values. In the case of split tensile strength the additive type 2 resulted in biggest values. The admixtures were used with dosages recommended by the producer, but for establishing how they can influence the concrete properties it must analyse concretes with different dosage, fact that is not studied in the article.

References

1. Ionescu, I., Ispas, Tr. and Popăescu, A.: *High Performance Concrete*, Technical Edition, București 1999
2. Rujanu, M.- *Construction stones, mineral binding materials and their composites*, TEHNICA-INFO Edition ,Chișinău 2001
3. AL-SUGAIR.- *Analysis of the time-dependent volume reduction of concrete containing silica fume*, Magazine of Concrete Research,47, No. 170, Mar., p.77-81,1995

Notes on microtriangulation network types as applied to the study of construction displacements

Carmen Nutiu

*Ph. D. Eng., Senior Lecturer, Faculty of Civil Engineering, Technical University of Cluj-Napoca,
400363, Romania*

Summary

The wide diversity of construction types and methods of designing and building various structures made it necessary that the civil engineer expert should be involved in topographical measurements and observation in time of the edifices; these observations are made over long periods of time, including the building process itself and the commissioning.

The study herein aims to present several types of microtriangulation networks used in topographical measurements, along with observation points and supporting points, which make part of topographical methods applied to the study of construction displacements.

In fact, every objective to be analysed poses different problems pertaining to location, type of terrain, size, purpose and utility; this leads to choosing a type of network that has to meet all the requirements in terms of accuracy and to offer the possibility of performing the measurements and satisfy all demands imposed by such experiments.

KEYWORDS: topographical-geodetical methods, microtriangulation network, displacements and deformations in construction, control points, observation points, orienting points.

1. INTRODUCTION

In choosing best options for designing and commissioning the construction buildings we must consider a thorough and complex study which is to be made at the beginning of the construction process, during inspection, execution and commissioning.

During designing phase, the experimental study consisting of construction testing has the following objectives:

- Numerical values for all parameters that describe the construction from the physico-mechanical point of view;

- Analysis of global characteristics of the construction/element using some coefficients which describe the behaviour of the structure in certain stress conditions that may be specific to the commissioning process, or may appear in special circumstances;
- A generalization of the results so that they can be applied on a large scale for a wide variety of construction structures, in different commissioning conditions.

The accuracy of the experimental parameters influences the accuracy of all the other parameters. For this reason, the selection of the equipment and methods cannot be randomly made, but in strict relation to their degree of sensitivity and accuracy so as the value for a parameter that cannot be measured directly should be obtained with best accuracy, regardless of the intermediate parameter used for this measurement. The accuracy depends on the accuracy of the measurements, and must ensure safe values for all parameters and indexes that characterize the construction.

The following reasons are given for the observation in time of the building:

- All common building material undergo certain processes of an evolutive nature, such as: quiet flow, relaxation, shrinkage, settlement, fatigue or ageing; in time, all these processes trigger changes of physico-mechanical characteristics, or alteration of effort distribution between the elements of the supporting structure of the building;
- In time, the behaviour of the construction can be altered by changes in environmental conditions
- In spite of all measures taken during design phase, there can be no accurate prediction as to what kind of future stress can be put on the construction structure.

The observation of construction behaviour is in fact a special type of testing triggered by the necessity of ensuring building safety during commissioning. By this type of observation we can determine the changes in form and position of the construction elements and the identification of the evolutive processes, which can threaten the safety of the building.

The optimisation of the construction eliminates the overmeasuring and reduces the use of raw material and consumption of energy, industrializes the construction and cuts down on costs.

2. BRIEF CLASSIFICATION OF CONSTRUCTION DISPLACEMENT MEASURING METHODS

The development of the measuring techniques made it possible to observe and identify the behaviour of the construction structures. There are many classification criteria for these methods of analysis and observation. The classifications were made according to the type of deformation, the type of measuring equipment, or the place where this equipment is placed during the analysis.

2.1. *Physical methods*

- made with the measuring equipment mounted inside the construction structure. In this case, the measuring equipment is displaced simultaneously with the structure, so the relative deformation and displacement can be measured. This type of measurement can be made using mechanical, physical, electrical or electronic methods. For this case, we can define a relative model, as there are no external supporting points. We have only results for relative movements between the points that are moving on the same object. According to the type of the parameters to be determined, we can include in this group:

- Measuring of linear displacement and deformations (settlements, arches, horizontal displacements) using the arch amplifier, stick gauge, thread comparator (for transmission of the displacement over long distance);
- Measuring of angular displacement (turnings) using the lever clinometer, spirit level clinometer and pendulum clinometer;
- Measuring of relative sliding displacement using the caliper beam or the stick gauge;
- Measuring of specific crippings using tensiometers or electrical, mechanical, optical-mechanical, pneumatic, photoelastic or electroacoustical (with vibratory chord) strain gauges;
- Measuring of displacements, speeds, accelerations and dynamic deformations using the vibration meter, vibration-measuring apparatus, seismic accelerograph, electrodynamic accelerometer (piezoelectrical or resistive), transducer of seismometric type, magnetolectrical recorder, cathode-ray oscillograph;
- Measuring of the deformations for the expansion joints using a tele-dilatometer and a micrometer for measuring expansion joints.

2.2. Geometric methods

- used when the measuring equipment is placed outside the construction structure; the measurements will be made using a network of fixed points placed outside the influence area of all the elements that impinge on the construction and the terrain. This method determines absolute values for the horizontal and vertical displacements. In this category we can include topographical-geodetical methods. The object itself is represented by several object points; the measurements are made between these points. Outside the analysis field, where the deformations are not present, we have a number of supporting points, considered to be very stable from the construction technique and geology issues point of view.

In this case we can say that we have defined an absolute model (if the displacements are determined as against the external supporting points).

According to the deformation type, we have the following topographical-geodetical methods:

Methods for measuring horizontal displacements and deformations:

- Trigonometrical method – microtriangulation
- Alignment method
- Accuracy traverse method

Methods for measuring vertical displacements and deformations:

- Highly accurate geometric levelling method
- Highly accurate trigonometric levelling method
- Hydrostatic levelling method

Methods for measuring the tilt of high buildings:

- Method of vertical projection
- Method for measuring the horizontal angles, using two or more base points
- Method of coordinates
- Method for measuring horizontal and vertical angles, using one base point.
- Method for measuring small zenith distances, using two points at the base of the construction
- Method for measuring the settlement of the foundation.

These methods can be used separately or in combination, according to the nature of the parameters that must be identified for the construction to be studied. The analysis of the construction using topographical-geodetical methods is made by cyclical measuring processes (angular and linear), using points outside the structure with projection on points placed on the construction.

As the degree of accuracy is very high with these procedures of data processing and assessment, the topographical-geodetical methods represent a fundamental system in the process of construction analysis.

3. TYPES OF SUPPORTING NETWORKS IN OBSERVATION OF CONSTRUCTION STRUCTURES

When processing the linear and angular measurements, either the vector of vertical or horizontal displacement can be obtained, or, first, the values of the components laid on the orthogonal axes, then the value for the displacement vector.

The microtriangulation method is used to observe in time the behaviour of massive construction structures (dams, locks, viaducts, bridges, monumental edifices) and the terrain pertaining to these.

The valuation of the vector for the horizontal displacement and construction settlement involves repeated measurements of the microtriangulation network, maintaining the same accuracy used when the network was set. The compensation calculations must be rigorously performed, using the method of smallest squares, for obtaining the most probable values for the coordinates of the network points.

The network consists of the following points:

- Control points - named also settling benchmarks, they are mounted on the construction structure that is to be observed. They are marked with beacons of different shapes and made of chrome-plated bronze for protection against corrosion. The research showed that the best beacons are disc-shaped.
- Observation points – from here repeated observations are made towards the control points placed on the construction structure.
- Fiducial points - from here the changes in position for the observation points are identified; they are placed on solid ground, 200-300 m away from the observed construction to eliminate any impingement of the latter.
- Orienting points - are placed at long distances, on grounds with a high degree of stability, mentioned in the geotechnical studies.

The microtriangulation network can have the following structures: simple network, partial network and full network. In the below representations there are the notations as follows:

B_1, B_2, \dots, B_n - benchmarks set on the object

S_1, S_2, \dots, S_n - observation stations

C_1, C_2, \dots, C_n - control points

O_1, O_2, \dots, O_n - orienting points

3.1. Simple network

- consisting of observation points and fiducial points

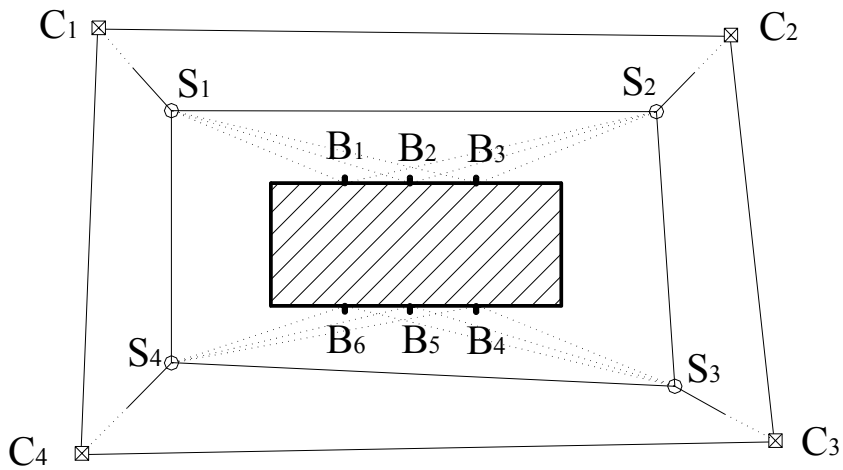


Figure 1 – Simple Observation Network

Partial network

- there are no reciprocal sight lines between observation points and fiducial points;

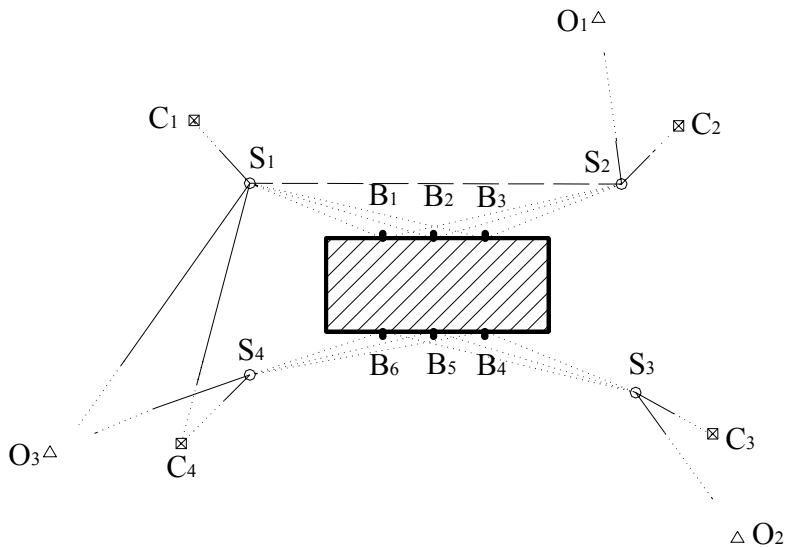


Figure 2 – Partial Observation Network

Full network

- consisting of all four types of points, with reciprocal sight lines between the observation points and the fiducial points;

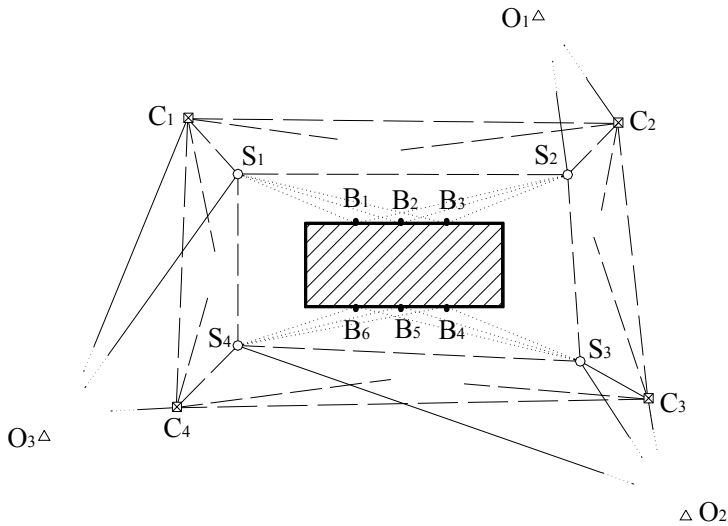


Figure 3 – Full Observation Network

When setting up a microtriangulation network we aim to obtain the best layout for the geometric figures involved for the purpose of gaining an accuracy that will fully meet all the requirements. The observations in the microtriangulation network points are made with the accuracy that corresponds to the 1st, 2nd and 3rd degree networks, using the method of complete series (reiterations). During measuring process, measures will be taken for eliminating the effect of systematic errors and for reducing the random errors to a minimum.

4. CONCLUSIONS

Based on what was stated so far, there remains the possibility to set up new types of microtriangulation networks as applied to the observation of the construction structure.

In the last decade, the development of the spatial geodetical technologies applied in the study of the construction behaviour led to the implementation of these methods that use observation networks focused rigorously upon constructions like hanging bridges. Also, specially designed networks can be set up in mining areas.

In fact, every objective to be analysed poses different problems pertaining to location, type of terrain, size, purpose and utility; this leads to choosing a type of network that has to meet all the requirements in terms of accuracy and to offer the possibility of performing the measurements and satisfy all demands imposed by such an experiment.

References

1. Neamțu, M., - Complemente de topografie inginerească – Partea I. Măsurarea deplasărilor și deformațiilor construcțiilor prin metode topografo-geodezice, Institutul de Construcții București, 1973.
2. Neamțu, M., Onose, D., Neuner, J., - Măsurarea topografică a deplasărilor și deformațiilor construcțiilor, Institutul de Construcții București, 1988.
3. Mușat, C., - Contribuții privind stabilirea tasărilor și deformațiilor construcțiilor utilizând metode și tehnici topografico-geodezice moderne, Referat doctorat, Timișoara, 2002.
4. *** - Măsurători terestre, Fundamente, volumul II, Editura Matrix Rom, București, 2002.

3D modeling and calculation of the fixed platform PFS-U (PESCARUS)

Alexandru Dima¹, Ionuț Radu Răcănel²

¹Assoc.Prof., PhD, Bridges Dept., Technical University of Civil Engineering, Bucharest, Romania

²Lecturer, PhD, Bridges Dept., Technical University of Civil Engineering, Bucharest, Romania

Summary

Fixed platforms for the exploitation of petroleum deposits in the continental Black Sea Romanian platform are usually built like 3D welded truss structures (called “jacket”), using circular hollow sections. The structure has lateral inclined faces and it is grounded using steel driven piles disposed at the interior part of the jacket columns. This construction solution asks that the drilling can be done through the jacket slots only after the placement of the offshore into position.

For the “PESCARUS” location a fixed 4-faces platform was designed, in a new solution, having an open jacket at one of the faces (this was called “Fixed support platform PESCARUS”). This structure should allow the earlier drilling of the offshore wells (using a self-lifting platform) and in this case the construction of the PFS-U platform can be done at a later time.

For the design and calculation of this platform a full finite element 3D model was built. The model takes into account the real dimensions of element cross sections, the stiffness of the structure and the structure-soil interaction respectively. For the evaluation of the dynamic response of the structure a 3D dynamic finite element model was considered, the position of masses on the structure being very close to the real one.

This paper present important aspects regarding the finite element model, the evaluation of the location specific actions and loading hypotheses, but also the resistance and stability checks according to the accepted norms.

KEYWORDS: platform, jacket, structure-soil interaction, dynamic response, loading

1. INTRODUCTION

The fixed marine platforms in the petroleum deposits of the Black Sea erected for water depths between 40.0 and 60.0 m consist, generally speaking, in two parts:

- a 3D welded truss structure (called “jacket”) with circular hollow sections, which is transported into position through floating, is placed in vertical position by bearing on the sea floor and then is fixed using steel driven piles disposed at the interior part of the jacket columns. The jacket height is established according to the water depth, so that his upper part reach the level +3.00 m above the water level (figure 1)
- a decks system, erected each like 3D steel parts above the jacket level, using columns and counterbraces. Those will sustain the equipments and materials which are necessary for the oil extraction technology (figure 1).

The jackets of the Romanian marine platforms were designed with 3, 4 and 6 steel columns and are called according to this number: tripod, tetrapod and hexapod respectively. In the same time the marine platforms are called according to their destination or functions in the oil extraction system::

- fixed platform flame support (tripod type);
- fixed platforms with offshore wells “PFS” for sustaining wells tubes (tetrapod type);
- central fixed platforms “PFC” for sustaining the installations necessary for the function and survey of the petroleum extraction equipments (hexapod type);
- platform for the social group and utilities “P.G.S.U.” (de tip hexapod).

Generally, for the marine platforms of P.F.S type, the drilling of the offshore wells is made through the jacket slots after the placement of the platform into position and this has as consequence a longer time for construction. For the fixed platform sustaining offshore wells PFS-U PESCĂRUȘ a special jacket was designed, in order to allow the assembling into location of the platform after the previous drilling of the offshore wells. This procedure lead to a lower value of the self weight of the platform and in this way the transport into location and the assembly of the structure could be done with equipments existing in Romania. The platform PFS-U has a tetrapod type jacket, with steel driven piles and has the following characteristics:

- decks system has 3 levels (+20.500, +16.500, +12.500), with a cantilever structure at the first two, at the face side II;
- the jacket is U-type (with face IV open, without braces and horizontals), other 3 side faces being foreseen with braces and horizontals; all side faces are inclined;
- the open side face will be closed in the future with braces, at the upper part, between levels +3.00 and +1.00, after the installation of the jacket into position;

The design and the final solution of the oil platform was made in two stages as a result of the revision in 1999 of the thicknesses for the marine growth, but also for the values and positions of the loading on the decks.

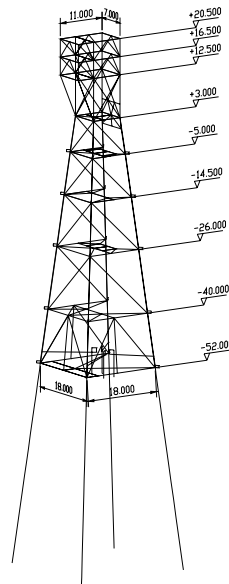


Figure 1 – The general scheme of the offshore wells platform PFS-U

2. FINITE ELEMENT MODELLING OF THE STRUCTURE

The finite element modelling of the fixed offshore wells platform PFS-U PESCĂRUȘ consist in a 3D model, with respect of the real geometry of the structure, of the structural elements stiffness, but also by taking into account the “jacket-piles-soil” interaction for the specific conditions of the platform. Thus, for the modelling of the jacket, decks and driven piles, two nodes straight beam elements were used (FRAME elements) and the steel plates at each deck level and at the level of the horizontal frames where the offshore wells are fixed in the slots were modelled using area elements with four nodes (SHELL).

At the upper part of the jacket (at level +3.00) the piles ends are directly welded at the corresponding columns and for this reason, at this level, the ends of piles and columns are connected through a common joint. In the model, the piles are disposed parallel to the jacket columns at the maximum distance allow by the movement between the pile and movable devices at the interior part of the pile (guiding devices).

The working connection between piles and jacket is modelled with elastic small frames placed at the joints of the jacket bellow level +3.00 and dimensioned in such a manner to allow elastic independent deformations between piles and jacket. This solution lead to the values of the horizontal displacements at each pile joints correlated with the displacements of the piles at the interior part of the columns and with the displacements of the jacket joints under loads. The calculation is made in some successive steps, for a applied load on the pile about 1000 to (value which is near to the maximum capacity of the pile), establishing in this way the cross section characteristics of the finite elements forming the frames according to their real stiffness. The first two elements of the working frames (the horizontal element at the bottom of the frame and the vertical element) results with a circular cross section having a 0.428 m diameter, and the top horizontal element, which allow relative independent displacements along the piles, between piles and jacket, was designed as a steel plate, having a very high stiffness value in horizontal plane and very small stiffness value in vertical plane (figure 2).

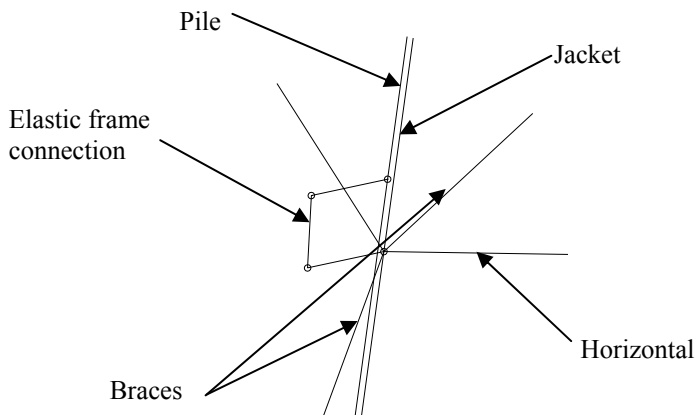


Figure 2 – Detail for the elastic frame connection between pile and jacket

The soil piles bearing is made through straight beam elements with two nodes which can take only axial force (pin ended beams) and having a unity length. These elements are placed along the piles at distances established according to each soil layer depth. The variable cross sections of these frames comes out from the condition that the settlement (which is dependent on the coefficient of soil reaction at the level of the corresponding frame element) under the pressure produced by the soil on the interaction surface of a pile from a unity load is equivalent with the axial deformation produced by the same load to a pin ended beam having 1m length, cross section A and elasticity modulus of the material E (2.1×10^7 to/m² for steel).

The values for the coefficients of soil reaction k_h [kN/m³] for each characteristic layer and their variation on the depth were established according to the physical-mechanical characteristics of the soil layers existing on the piles length.

3. LOAD HYPOTHESES FOR RESISTANCE AND STABILITY CHECKS

The loading hypothesis corresponds to the demands in Section C, “Loads” of API - RP 2A-LRFD and API RP 2A-WSD:

a) Hypothesis Q1 = 1,3(D1 + D2) + 1,5(L1 + L2) where:

D1 = self weight of the structure and equipments permanently mounted on the platform;

D2 = self weight of the equipments mounted on the platform. Their position can change according to the mode of operation;

L1 = includes the weight of consumable supplies and fluids in pipes and tanks;

L2 = live load exerted on the structure from operations such as lifting by cranes, machine operations vessel mooring etc.

b) Hypothesis Q2 = 1,1(D1 + D2 + L1) + 1,35(We + Dn) where:

D1; D2; L1 have been defined at point a);

We = sectional stresses in the analysed structural element produced by wind, wave and current loads action, in the most disadvantageous situation.;

Dn = sectional stresses in the analyzed frame coming from earthquake action (only for structures having a fundamental period over 3 sec.).

Taking into account the from, in plane, of the platform (figure 3) and the presence only of a load type L2, insignificant as value, the following load cases of the jacket, for resistance and stability checks, are considered:

a) For permanent actions D1+D2 and L1 type

Case 1: Loads coming from D1 and D2;

Case 2: Loads coming from L1 (having load L2 included).

b) For loads coming from wave actions H=14.1 m, current and wind

Case 1: Wave forces H=14.10 m, wind and current $\theta = 0^\circ$ with respect to Y axis, (W_e for $\theta = 0^\circ$)

Case 2: Wave forces H=14.10 m, wind and current $\theta = 45^\circ$ with respect to Y axis, (W_e for $\theta = 45^\circ$)

Case 3: Wave forces H=14.10 m, wind and current $\theta = 90^\circ$ with respect to Y axis, (W_e for $\theta = 90^\circ$)

Case 4: Wave forces $H=14.10$ m, wind and current $\theta = 225^\circ$ with respect to Y axis, (W_e for $\theta = 225^\circ$)

Case 5: Wave forces $H=14.10$ m, wind and current $\theta = 270^\circ$ with respect to Y axis, (W_e for $\theta = 270^\circ$)

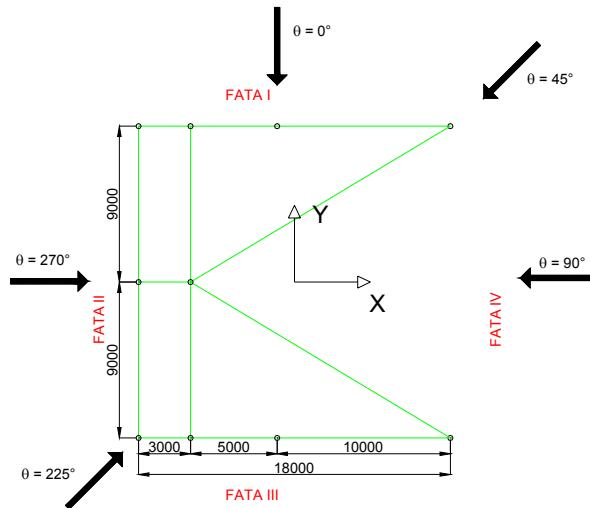


Figure 3 – Directions for wave and current loads

The sectional stresses (characteristic values) coming from these 2+5 loading cases are necessary to perform the resistance and stability checks for the structural elements of the jacket and for the resistance checks of the tubular joints respectively.

The maximum values of the sectional stresses are obtained by multiplication of the sectional stresses, determined according to the procedure presented above, through coefficients corresponding to hypotheses Q1 and Q2.

4. EVALUATION OF LOADS COMING FROM D1, D2, L1, L2 AND WIND ACTION

The values and positions of the loads coming from D1, D2, L1 and L2 on decks were established through survey of the specific equipments existing on decks but also by considering the technical data concerning the volume and the self weight of some installations, including live loads. For the evaluation of wind loads, the appropriate exposed surfaces are calculated, inclusive the perimeter protection shields disposed at levels 12.500 and +22.500.

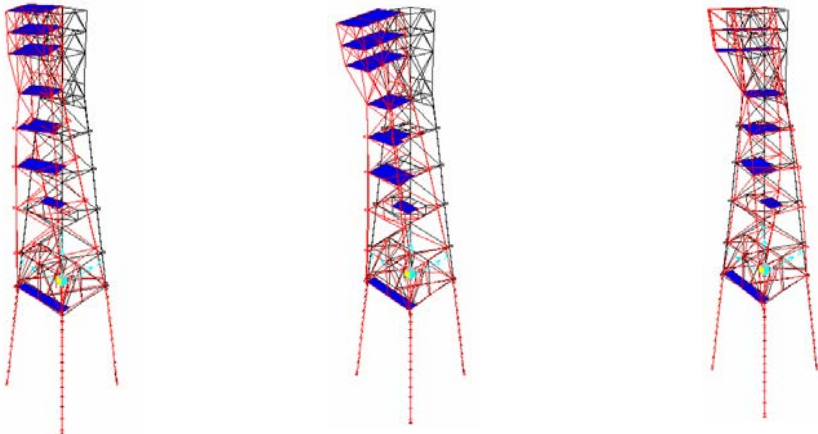
The exposed surfaces for the wind action directions (θ), are:

For $\theta = 0^\circ$ and $\theta = 180^\circ$	$A_1 = 110.0 \text{ m}^2$
For $\theta = 45^\circ, \theta = 135^\circ ; \theta = 225^\circ$ and $\theta = 315^\circ$	$A_2 = 137.0 \text{ m}^2$
For $\theta = 90^\circ$ and $\theta = 270^\circ$	$A_3 = 56.0 \text{ m}^2$

The wind loading hypotheses are taken according to the extreme wave loading hypotheses $\theta = 0^\circ, \theta = 45^\circ, \theta = 90^\circ, \theta = 225^\circ$ and $\theta = 270^\circ$ and they were coupled with each wave loading direction according to the load cases 3, 4, 5 and 6.

5. THE EVALUATION OF MAXIMUM WAVE LOAD FORCES AND CURRENT FORCES

For the computation of the maximum values of sectional stresses in structural elements from wave and marine current action, necessary to form Q2 hypothesis, in order to perform the resistance and stability checks, the load components at the joints of the finite element model are used. The forces corresponding to waves are computed for $H=14.1 \text{ m}$ water height with a period of 10.2 sec. For the forces coming from marine current, the current velocity was taken 1.10 m/s at the water surface and 0.28 m/s at sea floor, according to the data from ICIM București, given for all 5 directions of extreme wave.



a) Mode 1 – $T=1.207 \text{ sec.}$

b) Mode 2 – $T=0.985 \text{ sec.}$

c) Mode 3 – $T=0.686 \text{ sec.}$

Figure 4 – Deformed shapes from dynamic analysis

The considered marine growth have a thickness about 0.08 m/radius till a water depth of 25 m and a thickness of 0.04 m/radius below this level.

6. DYNAMIC MODEL AND EIGENMODES

The finite element model for the dynamic analysis has the same configuration like for the static analyses, but at joints, where the concentrated forces coming from dead loads acts (cases 1 and 2), are placed the additional masses corresponding to these loads. Using a linear eigenvector analysis, three eigenmodes are computed. The deformed shapes are presented in figure 4.

7. RESISTANCE AND STABILITY CHECKS

The design values for the sectional stresses, obtained through multiplication of characteristic values (from finite element analyses) with the corresponding coefficients (hypotheses Q1 and Q2) were used to perform the resistance and stability checks for structural elements and joints. In figure 5 is presented the distribution of axial force for jacket and piles under static loads.

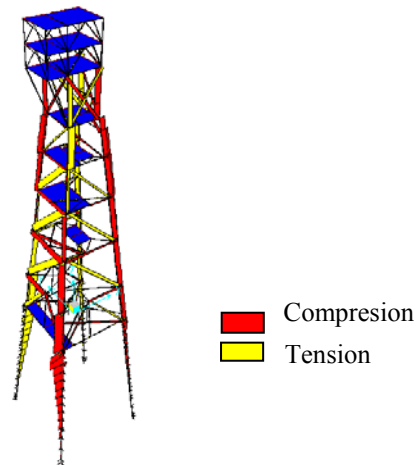


Figure 5 – Axial forces from wave and wind action (Case 1)

7.1 Tubular joints checks (API-RP 2A WSD)

- a) The geometrical condition for tubular joints check in tension and compression:

$$\left[\frac{F_{yb} (\gamma \sin \theta)}{F_{yc} (11 + 1.5/\beta)} \right] \leq 1 \quad (1)$$

where:

F_{yb} the yield strength of the brace member
 F_{yc} the yield strength of the chord member

β, γ, r, θ joint geometry parameters

b) The adequacy of the joint may be determined on the basis of:

Punching shear, considering the equations:

$$v_p = rf \sin \theta / \beta \leq v_{pa} = Q_q \cdot Q_f (F_{yc} / 0.6\gamma) \quad (2)$$

$$\left(v_p / v_{pa} \right)_{IPB}^2 + \left(v_p / v_{pa} \right)_{OPB}^2 \leq 1 \quad (3)$$

$$\left| v_p / v_{pa} \right|_{AX} + (2/\pi) \arcsin \sqrt{\left(v_p / v_{pa} \right)_{IPB}^2 + \left(v_p / v_{pa} \right)_{OPB}^2} \leq 1 \quad (4)$$

In the above equations Q_q and Q_f are factors and AX , IPB and OPB means axial, in plane bending and out of plane bending moments respectively.

c) **Nominal loads**, considering the equations:

$$N \leq N_a = Q_q^N Q_f^N F_{yc} T^2 / (1.7 \sin \theta) \quad (5)$$

$$M_{IPB} \leq (M_a)_{IPB} = \left(Q_q^M \right)_{IPB} \left(Q_f^M \right)_{IPB} F_{yc} T^2 (0.8d) / (1.7 \sin \theta) \quad (6)$$

$$M_{OPB} \leq (M_a)_{OPB} = \left(Q_q^M \right)_{OPB} \left(Q_f^M \right)_{OPB} F_{yc} T^2 (0.8d) / (1.7 \sin \theta) \quad (7)$$

$$\left(M / M_a \right)_{IPB}^2 + \left(M / M_a \right)_{OPB}^2 \leq 1 \quad (8)$$

$$\left| N / N_a \right| + (2/\pi) \arcsin \sqrt{\left(M / M_a \right)_{IPB}^2 + \left(M / M_a \right)_{OPB}^2} \leq 1 \quad (9)$$

In the above relationships N , M_{IPB} and M_{OPB} are the axial force, in plane bending moment and out of plane bending moment respectively, N_a , $(M_a)_{IPB}$ and $(M_a)_{OPB}$ are the allowable values for the same stresses.

T thickness of the chord wall

d diameter of the brace

7.2 Buckling check of the structural elements

The buckling strength of the platform structural elements is checked according to the relationship given in Germanischer Lloyd's, Section 3, point 22.4:

$$\left(\Gamma_m N \right) / \left(k N_p \right) + \beta_m \left(\Gamma_m N \right) / M_p + \delta_n \leq 1 \quad (10)$$

where:

$\Gamma_m, k, \beta_m, \delta_n$ coefficients

N elastic axial force in the brace

N_p, M_p plastic axial force and in plane bending moment in the brace.

8. RESULTS AND CONCLUSIONS

The analyses results, which are given for some elements in tables 1-3, have shown that for some structural elements, the checks are satisfied near to the limit value.

Table 1 Results for tubular joints checks

Joint / Frame	Equation number						
	1	2	3	4	5	8	9
Joint 10 Frame 204	0.66 <1.0	321.4 < 411	0.012 <1.0	0.849 <1.0	294 to <376.2 to	0.012 <1.0	0.851 <1.0
Joint 19 Frame 205	0.76 5 <1.0	342.5 < 411	0.018 <1.0	0.918 <1.0	271.3 to <325.2 to	0.018 <1.0	0.920 <1.0
Joint 31 Frame 206	0.72 6 <1.0	near limit 400.0 < 430	0.012 <1.0	near limit 0.999 <1.0	near limit 242.2 to <262.3 to	0.011 <1.0	near limit 0.992 <1.0
Joint 39 Frame 207	0.66 2 <1.0	122.0 < 470	0.007 <1.0	0.313 <1.0	55.1 to <216.6 to	0.006 <1.0	0.305 <1.0
Joint 60 Frame 88	1.06 <1.0	58.1 < 421	0.008 <1.0	0.196 <1.0	16.4 to <121.1 to	0.007 <1.0	0.189 <1.0

Table 2 Results for buckling checks for jacket columns (chords) and horizontals

Frame type	Frame number	Buckling checking condition
Column	135	0.509 < 1.0
Column	148	0.261 < 1.0
Column	164	0.517 < 1.0
Column	167	0.278 < 1.0
Column	171	0.406 < 1.0
Horizontal	25	1.03 < 1.0 (near limit)

Table 2 Results for buckling checks for braces

Frame type	Frame number	Buckling checking condition
Diagonal	136	0.513 < 1.0
Diagonal	143	0.952 < 1.0 (near limit)
Diagonal	151	0.352 < 1.0
Diagonal	205	0.794 < 1.0
Diagonal	206	0.933 < 1.0 (near limit)
Diagonal	207	0.450 < 1.0

The fundamental period of the structure resulting from the dynamic analysis is 1.207 sec. < 3 sec. so that the consideration only of the first 3 eigenmodes according to API is allowed.

The resistance checks results for the joints and also the buckling check results for braces shows that, reconsidering the position of some structural elements and also

their dimensions, the check criteria in API are satisfied. For the joints where these conditions are satisfied near limit it is necessary to introduce a chord clutch with larger wall thickness in the joint region.

References

1. Foundation Analysis and Design – Joseph E. Bowles (Capitolul 3, paragrafele 3-6, 3-7, 3-8, 3-9),
2. The Standard Penetration Test: Methods and use – Report 143/1995, , CIRIA
3. API RP 2A-LRFD - Load and Resistance Factor Design (Edition 1993);
4. API RP 2A-WSD, - Working Stress Design (Edition 1993);
5. GERMANISCHER LLOYD - Rules for Classification and Construction, Offshore Technology (Edition 1990)

Dynamic thermal behavior of building components. Calculation methods

Rodica Rotberg¹

¹Ph.D., Technical University “Gh. Asachi” Iasi

Summary

European standard prEN ISO 13786 specifies the characteristics related to dynamic thermal behaviour of complete building components and gives methods for their calculation, data required, period of thermal variations.

The paper presents matrix transfer method for thermal calculus of building elements, and examples of application

KEYWORDS: building, dynamic thermal characteristics, calculation methods

1. INTRODUCTION

The steady-state R value, traditionally used to measure energy performance of a building envelope does not accurately reflect the dynamic thermal behaviour of all complex building envelope systems. In this way, the effects of thermal inertia are neglected, or, in a better case, are taken into account by means of some correction coefficients.

Currently, the standard modeling practice is to replace complex material configurations by one dimensional multi-layer structures with similar R values and similar material arrangements. Unfortunately, such simplifications cannot accurately represent the complicated dynamic heat transfer that takes place in many currently used wall and roof assemblies.

Simplified models were developed based on classical heat transfer theory and resistance-capacitance analogues. The simplified procedures apply only to plane components. They are based on the penetration depth of a heat wave calculated for the material adjacent to the surface.

European standard prEN ISO 13786 specifies the characteristics related to dynamic thermal behaviour of complete building components and gives methods for their calculation, data required, period of thermal variations.

2. EUROPEAN STANDARDS STIPULATIONS

European standard prEN ISO 13768 recommends matrix transfer method for dynamic thermal characteristics calculus of building elements.

The procedure is as follows:

- identify the materials comprising the layers of the building component and the thickness of these layers, and determine characteristics of the materials ;
- specify the period of the variations at the surfaces ;
- determine the elements of transfer matrix for each layer ;
- multiply the layer transfer matrices, including those of boundary layers, in the correct order to obtain the transfer matrix of the component – Z –

The transfer matrix of the building component from surface to surface is:

$$Z_{SS} = \begin{pmatrix} Z_{11} & Z_{12} \\ Z_{21} & Z_{22} \end{pmatrix} = Z_N Z_{N-1} \dots \dots Z_2 Z_1 \quad (1)$$

where Z_1, \dots, Z_N are the transfer matrices of the various layers of the building component, beginning from layer 1. As a convention for building envelope components, layer 1 shall be the innermost layer.

The transfer matrix from environment to environment through the building component is:

$$Z = Z_{s2} Z_{ss} Z_{s1} \quad (2)$$

where Z_{s1} and Z_{s2} are the transfer matrices of the boundary layers, given by:

$$Z_s = \begin{pmatrix} 1 & -R_s \\ 0 & 1 \end{pmatrix} \quad (3)$$

R_s being the surface resistance of the boundary layer including convection and radiation.

The elements of the heat transfer matrix have the following physical interpretation:

$|Z_{11}|$ is a temperature amplitude factor, that is the amplitude of the temperature variations on side 2 resulting from an amplitude of 1 K on side 1 ;

$\varphi_{11} = \arg(Z_{11})$ is the phase difference between temperatures on both sides of the component ;

$|Z_{21}|$ gives the amplitude of the density of heat flow rate through side 2 resulting from a periodic variation of temperature on side 1 with an amplitude of 1K ;

$\varphi_{21} = \arg(Z_{21})$ is the phase difference between the density of heat flow rate through side 2 and the temperature of side 1 ;

$|Z_{12}|$ gives the amplitude of the temperature on side 2 when side 1 is subjected to a periodically varying density of heat flow rate with an amplitude of 1 W/m² ;

$\varphi_{12} = \arg(Z_{12})$ is the phase difference between the temperature on side 2 and the density of heat flow rate through side 1 ;

$|Z_{22}|$ is the heat flow rate amplitude factor, that is the amplitude of the variation of the density of heat flow rate through side 2 resulting from an amplitude of density of heat flow of 1 W/m² through side 1 ;

$\varphi_{22} = \arg(Z_{22})$ is the phase difference between the densities of heat flow rate through both sides of the component.

3. DYNAMIC THERMAL CHARACTERISTICS

Dynamic thermal transfer properties relate physical quantities on one side of the component on those on the other side.

The dynamic thermal characteristics for building components made of plane and homogeneous layers are thermal admittances and periodic thermal conductances.

The thermal admittances are:

- $Y_1 = \frac{Z_{11}}{Z_{12}}$ and $Y_2 = \frac{Z_{22}}{Z_{12}}$, Y_1 is for the internal side of the component, while Y_2 is for the external side;

Thermal admittance quantifies the heat storage property of a component.

- The periodic thermal conductances are :

$$L_{12} = AY_1 = A \frac{Z_{11}}{Z_{12}} ; ; ; L_{21} = AY_2 = A \frac{Z_{22}}{Z_{12}} \quad (4)$$

- The thermal capacities are:

$$C_1 = A \frac{T|Z_{11}|}{2\pi|Z_{12}|} \text{ and } C_2 = A \frac{T|Z_{22}|}{2\pi|Z_{12}|} \quad (5)$$

where A is the area of the building component.

- The decrement factor f is given by:

$$f = \frac{1}{|Z_{12}|U} \quad (6)$$

where the thermal transmittance, U , is calculated with $U=1/R$, R being the thermal resistance ;

The decrement factor is always less than 1.

4. EXAMPLES OF APPLICATION

The dynamic thermal characteristics of the closing elements were determined under harmonic boundary conditions for one day period, corresponding to daily meteorological variation and temperature setback.

Thermophysical characteristics of the materials used in the closing elements are:

a) for homogeneous elements:

Brick masonry wall (the thickness, $d = 0,36$ m) ;

- the thermal conductivity, $\lambda = 0,8$ W/mK ;
- the specific heat capacity, $c = 0,87$ KJ/KgK ;
- the density, $\rho = 1800$ Kg/m³

The four elements of the transfer matrix Z are :

$$\begin{aligned} Z_{11} &= -10.395 + 1.08i & Z_{12} &= 0.686 - 0.847i \\ Z_{21} &= 77.172 + 62.529i & Z_{22} &= -10.395 + 1.08i \end{aligned}$$

Taking account of surface resistances of $0,13$ W/(m²K) inside and $0,04$ W/(m²K) outside, the transfer matrix of the wall is:

$$\begin{aligned} Z_{11} &= -13.482 - 1.421i & Z_{12} &= 2.855 - 0.705i \\ Z_{21} &= 77.172 + 62.529i & Z_{22} &= -20.428 - 7.049i \end{aligned}$$

Decrement factor, $f = 0.211$, thermal transmittance $U = 1.613$ W/(m²K)

Table1 Dynamic characteristics of the homogenous element

	<i>thermal admittance</i>	
	modulus	time shift
internal side (Y_1)	4.611 W/(m ² K)	-10.679 h
external side (Y_2)	7.349 W/(m ² K)	-9.811 h
	areic heat capacities	
internal side (C_1)	6.343 (J/K)	-
external side (C_2)	10.111 (J/K)	-

b) Dumping and phase lagging for different multi-layer elements was calculated with matrix transfer method (table 2):

Table 2 Dumping and phase lagging of multi-layer elements

<i>Wall:</i> <i>(layer 1..n)</i>		<i>thermophysical characteristics</i>			<i>Dumping</i>	<i>phase lagging ε</i>
<i>(layer 1: internal;; external)</i>	<i>layer n</i>	λ W/mK	ρ Kg/m ³	c KJ/KgK	v []	<i>(hours)</i>
1. Brick (25 cm)		0.7	1600	0.87	14.015	-9.803
2. B.C. A (15 cm)		0.21	600	0.84		
1. B.C.A. (15 cm)		0.21	600	0.84	38.357	-10.25
2. Brick (25 cm)		0.7	1600	0.87		
1. Reinforced concrete (15 cm)		1.74	2500	0.84	72.435	7.714
2. Mineral wool (12 cm)		0.04	40	0.75		
1. Brick (25 cm)		0.7	1600	0.87	75.989	11.184
2. Mineral wool (8 cm)		0.04	40	0.75		
1. Mineral wool (8 cm)		0.04	40	0.75	5.488	9.628
2. Brick (25 cm)		0.7	1600	0.87		
1. B. C. A. (25 cm)		0.21	600	0.84	33.637	11.766
2. Mineral wool (8 cm)		0.04	40	0.75		
1. Mineral wool (8 cm)		0.04	40	0.75	5.957	10.084
2. B.C. A. (25 cm)		0.21	600	0.84		

3. CONCLUSIONS

The definitions given in this standard are applicable to any building component. The dynamic thermal characteristics defined in this standard can be used in product specifications of complete building components.

The dynamic thermal characteristics can also be used in calculation of:

- the internal temperature in a room ;
- the daily peak power and energy for heating or cooling ;
- the effect of intermittent heating or cooling; etc.

References

1. NP 107/7 –2002 *Normativ pentru proiectarea la stabilitate termică a elementelor de închidere a clădirilor.*
2. Asanache, Horia - *Higrotermica clădirilor*, vol. I, Ed. MATRIX ROM – București, 1999.
3. Roulet, Claude-Alain - *Energetique du batiment I*, Presses polytechniques romandes, 1987
4. Chemiller, Pierre – *Sciences et batiments*, Cours de l’Ecole Nationale de Ponts et Chaussées, Paris, 1992
5. European Standard pr EN ISO 13786 – *Thermal performance of building components. Dynamic Thermal characteristics, Calculation method*

Designing reticulated space systems

Constantin Jantea¹, Florin Varlam¹

¹Prof. Ph. D. eng. “Gh. Asachi” Technical University, Iași

Summary

The results of static and structural analysis, by means of a computer program, of two reticulated space structures made up of metal pipes are being presented.

1. INTRODUCTION

Reticulated space systems are structures made up of connected bars, either directly, if they are connected by hinges, or by gusset plates, aided by the weld. A system of bars, spatially developed from the point of view of static analysis is a multiply indeterminate structure whose solving in various assumptions of loading becomes possible only if we use computer programs. In what follows several aspects concerning the computation of two such structures will be made:

- Power line poles for night games, Onești stadium;
- Brine pipe duct over Trotuș river at Onești.

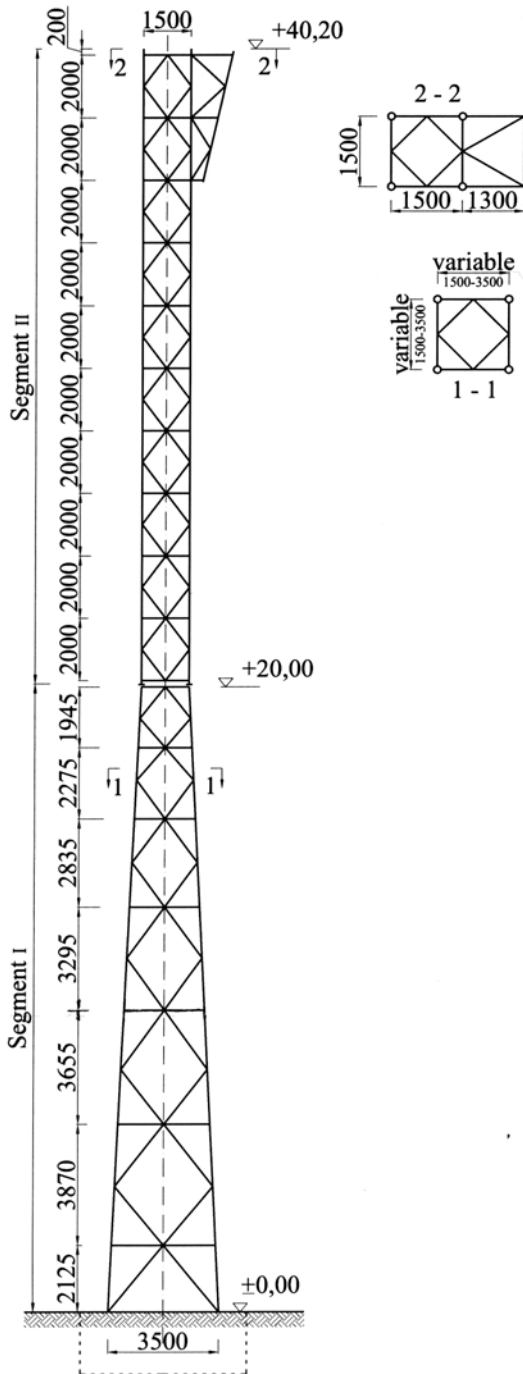
Of the two structures, the first has not been implemented, while the latter was built in 1995.

2. POWER LINE POLES FOR NIGHT GAMES, ONEȘTI STADIUM

2.1. Constructive solution

A pole (Fig. 1) is 40.20 m high considered from the upper surface of its foundation. It is a space structure made up of four branches which are hinge-connected in vertical plane by diamond shaped cross studs and additional struts (combined system). Furthermore, on the horizontal, at the strut level, diagonal bars are provided which form with the struts diaphragms that confer torsional rigidity to the pole. (section 1-1, Fig. 1).

The pole is built up of two segments, the bottom one - 20.00 m high, and a variable section ranging from 3.5×3.5 m at the base to 1.5×1.5 m at top, the upper one having a height of 20.20 m and a constant section of 1.5×1.5 m; this way the pole being subjected in its lower half to the bending moment diagram produced by the horizontal loads acting upon it (wind loads).



- vertical branches pole segment I $\varnothing 114 \times 8$
- vertical branches pole segment II $\varnothing 83 \times 8$
- diagonals pole segment I $\varnothing 48 \times 4$
- diagonals pole segment II $\varnothing 42 \times 4$
- horizontal struts segment I $\varnothing 60 \times 4$
- horizontal struts segment II $\varnothing 48 \times 4$
- diagonals diaphragms segment I, II $\varnothing 48 \times 4$

Fig. 1

The connection between sections is made using a flange and pin system. The joints between the pole bars made of seamless pipe are made by direct, welded joining (in fig. 2 is shown such a tie-bar joint).

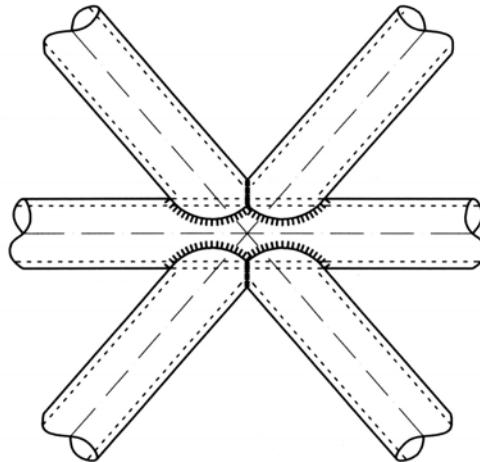


Fig. 2

At the top of the pole is located the support, made up of the same seamless pipe, for the electric lamps (Fig. 1).

2.2 Static analysis of structure

The structure is made up of 633 bars connected in 214 tie-bar joints. The structural analysis was made by means of a software SAP based on the bar-type finite element method. In a system of space co-ordinates $X-Y-Z$ in which Z is orientated along the pole, were written the input data: the co-ordinates of nodes that define the structure, the pole-ground embedding type, the characteristics of structure's bars cross-sections, the characteristics of material used in the structure, and the concentrated live loads in the nodes. Several sets of values were considered for the bar section, from which was chosen the most convenient set in terms of steel consumption. The final dimensions for the structure's bars are those shown in Fig. 1.

The loads for which the structure was analyzed were the following:

- dead load (including electric lamps weight);
- wind load;
- white frost weight.

The structure was analysed for the combination of live + wind loads which resulted as being more unfavorable than the combination of dead + wind + white frost loads, as the arrangement coefficient in the case of a single transitory load is 1,

while in the case of two transitory loads it is 0.9 (see STAS 10101/OA – 77), the arrangement coefficient 1.0 covering the effect of white frost loads neglect. The structural calculus was made at its ultimate state of strength and stability.

The computer program that we used highlighted both the sectional stresses in each bar, six in number - N_x , T_y , T_z , M_x (M_t), M_y , M_z – in a local space coordinates system (axis x orientated along the bar), and the unit stresses. Both sectional and unit stresses were determined for each load in its turn and for the dead + wind loads combination. The result was a large amount of data.

For a global, easier analysis of the structural stress state, the unit stresses in bars from each type of load were visualized in colors, and Fig. 3 shows the loading in the whole structure, while Fig. 4 details the loading level in the mean area of the pole, due to wind action.

These images, together with the tabulated values show us that the most loaded bars are those which compose the pole branches, in the zone where the variable section gives way to the constant one, the maximum unit stress in the structure being 1723 daN/cm^2 from the live + wind loads combination.

For the pole's nodes, the same program served to determine the displacements δx , δy , δz of the structure's nodes (in the general coordinates system from Fig. 3), of great interest being the horizontal deflection of the pole from wind loading, with a maximum displacement at the pole's end of 25.99 cm.

3. BRINE PIPEDUCT OVER TROTUȘ RIVER AT ONEȘTI.

3.1. Constructive solution

To make it possible for two pipe ducts to pass over Trotuș river, in order to transport brine between Tg. Ocna and Borzești, a metal space structure was designed out of seamless pipes. The solution for the duct structure (Fig. 5) comprises the two pipe ducts made of $\phi 351 \times 12$ are doubled by other two pipes of the same dimensions, meant to be a spare unit in the situation when a higher amount of brine is to be transported.

The four ducts located in the corners of a regular quadrangle with the side of 1400 mm are connected two by two with the diagonals of the triangular system, thus creating two trusses which in horizontal plan, at the upper and lower flanges level, are braced with struts to form a multiple framework, capable to take over the stresses from wind loads (Fig. 5, 6).

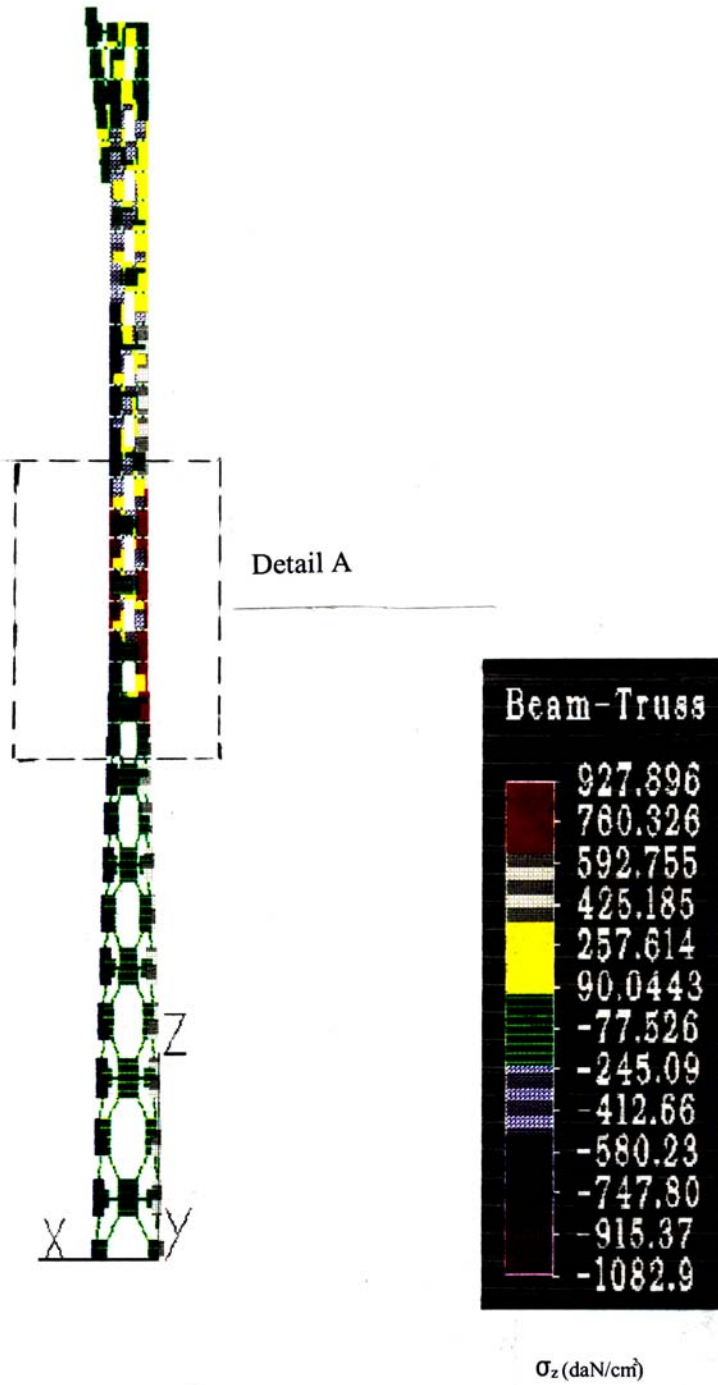


Fig. 3

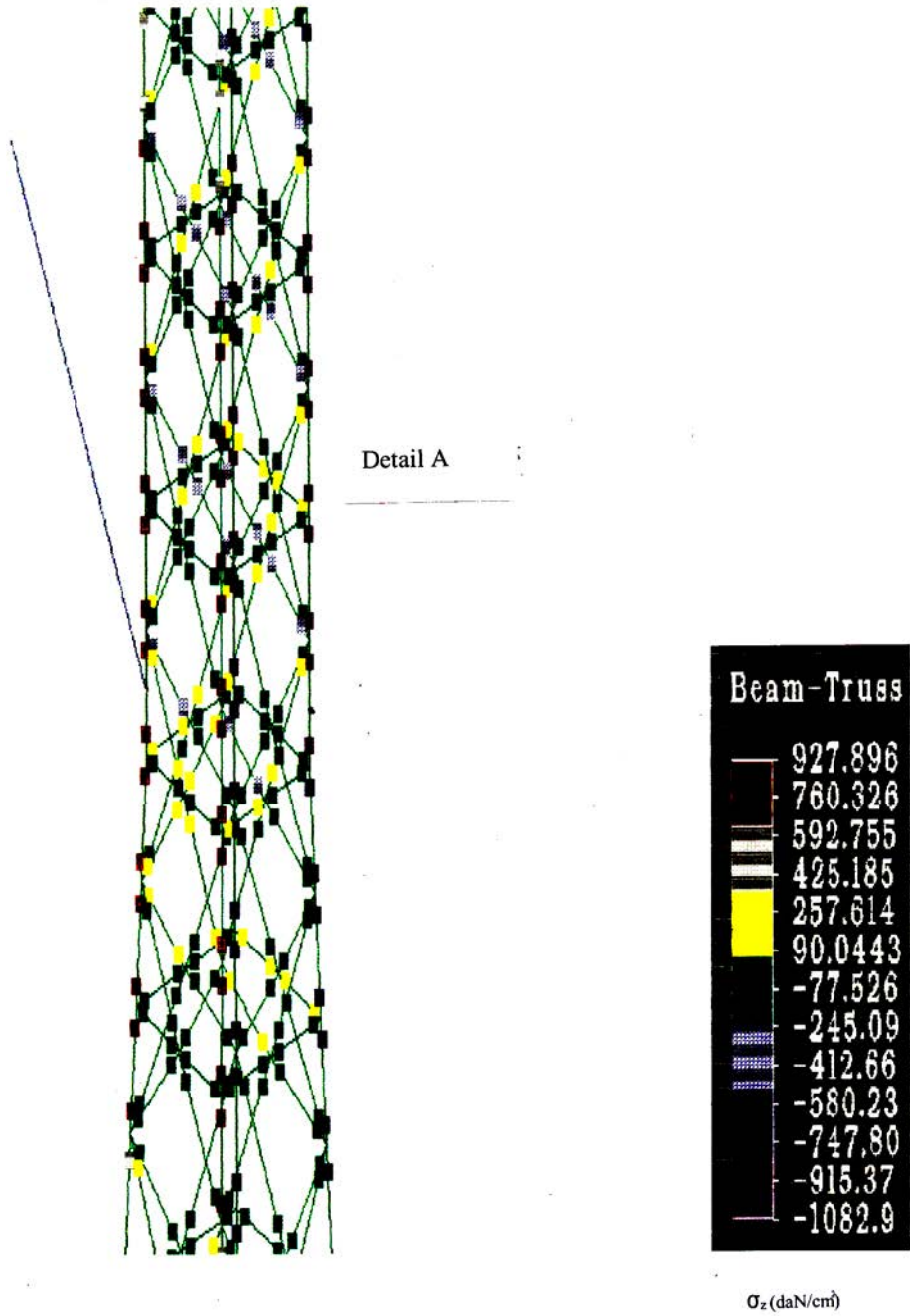


Fig. 4

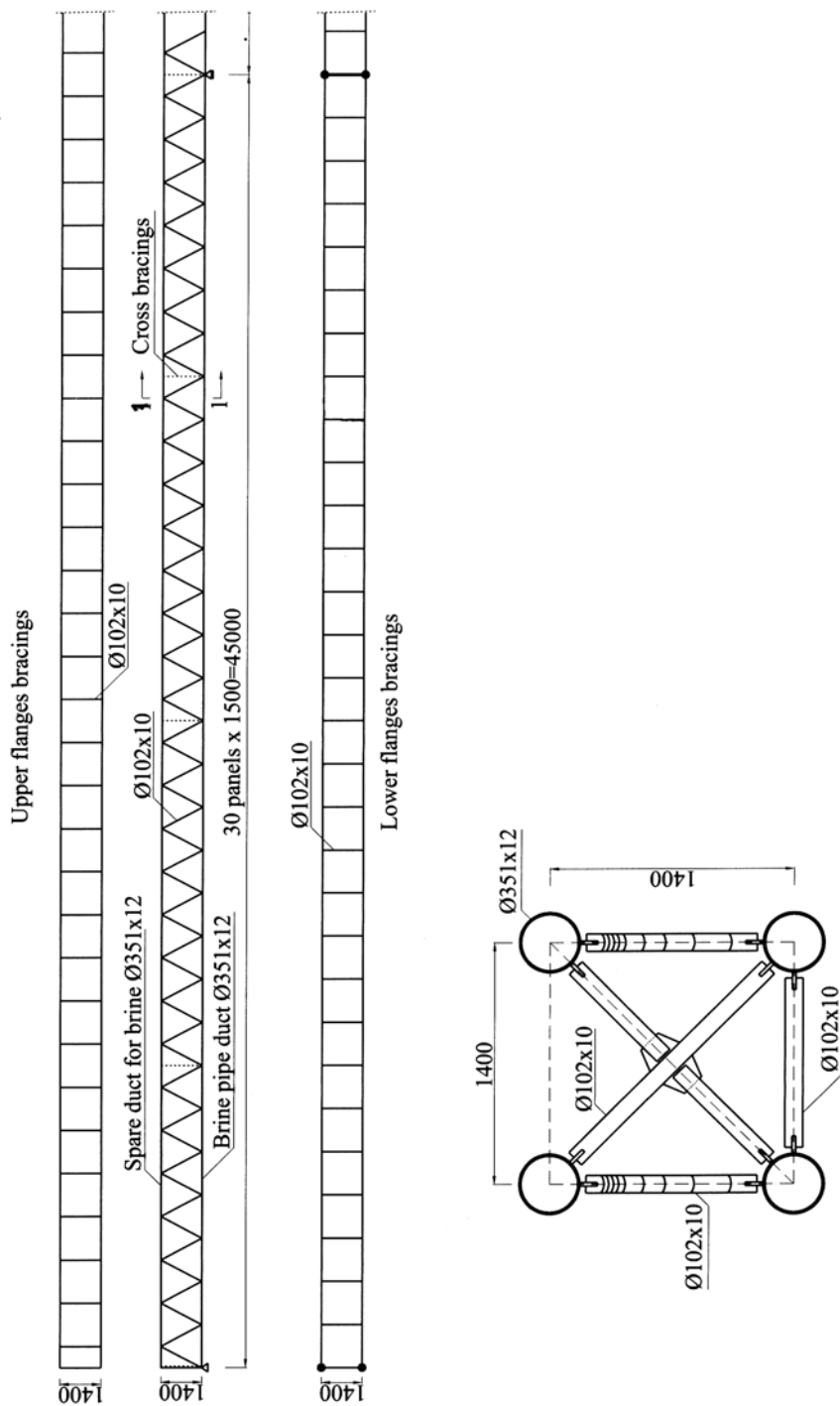


Fig. 5



Fig. 6

Furthermore, in order to increase the torsional rigidity of the structure, in various sections along the structure were provided cross bracings.

The over-crossing of Trotuș River is achieved by two continuous spans, 45 m each, supported on reinforced concrete piles (Fig. 7).



Fig. 7

The diagonals of the trusses and the bracing struts are made from pipe $\phi 102 \times 10$. The joining of the bars which ensure the connection between the main pipes is made by welding with gusset plates.

3.2. Structure’s dimensioning

The structure is a reticulated space one which is dimensioned for the following loads:

- dead load of the structure;
- weight of brine being carried by the ducts;
- wind load;
- snow load.

The structure is made up of 739 bars and 142 nodes. To determine the sectional stresses in the bars we used the same computer program, SAP that was used in designing the poles for night games. Six loading assumptions were made and from their combinations resulted the maximum sectional stresses (Fig. 8)

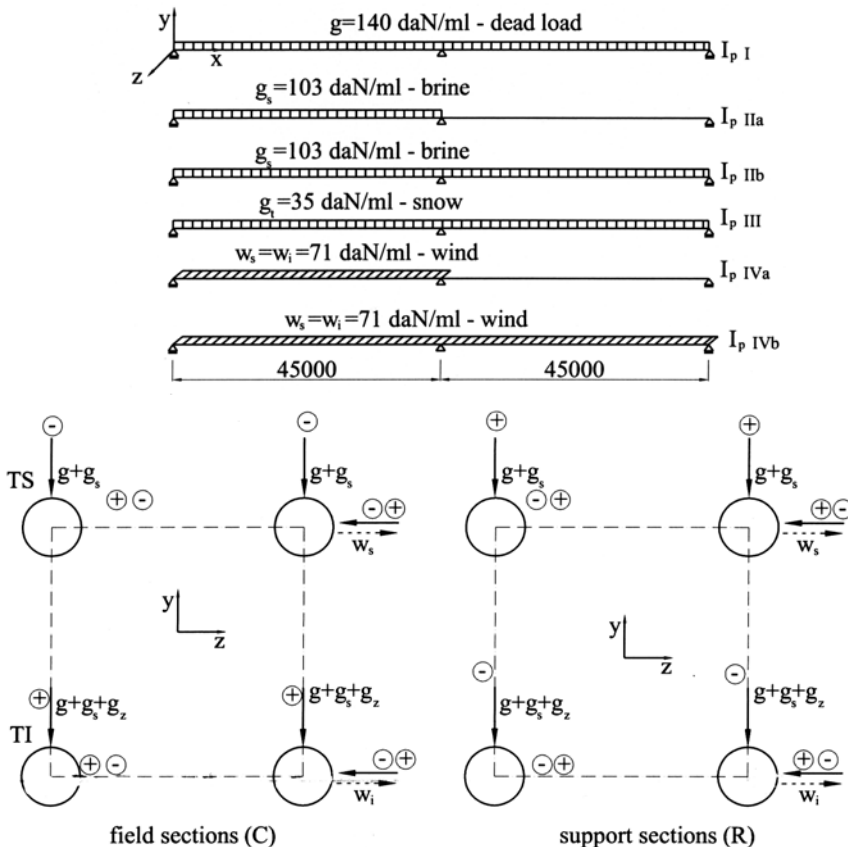


Fig. 8

By attaching a space system of coordinates $X - Y - Z$ to the structure, the program running produced the sectional stresses for each bar. The paper presents only the sectional stresses for the most loaded bars of the flanges in the span field (C) and in the central support (R) of the structure.

The assumptions II-a and IV-a are taken account of in determining the maximum stresses for the bars found in the span field, while the assumptions II-b and IV-b will be used in determining the bars at the side of the central support.

Table 1 shows the maximum sectional and normal unit stresses for these bars. From the six stresses, only the significant values were retained (T_y, T_z and $M_x(M_z)$ have low values). The most unfavorable loads combinations gave a maximum unit stress of 1337 daN/cm^2 .

Table 1

Loading Ipoteze	I		II a		II b		III		
	Nx	Mz	Nx	Mz	Nx	Mz	Nx	Mz	
T.I	C	29832	68154	27660	60000	-	-	3455	7492
	R	48644	224300	-	-	33180	152900	5639	26090
T.S	C	29813	63680	26930	60200	-	-	3457	7791
	R	51964	172260	-	-	35450	117600	6020	19660

Tabel 1 (continued)

IV a		IV b		Total stresses daN cm			Total unit stresses daN/cm ²
Nx	My	Nx	My	Nx	Mz	My	
7300	117500	-	-	68247	135646	117500	776
-	-	11630	184400	99093	403290	184400	1337
7291	193100	-	-	67491	131671	193100	839
-	-	9664	80740	103098	309520	80740	1179

4. CONCLUSIONS

- 1) In the case of multiple statically indeterminate structures, as are the reticulated ones, determining the stress-strain state is not possible without using performant computer programs, SAP being one of them, in different variants, all using finite element method.
- 2) In order to obtain accurate results, it is necessary to consider in the program a model of the structure that should represent it as accurately as possible, in

terms of connections between the component parts of the structure, of connections to the ground, and of loading assumptions.

- 3) As in general, such a computer program yields a very large amount of results, from these it will be necessary to extract the possible combinations which provide the highest loading and strain values to be used in comparing them with the design limit values.
- 4) In the case of the investigated structures, we consider that the adopted models and the results obtained were the correct ones, being confirmed by the 10 years of service life of brine pipe duct during which no defects have been discovered.

References

1. Jantea C., Varlam F., *Poduri metalice*. Editura Venus, Iasi, 1996
2. Dalban C., Juncan N., Varga Al., Dima S., *Construcții metalice*, București, editura Didactică și pedagogică, 1984
3. *** SR 1911 – 98, *Poduri metalice de cale ferată. Prescripții de proiectare*.
4. *** STAS 10101/20 – 1990, *Acțiuni în construcții. Încărcări de vânt*

The study of geocomposite influence on wearing course asphalt mixture behavior at permanent deformation

Elena Diaconu, Carmen Răcănel

¹Prof., Ph.D., Road Department, Technical University of Civil Engineering, Bucharest, Romania

²Assoc.Prof., Ph.D., Road Department, Technical University of Civil Engineering, Bucharest, Romania

Summary

Following the research, it was demonstrated that can be used the octahedral shear stress theory to analyze the premature deformation that appear in pavement asphalt layers.

This paper has an intention to study the influence of the place of geocomposite under the asphalt layer on the values of octahedral shear stress ratio.

To solve this problem we use the material characteristics obtained in laborator from triaxial test and an analyze of stresses and strains state in pavement structure, with and without geocomposite obtained using an elastic linear software.

The conclusion that can de drawn is the following: the placement of geocomposite lead to smaller octahedral shear stress ratio values in wearing course than in the case of structure without geocomposite.

KEYWORDS: geocomposite, asphalt mixture, permanent deformation

1. INTRODUCTION

One of the most important distresses that can appear in a flexible pavement structure is the permanent deformation. This kind of distress has considerable effects on circulation comfort and safety and for this reason the asphalt mixture that can become deformed under traffic and temperature, must be taken into account.

During the time it was demonstrated that the octahedral shear stress ratio (OSSR) is a very important parameter from pavement deformation point of view and gives the potential for rutting of mix. The OSSR (equation (1)) is the ratio of the critical induced octahedral shear stress in the pavement layer (τ_{oct}) to the octahedral shear strength of the material ($\tau_{oct, strength}$):

$$OSSR = \frac{\tau_{oct}}{\tau_{oct,strength}} \tag{1}$$

A detailed calculus for OSSR value is presented in references number [3], [4], [5].

In order to reduce the OSSR value in asphalt mixture it is suitable to place geocomposite under the new asphalt layer, if we discuss about the consolidation of an existing pavement structure.

The geocomposites are a combination of geosintetics and geogrids and they profit by the all advantages related to properties and functions of geosintetics and geogrids.

The geocomposites are polymer structures with a high tensile strength. This gives the possibility to use in pavement structures domain:

- the reinforcing of bituminous wearing course for roads, highways, airport runways;
- the avoidance of cracks propagation in pavement structure;
- the decrease of permanent deformation in pavement structure.

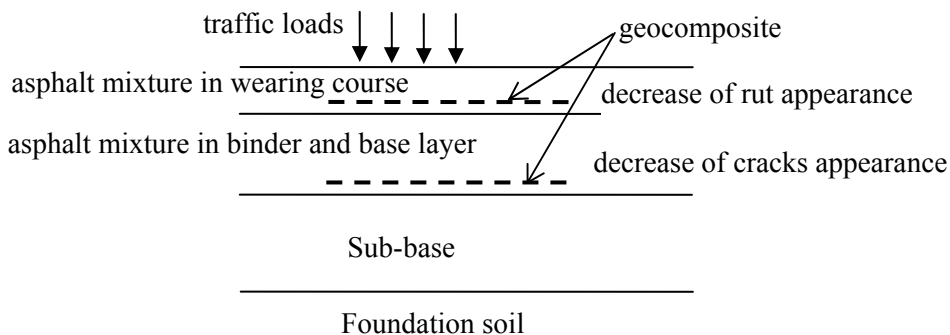


Figure 1. The use of geocomposites in flexible pavement structure

Thus, the use of geocomposites in asphalt layers leads to an improvement of behavior in service by increasing the resistance to transmitted cracks and to formation of rut in the higher layers (fig.1).

2. ANALYSIS

In this paper we will estimate the potential to rutting for four types of asphalt mixtures layed on an existing pavement structure, first without geocomposite (1) and second with geocomposite (2).

To have the OSSR values for wearing course mixture it is necessary to make a laboratory analysis in the beginning and then a computational analysis.

Table 1. Intrinsically characteristics of asphalt mixtures

Mixture	Loading rate, mm/min	ϕ_o	c , MPa
BA16-A in wearing course	0.46	45°51'49"	0.06129
BA16-B in wearing course	0.46	46°38'10"	0.07258
	12.5	47°33'3"	0.19496
	50.0	46°50'22"	1.76843
MASF16-A in wearing course	0.46	47°31'53"	0.15389
MASF16-B in wearing course	0.46	48°57'4"	0.18859
	12.5	48°57'4"	0.29014

The laboratory analysis consists in static triaxial tests performed on cylindrical samples ($\Phi = 70$ mm and $h = 140$ mm) made by the following asphalt mixtures: BA16 asphalt concrete and MASF16 asphalt mixture with fiber, with 16 mm maximum size, both for wearing course, containing ESSO asphalt binder, D 50/70 pen (noted by A) and Suplacu de Barcau asphalt binder, D 60/80 pen (noted by B). During the test, the loading rate was maintained constant, at a value equal to 0,46 mm/min. to simulates a stationary load and 12.5 mm/min. and 50 mm/min. to simulates a mobile loads on pavement structure.

Table 2. The pavement structure without geocomposite (1), taking in accounts

Mixture	h_{layer} m	Poissson ratio, μ	Elastic modulus, MPa
wearing course BA16-A	0.04	0.35	266
or wearing course BA16-B			278
or wearing course MASF16-A			312
or wearing course MASF16-B			352
existent asphalt layers	0.095	0.35	300
macadam	0.08	0.27	400
ballast	0.20	0.27	239
soil	∞	0.35	110

From this test, result the shear strain of cylindrical samples and then we can have the angle of internal friction and cohesion for the asphalt mixture tested. For each recipes of asphalt mixture it is necessary to make triaxial test at failure for minimum two samples with different lateral stress ($\sigma_3 = 2$ daN/cm², $\sigma_4 = 4$ daN/cm²) (table 1).

The computational analysis consists in obtaining the strain and stress state within pavement structure (table 2 and 3) by using elastic linear software, ALIZE 5, under standard load of our country (115 kN).

Table 3. The pavement structure with geocomposite (2), taking in accounts

Mixture	h_{layer} m	Poissson ratio, μ	Elastic modulus, MPa
wearing course BA16-A			266
or wearing course BA16-B			278
or wearing course MASF16-A	0.04	0.35	312
or wearing course MASF16-B			352
geocomposite	0.002	0.3	73000
existent asphalt layers	0.095	0.35	300
macadam	0.08	0.27	400
ballast	0.20	0.27	239
soil	∞	0.35	110

To estimate the dynamic elastic modulus (E) for the four asphalt mixtures from wearing course it was used the indirect tensile fatigue test. The frequency for indirect tensile fatigue test was 1 Hz.

The samples were subjected to conditions that can appear in summer period (40°C temperatures) for both tests performed.

The calculus was made at two depths of asphalt wearing layer: at the top of the layer ($z = 0$ m) and at the bottom of the layer ($z = 0.04$ m), in the axis of applied load.

3. RESULTS

Base on those presented above we can calculate the octahedral shear stress ratio (OSSR) for asphalt mixture from wearing course. Thus, we have the results presented in table 4.

4. CONCLUSIONS

From this research the following conclusions can be drawn:

- the OSSR parameter indicate potential for rutting of an asphalt mixture under traffic loads;

- OSSR presents greater values at the top of asphalt layer than at the bottom of asphalt layer for 40°C test temperature, irrespective of mixture;
- the all of the OSSR values (table 4) are below 1, which signify that octahedral shear strength of material in the layer is not exceeded; the asphalt mixtures are suitable from permanent deformation point of view;

Table 4. The OSSR values for asphalt mixtures in wearing course

Loading rate mm/min.	Asphalt mixture	Pave-ment structure	z, m	σ_1 , MPa	σ_3 , MPa	σ_{oct} MPa	σ_{oct} MPa	$\sigma_{oct,s}$ MPa	OSSR
0,46	BA16-A	1	0	0,5793	0,0685	0,24	0,24	0,54	0,952
			0,04	0,467	0,2257	0,31	0,11	0,44	0,368
		2	0	0,5667	0,08743	0,25	0,23	0,52	0,870
			0,04	0,4444	0,2691	0,33	0,08	0,42	0,253
	BA16-B	1	0	0,5851	0,05991	0,23	0,25	0,59	0,902
			0,04	0,4674	0,2252	0,31	0,11	0,48	0,337
		2	0	0,5731	0,07784	0,24	0,23	0,58	0,829
			0,04	0,4447	0,2687	0,33	0,08	0,46	0,232
	MASF16-A	1	0	0,6009	0,03612	0,22	0,27	0,68	0,790
			0,04	0,4679	0,2245	0,31	0,11	0,56	0,279
		2	0	0,5912	0,05077	0,23	0,25	0,68	0,743
			0,04	0,4457	0,2675	0,33	0,08	0,54	0,195
MASF16-B	1	0	0,6189	0,00908	0,21	0,29	0,74	0,804	
		0,04	0,4678	0,2248	0,31	0,11	0,60	0,257	
	2	0	0,6123	0,01911	0,22	0,28	0,74	0,773	
		0,04	0,4465	0,2663	0,33	0,08	0,58	0,182	
12,5	BA16-B	1	0	0,5851	0,05991	0,23	0,25	0,70	0,649
			0,04	0,4674	0,2252	0,31	0,11	0,60	0,256
		2	0	0,5731	0,07784	0,24	0,23	0,69	0,601
			0,04	0,4447	0,2687	0,33	0,08	0,57	0,178
	MASF16-B	1	0	0,6189	0,00908	0,21	0,29	0,83	0,651
		0,04	0,4678	0,2248	0,31	0,11	0,68	0,216	
50	BA16-B	1	0	0,5851	0,05991	0,23	0,25	2,04	0,144
			0,04	0,4674	0,2252	0,31	0,11	1,93	0,064
		2	0	0,5731	0,07784	0,24	0,23	2,03	0,135
			0,04	0,4447	0,2687	0,33	0,08	1,91	0,046

1 - the structure without geocomposite

2 - the structure with geocomposite

- in all the studied cases it is observed that the geocomposite improve the OSSR value;
- it results that the values OSSR decrease when is a geocomposite in pavement structure, by following:
 - for 0.46 mm/min rate of loading:
 - BA16-A: 8.7% at the top of the layer and 31.3% at the bottom of the layer
 - BA16-B : 8.1% at the top of the layer and 31.3% at bottom of the layer
 - MASF16-A: 6% at the top of the layer and 30.1% at bottom of the layer
 - MASF16-B: 3.9% at the top of the layer and 29% at bottom of the layer
 - for 12.5 mm/min rate of loading:
 - BA16-B : 7.5% at the top of the layer and 30.4% at bottom of the layer
 - MASF16-B: 3.7% at the top of the layer and 28.5% at bottom of the layer
 - for 50.0 mm/min rate of loading:
 - BA16-B : 6.1% at the top of the layer and 28.1% at bottom of the layer
- in the case of BA16 asphalt mixture the loading rate has a little influence on the above percent and in the case of MASF16 asphalt mixture has almost no influence;
- at the same loading rate (0.46 mm/min), the BA16 asphalt mixture presents higher OSSR values than the MASF16 asphalt mixture.

References

1. Diaconu E., Burlacu A., *Locul si rolu geocompozitelor in structurile rutiere*, Simpozionul Tehnologie si Siguranta, Cluj Napoca, 2004.
2. Diaconu E., Lazar S., Burlacu A., *Caracteristici de stabilitate ale mixturilor asfaltice utilizate la remedierea imbracamintilor bituminoase uzate*, Simpozion Stiintific Investigarea Starii Tehnice si Procede de Remediere Utilizate la Drumuri , UTCB, Bucuresti, 2002.
3. Răcănel C., *Establishing the curves of equal value of octahedral shear stress ratio for asphalt mixtures from wearing course*, Computational Civil Engineering, International Symposium, Iasi, Ed. Societății Academice Matei-Teiu Botez , 2003.
4. Răcănel C., *Aprecierea calitatii mixturii asfaltice pe baza caracteristicilor intrinseci ale materialului*, Simpozion “Infrastructuri eficiente pentru transporturi terestre”, Zilele Academice Timisene, editia a VIII-a, Timisoara, 2003 (in Romanian)
5. Răcănel C., *Efectele din fluaj și oboseală asupra comportării mixturilor asfaltice*, teză de doctorat, U.T.C.B., 2002.
6. Dallas L., Hisham Y., *Improved ACP Mixture Design: Development and Verification*, Research Report 1170-1F Texas Transportation Institute, 1992

A viscoelastic-plastic prediction of rutting in asphalt mixtures

Mircea Balcu¹, Ștefan Marian Lazăr²

¹ Professor dr.eng., Faculty of Railways, Roads and Bridges, Technical University of Civil Engineering, Bucharest, Romania

² Assistant drd.eng., Faculty of Railways, Roads and Bridges, Technical University of Civil Engineering, Bucharest, Romania

Summary

In this paper, asphalt mixtures are described as viscoelastic-plastic materials for which the responses of the mixtures to the loads are categorized into three groups as elasticity, viscoelasticity and viscoplasticity, depending on whether they are time dependent and recoverable during the unloading period.

Rowe's stress dilatancy theory is used to obtain the relationship between the permanent volumetric and vertical strains as well as the hardening law for the changes in the sizes of the plastic moduli caused by cyclic loading.

A computer program, RAM (Rutting in Asphalt Mixtures), is under completion to determine the plastic deformation under cyclic loading. To date, an agreement between the model prediction and laboratory tests are under inspection.

KEYWORDS: rutting, viscoelastic-plastic, asphalt mixtures, model prediction

1. INTRODUCTION

Non-linear viscous behaviours of asphalt mixtures have been investigated by many researchers [1-4]. Their work shows that the responses of asphalt mixtures to loads are very complex. But, as an approximation, mechanical properties of an asphalt mixture can be considered separately, according to whether the deformations measured in creep/recovery tests are time dependent and recoverable or not, during unloading [5, 6]. Sides et al. [7] proposed a comprehensive constitutive model for asphalt mixtures in which elastic, plastic, viscoelastic and viscoplastic strains are evaluated individually. Such a classification can be of great importance to the effort of developing a finite element code for visco-elastoplastic analysis for these materials.

Applications of the finite element method (FEM) to the structural analysis of non-linear, time dependent materials have been well documented in many papers. Desai and Zhang [8], for example, employed the FEM to investigate time dependent behaviour of a rock salt. Zienkiewicz and Corneau [9] simulated the viscous

behaviour of a lined tunnel by the FEM. Later, Zienkiewicz [10] provided a thorough review of finite element solutions to the time dependent materials. He indicated that time dependent problems can be solved efficiently using a step-by-step approach. To perform the computation, stress is assumed to be constant in a small time interval. Strains can be evaluated and corrected at the end of the time interval. Step-by-step, strains in the whole time domain are then determined.

Problems of utilizing the viscoplastic approach in the performance assessment of flexible pavements have been detailed by Barksdale [11]. He pointed out that one of the key problems for viscous analysis of asphalt mixtures is the proper choice of parameters required by the models. Goacolou [12] suggested that the viscoplastic strain rate of asphalt mixtures can be directly related to the stress by a special matrix which is equal to the classical stiffness matrix multiplied by the three functions of temperature, loading cycle and the characteristics of stress non-linearity. Based on experiments, Bonnier [3] proposed that strains of asphalt mixtures be resolved into viscoelastic and viscoplastic components. Kelvin-Woigt elements were used in the simulation of viscoelasticity while the general flow rule was employed to model viscoplasticity.

In this paper, mechanical models of asphalt mixtures are extended from one dimension to multi-dimensions on the basis of Perzyna's theory of the viscoplastic flow rule [13]. A computer program of FEM denoted RAM (**R**utting in **A**sphalt **M**ixtures) is implemented and verified with respect to experimental data and theoretical analyses. Using it in the pavement performance evaluation, development of permanent deformations within the surface layer of the road is simulated.

2. MECHANICAL MODELS OF ASPHALT MIXTURES

Creep and recovery tests are widely used in the determination of viscous parameters of asphalt mixtures. Sides et al. [7] suggested that recorded deformations from compressive creep and recovery tests can be divided into elastic, plastic, viscoelastic and viscoplastic components, according to whether the components are time dependent and recoverable during unloading. Typical strain-time relationships during one loading cycle are illustrated in Figure 1, where ε_e , ε_p , ε_{ve} and ε_{vp} denote the four components stated above. Due to the uncertainty of loading magnitude, it is difficult to quantify stress and strain relationships during the period before the load reaches the designed value. Therefore, it is decided that the plastic component is not considered separately but is treated as a part of the viscoplastic component. In a uniaxial context, the constitutive models of asphalt mixtures during the N th creep period can then be expressed as

$$\epsilon_e = \frac{1}{E} \cdot \sigma \tag{1}$$

$$\epsilon_{ve} = A(\sigma) \cdot t^\alpha = A \cdot \sigma^h \cdot t^\alpha \tag{2}$$

$$\epsilon_{vp} = B(\sigma) \cdot f(N) \cdot t^\beta = \beta \cdot \sigma^\omega \cdot f(N) \cdot t^\beta \tag{3}$$

where $f(N) = N^b - (N - 1)^b$; $A(\sigma)$, $B(\sigma)$ are viscous stress functions; $A, B, h, \omega, E, \alpha, b$ and β are test constants under a constant temperature. Instead of polynomials used by Sides et al., power functions were adopted in this paper for stress functions $A(\sigma)$ and $B(\sigma)$. Regression shows that there is not much difference between them. Therefore, the adoption of the power functions is purely from the consideration of simplifying the constitutive equations for numerical analysis.

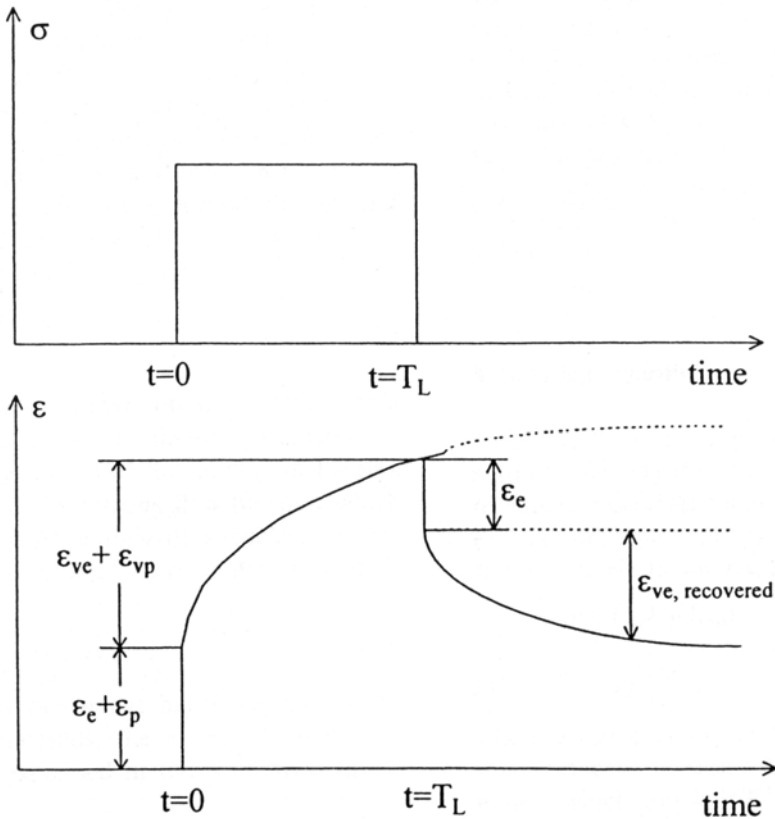


Figure 1. Typical σ and ϵ -time relation in creep and recovery tests.

When the models are extended to multidimensions, Eq. (1) is written as

$$\{\varepsilon_e\} = [C] \cdot \{\sigma\} \tag{4}$$

where $[C]$ is the compliance matrix defined by

$$[C] = \frac{1}{E} \begin{bmatrix} 1 & -\nu & -\nu & 0 & 0 & 0 \\ & 1 & -\nu & 0 & 0 & 0 \\ & & 1 & 0 & 0 & 0 \\ & & & 2 \cdot (1 + \nu) & 0 & 0 \\ & & & & 2 \cdot (1 + \nu) & 0 \\ & & & & & 2 \cdot (1 + \nu) \end{bmatrix} \tag{5}$$

in which E is Young’s modulus; ν denotes Poisson’s ratio and it can be approximated as a parameter of time independence.

Constitutive Eq. (2) in multidimensions may be replaced by

$$\{\varepsilon_{ve}\} = A \cdot t^\alpha \cdot [R] \cdot \{\sigma^h\} \tag{6}$$

where

$$[R] = E \cdot [C] \tag{7}$$

$$\{\sigma^h\} = \{\sigma_X^h \quad \sigma_Y^h \quad \sigma_Z^h \quad \tau_{XY}^h \quad \tau_{YZ}^h \quad \tau_{ZX}^h\}^T \tag{8}$$

In the effort of establishing constitutive equations in multidimensions, the most delicate problem is the coupling of the plastic response of the mixtures with loading times. Presently, Perzyna’s theory [13] is generally accepted as one of the most efficient means to tackle this problem. In it, the classical plastic flow law is replaced by the time rate flow rule which relates the rate of viscoplastic strains to the current stresses and loading history. For an associative viscoplastic flow, such a rule is formulated as

$$\{\dot{\varepsilon}_{vp}\} = \gamma \cdot \langle \phi(F) \rangle \cdot \frac{\partial F}{\partial \{\sigma\}} \tag{9}$$

where $\{\dot{\varepsilon}_{vp}\}$ denotes derivative of viscoplastic strain with respect to time t ; γ is the fluidity parameter associated with loading time, and the number of loading applications; $\langle \phi(F) \rangle$ is the viscous flow function which represents the current

magnitude of viscoplastic strain rate; F denotes the general yield criterion and is expressed by

$$F(\{\sigma\}, \kappa) = f(\{\sigma\}, \kappa) - y(\kappa) = 0 \quad (10)$$

where κ is a history dependent hardening parameter. For the isotropic materials, the explicit form of this equation is usually expressed in terms of stress invariants

$$F(\sigma_m, \bar{\sigma}, \theta, \kappa) = 0 \quad (11)$$

where

$$\sigma_m = \frac{J_1}{3} = \frac{1}{3}(\sigma_x + \sigma_y + \sigma_z) \quad (12)$$

$$\bar{\sigma} = J_2^{\frac{1}{2}} = \left[\frac{1}{2}(s_x^2 + s_y^2 + s_z^2) + \tau_{xy}^2 + \tau_{yz}^2 + \tau_{zx}^2 \right]^{\frac{1}{2}} \quad (13)$$

$$\theta = \frac{1}{3} \sin^{-1} \left[-\frac{3\sqrt{3}}{2} \cdot \frac{J_3}{\bar{\sigma}^3} \right] \text{ with } -\frac{\pi}{6} < \theta < \frac{\pi}{6} \quad (14)$$

where

$$J_3 = s_x s_y s_z + 2\tau_{xy} \tau_{yz} \tau_{zx} - s_x \tau_{yz}^2 - s_y \tau_{zx}^2 - s_z \tau_{xy}^2 \quad (15)$$

and

$$s_x = \sigma_x - \sigma_m, \quad s_y = \sigma_y - \sigma_m, \quad s_z = \sigma_z - \sigma_m \quad (16)$$

Derivative yield function Eq. (11) with regard to stress, gives

$$\frac{\partial F}{\partial \sigma} = \frac{\partial F}{\partial \sigma_m} \cdot \frac{\partial \sigma_m}{\partial \sigma} + \frac{\partial F}{\partial J_2} \cdot \frac{\partial J_2}{\partial \sigma} + \frac{\partial F}{\partial J_3} \cdot \frac{\partial J_3}{\partial \sigma} \quad (17)$$

where

$$\frac{\partial F}{\partial J_3} = \frac{\partial F}{\partial \theta} \cdot \frac{\partial \theta}{\partial J_3} \quad (18)$$

According to one-dimensional constitutive Eq. (3), viscoplastic strain increases monotonically with loading time, no matter how small the stress. In other words, there is no threshold of yield stress for asphalt mixtures. Such phenomena were

observed in our tests as well as by Drescher et al. [5] and Sides et al. [7]. From this fact and Eq. (3), the viscous flow function in Eq. (9) is postulated to be

$$\phi[F] = [f(\{\sigma\})]^w \quad (19)$$

3. SOLUTION ALGORITHM

Similar to the assumptions employed by Perzyna, we assume that: (1) the total strain rate $\{\dot{\epsilon}\}$ is composed of elastic, viscoelastic and viscoplastic strain rates; and (2) the stress rate $\{\dot{\sigma}\}$ is related to the elastic strain rate by the elastic matrix, i.e.

$$\{\dot{\epsilon}\} = \{\dot{\epsilon}_e\} + \{\dot{\epsilon}_{ve}\} + \{\dot{\epsilon}_{vp}\} \quad (20)$$

$$\{\dot{\sigma}\} = [D] \cdot \{\dot{\epsilon}_e\} \quad (21)$$

where a dot over $\{\sigma\}$ or $\{\epsilon\}$ denotes the derivative of this vector with regard to time t ; $[D]$ is the elastic matrix which equals $[C]^{-1}$. Obviously, it is difficult to provide analytic solutions to these differential equations. But if we break the loading time into small increments, strains at any time can be determined using the step-by-step time integration approach with a Newton-Raphson iteration procedure [10]. To do this, substitute Eqs. (6)-(9) and (21) into Eq. (20) and rewrite Eq. (20) in the incremental form. The increment of the stress vector during the time $t_n \sim t_{n+1}$ (the n th iterative step) is then written as

$$\Delta\{\sigma\}^n = [D] \cdot \left(\Delta\{\epsilon\}^n - A \cdot \alpha \cdot t^{\alpha-1} \cdot [R] \cdot \{\sigma^h\}^n - \Delta\{\epsilon_{vp}\}^n \right) \quad (22)$$

Now, the increment of viscoplastic strain during $t_n \sim t_{n+1}$ is approximated by

$$\Delta\{\epsilon_{vp}\}^n = \Delta t_n \left[(1 - \lambda) \{\dot{\epsilon}_{vp}\}^n + \lambda \{\dot{\epsilon}_{vp}\}^{n+1} \right] \quad (23)$$

in which superscript n denotes the n th time step of computation and $\Delta t_n = t_{n+1} - t_n$. λ is the integration parameter yet to be determined. Zienkiewicz [10] discussed in detail the choice of λ . The most reliable results can be achieved when $\lambda = 0.5$.

Using Taylor series and curtailing at the term of the 2nd order, viscoplastic strain rate at the $(n + 1)$ th time step $\{\dot{\epsilon}_{vp}\}^{n+1}$ can be approximated. On the substitution of $\{\dot{\epsilon}_{vp}\}^{n+1}$ in Eq. (23), the increment of viscoplastic strain during the n th time step is determined. Then, Eqs. (22) and (23) can be rewritten as

$$\Delta\{\sigma\}^n = [\tilde{D}] \cdot \left(\Delta\{\varepsilon\}^n - \{\dot{\varepsilon}_{vp}\}^n \Delta t_n \right) - A \cdot \alpha \cdot t^{\alpha-1} \cdot [\tilde{D}] \cdot [R] \cdot \{\sigma^h\}^n \quad (24)$$

$$\Delta\{\varepsilon_{vp}\}^n = [B]\Delta\{d\}^n - A \cdot \alpha \cdot t^{\alpha-1} \cdot [R] \cdot \{\sigma^h\}^n - [D]^{-1} \Delta\{\sigma\}^n \quad (25)$$

where

$$[\tilde{D}] = ([D]^{-1} + [G]^n)^{-1} \quad (26)$$

$$[G]^n = \lambda \cdot \Delta t_n \cdot \left(\frac{\partial\{\dot{\varepsilon}_{vp}\}}{\partial\{\sigma\}} \right)^n \quad (27)$$

$$\left(\frac{\partial\{\dot{\varepsilon}_{vp}\}}{\partial\{\sigma\}} \right)^n = \gamma \left[\phi(F) \cdot \frac{\partial\{a\}^T}{\partial\{\sigma\}} + \frac{d\phi(F)}{dF} \cdot \{a\}\{a\}^T \right] \quad (28)$$

$$\{a\} = \frac{\partial F}{\partial\{\sigma\}} \quad (29)$$

With Eqs. (24) and (25), stresses and viscoplastic strains at the end of n th time step are approximated by

$$\{\sigma\}^{n+1} = \{\sigma\}^n + \Delta\{\sigma\}^n \quad (30)$$

$$\{\varepsilon_{vp}\}^{n+1} = \{\varepsilon_{vp}\}^n + \Delta\{\varepsilon_{vp}\}^n \quad (31)$$

4. FINITE ELEMENT PROCEDURE

The adaptation of constitutive equations to numerical formulations makes it possible to produce a computer program from the finite element method so that the response of asphalt mixtures to the loads can be solved numerically. Here, we shall start from the well-known equilibrium equation of FE analysis

$$\int_{\Omega} [B]^T \{\sigma\}^n d\Omega + \{f\}^n = 0 \quad (32)$$

where $\{f\}^n$ is the equivalent nodal forces caused by external forces; Ω is the integration domain.

Obviously, Eq. (32) holds at all times during loading. Using an incremental expression, we have

$$\int_{\Omega} [B]^T \Delta\{\sigma\}^n d\Omega + \Delta\{f\}^n = 0 \quad (33)$$

where $\Delta\{f\}^n$ is the change of $\{f\}^n$ during $\Delta t_n = t_{n+1} - t_n$. Substitute Eq. (24) into Eq. (33) and we obtain

$$\int_{\Omega} [B]^T \left([\tilde{D}] \cdot (\Delta\{\varepsilon\}^n - \{\dot{\varepsilon}_{vp}\}^n \Delta t_n) - A \cdot \alpha \cdot t^{\alpha-1} \cdot [\tilde{D}] \cdot [R] \cdot \{\sigma^h\}^n \right) d\Omega + \Delta\{f\}^n = 0 \quad (34)$$

Replace $\Delta\{\varepsilon\}^n$ by $[B]\Delta\{d\}^n$ and Eq. (34) gives

$$[K_T]^n \Delta\{d\}^n - \Delta\{\Psi\} = 0 \quad (35)$$

where

$$[K_T]^n = \int_{\Omega} [B]^T [\tilde{D}]^n [B] d\Omega \quad (36)$$

$$\Delta\{\Psi\} = \int_{\Omega} [B]^T [\tilde{D}]^n \{\dot{\varepsilon}_{vp}\}^n \Delta t_n d\Omega + A \cdot \alpha \cdot t^{\alpha-1} \cdot \int_{\Omega} [B]^T [\tilde{D}]^n [R] \{\sigma^h\}^n d\Omega - \Delta\{f\}^n \quad (37)$$

and $\Delta\{d\}^n$ is the increment of total deformation at the n th time step.

Initial conditions of visco-elastoplastic computation are the equilibrium of elasticity. After the n th time step, displacement and stress increments are evaluated by Eqs. (35) and (30). Substitute them into Eq. (25) and the increment of viscoplastic strains can be determined. Stresses and viscoplastic strains calculated by Eqs. (30) and (31) are then treated as the initial conditions during the next iteration. Computation is repeated in the same way until the whole loading time is covered.

It should be pointed out here that convergence of computation is not involved in the stated procedure since viscoplasticity goes on as long as the loading is applied. As stated in the foregoing sections, such phenomena were observed in the experiments and are reflected by the viscous flow function Eq. (19).

5. CHOICE OF PARAMETERS FOR COMPUTATIONS

From the constitutive equations of multidimensions, it is easy to see that elastic and viscoelastic parameters determined from tests are utilized directly in the

computation. The application of viscoplastic parameters, however, is not so straightforward. They are associated with the determination of the fluidity parameter γ in Eq. (9). To evaluate γ , derivative $\dot{\varepsilon}_{vp}$ of Eq. (3) with respect to loading time t , we have

$$\dot{\varepsilon}_{vp} = B \cdot f(N) \cdot \sigma^\omega \cdot \beta \cdot t^{\beta-1} \quad (38)$$

where $f(N) = N^b - (N-1)^b$. The average value of $\dot{\varepsilon}_{vp}$ during loading period t can be approximated by

$$\dot{\varepsilon}_{vp} = B \cdot f(N) \cdot \sigma^\omega \cdot \frac{1}{t} \int_0^t \beta \cdot \tau^{\beta-1} d\tau = B \cdot f(N) \cdot \sigma^\omega \cdot t^{\beta-1} \quad (39)$$

Compare the above equation with Eq. (3) and the fluidity parameter can then be approximated by

$$\gamma = B \cdot f(N) \cdot t^{\beta-1} \quad (40)$$

Three points are noted for Eq. (40). Firstly, the fluidity parameter of an asphalt mixture is an average value over the loading period t . This means that γ in the iteration is a variable which changes with the increase of loading time t . This characteristic is different from that of many other materials for which constant fluidity parameters can be employed. Secondly, the fluidity parameter is associated with parameter β . If $\beta \geq 1.0$, it may indicate the steady plastic flow or collapse of the sample which Bonnier [3] described as the second or the tertiary creep. For $\beta < 1.0$, the rate of viscoplastic strains deteriorates monotonically during the computation. For a given tolerance, therefore, the convergence can always be expected if the relative value of viscoplastic strain rate is used as a discriminant. Lastly, it is noted that the fluidity parameter $\gamma \rightarrow \infty$ when $t \rightarrow 0$. To avoid the singular solution, it is necessary to assign a minimum value for the initial tie step t_0 . Based on our experience of computation, $t_0 = 1.0 \times 10^{-5}$ s should be employed for the asphalt mixture specimen used in our experiments.

Besides the parameters of the mechanical properties of asphalt mixtures, the choice of time steps can make a great difference to the accuracy and efficiency of the computation. Generally, computational accuracy deteriorates with the increase of the time step length. Zienkiewicz and Corneau [9] suggested that the maximum length of the time step should not exceed the ratio of total strains against the second strain invariants. Based on our experiences, an additional restriction is imposed which requires length of the time step to be smaller than a critical value to which may be in the range of 0.1-1.0 s for asphalt mixtures. On the grounds that

both of the criteria are met, formulae $\Delta t_{n+1} = 1.2 \cdot \Delta t_n$ (where Δt_0 denotes the initial time step) is adopted to determine the increment of the time step. In this way, the number of iterations is greatly reduced while accuracy is satisfied.

6. A NUMERICAL APPLICATION WITH THE RAM PROGRAM

It is well known that rutting in flexible pavement is a gradual damaging process caused by the accumulation of permanent deformations. In this paper, the visco-elastoplastic method stated above is employed to give an estimation of its development. To do this, a structure of three layers is modelled with the pulse strip loads being used to represent the moving vehicles, Figure 2. Apparently, this system can be simplified as a plain strain configuration with its vertical boundaries being held in the horizontal direction and its lower boundary being completely fixed.

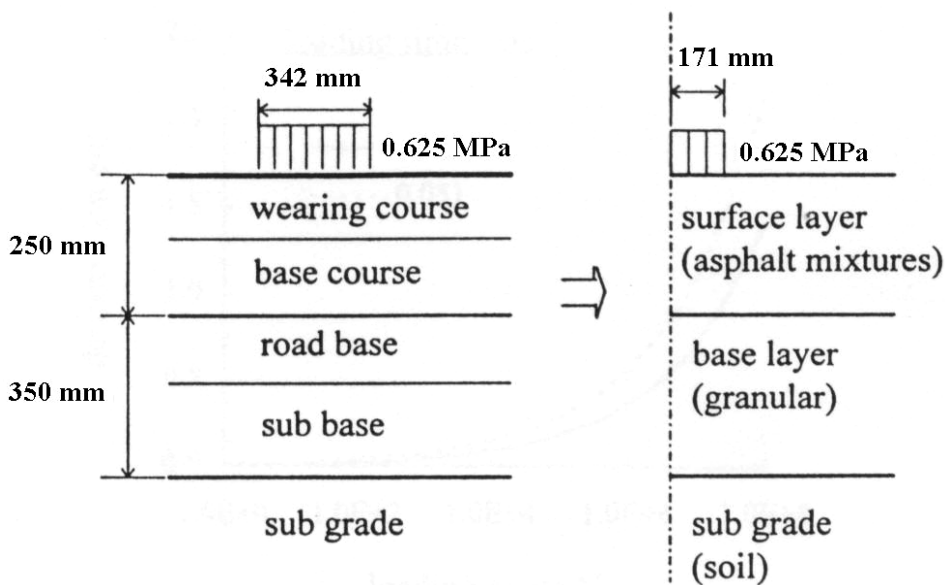


Figure 2. Structure of flexible pavements

Since our main interest in this paper is the mechanical behaviour of asphalt mixtures, the cement bound granular sub-base and the cohesive soil are idealized as perfectly plastic materials and it is assumed that Mohr-Coulomb criterion can be used as their yield functions. The surface layer is assumed to be made up of hot rolled asphalt with the design parameters being chosen from Table 1 [7].

Table 1. Parameters of asphalt mixtures for computation

Materials	E (MPa)	$A \times 10^3$	h	a	$B \times 10^3$	w	b	b
Asphalt concrete	613	0.488	0.716	0.290	1.222	0.795	0.190	0.220
Hot rolled asphalt	1377	0.816	0.842	0.449	2.110	0.750	0.338	0.344

To investigate the development of rutting, values of viscoplastic displacement at various loading cycle n , say, at $n = 10^1, 10^2, 10^3, 10^4, 10^5, \dots$, are computed first. Using the obtained values, viscoplastic displacement $u(n)_{vp}$ and loading cycle n can be related by a regression equation. Now, replace integer n by a real x . Accumulation of viscoplastic deformations $U(N)$ can therefore be viewed as a pseudo-continuous function expressed as

$$U(N) = \sum_{n=1}^N u(n)_{vp} \approx \int_0^N u(x)_{vp} dx \quad (41)$$

Plot $U(N)$ vs. N , the accumulation of viscoplastic deformations after the N th wheel loading is determined. Further on, rutting after the N th wheel loading can be estimated. The $u(n)_{vp} \sim n$ relationships can be determined using the least square technique. Replace $u(n)_{vp}$ by $u(x)_{vp}$ and substitute it into Eq. (41), and the accumulation of viscoplastic deformations are evaluated. A plot at different loading cycles allows one to see the development of permanent deformations along the pavement surface. With it, rutting and loading application relationships might be obtained. As expected, rutting under a specific length of loading time is a power function with regard to the loading applications. This result is generally in agreement with the phenomena observed in practice, see, e.g. Thompson and Nauman [14].

7. CONCLUSION

Constitutive models of viscous behaviour of asphalt mixtures under repeated loads are incorporated in a finite element code, RAM, using the general approach of visco-elastoplastic analysis. One of the main attractions of this work is the fact that the response of the material to the loads can be simulated during the whole loading period and the development of deformations with time is hence accounted for. A computer program, RAM (Rutting in Asphalt Mixtures), is under completion to determine the plastic deformation under cyclic loading. To date, an agreement between the model prediction and laboratory tests are under inspection.

References

- [1] Kim, Y.R., Little, D.N. *One dimensional constitutive modelling of asphalt concrete.*, J Engng Mech 1989; 116(4) pp 751-771.
- [2] Van de Loo, P.J. *The creep test, a key tool in asphalt mix design and in the prediction of pavement rutting.*, Proc Assoc Asph Pav Tech 1978; 47 pp 522-557.
- [3] Bonnier, P.G. *Testing modelling and numerical analysis of the mechanical behaviour of bituminous concrete.*, PhD thesis, Delft University of Technology, The Netherlands, 1993.
- [4] Judycki, J. *Non-linear viscoelastic behaviour of conventional and modified asphaltic concrete under creep.*, Mater and Struct 1992; 25 pp 95-101.
- [5] Drescher, A., Kim, J.R., Newcomb, D.E. *Pavement deformation in asphalt concrete.*, J Mater Civ Engng 1993; 5(1) pp 112-128.
- [6] Florea, D. *Associated elastic/viscoplastic model for bituminous concrete*, Int J Engng Sci 1994; 32(1) pp 79-86.
- [7] Sides, A., Uzan, J., Perl, M. *A comprehensive viscoelastoplastic characterization of sand-asphalt compressive and tensile cyclic loading.*, J Test Evaluat 1985; 13(1) pp 49-59.
- [8] Desai, C.S., Zhang, D. *Viscoplastic model for geological materials with generalized flow rule.*, Int J Num Meth in Geomech 1987; 11 pp 603-620.
- [9] Zienkiewicz, O.C., Corneau, I.C. *Visco-plastic – plasticity and creep in elastic solids – a unified numerical solution approach.*, Int J Num Meth Engng 1974; 8 pp 821-845.
- [10] Zienkiewicz, O.C. *The finite element method, 3rd ed.*, London: McGraw-Hill, 1977; pp 450-496.
- [11] Barksdale, R.D. *A nonlinear theory for predicting the performance of flexible highway pavements.*, Hwy Res Rec 1970; 337 pp 22-39.
- [12] Goacolou, H. *Calculation of the rutting of structures – CASTOR program method for prediction of permanent deformations in asphaltic structures.*, In: Proc 6th Int Conf Struct Des Asp Pay, 1987; pp 191-199.
- [13] Perzyna, P. *Fundamental problems in viscoplasticity.* In: *Advanced Applied Mechanics.*, New York: Academic Press, 1966; 9 pp 243-377.
- [14] Thompson, M.R., Nauman, D. *Rutting rate analyses of the AASHO road test flexible pavements.*, Trans Res Rec 1993; 1384 pp 36-48.

AutoLISP Automated Drawing Programming under AutoCAD

Mircea Petrina¹, Roxana Balc², Cristian Ciplea³, and Marchis Ciprian³

¹Professor, Technical University, Cluj-Napoca, 3400, Romania

²Assistant, Technical University, Cluj-Napoca, 3400, Romania

³Student, Technical University, Cluj-Napoca, 3400, Romania

Summary

The AutoLISP program that is presented in this paper has the purpose to generate and draw reinforcement tables into AutoCAD drawings, using the information given by the user. AutoLISP is a programming language that can substantially enhance user's productivity by automating often used or repetitive tasks.

KEYWORDS: reinforcement table, AutoLISP, AutoCAD, drawing, programming, automated.

1. INTRODUCTION

AutoLISP is a programming language that can substantially enhance user's productivity by automating often used or repetitive tasks. An AutoLISP routine gives complete control of its interaction with the user and what it does once it is loaded.

LISP stands for *LISt Processing*. AutoLISP expressions can be typed at the command line in response to prompts or can be saved to a file to be loaded and used when needed. AutoLISP offers wide and varied possibilities for shortcuts. Best of all, AutoLISP can be customized to any level of complexity.

2. PROGRAM DESCRIPTION

The AutoLISP program that is presented in this paper has the purpose to generate and draw reinforcement tables in AutoCAD drawings, using the data given by the user. This program has three important parts :

A. AutoLISP function “MARCA”

B. Fortran Program “Sort”

C. AutoLISP function “TABLE”

A. AutoLISP function “MARCA”

By using this function, the user is guided step-by-step to give the following information: scale of the AutoCAD drawing, element name, for which the user

wants to create the reinforcement table and also the reinforcement characteristics: name, steel grade, number of pieces, diameter. After the user inputs this information, he/she will have to choose the point where the reinforcement name should be placed in the AutoCAD drawing.

Below you can find the function which is computing the length of the reinforcement that is selected by the user. The reinforcement can be represented in the AutoCAD drawing by one of the following types: Line, Arc, Circle, Spline, PolyLine, 3DPolyLine or Ellipse.

```
(defun length_reinforcement (/ ss n ent itm obj l)
  ;// the user is selecting in the AutoCAD drawing the reinforcement
  (setq ss (ssget)
        lt 0
        tl 0
        n (1- (sslength ss)))
  (while (>= n 0)
    (setq ent (entget (setq itm (ssname ss n)))
          obj (cdr (assoc 0 ent)))
    ;// the typed of the selected object is checked
    l (cond
      ((= obj "LINE")
       (distance (cdr (assoc 10 ent))(cdr (assoc 11 ent))))
      ((= obj "ARC")
       (* (cdr (assoc 40 ent))
          (if (minusp (setq l (- (cdr (assoc 51 ent))
                                (cdr (assoc 50 ent)))))
              (+ pi pi l) l)))
      ((or (= obj "CIRCLE")(= obj "SPLINE")(= obj "POLYLINE")
          (= obj "LWPOLYLINE")(= obj "ELLIPSE")))
      (command "_area" "_o" itm)
      (getvar "perimeter"))
    (T 0))
  tl (+ tl l)
  n (1- n)))
```

;// The total length of the selected reinforcement it will be given to the global ;//variabile lt which will be used in the MARCA function

```
(setq lt tl)
); close length function
```

Below you can find important parts of the AutoLISP function "MARCA" :

```
(defun C:MARCA ()
  (setvar "cmdecho" 0)
  (command "._color" 7)
  ;creating the block for writing the reinformants description
  (setq htext 1
        rotext 0)
  (setq tes0
        (getint "Measuring unit in the drawing (<1>=m,<2>=cm,<3>=mm):"))
  (if (= tes0 1) (setq tes1 1))
  (if (= tes0 2) (setq tes1 100))
  (if (= tes0 3) (setq tes1 1000))
  .....
  ;//choosing the name of the block for the current reinforcement description
  (setq marcbv "qw1")
  (setq marcb (getstring T "Block name for the current reinforcement : "))
  (if (= (strlen marcb) 0) (setq marcb marcbv))
  ;//reading the drawing scale
  (command "line" (list 0 0) (list 0 0.001) "")
  (setq sxv 1 syv 1 ro 0)
  (SETQ SX (GETstring "\nScale for x:")
          sy (GETstring "\nScale for y:")
          ro (GETstring "\nRotation angle :"))
  .....
  //the AutoCAD block elements are created
  (command "attdef" "i" "" "ELEMENT" "Element" "" "f" p1 p2 htext )
  (command "attdef" "" "NRE" "Nr.elemente" "1" p9 htext rotext )
  (command "attdef" "" "OTEL" "Otel" "OB37" p10 htext rotext )
```

```
(command "attdef" "I" "" "M" "Marca" "1" "f" p2 p21 htext )
(command "attdef" "" "NR" "Nr.buc" "1" "f" p3 p31 htext )
(command "attdef" "" "D" "Diametrul" "10" "f" p5 p51 htext )
(command "attdef" "" "L" "Lungimea" "1" "f" p7 p8 htext )
(command "circle" (list (+ (car p2) 0.50) (+ (cadr p2) 0.5)) 0.75)
(command "circle" (list (- (car p5) 0.75) (+ (cadr p5) 0.5)) 0.5)
(command "line" (list (- (car p5) 1.25) (cadr p5) )
              (list (- (car p5) 0.25) (+ (cadr p5) 1) ""))
(command "text" "f" p6 p7 htext "-L= ")
(while ent0
  (setq setsel (ssadd ent1 setsel)
        ent1 (entnext ent0)
        ent0 ent1)
  )
);inchide while ent0
(command "block" marcb (list 0 0) setsel "")
```

.....
*;//reading the information given by the user : element name, steel grade, number of
 ;//pieces, diameter.*

```
(setq i 0
      j nrmarci
      marcav 0
      code T)
(while (= code T)
  (setq elem (strcase (getstring T "Element name :")))
  (if (> (strlen elem) 0)
    (progn
      (setq i (+ i 1))
      (setq nre (getint "Number of the same element :"))
      (setq otelv "OB37")
      (setq codm T)
      (while (= codm T)
```

```

(print (strcat "Marca:" (itoa (+ J 1))))
(setq marc (getstring "\nReinforcement name :"))
.....
  (progn
    (length_reinforcement )
    (setq j (+ j 1)); contor marci.
    (setq nrb (getint "\nNumber :"))
    (setq dfi (getreal "Diameter (mm):"))
    (setq lt (/ lt tes1))
    (setq otel (STRCASE (getstring "Steel grade <prv>:")))
    (if (= (strlen otel) 0) (setq otel otelv))
.....
    (setq p (getpoint "\nInsertion point of the reinforcement description :"))
    (command "insert" marcb p SX SY RO elem nre otel marc nrb fi l1)
.....
);closing progn marci
  (setq codm nil) ;cicle marci
); closing if marci
); closing while marci
; closing marcile
); closing progn
  (setq code nil)
); closing if
); Closing WHILE

; writing in a file reinforcement descriptions using an AutoCAD template file
(command "atttext" "s" "templ1.txt" "fis1")
  (command "._color" 7)
); close marca

```

B. Fortran Program “Sort”

The purpose of the FORTRAN program is to sort the information that has been exported from the AutoCAD drawing by “Marca” AutoLISP function and generate

a file with the data needed by “Table” AutoLISP function, to draw the reinforcement table into AutoCAD drawing.

C. AutoLISP function “TABLE”

This function will create in the AutoCAD drawing, the reinforcement table using the data from the input file, generated previously by the sort program.

```
(defun C:EXTRAS ()
.....
;// the user has to give the path and filename for the input file
(setq file1 (getstring "\nFilename <T1>:" ))
(setq file1 (strcat file1 ".rfg"))
(setq fl (open file1 "r"))
  (setq titlu (read-line fl))
  (setq ln (read-line fl));
;// the reinforcement table will be an AutoCAD Block object
(setq ext (getstring T "Block name for the table : "))
;//drawing the table heading
(setq h 1.0
  lc (* h 4.0)
  htext (* h 0.7)
  d (* h 0.1)
  d0 (* lc 2.0)
  dmax (* lc (+ ncd 8)))
  (setq t1 "Elementul" t2 "Marca" t3 "D" t4 "Lungimea" t5 " Numar bare "
    t6 "pe element" t7 "total" t8 " Lungimi pe diametre "
    t9 "OB37" t10 "PC52" t11 "PC60" t12 "STNB"
    t13 "STPB" t14 "Nr.marca" )
.....
;// drawing into the table the total lengths etc
(command "_line" (setq z1 (list (* lc 3.0) (- y (* h 1))))
  (list dmax (- y (* h 1))) ""))
(command "_line" (setq z2 (list (* lc 3.0) (- y (* h 2))))
  (list dmax (- y (* h 2))) ""))
```

```
(command "._line" (setq z3 (list (* lc 3.0) (- y (* h 3))))
      (list      dmax (- y (* h 3))) "")).....
(setq pii (getpoint "\nGive the insertion point for the table :"))
(close fl)
(if (tblsearch "block" ext)
  (command "._block" ext "Y" (list 0 0) setsel ""))
  (command "._block" ext (list 0 0) setsel ""))
  (command "._insert" ext pii SX SY RO )
);closing lisp function
```

3. PROCEDURE OF EXECUTION PROGRAM

The following describes step-by-step how the user can draw the reinforcement table into an AutoCAD drawing:

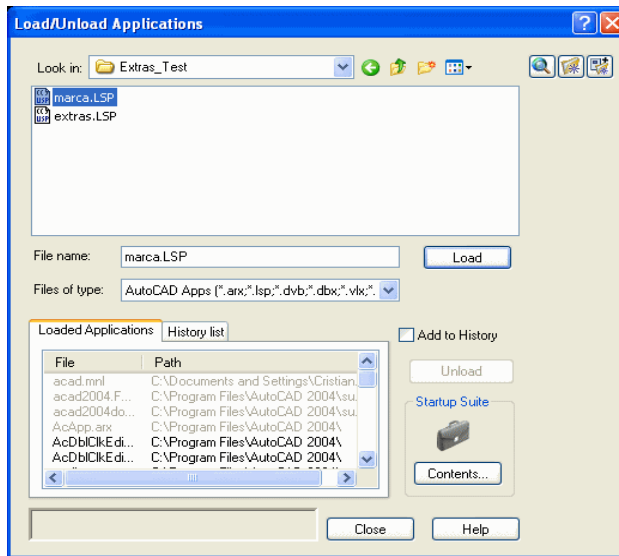
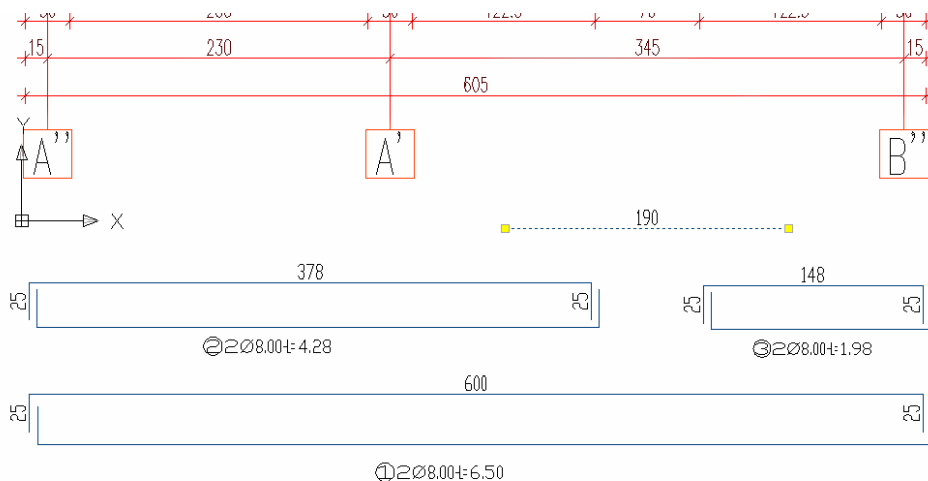


Figure 1. Load/unload applications window

1. In AutoCAD the user has to choose from Tools menu the “Load Application ...” option. In the window that will open, the user has to select the files that contain the AutoLISP functions and to load them.

2. After the routines are loaded, you can type the function’s name on the command line like any other AutoCAD command.
3. In the AutoCAD command prompt the user has to write “MARCA” in order to launch “Marca” function. The routine contains prompts to guide the user to input the information needed for the reinforcement table: name, steel grade, number of pieces, diameter. Also the user has to select in the AutoCAD drawing the reinforcement as shown in figure 2.. The information that was entered is then saved into a text file.



```

Command: marca
Unitatile de masura in desen(<1>=m,<2>=cm,<3>=mm): 2
Exista marci introduse(Y N)? : n
Nume block pentru marca curenta: Diafragma
Scara dupa x: 50
Scara dupa y: 50
Unghiul de rotire:
Nume element: Diafragma
Numarul de elemente asemenea: 1
"Marca: 1"
Marca: 1
Select objects: 1 found
Select objects:
Numarul de bucati: 8
Diametrul (mm): 8
Otel<prv>: PC52
Punctul de plasare a marcii:
"Marca: 2"
Marca: 2
Select objects: 1 found
Select objects:
    
```

Figure 2. Work example

4. The FORTRAN sort program is executed and the filename for the file that has to be processed is given, the filename of the previously created file by

AutoLISP “Marca” function. The sorting program will create the file with the needed data to draw the reinforcement table.

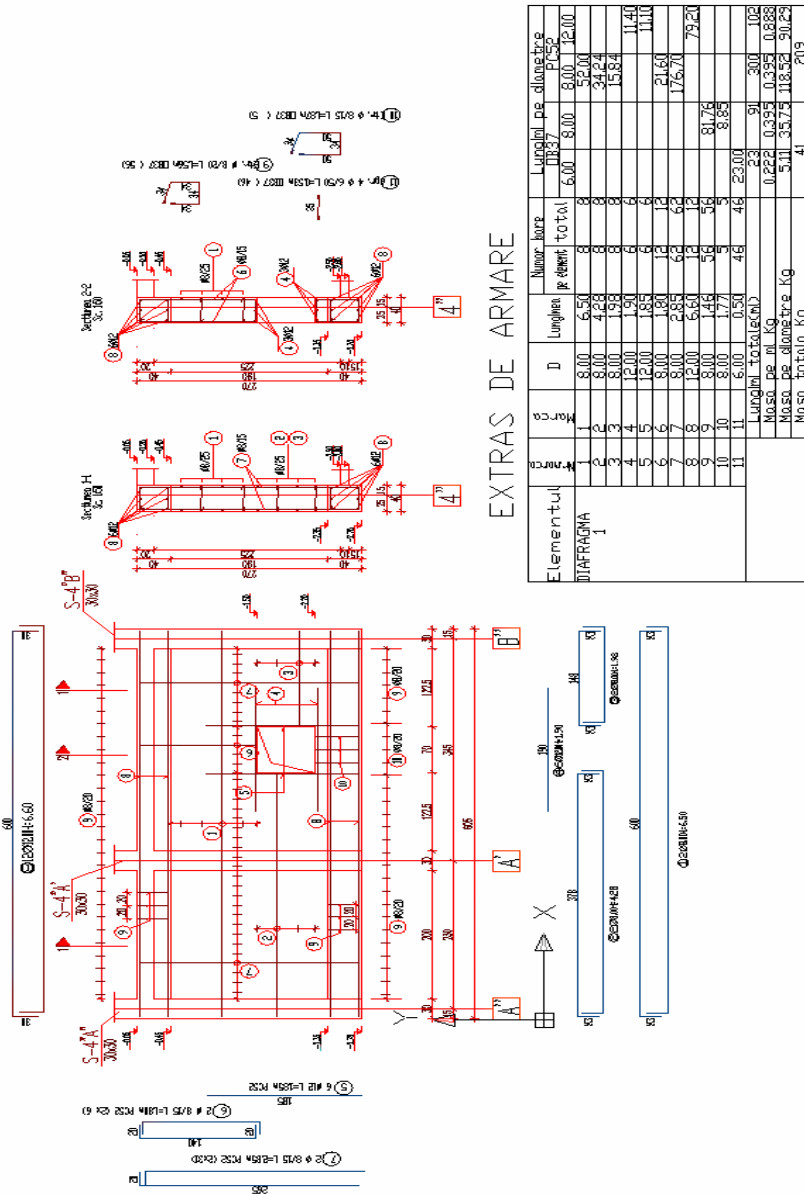


Figure 3. Drawing example

- The user has to launch “TABLE” function, enter the filename of the text file that was generated by sort program and choose the insertion point where the reinforcement table will be placed in the AutoCAD drawing.

The result obtained by following the steps above are presented in figures 3. and 4.:

EXTRAS DE ARMARE

Elementul	Nr.marca	Marca	D	Lungimea	Numar bare		Lungimi pe diametre			
					pe element	total	ØB37		PC52	
							6,00	8,00	8,00	12,00
DIAFRAGMA 1	1	1	8,00	6,50	8	8			52,00	
	2	2	8,00	4,28	8	8			34,24	
	3	3	8,00	1,98	8	8			15,84	
	4	4	12,00	1,90	6	6				11,40
	5	5	12,00	1,85	6	6				11,10
	6	6	8,00	1,80	12	12			21,60	
	7	7	8,00	2,85	62	62			176,70	
	8	8	12,00	6,60	12	12				79,20
	9	9	8,00	1,46	56	56		81,76		
	10	10	8,00	1,77	5	5		8,85		
	11	11	6,00	0,50	46	46	23,00			
Lungimi totale(ml)							23	91	300	102
Masa pe ml Kg							0,222	0,395	0,395	0,888
Masa pe diametre Kg							5,11	35,75	118,52	90,29
Masa totala Kg							41		209	

Figure 4 Final output

References

- John Wiley & Sons - AutoCAD 2004 Bible , 2004
- Burchard B. , Pitzer D. - Totul despre AutoCAD 2000, Editura Teora, 2000.

Static analysis of semi-rigid structures - Computation program

Mircea Petrina¹, Roxana Balc²

¹Structural's Mechanics, Technical University, Cluj-Napoca, 3400, Romania

²Structural's Mechanics, Technical University, Cluj-Napoca, 3400, Romania

Summary

The study presents an analysis of the behavior of semi-rigid steel structures using a computation program. A synthetic description of the behavior of semi-rigid structures was presented. The effect of the linear behavior of the beam-column connections is discussed. The static analysis of a steel frame in the ultimate limit states was developed. A comparative study with experimental results is made.

KEYWORDS: semi-rigid frames, computation program, linear static analysis, beam to column connection.

1. INTRODUCTION

Conventional analysis of steel frame structures is usually carried out under the assumption that the beam-to-column connections are either fully rigid or ideally pinned.

However, most connections used in current practice are of semi-rigid type whose behavior lies between these extreme cases.

The moment-rotation relation describes the joint behavior. Experimentally tests developed from elements connections have generated a database for moment-rotation curve. Using this database, more models for connections behavior are developed as: linear, bi- or tri- linear, polynomial, exponential.

There is a great variety of possibilities for practical realization of beam-to column connections. Modifying the structural connection's details, different non-linear behaviors are obtained, starting with quasi-perfect rigid connections (connections welded with the flush end plate) and ending with flexible connections (bolted connections of double angles on the beam web, bolted connections of flush end plate and angles on the beam web, bolted connections of angles on the beam flanges etc).

Considering the connections effect on the global structural analysis, the following observations have to be made regarding the frame joints modeling:

- The elastic analysis is based on a linear moment-rotation relation of the connection

- The rigid-plastic analysis is using a calculus capable moment of the connection, but only if the connection can develop a satisfactory rotation capacity.
- The elasto-plastic analysis is based on non-linear modeling of the moment-rotation characteristic of the connection.

2. LINEAR ELASTIC ANALYSIS FOR RIGID AND SEMI-RIGID FRAMES

2.1. Basic concept description

The linear analysis is the most widely used method in practice and it has been used by engineers in designing the majority of structures in human history. The method has the advantages of being easy-to-understand, and simplicity in computation. The superposition effects principle can be applied in a linear analysis knowing that the response of the structure is equal to the sum of all the effects due to different load cases.

In conventional linear analysis, the deflection of a structure is assumed to be very small and the second-order effects due to the geometrical changes can be ignored. The stiffness of the structural members is also considered as constant and independent of the axial force. The linear assumption for structure behavior ignores the $P-\delta$ and $P-\Delta$ effects due to the element and global structural deflections as well as any material non-linearity including yielding and the plastic hinges formation. Over the last century, a number of manual and automatically methods for linear analysis of frame structures has been developed. The most general methods suitable for computer applications are the stiffness and the flexibility methods.

2.2. Computer program

This section describes a FORTRAN- based computer program which can be used for the linear analysis of two-dimensional frames.

The computer program is divided into two parts, the first one consisting in a FORTRAN program which generates the working data file and the second, which reads the data file and generates the output files. The schematic diagram shown in figure 1., explains the operation procedure of the computer program.

Program CADRE.EXE is developed based on the matrix formulation of the displacement method. The program performs first-order elastic analysis of planar frames with or without semi-rigid connections.

The input data file contains two categories of data: information of the structure geometry and external loads.

The algorithm of the program is schematic presented in figure 2.

The element stiffness matrix was calculated for the model of the element s connected with the elastic springs by the rigid nodes with finite dimensions.

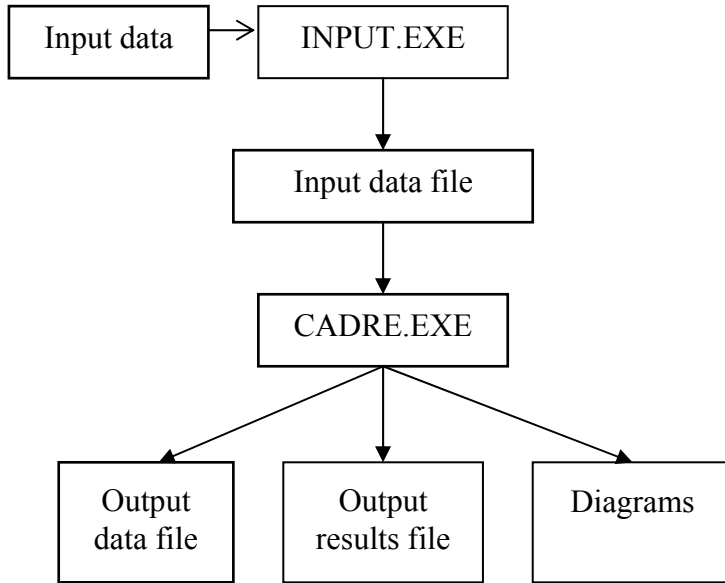


Figure 1. Operating procedure of the program

The stiffness element matrix should by first formed, transformed and assembled to form the stiffness matrix for the global structure from which the displacements are solved. They will be used for the calculation of the element efforts.

The structure stiffness matrix was assembled and then transformed in a band matrix using the band-width technique. The maximum band width for the structure stiffness matrix is calculated, and making use of the symmetry, only a half of stiffness matrix is stored. A nxn dimension stiffness matrix can be stored in a nxh rectangular matrix, in which h is the band width.

The matrix equation may be arranged by separating the unknown nodes displacements (1)

$$\begin{Bmatrix} A_S^D \\ A_S^R \end{Bmatrix} = \begin{bmatrix} K_D & K_{DR} \\ K_{RD} & K_R \end{bmatrix} \begin{Bmatrix} Z \\ D_S^R \end{Bmatrix} \tag{1}$$

Where, A_S^D is the vector of external loads applied of the nodes structure on the degree of elastic freedom directions;

A_S^R is the vector of external loads applied on the frame nodes on the direction of supports;

Z is the vector of nodes displacements by the elastic degrees of freedom direction (unknown);

D_S^R is the vector of nodes displacements in foundations (known);

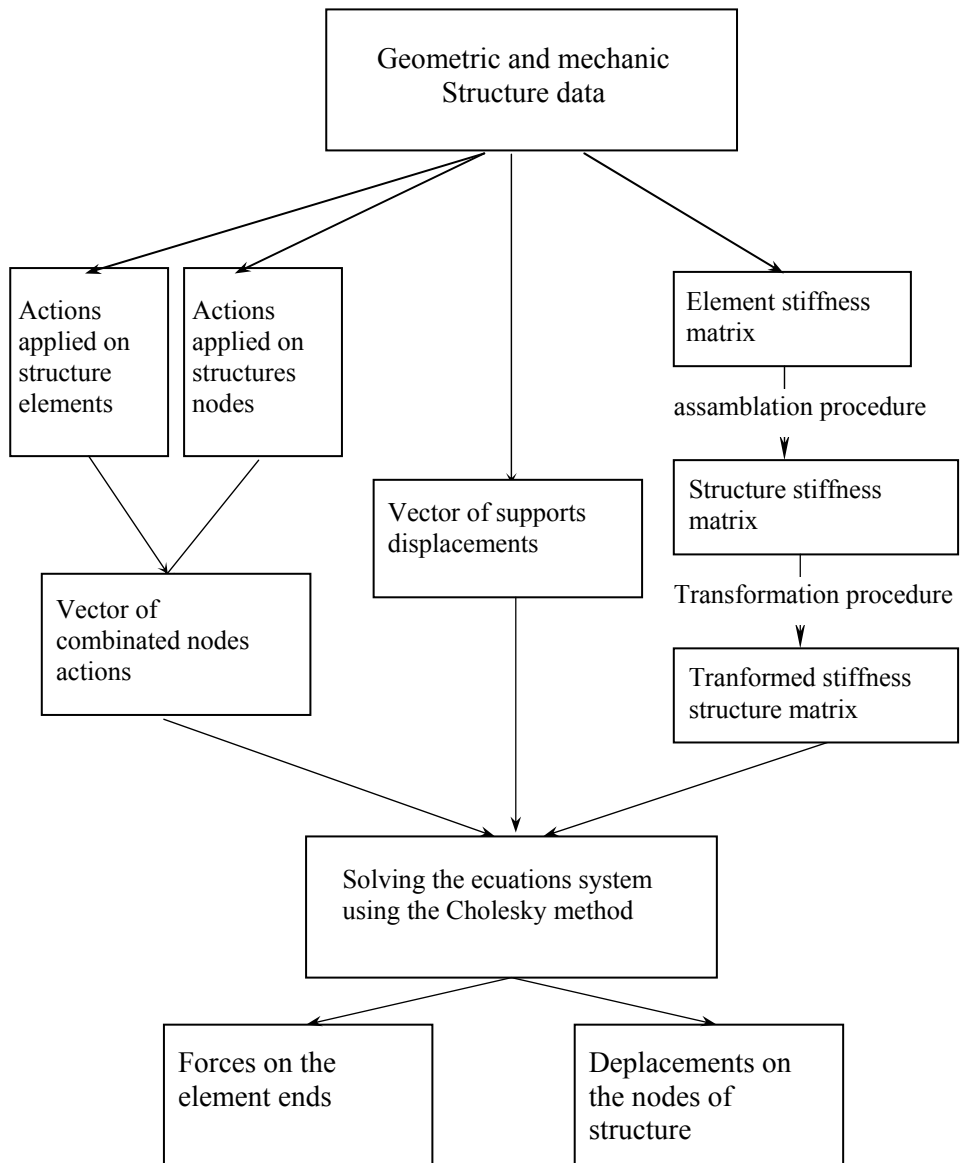


Figure 2. Program algorithm

The beam-to-column connections considered in the portal design are corresponding as rigid by full welding, pinned by angles web cleats and as semi-rigid by top and seat angles or flush end plate. For demonstrative purposes, the stiffness for the semi-rigid connection is related to the beam stiffness as $4EI_b/L_b$ in which, I_b is the beam moment of inertia and L_b is the beam length.

The moment diagrams for the three assumed beam connection types are presented in Fig. 4.a., for the references model and in Fig. 4.b for the proposed program.

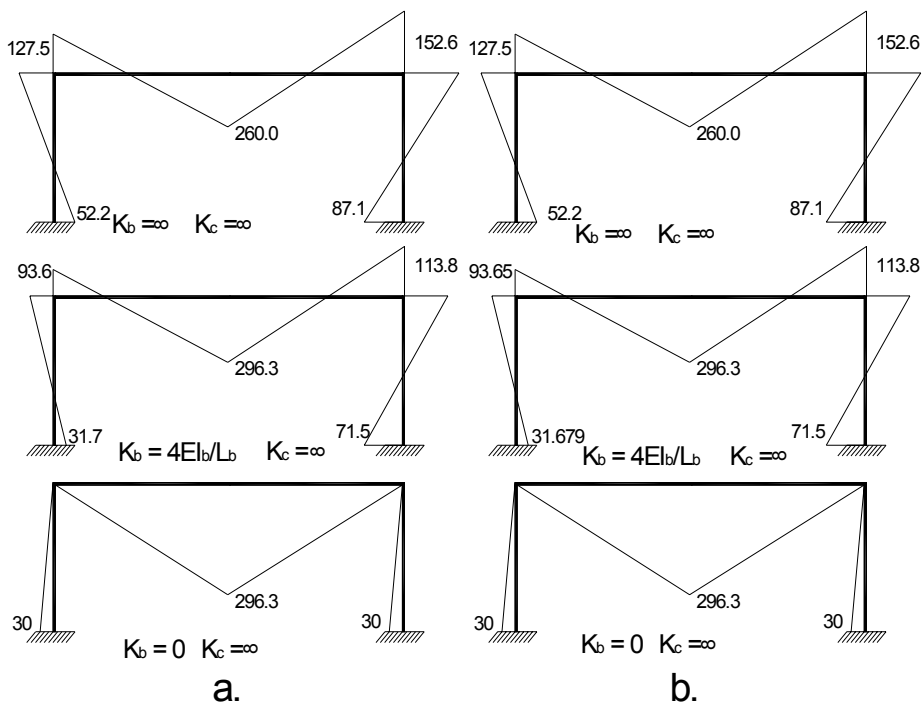


Figure 4. Bending moments in a portal (kNm).

It can be seen that the bending moment for the members are very much influenced by the connection details.

Practically, the beam-to column connections and the column-to-foundations connections have finite stiffness.

An other example studied with the same program, consist in an elastic analysis of a multi-storey unbraced steel frame.

The six storey frame with rigid joints has been proposed by Vogel (1985) as calibration example for checking the accuracy of an ultimate strength analysis. The frame has a total height of 22.5 meters and the width is 12 meters. No bracing is provided to the frame. Frame elements are realized by European profiles, shown in Fig.5. This frame was analysed for two types of beam-to-column connections.

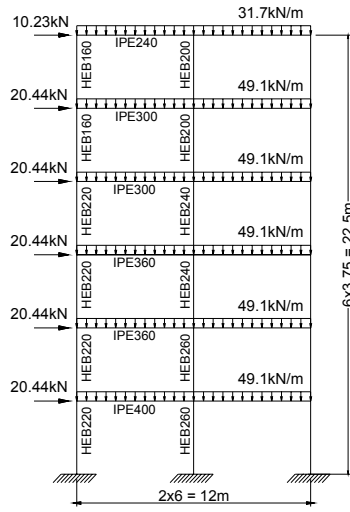


Figure 5. Structure schema

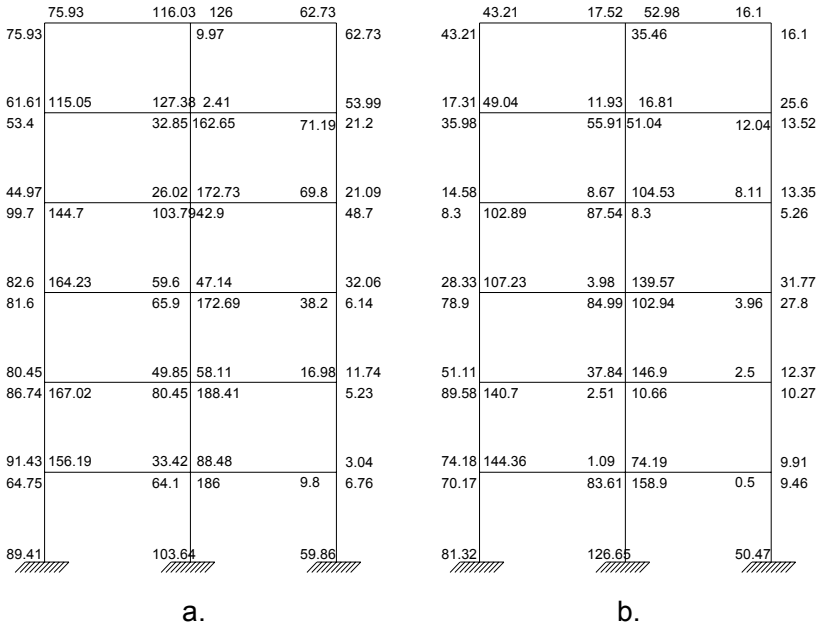


Figure 6. Bending moments on six storey frame (kNm).

The moments at beams and columns are shown in fig.6a., for rigid joins and in fig.6.b. for semi-rigid beam-to column connections, corresponding of a flush end plate connection.

The bending moment diagrams resulted by this analysis, show that the difference between the behavior of the frame with rigid and semi-rigid connections.

3. CONCLUSIONS

This paper present a computation program based on the basic concept and formulation for linear elastic analysis.

The analyses procedure is simple and can be very effective in analyzing steel frames with different connection stiffnesses.

The bending moment diagrams resulted by this method, show that the difference between a rigid and a semi-rigid frame is significant.

An elastic analysis for the semi-rigid frames, implies a few additional data defining the type and stiffness connections at the ends of the beam and the time allocated for such analysis is minimal.

The proposed program give the results closed by the other programs based on a linear analysis of steel frames.

References

1. Eurocode 3, *Design of steel structure*, - 2003
2. Load and Resistance *Factor* design (LRFD).
3. Chan, S.L. and Chui, P.P.T. *Non-linear Static and Cyclic Analysis of Steel Frames with Semi-rigid connections* , Elsevier, Amsterdam, 2000
4. Faella, C., Piluso, V., Rizzano, G., A. *Structural Steel Semirigid Connections*, CRC Press LLC U.S.A.,2000.
5. Catarig,,Al., Petrina, M., *Statica Constructiilor-Teorie si Aplicatii* Ed..Dacia, 1991. (in Romanian)

Considerations on the quality and importance of the existing high-accuracy levelling networks on the territory of Romania

Carmen Nutiu

*Ph. D. Eng., Senior lecturer, Faculty of Civil Engineering, Technical University of Cluj-Napoca,
400363, Romania*

Summary

The goal of this paper is to highlight the importance of the modernisation of the grade 1 levelling network of our country, correlated with the efforts to create a transcontinental line for linking the Black Sea and the Baltic Sea marigraphs. In the same time, in order to study the vertical movements of the crust of the earth in this area, a levelling network at Eastern-European level had to be accomplished.

After the analysis of the existing earlier measurements, we introduce the works of modernization on the grade 1 levelling network by means of high-accuracy geometrical levelling. Next we present the database for the high-accuracy levelling.

KEYWORDS: state-owned levelling network, *grade 1 levelling network*, high-accuracy geometrical levelling, level system zero, levelling line, levelling polygon, nodal benchmark, fundamental benchmark, leveling database.

1. INTRODUCTION

The measurements for the state-owned levelling network have been made using the geometrical levelling method and by means of different devices, accuracies and adjustments. The classification of the points in the state-owned levelling network has been made based on different reference levels, such as: the Adriatic Sea, the Black Sea with the zero level at Constanta, the Black Sea with the zero level at Sulina, and the Baltic Sea. This is due to the fact that the measurements the state-owned levelling network were based on small areas within the country, by creating polygons to be adjusted.

Thus the following versions of level systems have been created:

- the level system with zero at the Adriatic Sea – “MA”,
- the level system with zero at the Black Sea - Constanta – “MNC”,
- the level system with zero at the Black Sea - Sulina – “MNS”,

- the level system with zero at the Baltic Sea – “MB”,

The heterogeneity of the distribution of these systems on the territory of our country, as well as of the datum levels has led to the necessity of creating a compact and homogenous network for the whole territory of our country, having as datum level the Black Sea. This network was called “level system with zero at the Black Sea, adjusted in 1975” and marked “0” – 1975.

2. THE IMPORTANCE OF THE HIGH-ACCURACY LEVELLING NETWORKS EXISTING ON THE TERRITORY OF ROMANIA

The general conclusion drawn from the studies and research made is that the earlier measurements have enough accuracy, and are a reliable database and information base for later processing. Thus, the differences between the measurement of level differences made earlier and the new ones are acceptably small, and are within $\pm 2-3$ mm for the common points.

After analysing the abovementioned level systems we were able to formulate general considerations on the quality and importance of the existing high-accuracy levelling networks.

2.1. *The level system with the datum level at the Adriatic Sea - MA*

This network includes points especially in the Banat area. Considering the age of these points, as well as the fact that most of them have disappeared from the land and can only be found in the level archives, the need of points with level in this system is very reduced.

2.2. *The level system with the datum level at the Black Sea - Constanta - MNC*

The findings based on the points that make up this type of network, as well as the large dimensions of the areas in which the works in this system have been carried out lead to the conclusion that this network represents a fundamental structure on the territory of our country.

Thus there is a relatively large area covered by a basic topographic plan, with levelling carried out in the MNC reference system; a large part of the state-owned triangulation system's points have levels in this system; on the majority of the levelling lines there are many other materialised points.

Moreover, the high-accuracy levelling routes of grades 1-4 in the MNC system are linked to a series of other geometrical levelling routes of grade 5 and technical ones (which also have levels in the MNC system).

2.3. The level system with the datum level at the Black Sea - Sulina - MNS

There are just a few points in the land (apart from the points in the ports that make up the network), and the need for levels at national level in this system is reduced. This network is developed along the Danube, and includes the levels of the hydrometric staffs placed in the main ports on the Romanian bank of the Danube.

2.4. The level system with the datum level at the Baltic Sea - MB

It is the main network the earlier levelling measurements were carried out, and consists of good quality data, complying with the accuracy and tolerance limits in force. After analysing the performance of this type of network, we made the following observations: the topographic description of the points are made on standard form and are recorded in the national geodesic system; the levelling on the basic topographic plan is drawn in this reference system; in the land, the levelling routes are roughly maintained between 60-80% of the total of the placed points; there are a large number of grade 5 and technical levelling routes (each having its own number) linked to the levelling routes of grades 1-4 in the MB system; the majority of the points in the state-owned triangulation system have reference levels in the MB – Baltic Sea system.

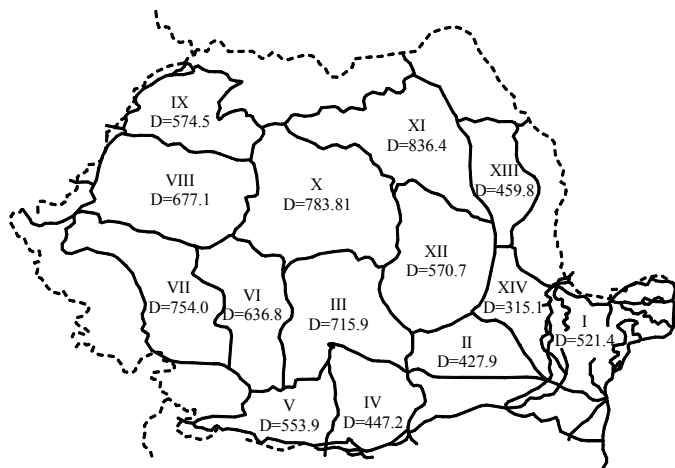


Figure 1. Outline of the grade 1 geometrical levelling network "0" – Black Sea 1975

2.5. The level system with the datum level at the Black Sea, adjusted in 1975 – "0" – 1975

This network was created using the selected, adjusted and recalculated results of the earlier measurements. The findings that resulted from the analysis of this system and from the checks are as follows: not all the points in the coordinate

archives can be found in the land (30-35% of the points can be considered destroyed); 14 polygons of grade 1 have been created and bulkily adjusted (Fig. 1). Within these polygons the levelling lines of grades 2, 3 and 4 have been adjusted. The resulting constant terms have not exceeded the admissible tolerances; the checks carried out revealed that the state-owned levelling in the networks of grades 1-4 is relatively homogenous; in the MN “0” – 1975 reference system just a few works have been carried out that preserved the description of the exiting topographic points created when measurements in the MB or MNC system have been carried out.

3. MODERNISATION OF THE ROMANIAN GEOMETRICAL LEVELLING NETWORK OF GRADE 1 USING HIGH-ACCURACY GEOMETRICAL LEVELLING

The main goal of these modernisation works was the creation of transcontinental lines that link the Black Sea and Baltic Sea marigraphs. In the same time, in order to study the vertical movements of the crust of the earth in this area, a levelling network at Eastern-European level had to be accomplished.

The works of creating the new network, i.e. the planning, land recognition and execution have started in 1972, while the land measurements were set to start in 1974. Consequently, in the planning phase the levelling routes of the new network have been overlapped with the grade 1 levelling routes executed previously, and five new lines have been added. These new lines have created smaller polygons and useful values for the enclosure in the common polygons to neighbouring states. These line are: Mangalia – Negru Voda, Giurgiu – Calarasi, Calafat – Simian, Orsova – Socol, Socol – Timisoara.

The Romanian high-accuracy levelling network consists of 19 polygons with a perimeter of 82-850 km, consisting of 62 lines of 24-247,55 km in length; the network has 6400 benchmarks and has a total length of 6620 km. The 19 levelling polygons are distributed uniformly within the country, and have as marginal lines the borders and 24 links to the neighbouring countries, as follows: 6 links to Bulgaria, 10 links to Yugoslavia, 5 links to Hungary and 3 links to Ukraine.

The fundamental point of the levelling network was designed and realised in the area of Tariverde, Constanta County. This was linked by its own levelling network to the three marigraphs which were to provide the most probable height as compared to the “0” Black Sea.

The levelling lines have been divided into sectors of around 50 km in length, allowing the error analysis to be made within the tolerances.

In 1988 the land measurements have been completed in the entire Romanian high-accuracy geometrical levelling network. In 1990 the phase of adjustment and creation of the level registers has started for each line. The calculation algorithm followed the principles of adjustment by means of indirect observations in free geodesic networks, applied to the high-accuracy geometrical levelling networks.

The creation of the new network determined the need for extending the new level system to the geometric levelling networks of grade 1-4, both in order to homogenise the accuracy of these networks and to meet the various needs of the national economy.

In order to integrate the Romanian geometric levelling network of grade 1 in the Eastern-European U.P.L.N. (E.V.N.S.) this was adjusted to the Baltic Sea reference system. The adjustment was made using the method of indirect observation, restricted to the benchmarks with levels in the Baltic Sea system, as a result of the international adjustment of the network (E.V.N.S.).

The network with the levels specified in the Baltic Sea system consists of the following: 46 nodal benchmarks of the national network, 14 benchmarks previously with levels in the (E.V.N.S.) network and the 5 nodal benchmarks of the polygon of the Tariverde fundamental benchmark, adjusted as a reduced network for the 14 benchmarks of the (E.V.N.S.) network. The differences between the levels calculated in the Black Sea reference system and the Baltic Sea reference system are: the minimum difference of 0.13908 m in the nodal point Negru Voda, the maximum difference of 0.17506 m in the nodal point Calafat; average difference: 0.14966 m.

In the future the creation of a European levelling network (E.U.V.N.) will be proposed, by unifying the Western-European U.E.L.N. network and the Eastern-European U.P.L.N. (E.V.N.S.) network. Our country will take part in this project with five points.

4. THE LEVELLING DATABASE

The high-accuracy geometrical levelling creates a topographic database and information base as a separate domain. This is hierarchically structured on two levels, as follows: state-owned networks and levelled detail points. For each of these levels there will be some databases with functionalities specific to the goal and adapted to the level they are located at. The levels consist of three zones that will be created in modular fashion and will be implemented in phases. These zones are:

- zone 1 = the data and information set,
- zone 2 = data processing,

- zone 3 = the selection and decisional module.

Each of these zones covers a well-defined functional domain within the database, has its own logic segment, completed with the one of the related zones. For a levelling point a large variety of elements may be stored, however the larger their number, the more difficult and costly to create the database.

Based on the statistical studies created in order to solve this problem, it was found that the data and elements to be introduced in the database and information base will be structured as follows: positioning data of the point; description data of the point; data, elements and information on the content; execution data; miscellaneous data.

- Positioning of the point can be made within the levelling polygons, based on the topographic description of the point in question.
- The description data refer to: the name of the point, in some cases the brief description of the location and its topographic description.
- The data, elements and information on the content refer to the data and information set the levelling database and information base is created for. The following fall in this category: data referring to the altimetric position of the point (the levelling reference system, the z level of the point, the precision of level determination, the altitude difference ΔH measured to the next point) and data on the gravimetric position of the point.
- The data concerning the execution, i.e. the contractor, the method and year of execution, are recorded on basis of an existing code that can be accessed via the levelling database and information base.
- The miscellaneous data provide security for the database in terms of integrity and for the situations that appeared and are unforeseen at the date of planning.

5. CONCLUSIONS

The modernisation of the Romanian levelling network of grade 1, using high-accuracy geometrical levelling, played a decisive role in its integration into the Eastern-European U.P.L.N. (E.V.N.S.). levelling network. The phase of adjustment and creation of the level registers, made on the basis of the land measurements completed in 1988, was accomplished restricted to the benchmarks with levels in the Baltic Sea system, as a result of the international adjustment of the network (E.V.N.S.).

The database separately created on two levels, namely: state-owned networks and levelled detail points, provide full high-accuracy topographic information on the studied points.

The results of this modernisation allowed Romania's participation (with five points) in the project of creating a European E.U.V.N. levelling network, by unifying the Western-European U.E.L.N. network and the Eastern-European U.P.L.N. (E.V.N.S.) network.

References

1. Ghitau, D., *Geodezie și gravimetrie geodezică*, Editura Didactică și Pedagogică, București, 1983.
2. *** *GPS Tehnology Applications* - International Symposium Volume, Bucharest, 1995.
3. *** *Revista de Geodezie, Cartografie și Cadastru*, București, 1999.
4. Grecea, C., *Tehnologii topografice utilizând Sistemul Global de Poziționare GPS pentru rețele de sprijin cadastrale - Teza de doctorat*, București, 1999.
5. Colectiv Facultate Geodezie București, *Măsurători terestre – Fundamente*, Editura Matrix, București, 2001.
6. Moldoveanu, C., *Geodezie*, Editura Matrix, București, 2002.

Prediction of condition of structures using Markov chains

Rodian Scînteie¹, Constantin Ionescu²

¹CESTRIN Bucharest, Romania

² Technical University "Gheorghe Asachi" Iasi, Romania

Summary

The article considers the derivation of prediction models for highway bridge condition indices. The prediction is needed as an important part of bridge management system. Deduction of equations, graphics and probabilities of transition is presented for a significant sample of bridge inspection records. The results are used to simulate the evolution of the technical condition of a bridge.

KEYWORDS: bridge, Markov chains, prediction, bridge inspection, bridge management.

1. INTRODUCTION

A modern road management implies a set of technical, mathematical, economic and informational instruments to perform analysis concerning the behavior of the structures and the corresponding costs to maintain the functional parameters in the admitted limits.

It is important to assess the present technical condition of the bridges to verify the necessity of urgent intervention works, their type and costs. In the same time, it is important that condition prediction methods are available to estimate the effects induced to the system or its components by committing or delaying of works.

The approach of condition prediction consists from the following consecutive steps: monitoring the bridges, data collection, statistical analysis, regression analysis, development of transition diagrams.

By monitoring the bridge over its life time most exact results are obtained. Unfortunately, these results may not be applied anymore once the system they are deduced for is out of use. The most effective approach consists in collecting and analyzing data from a set of similar entities. The implied assumption is that similar systems have similar behavior. In such manner, we obtain a cross section through data.

2. ANALYSIS OF CONDITION INDEX I_{ST}

A significant sample of 1795 condition reports is used. All reports were collected after last change in inspection regulations, so respecting the same rules. For obtaining the correct results data must be consistent and the measurement system coherent. The total condition index I_{ST} and the time from construction or last rehabilitation/reconstruction were considered. The values are presented in Figure 1.

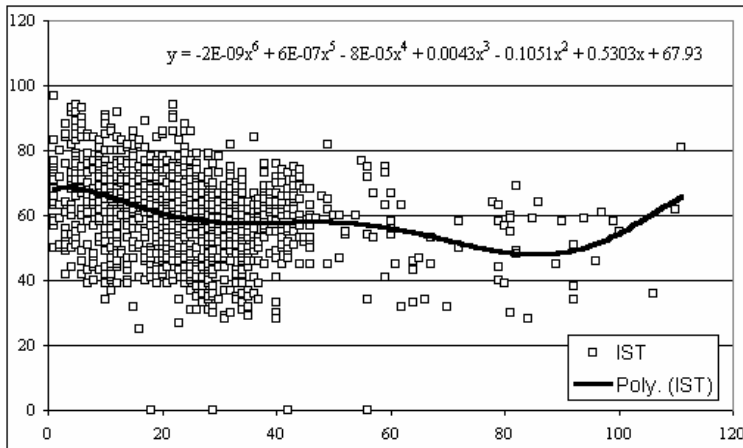


Figure 1. Values of the technical condition index and preliminary regression curve

Reviewing available data one can see that they are on a very large time interval (111 years). On the available sample a polynomial regression analysis was performed for the entire period. The 6th degree equation and the resulted curve are also presented into Figure 1.

This shape presents the inconveniences that make it useless because it does not satisfy some physical considerations. The curve must be descendant for the entire length (condition cannot improve by itself). It must also start from the maximal possible value (at the beginning, the bridge should be in perfect condition, at least in theory).

Another aspect, that must be considered, is the very long period of time. It is very probable that this situation to be the result of lack of records for the moment of the reconstruction, rehabilitation or capital reparation. To eliminate possible perturbations due to incompleteness, truncation of data was considered. Truncation reduces the applicability domain of the obtained equations and values, but one must not forget that the normal life length for a bridge is 50 years, according to regulations, and for some components it is even lower (25 years for the deck). Also, according to present regulations, some works are mandatory to be performed (maintenance, small repairing etc.) and which are not always recorded.

As a consequence, it is not probable that bridges are in a free process of degradation. The longer the period of time, the higher chances are that more interventions were performed with out records. For the truncated period, extrapolation can be performed assuming and accepting a certain degree of uncertainty.

After truncation and regression analysis one can note that the evolution respects the rules of the theory of reliability: an initial zone of rapid degradation, followed by an interval of relative evenness, and finally a zone of fast degradation due to obsolescence.

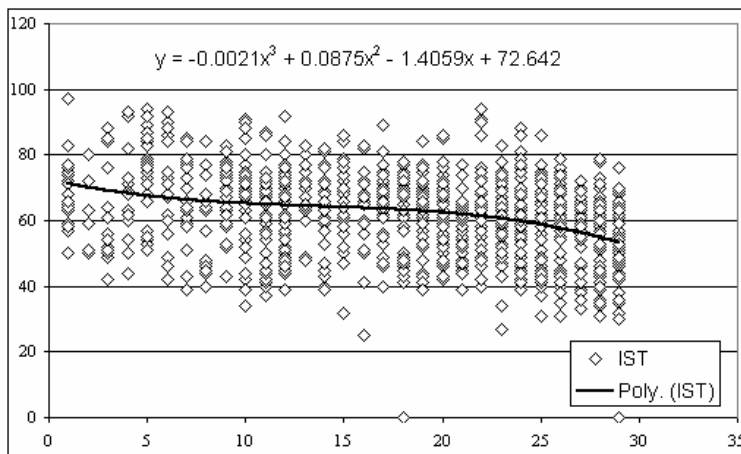


Figure 2. Analysis of I_{ST} values on truncated interval

3. ANALYSIS OF A PARTICULAR CONDITION INDEX (C_1)

Even the analysis of an index like I_{ST} requires strong statistical knowledge and a special attention, it is however relatively simple to perform the computation for this part as the characteristics are visible or intuitive. It is Much more difficult to analyze the indicators with a reduce domain, i.e. analysis for the evolution of C_1 (main resistance elements of the superstructure) which is presented in Fig.3. The value cloud is extremely scattered and the regression consistence does not present consistence (is ascendant for some range).

Due to the fact that no result may be deduced from raw data the evolution will be studied based of annual average, Fig.4. The time interval is partitioned in 3 zones and regression will be performed on each one. For the first zone the trend line is forced to pass through the value 10 for $t=0$.

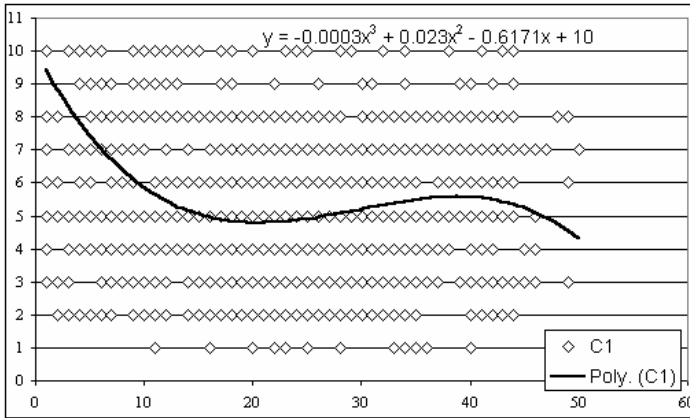


Fig 1. Value of C_1 (main resistance elements of the superstructure)

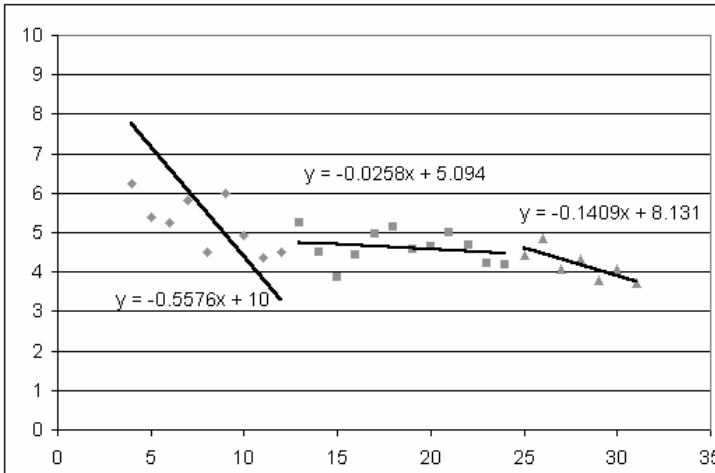


Fig 2. Analysis of the condition index through annual average

It is usual for the management systems to use models based on Markov chains and transition matrix. This refers to computing the probabilities of evolution of the system from one state to another.

The transition chain is described in Figure 5.

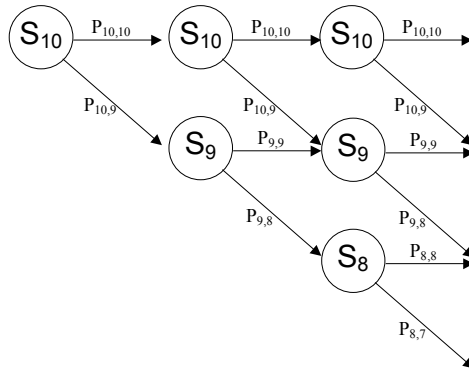


Fig 3. Transition between states and transition probabilities

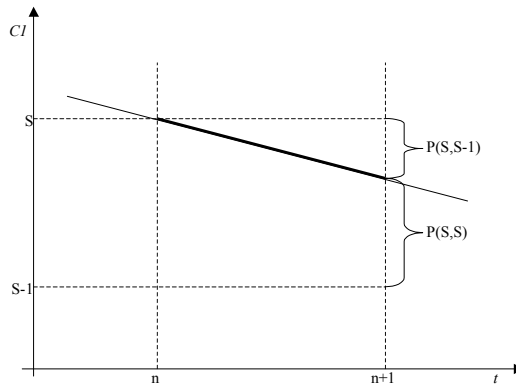


Fig 4. Principle of computation of the probabilities from trend diagram

The process of transformation from diagram to transition matrix starts from the assumption that bridge condition evolution is a quasi-stationary process. This means that the slope is sub-unitary and the transition is done from a state into the immediate next one (no catastrophic transition occurs).

Mathematically, the enounced principle is comprised in the following equation:

$$P(S, S) + P(S, S - 1) = 1$$

Where: $P(S, S)$ represents the probability of remaining in the same state after the unity interval, and

$P(S, S - 1)$ - the transition probability into the immediately next state after the unity interval.

Analysis of Figure 6 reveals immediately the aspect that $P(S, S - 1)$ is equal with the slope of the diagram in point S . Processing the available data the transition probabilities were deduced (see Tabell.).

Table 1.

Condition	Time moment	Slope
10	0.000	0.5576
9	1.790	0.5576
8	3.586	0.5576
7	5.379	0.5576
6	7.173	0.5576
5	8.966	0.0491
4	29.322	0.1409
3	36.420	0.1409
2	43.518	0.1409
1	50.616	0.1409
0	57.714	0

Starting from the table of the slopes the transition matrix can be immediately deduced. This is presented in Table 2.

Table 2. Transition matrix

	10	9	8	7	6	5	4	3	2	1	0
10	0.44	0.56	0	0	0	0	0	0	0	0	0
9	0	0.44	0.56	0	0	0	0	0	0	0	0
8	0	0	0.44	0.56	0	0	0	0	0	0	0
7	0	0	0	0.44	0.56	0	0	0	0	0	0
6	0	0	0	0	0.44	0.56	0	0	0	0	0
5	0	0	0	0	0	0.95	0.05	0	0	0	0
4	0	0	0	0	0	0	0.86	0.14	0	0	0
3	0	0	0	0	0	0	0	0.86	0.14	0	0
2	0	0	0	0	0	0	0	0	0.86	0.14	0
1	0	0	0	0	0	0	0	0	0	0.86	0.14
0	0	0	0	0	0	0	0	0	0	0	1

The resulted matrix was used to simulate the behavior of a bridge over the life time. The evolution of is presented in Figure 7. The use of the matrices is a simple operation easy to implement in computation systems.

The result of the simulation (dotted line) closely follows the trend line obtained through regression. For long forecast periods (over 20 years) one may see a difference. However, this difference is covered by data variance.

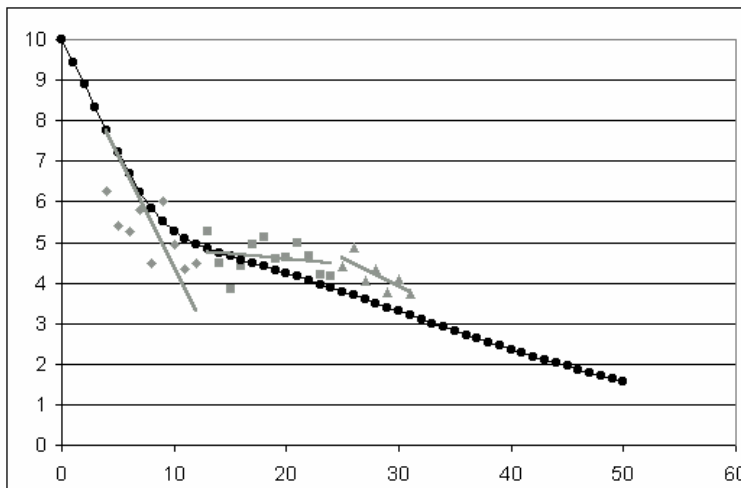


Figure 7. Simulation of the evolution of C_1 condition index

4. CONCLUSIONS

The bridge management system represents a necessity by its effects on enhancing the allocation on resources. An important element of the system is represented by the prediction model for evolution of technical condition.

For development of the model data obtained for similar systems should be analyzed. To analyze acquired data, mathematical regression was used.

The value of the transition probabilities might be deduced from the equations of evolution of condition indices. The probabilities are grouped in transition matrix, an extremely convenient instrument for prediction and simulation of the condition evolution over the lifetime.

It is important to study in the immediate future if there is a significant difference behavior for new bridges and rehabilitated bridges.

References

1. Scînteie Rodian, Ionescu, Constantin, Considerații asupra inspecției de evaluare a stării tehnice a podurilor (Considerations on inspection for bridge condition assessment); Chisinau, Noiembrie 2002.
2. AND522 – Instrucțiuni pentru determinarea stării tehnice a unui pod de șosea (Instruction for assessment of technical condition of a highway bridge), AND, Buletinul Tehnic Rutier nr. 3-4/2002, Bucuresti.

Single exciter techniques for structural identification

Cristian-Claudiu Comisu

¹*Catedra Cai de Comunicatii si Fundatii, Facultatea de Constructii, Iasi, 70050, Romania*

Summary

The main objective of structural identification is the development of an analytical conceptualization of a structure, and quantifying, testing, improving, and validating the resulting analytical model by correlating responses simulated by the model with those measured from the structure. The structural identification requires integrated analytical and experimental components of research or applications. The experimental techniques can be further sub-divided into two categories - single exciter techniques and multiple exciter techniques.

This paper is focus to find an algorithm to quantify modal parameters obtained by the single exciter techniques. The advantages and disadvantages of the various exciter techniques will be discussed. The objectives of this paper are to integrated analytical research (to find the mechanisms of flexibility, inertia and damping that govern the dynamic responses) with the experimental components of research (apply an algorithm to quantify modal parameters).

The simplest and most commonly used technique is the peak amplitude method, in which the structure is excited by a sinusoidal force from a single exciter and the response curves of total amplitude, obtained at several points on the superstructure of bridge, are recorded as a function of frequency. Measurement of the exciting force and the resulting motion at a number of points over a range of frequencies would be sufficient to describe the vibrator behavior of the structure.

The limitations of the peak amplitude method, when there are close resonances (which may be further aggravated by heavy damping) are summarized in the following:

- 1. A mode may be completely missed out;*
- 2. Errors may occur in estimation of damping and the principal modes;*
- 3. If the damping is very light experimental difficulties lie in making measurements around the resonant frequencies.*

KEYWORDS: structural identification, exciter, analytical model, modal parameters, flexibility, inertia, damping

1. INTRODUCTION

The definition of structural identification is the development of an analytical conceptualization of a structure, or region thereof (including supports and continuity), and quantifying, testing, improving, and validating the resulting analytical model by correlating responses simulated by the model with those measured from the structure [1]. The structural identification requires integrated analytical and experimental components of research or applications.

The identification methodology proposed for large structures such as superstructures of bridges, have 10 steps [1]:

1. Study the structure to be identified, including its support mechanism, by examining existing information about the structure, e.g. construction drawings, record drawings, inspection records, and visiting the site.

2. Based on synthesis of the data from step 1, develop a reference analytical model of the structure. The model should include all potentially critical mechanisms of flexibility/stiffness, inertia, and if possible energy dissipation.

3. Establish reasonable upper and lower bounds of the values of the modal parameters in the model.

4. Conduct parametric sensitivity studies to find the mechanisms of flexibility, inertia and damping that govern response. Determine which particular responses are most affected by these mechanisms.

5. Reduce the reference model to include only those parameters, termed the “critical” parameters that model the governing mechanisms.

6. Conduct experiments on the structure to reliably generate and measure the responses most sensitive to the governing mechanisms. Use the upper and lower bounds of responses established in step 4 to guide selection of the type and manner of use of equipment.

7. Apply an algorithm to the measured data to quantify modal parameters and then those dealing with inertia [m], flexibility [k], and, if possible, energy dissipation [c].

8. Alter values of the parameters of the reduced-reference analytical model until a best fit between model and experimentally generated flexibilities is reached.

9. Validate the reliability of the process.

10. Return to step 1 or some other intermediate step as indicated by the validation procedure.

Based on this proposed identification methodology, the objectives of this paper are to integrated analytical research of step 4 (to find the mechanisms of

flexibility, inertia and damping that govern the dynamic responses) with the experimental components of research in step 7 (algorithm to quantify modal parameters).

The experimental techniques can be further sub-divided into two categories - single exciter techniques and multiple exciter techniques. This paper is focus to find an algorithm to quantify modal parameters obtained by the single exciter techniques.

2. STRUCTURAL DYNAMICS

Consider a simple free-free beam shown in figure 1, and assume it has only the first three degrees of freedom. To determine the total vibration of the beam, it must be excited at some point and the vibration measured at several points on the beam. If this time domain information were transformed to the frequency domain, the frequency response curves obtained at the three points would be as shown in figure 1. That the sharp peaks (resonances) occur at the same frequencies, independent of where they are measured on the beam; the only difference is the relative height of the resonances.

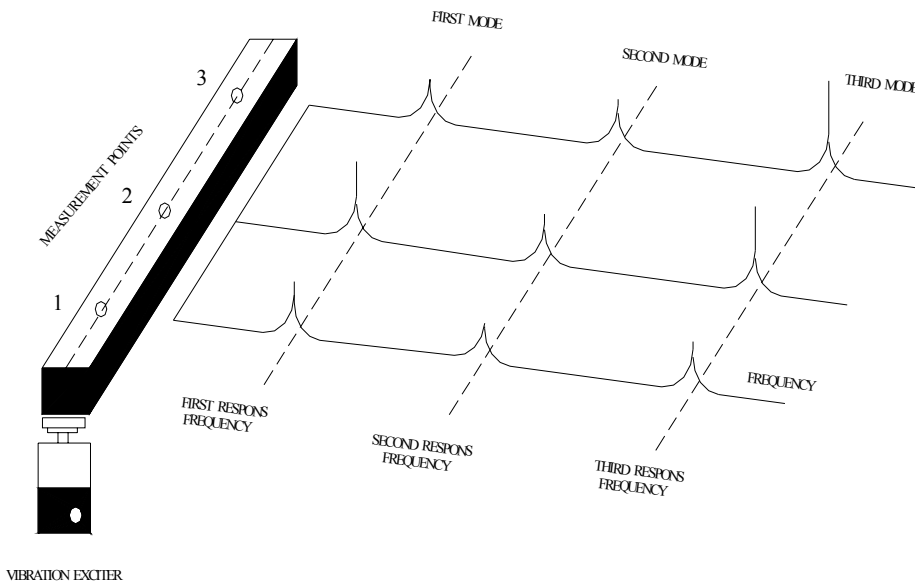


Fig. 1. Frequency response of a free-free beam at three measurement points [2]

In figure 2 the frequency response curves are obtained at several accelerometer positions on the beam. By connecting the peaks of the resonances of a given mode, and considering the phase, the mode shape at each resonance frequency can be traced out. Thus by viewing the figure along the distance axis, obtain a combined frequency response.

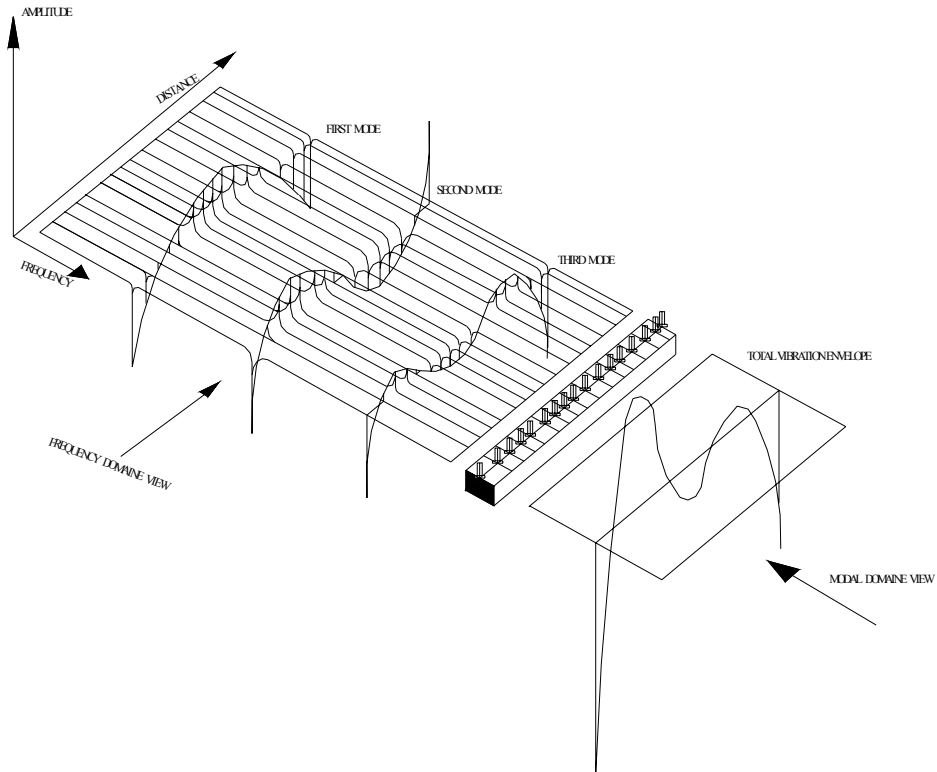


Fig. 2. Three-dimensional view illustrating the frequency and the modal domain

The figure when viewed along the frequency axis shows the three mode shapes, and is referred to as the **modal domain** view. Just as any real waveform can be expressed as a sum of simple sine waves, any vibration can be represented as a sum of principal modes. The right side of figure 2 shows the total vibration envelope, as a sum of the three modes.

It can be seen that the same amount of information is available from the three-dimensional plot of figure 2, whether it is viewed in the frequency domain or in the modal domain. In other words, there is no loss of information by this change of perspective, similar to the case of transforming data mutually between the frequency and the time domain.

To determine the mode shapes, therefore, one can either excite the structure at the resonance frequencies or measure the structural deformation in each vibration mode, or they can be deduced from the frequency responses measured at various points on the superstructure of bridge.

The simplest and most commonly used technique is the *peak amplitude method*, in which the structure is excited by a sinusoidal force from a *single exciter* and the *response curves* of total amplitude, obtained at several points on the superstructure of bridge, are recorded as a function of frequency. The required information is then extracted from these curves. This method has inherent deficiencies, in that not enough is measured, and what is measured is displayed unsatisfactorily. Since the vibratory response of a structure is due to the response in all the principal modes simultaneously, the measured mode shapes are often distorted. This problem is further exacerbated in the case of structures with close natural frequencies where separation of modes becomes mandatory.

In contrast to the traditional sinusoidal excitation, measurement of response to *wide band excitation signals* has been made possible. In this technique, the frequency response function of the superstructure of bridge can be measured at a single point, due to impulse excitation at various points on the structure, or the superstructure can be excited at a single point using various forms of wide band random signals, and the frequency response function measured at several points. The modal parameters are then extracted by analytic curve-fitting the measured data in both the time and the frequency domains [2], [3].

The testing a superstructure of bridge is carried out in two steps.

In the first step the number of modes and their resonant frequencies are roughly established using single shaker sweeps. These presences of modes are indicated by resonant phenomena and phase shifts in the response, and can be difficult to detect when modes have similar shapes and natural frequencies.

Once the existence of a mode has been established, **the second step** involves isolation (tuning) of the mode. This is achieved by distributing the available number of shakers around the superstructure of bridge, guided by experience and heuristic reasoning, and adjusting (appropriating) the amplitudes of the mono-phase forces on the shakers, such that only the mode of interest is dominantly excited in that particular frequency range.

The superstructure thus responds predominantly in the principal mode as a single degree of freedom system, and the modal parameters can then be easily calculated. The number of shakers used and their judicious distribution around the superstructure govern the accuracy of the results.

3. SINGLE EXCITER TECHNIQUES

3.1. Peak Amplitude Method

The simplest and most commonly used technique is the *peak amplitude method*, in which the structure is excited by a sinusoidal force from a *single exciter* and the *response curves* of total amplitude, obtained at several points on the superstructure of bridge, are recorded as a function of frequency. Measurement of the exciting force and the resulting motion at a number of points over a range of frequencies would be sufficient to describe the vibrator behavior of the structure. This information can be presented by plotting the ratio of motion to force as a function of frequency. This is the most commonly used method of carrying out a resonance test [4].

In the instrumentation set-up used for obtaining a response curve the vibration exciter is fed with a certain amount of power at a slowly changing frequency. Due to resonances in the structure and the vibration exciter, the power necessary to subject the structure to a constant force level will not remain constant during the test, but will be a function of frequency. To keep the force level constant, a servo-loop is used in which the output from the force transducer, mounted between the exciter and the superstructure of bridge, is fed back to the exciter control via a preamplifier. The output from the accelerometer mounted on the specimen is fed to an X-Y recorder, which traces out a response curve as the frequency is scanned (fig. 3).

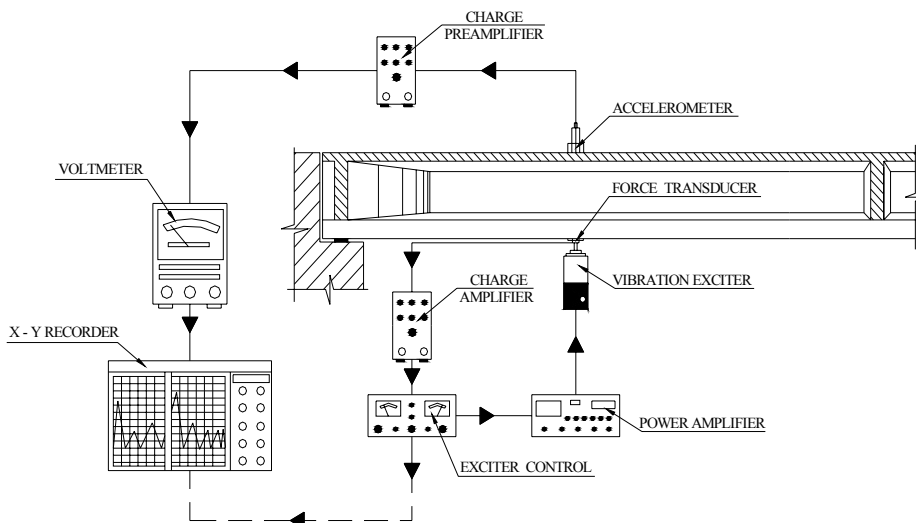


Fig. 3. Instrumentation set-up for the peak amplitude method

The response should be measured at enough points on the superstructure to ensure that all modes will display their resonant characteristics in the response curve of at least one of the points.

The first piece of information that can be extracted from an amplitude response curve is the natural frequencies of the specimen, which are usually identified as the frequencies where peaks are attained – and thus the name peak-amplitude method.

Theoretically, the peaks do not occur exactly at the natural frequencies but at a frequency displaced slightly on one or the other side of them. This is partly due to the damping which couples the modes (non-proportional damping) and partly due to the contribution from the other off-resonant modes at that frequency. The latter contribution will still be there, even if the damping does not couple the motion in the principal modes. However, if the system is lightly damped and the natural frequencies are widely spaced, these errors would be relatively small compared to the experimental errors involved in locating the peaks.

The second piece of information that can be extracted from a response curve is the amount of damping in a particular mode [2]. Damping is determined from the sharpness of the peak (fig. 4) and is normally measured in terms of the Loss Factor given by

$$\eta = \frac{\omega_1 - \omega_2}{\omega_0}$$

where ω_0 is the natural frequency and ω_1 and ω_2 are frequencies on either side of the natural frequency where the peak amplitude is reduced by a factor of $\sqrt{2}$.

Other parameters in terms of which damping is quoted are all related to each other and are given by:

$$\eta = \frac{2 \cdot c}{c_c} = \frac{\delta}{\pi} = \frac{E}{2 \pi w}$$

where $\frac{c}{c_c} = \frac{c}{2 \cdot m \cdot \omega_0}$ is the dimensionless damping ratio

c_c is the critical damping

δ is the logarithmic decrement

E is the energy dissipated per cycle at resonance

w is the energy stored in the system.

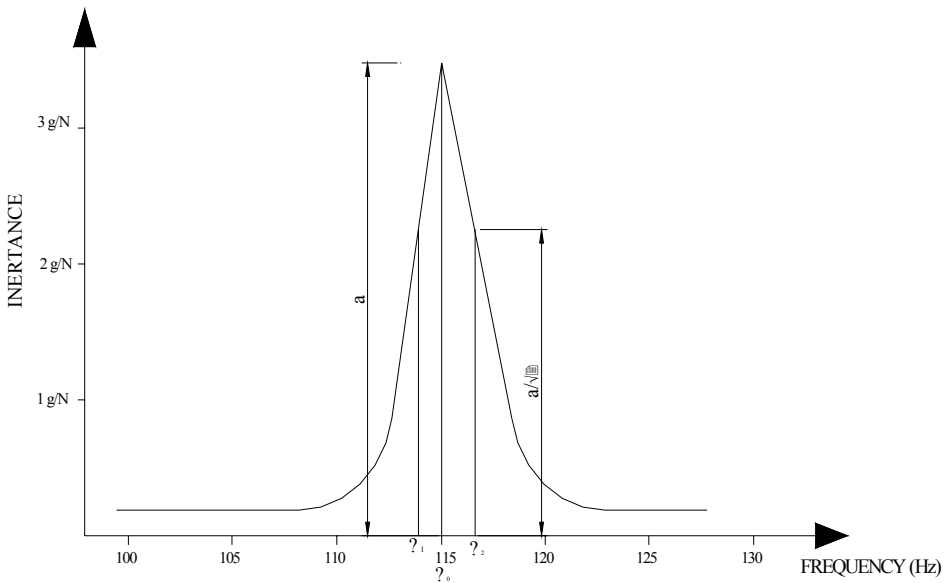


Fig. 4. Third resonance plotted on enlarged linear scales

In the calculation of the damping by this method, it is assumed that each peak represents motion in only one mode, i.e. the contribution from the off-resonant modes is negligible. For resonances that are well separated, however, sufficiently accurate estimates of damping can be achieved, provided $\eta < 0,1$. If the off-resonant vibration is not negligible, but however, constant, it may appear at first that the off-resonant vibration could be extracted from the measured amplitude. Unfortunately, this cannot be done directly, as accelerations are vector quantities and phase angles of the responses have to be taken into consideration. Thus the effect of the off-resonant vibration will be different above and below resonance of the mode under consideration, resulting in a non-symmetrical peak [5], [6].

To determine the mode shape, the superstructure of bridge is excited at a natural frequency, and the ratios of the amplitudes at various points on the structure are determined (fig. 5). As the acceleration goes through a phase change of 180^0 as one passes through a node, the relative phase of the accelerations at various points should also be taken into account.

Since the beam has uniform cross-section, the mode shape ideally be symmetrical; however, the asymmetry of the mode shape is evident. This is because more that one mode is represented in general, at any one frequency, and therefore the mode shape is not a true principal mode. In other words, the phase angle between the force and the acceleration would not be exactly 90^0 at all points on the superstructure.

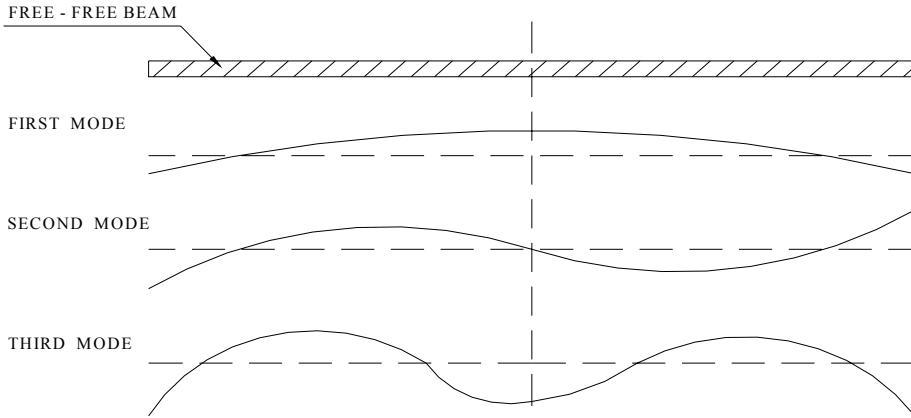


Fig. 5. Mode shape for the third natural frequency

3.2. Contribution from Off-Resonant Modes

The response of a continuous structure (multiple degree of freedom system) can be represented by the superposition of the responses in its individual modes, considering each mode to responses as a single degree of freedom system. Differences between the resonance characteristics of the response of a single degree of freedom system and those of a multiple degree of freedom system are, however, manifested by the contribution of the off-resonant modes to the mode that is excited.

These responses can be derived from equation of motion for a single degree of freedom system with structural (hysteretic) damping [5]:

$$m \cdot \ddot{x} + \frac{\gamma \cdot k}{\omega} \dot{x} + k \cdot x = F \cdot e^{j \cdot \omega \cdot t}$$

or

$$m \cdot \ddot{x} + k(1 + j \cdot \gamma) \cdot x = F \cdot e^{j \cdot \omega \cdot t}$$

where

$k(1 + j \cdot \gamma)$ - is called the complex stiffness

γ - is called the structural damping factor.

The steady state solution is given by:

$$x = X \cdot e^{j\omega t} = \left[\frac{1}{1 - \left(\frac{\omega}{\omega_0}\right)^2 + j \cdot \gamma} \right] \cdot \frac{F \cdot e^{j\omega t}}{k}$$

By multiplying the numerator and the denominator of the square brackets by its complex conjugate, the real and the imaginary components of the displacement can be obtained:

$$x = \left[\frac{1 - \left(\frac{\omega}{\omega_0}\right)^2}{\left\{1 - \left(\frac{\omega}{\omega_0}\right)^2\right\}^2 + \gamma^2} - \frac{j \cdot \gamma}{\left\{1 - \left(\frac{\omega}{\omega_0}\right)^2\right\}^2 + \gamma^2} \right] \cdot \frac{F \cdot e^{j\omega t}}{k}$$

Thus

$$\text{Re}(x) = \left[\frac{1 - \left(\frac{\omega}{\omega_0}\right)^2}{\left\{1 - \left(\frac{\omega}{\omega_0}\right)^2\right\}^2 + \gamma^2} \right] \cdot \frac{F \cdot e^{j\omega t}}{k}$$

and

$$\text{Im}(x) = \left[\frac{-\gamma}{\left\{1 - \left(\frac{\omega}{\omega_0}\right)^2\right\}^2 + \gamma^2} \right] \cdot \frac{F \cdot e^{j\omega t}}{k}$$

The total displacement is given by:

$$\left[\frac{1}{\sqrt{\left\{ 1 - \left(\frac{\omega}{\omega_0} \right)^2 + \gamma^2 \right\}}} \right] \cdot \frac{F \cdot e^{j\omega t}}{k}$$

which lags behind the force vector by an angle θ given by:

$$\theta = \tan^{-1} \left[\frac{\gamma}{1 - \left(\frac{\omega}{\omega_0} \right)^2} \right]$$

It can be seen that the quadrature response peaks more sharply than the total response, and is equal to the total response at resonance, since the in-phase response is zero. The total response on either side of resonance is relatively large, because the in-phase response varies more slowly than the quadrature response. Whilst the in-phase response is asymptotic to $1/m$ above resonance, the quadrature response rapidly approaches zero on either side of resonance.

The amplitude of the total response is larger than that of the quadrature response and that the peak of the total response occurs above the true resonant frequency. Although the difference in the frequency of the two peaks is small, the relative amount of the non-resonant mode response at the frequency of the peak total response is increased. Since the response of the resonant mode varies rapidly with frequency, the contribution of non-resonant modes to the total response is increased from approximately 25% at the actual resonant frequency to approximately 65% at the apparent resonant frequency indicated by the peak of the total response.

If the mode shape was determined from the quadrature response, adequate mode shape measurement would be obtained, since the error in the amplitude of the fourth mode as determined by the quadrature response is negligible for this simple system. In practical structures, however, resonant modes are often close to each other, causing modal interaction in the quadrature response.

2. 3. Close Resonances

Figure 6 shows two modes that are closely spaced in the frequency domain. Each mode responds to a sinusoidal excitation at any frequency. This response is small unless the excitation frequency is in the immediate vicinity of the mode's resonant frequency. Although the off-resonant contribution is relatively small at the

frequency of the mode to be excited, it adds to the distortion of the data and must, therefore be removed [7].

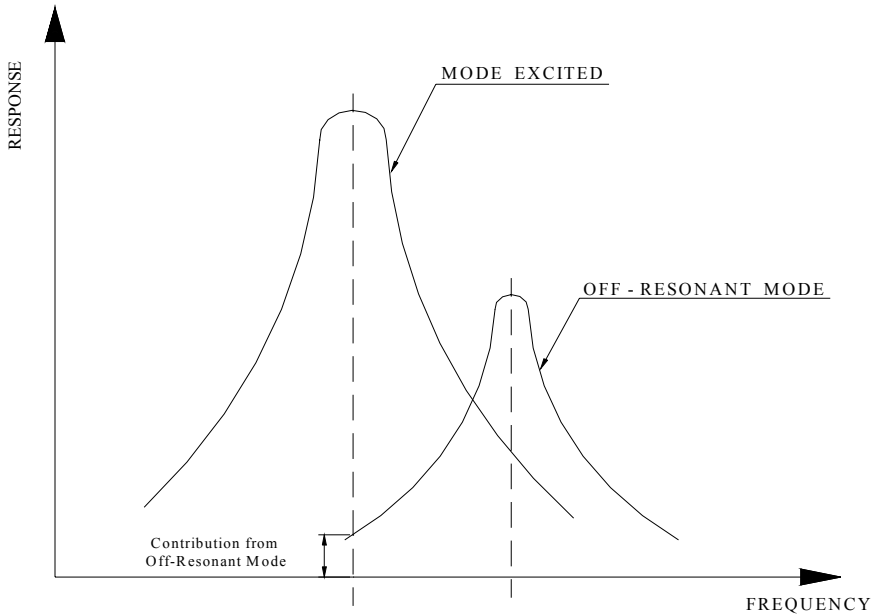


Fig. 6. Two closely spaced modes illustrating contribution from the off-resonant mode

The off-resonant vibration is constant, in amplitude and phase, as the excitation frequency is scanned through the resonance. Therefore, at first sign one might be inclined to extract the off-resonant vibration from the measured amplitude. Unfortunately, this cannot be done legitimately, as accelerations (or displacements) are vector quantities. Therefore, phase angles of the measured amplitude and of the off-resonant vibration have to be taken into account, and subtraction carried out vectorially. Although the off-resonant vibration does not go through a marked change in the phase response, the phase angle of the response in the resonant mode change from a small angle to almost π as it passes through the resonant frequency.

Another difficulty that arises in analyzing the amplitude frequency curves is when there is heavy damping. Firstly, a heavily damped mode may be completely obscured from some of the curves. Secondly, at the resonant frequency of a heavily damped mode, the amplitude of the off-resonant vibration may be comparable to the vibration in the resonant mode. This can induce serious errors in the estimation of damping and the principal modes.

3. CONCLUSIONS

The limitations of the *peak amplitude method*, when there are close resonances (which may be further aggravated by heavy damping) are summarized in the following:

1. A mode may be completely missed out;
2. Errors may occur in estimation of damping and the principal modes;
3. If the damping is very light experimental difficulties lie in making measurements around the resonant frequencies.

To overcome these limitations, either the off-resonant vibration has to be extracted from the response, or the structure must be excited in such a manner, so that only the mode of interest is excited.

References

1. Ibanez, P., Identification of dynamic structural models from experimental data. Univ. of Calif. At Los Angeles Engrg. Report, UCLA-ENG-7725, Univ. Of California at Los Angeles, Los Angeles, California, 1972
2. Zaveri K., Phil M., Modal Analysis of Large Structures. Multiple Exciter Systems. Bruel & Kjaer, 1984.
3. Kennedy C. C., Pancu C. D. P., Use of Vectors in Vibration Measurement and Analysis, J. Aeronautical Sciences, Vpl. 14, No. 11, 1947, pp. 603-625
4. Stahle C. V. Jr. Phase Separation Technique for Ground Vibration Testing, Aerospace Engineering, 1962
5. Comisu Cristian., *Contribuții la studiul caracteristicilor dinamice ale tablierelor de poduri cu structură compusă (mixtă)*, Facultatea de Construcții Iași, martie 1998
6. Comisu Cristian., Identificarea în concept dinamic a stării tehnice a podurilor cu structură mixtă oțel-beton, Editura Societății Academice "Matei-Teiu Botez", Iași, 240 pg., ISBN:973-7962-12-5, 2003
7. Cristian Claudiu Comisu, Constantin Ionescu, *Metodologia de investigare analitico-experimentală și de identificare în concept dinamic a tablierelor de poduri. Studii de caz*. Simpozion cu participare internațională "Computational Civil Engineering 2004" Iași, 11 iunie 2004.

Multiple exciter techniques for structural identification

Cristian-Claudiu Comisu

¹*Catedra Cai de Comunicatii si Fundatii, Facultatea de Constructii, Iasi, 70050, Romania*

Summary

The objectives of this paper are to integrated analytical research with the experimental techniques. These techniques can be further sub-divided into two categories - single exciter techniques and multiple exciter techniques. The various techniques used for obtaining the modal parameters, will be viewed from three aspects: the way in which the structure is excited and the instrumentation required, the data obtained and its presentation and the analysis of the data. Furthermore, the advantages and disadvantages of the various exciter techniques will be discussed.

This paper is focus to find an algorithm to quantify modal parameters obtained by the multiple exciter techniques.

For each frequency of excitation there are as many characteristic phase angle as there are number of degree of freedom, corresponding to certain sets of forces.

If the structure is non-proportionally damped, the structure can be excited in its principal mode, only at the corresponding natural frequency by a set of mono-phase forces. In this case, the response will be in quadrature with the forces at all points on the structure.

If the structure has n degrees of freedom, n number of shakers is required ideally to isolate a mode.

For each characteristic phase lag there is a corresponding mode shape which varies with frequency. At the undamped natural frequencies one of the mode shapes is identical to the corresponding undamped principal mode.

The mode shapes depend on the shape of the damping matrix and not on the intensity of damping.

In each mode the response at the coordinates are all in phase, but lag behind the excitation force by an angle θ . At the undamped frequency $\theta = 90^\circ$ for one of the modes which is the principal mode.

KEYWORDS: structural identification, exciter, analytical model, modal parameters, flexibility, inertia, damping

1. INTRODUCTION

Since a superstructure of bridge when excited vibrates in several modes simultaneously, and thus causes difficulties in the analysis of the results, the unwanted modes have to be somehow eliminated. This can be achieved for simple structures by placing the exciters or pick-ups at nodal points of the unwanted modes, or by making use of the symmetrical and anti-symmetrical properties of the mode shapes. In complex structures such as superstructures of bridge, this is not always possible, and systematic methods have to be used for exciting the structure with multiple shakers and forcing them to vibrate in their principal modes. However, this requires rather sophisticated equipment both on the excitation side, as well as on the data acquisition side, because of the large number of pick-ups, necessary for determining the mode shapes. To facilitate understanding of the multiple exciter techniques, it is necessary to first illustrate in practical terms the theoretical considerations and describe the instrumentation required, and the features that have been incorporated, that are obligatory for functioning of the test [1], [2].

2. EXPERIMENTAL PROCEDURE

That if a structure is proportionally damped, it can be excited at any frequency by a particular set of forces which are in phase or anti-phase with each other, such that the measured responses at all points are all in phase, or anti-phase, and that the common phase lag between the force and the response is unique at this frequency. At this frequency there are as many characteristic phase lags with their associated linearly independent force distribution, as there are degrees of freedom in the structure. The structure when excited in this manner for a particular ratio of forces will vibrate in the principal mode, and thus as a single degree of freedom system.

If the structure is non-proportionally damped, the structure can be excited in its principal mode, only at the corresponding natural frequency by a set of mono-phase forces. In this case, the response will be in quadrature with the forces at all points on the structure.

If the structure has n degrees of freedom, n number of shakers is required ideally to isolate a mode. To exemplify this statement, consider the mode shapes of the first three degrees of freedom of a free-free beam shown in figure 1.

In order to excite the third mode only, three shakers in phase would be required, one at each of points A, B and C. If only two shakers with equal force amplitudes were used in phase at A and B, the second mode could be eliminated, as points A and B move in anti-phase, however, the first mode would be excited together with the third one. Again, if only two shakers were used in phase at A and C, the first

mode could be eliminated, as point A and C move in anti-phase, however, the second mode could not be eliminated.

From this example, it can be appreciated how the symmetrical and anti-symmetrical properties of the mode shapes can be used to advantage, for judicious positioning of the shakers. In complex structures, however, this is not always possible. Furthermore, as continuous structures have infinite number of degrees of freedom, infinite number of shakers would be required. In practice, obviously a limited number of shakers are used, such that only the mode of interest is dominantly excited in a particular frequency range.

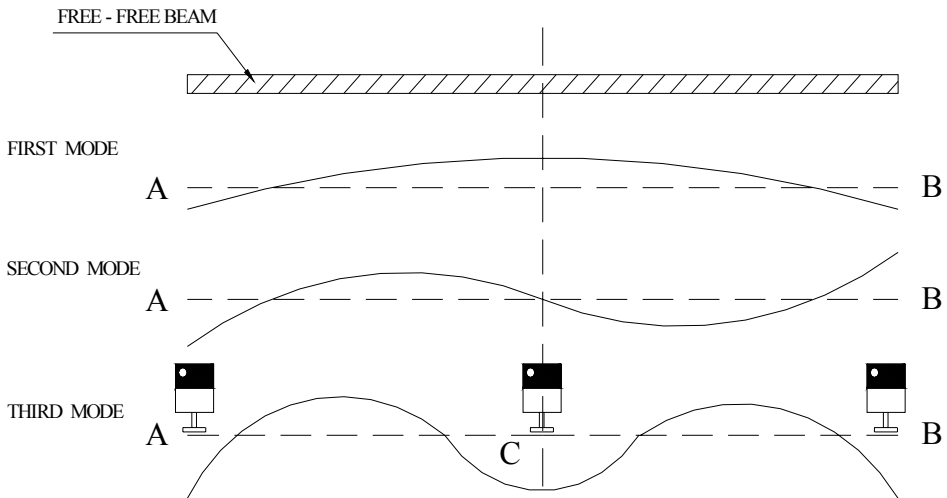


Fig. 1. Positioning of shakers to excite the third mode of a free-free beam

The testing of large structures, such superstructure of bridges, is carried out in two stages. In the first step the number of modes and their natural frequencies are roughly established using single shaker sweeps, by either plotting the peak amplitude or the quadrature component as a function of frequency, or preferably using the complex plot. The response should be monitored at several points to ensure that none of the modes is missed out in the frequency range of interest. Once the existence of a mode has been established, the second step involves tuning of the mode using multiple shakers.

The test is started using a single exciter, placed preferably at an anti-node of the mode to be excited, with an arbitrary force, and the response from an accelerometer placed at the same shaker, or an anti-node, is fed back to the generator. The natural frequency of the mode to be examined is now found by adjusting the frequency of the generator, and observing the relevant Lissajous

figure on the oscilloscope until it becomes a straight line, indicating that a quadrature relationship between the exciting force and the response is established. The automatic frequency control loop is now closed so that subsequent frequency control, the force level on the second shaker is adjusted on its power amplifier, until the quadrature relationship for it established on its Lissajous figure. The force level now is similarly adjusted on the third shaker, which may, however, cause a phase difference on the Lissajous figure of the second shaker. Thus, the force levels on the second and third shakers must be systematically adjusted. When force levels on more shakers are brought into play they would have effects on each others phase response. Thus, iterative adjustment of force levels on the shakers is generally necessary to minimize the phase error on the Lissajous figures of all the shakers.

It will be found that as more and more forces are applied and adjusted, the more uniform in phase are the various points on the structure, and the responses in quadrature with the force. Furthermore, the frequency at which the generator was initially set when the force to the first shaker was applied would have drifted and approached the true natural frequency of the mode being excited. These trends give definite indications that a principal mode is being approached.

When the correct force distribution has been determined, it may be found that the overall force input is too low for accurate response measurements. This occurs if the force level chosen on the first exciter is incorrect. This can be overcome by increasing the voltage output from the generator, so that the forces at all the shakers are increased equally, maintaining the same force distribution. This feature is also useful in checking the amplitude linearity of the structure, by gradually increasing the overall force level chosen on the first exciter is incorrect, is that one or more of the forces at the other shakers may be at a maximum, before the correct force distribution is found. In this case, the force at the first shaker has to be reduced and the force adjustment procedure repeated.

Once the correct force distribution has been obtained, such that the quadrature relationships have been established at the monitoring points, the rest of the structure should be examined for mono-phase response. If the phase scatter around the structure is unacceptably large, repositioning of the shakers and/or monitoring points of responses should be considered. If for some reason, for example, non-linearity in the structure, it is impossible to find the correct force distribution that gives a monophasic response, it may be necessary to accept some phase error at a couple of excitation points. It should be remembered, that unless the automatic frequency control loop is offset, no phase error could occur at the first exciter. Thus if minimum error is sought, the possibility of having to accept some phase error at the first exciter should not be overlooked.

With the correct force distribution established, a sinusoidal frequency sweep around the natural frequency is very useful in revealing the characteristics of the

mode. If the damping were proportional (non-coupling) and hysteretic, the complex response in the Argand plane would be a perfect circle, centered on the imaginary axis with its highest point passing through the origin. From this polar plot, the modal damping as well as the mode shape component could be determined. If the damping were proportional and viscous, the complex response would still be nearly circular. Even if the damping is non-proportional (i.e. damping couples the modes), the complex response plot is nevertheless useful in establishing the presence of a true mode. However, damping coupling of closely spaced modes causes deviation from circular shape of the polar plots, which may be difficult to interpret. It should be remembered that for non-proportional damping, according to the characteristic phase lag theory, the principal mode could be tuned only at the natural frequency, with the response in quadrature with excitation force.

If the mode is isolated, and all the forces at the shakers are suddenly stopped (for example by setting the generator on standby), the resulting decay curves will not exhibit “beating” and will be of a single frequency (the natural frequency of the mode). The modal damping could then also be evaluated from the logarithmic decrement of the decay curves.

3. PRACTICAL DETAILS

3.1. *Exciter Positions*

Some prior knowledge of the mode shapes, either obtained from theoretical calculations or from experience of similar structures, will often expedite judicious positioning of the shakers around the structure. Since nodal regions should be avoided, the extremities of free-free structures are generally a good choice. For exciting the symmetrical modes, positioning the shakers on the axis of symmetry is advisable, and conversely should be avoided for anti-symmetrical modes.

Since the aim of multiple shaker excitations is not only to excite the mode of interest, but also to cancel the contribution from the off-resonant modes, it should be remembered that the off-resonant component couldn't be cancelled, if all the shakers are placed at the nodes of that unwanted mode. The unwanted mode can nevertheless be excited due to damping coupling between it and the other modes.

3.2. *Response Monitoring points for Force Control*

That if the structure is excited in a pure mode, the response at all points on the structure would be in quadrature with the forces. Therefore, the minimum phase scatter that could be measured would be the minimum phase error of the equipment. Unfortunately, structures are never ideal in practice, and therefore a

realistic criterion for modal purity that is often used, is a phase scatter no greater than $\pm 10^0$ around the quadrature components.

4. CHARACTERISTIC PHASE-LAG MODES

For a n degree of freedom system with viscous damping, the equation of motion for steady state sinusoidal excitation can be written in its general form as:

$$[m]\{\ddot{x}\} + [c]\{\dot{x}\} + [k]\{x\} = \{F\}\sin \omega t \quad (1)$$

where the system inertia $[m]$, damping $[c]$ and stiffness matrices $[k]$ are assumed to be real symmetric and positive – definite.

If the damping is hysteretic, the equation of motion would be given by:

$$[m]\{\ddot{x}\} + \frac{1}{\omega}[d]\{\dot{x}\} + [k]\{x\} = \{F\}\sin \omega t \quad (2)$$

where $[d]$ is the hysteretic damping matrix.

In the general case damping would be non-proportional and thus the damping matrix cannot be diagonalized using the normal mode transformation. For an arbitrary set of forces $\{F\}$ and excitation frequency ω the solution of equation (1) is rather complicated. Although the responses at each coordinate x are harmonic with the excitation frequency, they are not all in phase with each other or with the excitation force. If a system with n degrees of freedom is excited by a n number of forces which are either 0^0 or 180^0 out of phase (often called monophasic or coherently phased forces), then for a particular ratio of forces, the response at each of the coordinates will be in phase with each other and lag behind the force by a common angle θ called the characteristic phase lag.

Thus we have to determine the conditions which will produce a solution of the form:

$$\begin{Bmatrix} x_1 \\ x_2 \\ \cdot \\ \cdot \\ x_n \end{Bmatrix} = \begin{Bmatrix} X_1 \\ X_2 \\ \cdot \\ \cdot \\ X_n \end{Bmatrix} \sin(\omega t - \theta) = \{\Psi\} \sin(\omega t - \theta) \quad (3)$$

For any given excitation frequency ω , there exist n solutions of the type given by equation (3), where each of the modes $\{\Psi\}$ is associated with a define phase θ_i and a corresponding distribution of forces $\{\Gamma_i\}$ which is required for its excitation. The response under these conditions is called the “forced normal modes” of the damped system, since every point of the system moves in phase and passes through its equilibrium position simultaneously with respect to the other points.

Substituting equation (3) in equation (2) gives:

$$\sin(\omega t - \theta) \left[[k] - \omega^2 [m] \right] \{\Psi\} + \omega \cos(\omega t - \theta) [c] \{\Psi\} = \{F\} \sin \omega t \quad (4)$$

Expanding the $\sin(\omega t - \theta)$ and $\cos(\omega t - \theta)$ terms and separating the $\sin \omega t$ and $\cos \omega t$ terms we obtain:

$$\cos \theta \left[[k] - \omega^2 [m] \right] \{\Psi\} + \omega \sin \theta [c] \{\Psi\} = \{F\} \quad (5)$$

$$\sin \theta \left[[k] - \omega^2 [m] \right] \{\Psi\} - \omega \cos \theta [c] \{\Psi\} = \{0\} \quad (6)$$

These equation contain three unknowns $\{F\}$, $\{\Psi\}$ and θ since ω is given. If $\cos \theta \neq 0$, equation (6) may be divide by $\cos \theta$ to give [2]:

$$\left[\tan \theta \left[[k] - \omega^2 [m] \right] - \omega [c] \right] \{\Psi\} = \{0\} \quad (7)$$

Equation (7) has a non-trivial solution if the determinat:

$$\left| \tan \theta \left[[k] - \omega^2 [m] \right] - \omega [c] \right| = 0 \quad (8)$$

It is evident, that for a given ω there are n values of $\tan \theta_i$ ($i = 1, 2, \dots, n$) corresponding to the n eigenvalues, and for each $\tan \theta_i$ there is a corresponding eigenvector $\{\Psi\}$ satisfying the equation

$$\left[\tan \theta_i \left[[k] - \omega^2 [m] \right] - \omega [c] \right] \{\psi_i\} = \{0\} \quad (9)$$

If equation (9) is premultiplied by the transpose $\{\psi_i\}^T$ and rearranged, we obtain:

$$\tan \theta_i = \frac{\omega \{\psi_i\}^T [c] \{\psi_i\}}{\{\psi_i\}^T \left[[k] - \omega^2 [m] \right] \{\psi_i\}} \quad (10)$$

From equation (10) it can be seen that each of the roots $\tan \theta_i$ is a continuous function of ω . For low values of ω , $\tan \theta_i$ is small i.e. θ_i is a small angle. As ω increases and approaches ω_i the undamped natural frequency, one of the roots θ_i , which can be named θ_i , approaches the value $\pi/2$. When ω tends to ∞ , $\theta_i(\omega)$ tends to π . In a similar manner the remaining roots $\theta_i (i = 1, 2, \dots, n)$ can be plotted as a function of frequency ω_i . Thus θ_k is that root which has the value $\pi/2$ at the undamped natural frequency $\omega = \omega_k$.

. If every element in the matrix $[c]$ is multiplied by a constant factor, then equation (8) shows that the roots $\tan \theta_i$ will all be increased by the same ratio. Thus equation (9) which determines the mode shapes, will be multiplied throughout by the same factor and the mode shape $\{\psi_i\}$ will be unchanged.

Equation (9) can be re-written as

$$\left[[k] - \omega^2 [m] - \frac{\omega \cdot [c]}{\tan \theta_i} \right] \{\psi_i\} = \{0\} \quad (11)$$

When ω is equal to one of the undamped natural frequency, say $\omega = \omega_i$, then one of the roots θ_i is 90° . Thus equation (11) which determines the mode shape for this root becomes:

$$\left[[k] - \omega_i^2 [m] \right] \{\psi_i\} = \{0\} \quad (12)$$

It can thus be seen, that when the frequency is equal to one of the undamped natural frequency, the mode shape for one of the roots (which is equal to $\pi/2$) is identical to the principal or normal mode shape.

Attention can now be paid to the force that is required to excite any one mode $\{\psi_i\}$ for the corresponding root $\tan \theta_i$ at any one frequency. The force ratio required can be calculated from equation (5) namely:

$$\cos \theta \left[[k] - \omega^2 [m] \right] \{\psi_i\} + \omega \sin \theta [c] \{\psi_i\} = \{\Gamma_i\} \quad (13)$$

In the special case when $\omega = \omega_i$ one of the undamped natural frequencies, one of the roots

$\theta_i = \theta_1 = 90^\circ$ and equation (13) reduces to:

$$\omega_1 [c] \{\psi_1\} = \{\Gamma_1\} \quad (14)$$

5. CONCLUSIONS

In conclusion:

1. For each frequency of excitation there are as many characteristic phase angle as there are number of degree of freedom, corresponding to certain sets of forces.

2. For each characteristic phase lag there is a corresponding mode shape which varies with frequency. At the undamped natural frequencies one of the mode shapes is identical to the corresponding undamped principal mode.

3. The mode shapes depend on the shape of the damping matrix and not on the intensity of damping.

4. In each mode the response at the coordinates are all in phase, but lag behind the excitation force by an angle θ . At the undamped frequency $\theta = 90^\circ$ for one of the modes which is the principal mode.

References

1. Ibanez, P., Identification of dynamic structural models from experimental data. Univ. of Calif. At Los Angeles Engrg. Report, UCLA-ENG-7725, Univ. Of California at Los Angeles, Los Angeles, California, 1972
2. Zaveri K., Phil M., Modal Analysis of Large Structures. Multiple Exciter Systems. Bruel & Kjaer, 1984.
3. Kennedy C. C., Pancu C. D. P., Use of Vectors in Vibration Measurement and Analysis, J. Aeronautical Sciences, Vpl. 14, No. 11, 1947, pp. 603-625
4. Stahle C. V. Jr. Phase Separation Technique for Ground Vibration Testing, Aerospace Engineering, 1962
5. Comisu Cristian., *Contribuții la studiul caracteristicilor dinamice ale tablierelor de poduri cu structură compusă (mixtă)*, Facultatea de Construcții Iași, martie 1998
6. Comisu Cristian., Identificarea în concept dinamic a stării tehnice a podurilor cu structură mixtă oțel-beton, Editura Societății Academice “Matei-Teiu Botez”, Iași, 240 pg., ISBN:973-7962-12-5, 2003
7. Cristian Claudiu Comisu, Constantin Ionescu, *Metodologia de investigare analitico-experimentală și de identificare în concept dinamic a tablierelor de poduri. Studii de caz*. Simpozion cu participare internațională “Computational Civil Engineering 2004” Iași, 11 iunie 2004.

Structures with active hinges, a step to Structural Robotics

Fideliu Păuleț-Crăiniceanu¹

¹"Gh. Asachi" Technical University of Iași, România

Summary

Previously, the concept of Structural Robotics had been founded and defined [1].

The need for this new term is based on tremendous development of many fields of activity as Computer Science and new materials, seen from the last 30 years of the XXth Century.

As a reaction to this development, researches in structural active control followed. Main faced problems were the high costs and the reliability. Imagining that the actual stage would be surpassed, concepts like Structural Active Control, defined by J.T.P. Yao in 1972, [2] or Intelligent Building, defined by T. Kobori in 1988, [3], it appears that they are not enough for covering the needs of the future society.

The reason of limitations in terms of [2] and [3] is the concern that, especially large structures should have a high degree of integration of active devices and the "independence" of the structures must be extremely increased. Intervention of humans in "structure's life" will surely be almost avoided. Therefore a new philosophy was proposed, the Structural Robotics.

Firstly, this paper describes some steps that led to the actual development in active and passive control of civil engineering structures. The author is expressing the idea that the use of Structural Active Hinges could lead to the wanted future's structures. The control for these structures shall be decentralized when referring to active devices systems and centralized for the whole structure.

According to the society's needs, robotic structures, or structure with active hinges, will be active members of the human society. The human intervention on these types of structures will be reduced and replaced with robots and artificial intelligence.

A robotic and robotized structure will never be a "final" structure because it will be self-adaptable and self-developing as a function of the changes in structures' loads, functions, or natural environment. The robot-structure will "think" in advance for calling robots needed in building, rebuilding, repairing or withdrawing parts of the structure.

As a consequence of robotic structures, civil engineers should prepare to strongly cooperate with all the members of the civil society for globalization and integration of their work.

KEYWORDS: active hinges, structural robotics, active control, intelligent buildings

1. INTRODUCTION

The trends from last 30 years have shown a tremendous development of many fields of activity as Computer Science and new materials. The logic step is to integrate the new findings at least into the new and important structures. It is already admitted that microchips and micro-mechanical devices are more and more efficient and at very affordable prices. Also, it can be supposed that sources of energy will be almost unlimited and easier to obtain.

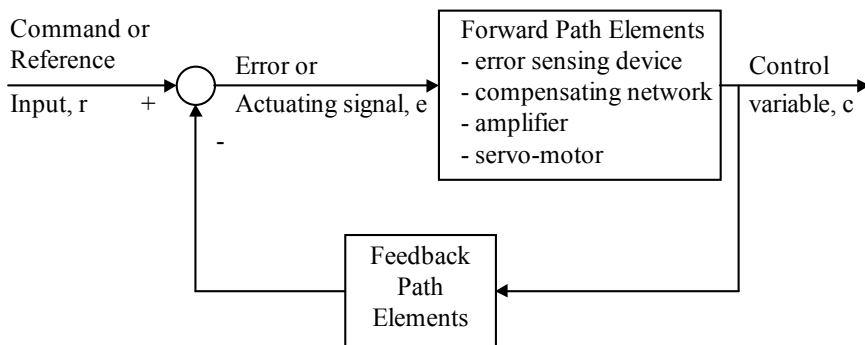


Fig.1 Closed-Loop Control System (Yao, 1972, [1])

Another aspect is that there are structures that need special attention from all members of the civil society. Between them life-line structures and civil engineering structures with inestimable material and spiritual values (as historical buildings) could be named. Also, the outer-space human activity needs light flexible safe structures with low vibration.

Ideas shown above led to an evolution in civil structures. In 1972, Prof. James T.P. Yao, in his paper entitled “Concept of Structural Control” [2], marks the beginning of this new field in Structural Analysis. He proposes the concept of Structural Control, stressing on closed-loop (feedback) control systems. Figure 1 shows the logic of a feedback system, as J.P. Yao viewed it.

At that time, passive devices like those in Figure 2 started to be largely used [4].

Soong & Manolis, in 1987, [5], proposed the concept of “active structures”. They show that “An active structure is one whose active and passive components are integrated and *simultaneously* optimized to produce a new strain of structural system.”

In Figure 3, the use of some structural control devices is suggested [6]. This figure is just a demonstration of how active and passive control could be installed in buildings in order to contribute to their safety.

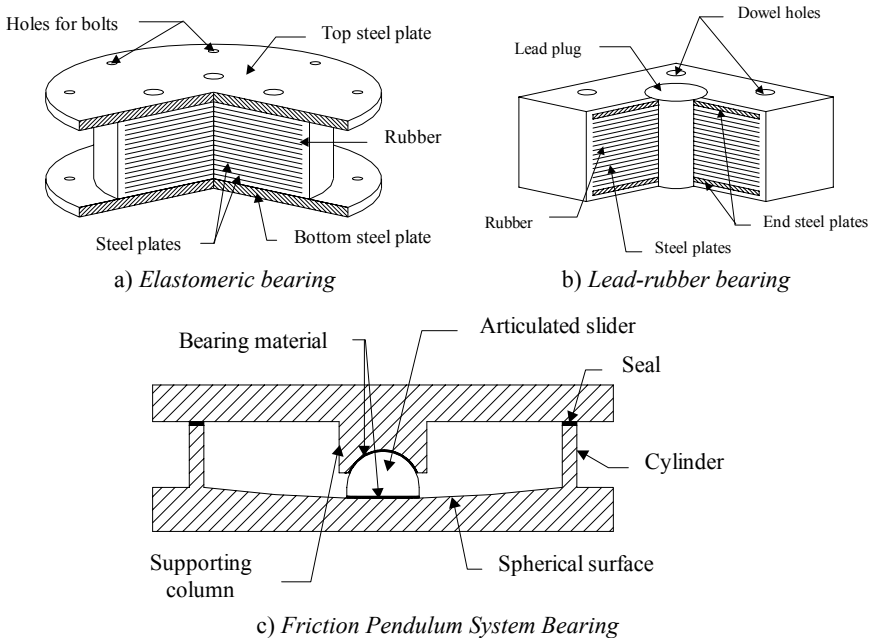


Fig.2 Passive Devices [4]

“Dynamic Intelligent Building” is an important concept introduced by Kobori & al., 1988, [3]. This concept tries to unify the perspective of lifeline systems belonging to an urban community. The information network, which is the infrastructure of very crowded metropolis, should include buildings with dynamic behavior. The data from the surroundings or from long distance, sent through cables, radio and via satellite should be processed by the general and local computers and, this way, the structures will be better prepared to respond to strong earthquakes, Figure 4.

Three prestigious scientists had shown, [7], that "at the present, several active control systems have been developed for real structural applications. These are, by large, discrete and localized sensing and control systems. In fact, only a single control mechanism, such as an active bracing system or an active mass damper, is usually incorporated into a structure. A logical extension of this research is distributed sensing and control".

Following the idea shown above, a research envisioning to control the response of large cable suspended bridge structures with many active devices was started [8]. The analytical study is succeeded to show that optimal active control can be used. An energy based method of generating the parameters of control was developed

and applied also to bridges [9]. The method was analytically tested to buildings, too, [10].

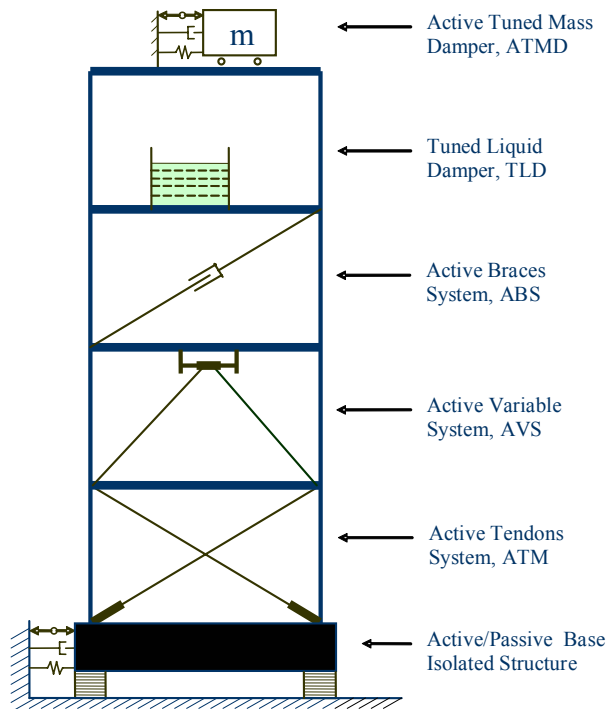


Fig.3 Use of some structural control systems [6]

2. STRUCTURAL CONTROL

In order to control a structure, a thorough identification of the structure should be done. The identification should be done not only in the normal condition but it must be done during the external severe events (strong winds or earthquakes). Sensors placed in structures are useful not only for structural control but also for structural identification.

In what follows, the problem of damage identification is seen to be solved. However, even for such situation, the problem remains very complex. The author's experience is showing that an increased number of sensors and active devices is the only solution for large active controlled structures; see Figure 5 for a model used in analysis [11]. The next methodology is not the only possible one. However, it is showing what happens when many active devices are placed into structures. This methodology does not limit the size of the structure or the number of devices.

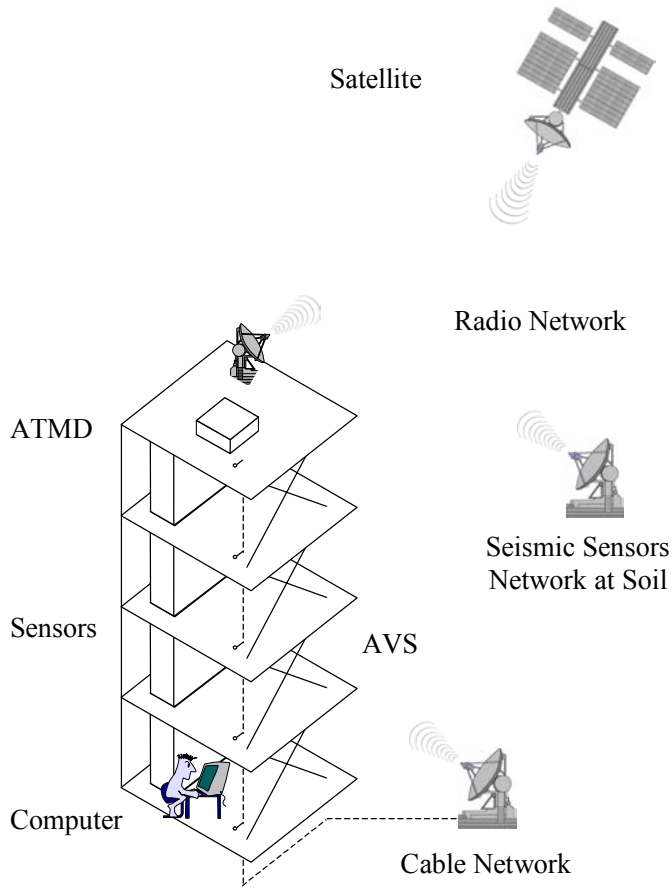


Figure 4. Concept of Dynamic Intelligent Building (Kobori, 1988, [3])

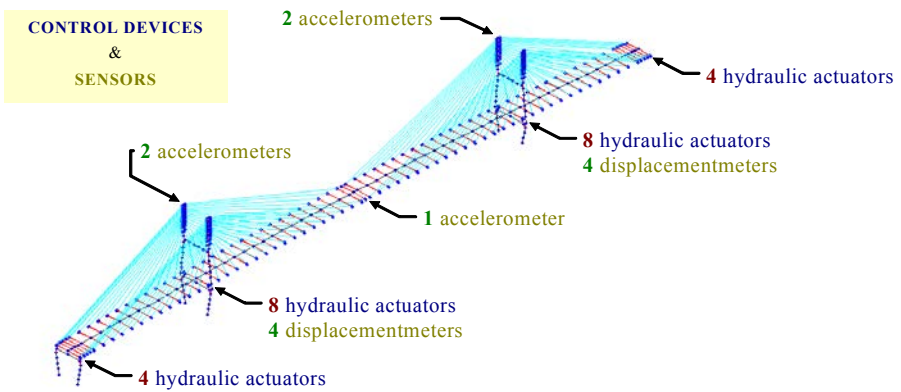


Fig.5 A FEM model of a cable bridge with instrumentation on it [11]

Optimal active control is a time domain strategy, which is appropriate for controlling the response of structures subjected to strong earthquakes. The strategy allows minimizing the energy induced in structures, which is the aim of the seismic design.

The equation of motion for a n degree of freedom controlled system under seismic action is:

$$\mathbf{M}_1 \ddot{\mathbf{z}}(t) + \mathbf{C}_1 \dot{\mathbf{z}}(t) + \mathbf{K}_1 \mathbf{z}(t) = \mathbf{f}(t) + \mathbf{u}(t) \quad (1)$$

where $\mathbf{M}_1 = n \times n$ mass matrix of the structure; $\mathbf{C}_1 = n \times n$ damping matrix; $\mathbf{K}_1 = n \times n$ stiffness matrix; $\mathbf{z}(t) = n$ -dimensional vector of generalized displacements; $\mathbf{u}(t) = n$ -dimensional vector of control actions; $\mathbf{f}(t) = n$ -dimensional vector of external actions.

$\mathbf{f}(t)$ is taken proportional to the seismic ground acceleration:

$$\mathbf{f}(t) = \mathbf{h}_1 \ddot{x}_g(t) \quad (2)$$

where $\mathbf{h}_1 = n$ -dimensional vector showing the points of application and the values for inertia.

Equation 1 can be written as a state equation:

$$\dot{\mathbf{x}}(t) = \mathbf{A}\mathbf{x}(t) + \mathbf{B}\mathbf{u}(t) + \mathbf{h}\ddot{x}_g(t) \quad (3)$$

where $\mathbf{x}(t) = 2n$ -dimensional vector of the states.

To obtain the above transformation, next equations must be employed:

$$\mathbf{x} = \begin{Bmatrix} \mathbf{z} \\ \dot{\mathbf{z}} \end{Bmatrix}, \quad \mathbf{A} = \begin{bmatrix} \mathbf{0} & \mathbf{I} \\ -\mathbf{M}_1^{-1}\mathbf{K}_1 & -\mathbf{M}_1^{-1}\mathbf{C}_1 \end{bmatrix}, \quad \mathbf{B} = \begin{bmatrix} \mathbf{0} \\ \mathbf{M}_1^{-1} \end{bmatrix}, \quad \mathbf{h} = \mathbf{B}\mathbf{h}_1 \quad (4)$$

The system of n second order differential equations, Equation 1, became a $2n$ first order differential equations, Equation 3, and therefore for \mathbf{A} , \mathbf{B} , and \mathbf{h} the dimensions are $2n \times 2n$, $2n \times 2n$, and $2n$ respectively.

Supposing that the control actions are a function of the states, i.e. $\mathbf{u}(t) = -\mathbf{K}(t)\mathbf{x}(t)$ then the goal is to obtain the feedback gain matrix $\mathbf{K}(t)$ such that to minimize a performance index J defined by

$$J = \int_0^{t_f} [\mathbf{x}'(t)\mathbf{Q}\mathbf{x}(t) + \mathbf{u}'(t)\mathbf{R}\mathbf{u}(t)]dt \quad (5)$$

where \mathbf{Q} and \mathbf{R} = weighting matrices. The prime sign in Equation 5 means the transpose.

\mathbf{Q} and \mathbf{R} show the relative importance of minimizing the states (structural response) or the actuating forces. These matrices are square. The first is n -dimensional and the second is m -dimensional, where m is the number of the actuators.

Minimizing J and considering the unknown a constant matrix \mathbf{P} , the next Riccati equation takes place:

$$\mathbf{P}\mathbf{A} - \frac{1}{2}\mathbf{P}\mathbf{B}\mathbf{R}^{-1}\mathbf{B}'\mathbf{P} + \mathbf{A}'\mathbf{P} + 2\mathbf{Q} = \mathbf{0} \quad (6)$$

and the control matrix gain is a constant matrix:

$$\mathbf{K} = \frac{1}{2}\mathbf{R}^{-1}\mathbf{B}'\mathbf{P} \quad (7)$$

With the established gain matrix, the necessary forces for actuators are calculated and the corresponding commands are generated for the actuators.

A difficult task for applying the classical method shown above is to choose the coefficients involved by weighting matrices \mathbf{Q} and \mathbf{R} . For large systems it is not possible to accept individual trial for each coefficient. Therefore general rules are better to envision.

The first term in the brackets of Equation 5 can be written as energy expression and thus leading to minimization of the energy of the structural response. A solution is got if the weighting matrix \mathbf{Q} is composed from the structural matrices \mathbf{M} and \mathbf{K} .

$$\mathbf{Q} = \begin{bmatrix} \mathbf{K} & \mathbf{0} \\ \mathbf{0} & \mathbf{M} \end{bmatrix} \quad (8)$$

A problem occurring when using Equation 8 is that of the embedded active devices' dynamics. It must be noted that the minimization from Equation 5 should refer only to the energy of structural response. Therefore, it is advisable to not use the true \mathbf{M} and \mathbf{K} matrices but matrices in which the terms provided by the active devices are considerably diminished.

In what is regarding the weighting matrix \mathbf{R} it can be taken as a diagonal matrix with terms showing the relative importance between the active devices.

$$\mathbf{R} = \begin{bmatrix} r_1 & \dots & 0 \\ \vdots & \ddots & \vdots \\ 0 & \dots & r_m \end{bmatrix} \tag{9}$$

where $r_1 \dots r_m$ = the corresponding relative importance factors for actuators. If all of these factors are equal, then the matrix \mathbf{R} becomes easier to generate:

$$\mathbf{R} = r\mathbf{I} \tag{10}$$

where r = unique relative importance factor; \mathbf{I} = diagonal 1 matrix (identity matrix).

Using the models like those in Figure 5, the idea that the active/passive controls are very effective (even if the energy request is large) was risen. Typical results as those in Figures 6 and 7 are obtained in all cases. The response reduction is seen in all forms: accelerations, velocities, displacements, stresses, in time domain or in frequency domain.

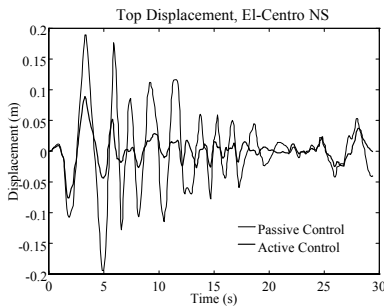


Fig.6 Time-history displacement response

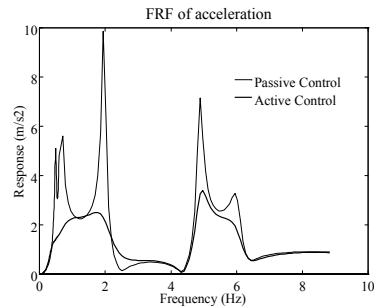


Fig.7 Acceleration frequency response

3. ACTIVE HINGED STRUCTURE AND STRUCTURAL ROBOTICS

Looking to living beings one should observe that the active joints are the keys of dynamic equilibrium.

In Figure 8 the concept of an active joint, *Structural Active Hinge* or *SAH*, is further developed as compared to proposal from [1]. This is only for 90 degrees connection but it is somehow easy to imagine versions for other situations. At the left of Figure 8, the action is done through a linear actuator. The right part of Figure 8, the active rotational moment is the mean for control.

The above concept of active hinge is based on what it can be seen at humans or animal joints, for example at the knee. One should think that these types of joints should be autonomous automatic systems, which must work in order to fulfill the

requirements of the general system, the whole structure. Therefore the device must have its self-controlled system.

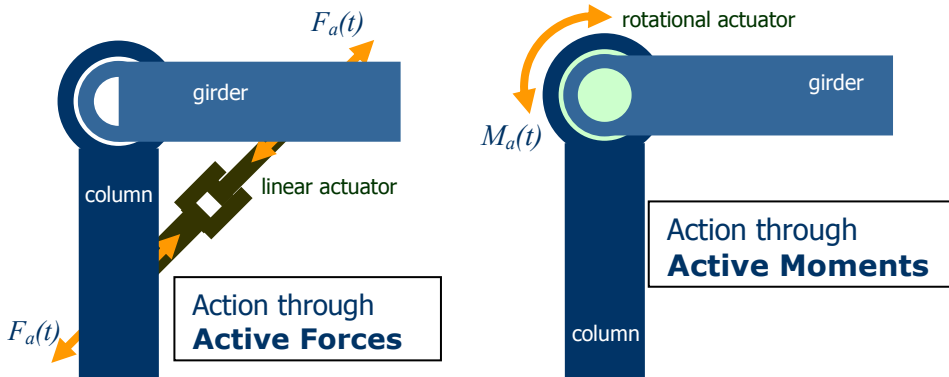


Fig.8 Structural Active Hinges development, SAH

A structure will then consist in a series of substructures interconnected with joints as those in Figure 8. In this case the structure becomes *robotic* [1].

Going further, the degree of autonomy of the structure can go until the idea that a structure can even *move* in case of danger in a better place (quite easy to image in outer-space).

Such structure is not only robotic but it is also *robotized*, i.e. robots should develop and maintain it.

Intervention of humans will surely be almost avoided. There are multiple reasons to support this idea. Mainly the high cost of humans' labor (eventually in outer-space) and danger are relevant.

In the future, the knowledge in structures' planning, designing, constructing, and managing will be huge. Only automatic work will be efficient in doing all these tasks. Coordination of the work must be also automatic.

The main needs of the society will be withdrawn from global databases and, therefore, the artificial intelligence brains will launch the project for a new robot-structure.

Planning and designing shall take care of all the necessary steps for future actions. Robots will build robotic structures based on a design flexible in terms of conceptions and adaptable to the latest findings in the field or related fields of activity. The final structure will never be a "final" structure because it will be self-adaptable and self-developing as a function of the changes in structures' loads, functions, or natural environment.

The robotic structure will "think" in advance for calling robots needed in building or withdrawing parts of the structure. Repairing or improvements based on newest materials or researches will be done. There will be an always work of self-control of the building and for interaction with the environment.

Civil and structural engineers should prepare to strongly cooperate with all the members of the civil society for globalization and integration of their work.

5. CONCLUSIONS AND FURTHER RESEARCH PROPOSES

Structural Robotics is a concept that tries to cope with the future of Structural Civil Engineering [1]. This paper shows that, at this moment, based on shown methodology, active hinges can make this concept be put into practice.

Compared to [1], the active hinges means are further developed. However, it is envisioned that analytical applications must be started for showing the effectiveness and requirements that this new concept and means are implying.

Acknowledgments

This paper is partially supported by CNCISIS Romania Grant code no. 540/2005.

References

1. Păuleț-Crăiniceanu, F.: Structural Robotics, *First Romanian American Workshop in Structural Engineering*, June 25-30, 1999, Iași, Romania pp. 43-52, “A.I.I. Cuza” University Publishing House Iași, 1999, ISBN 973-9312-59-4
2. Yao, T.P.J. 1972. Concept of Structural Control. *Journal of the Structural Division*. Vol. 98, No. St7: pp. 1567-1574
3. Kobori, T. 1988. Active Seismic Response Control (state of art report). *Proceedings of the 9th WCEE*.
4. Public Works Research Institute And 28 Companies, *Manual of Menshin Design of Highway Bridges*, Technical Note No.60, Public Works Research Institute, Tsukuba, Japan, 1993
5. Soong, T.T, Manolis, G.D. 1987. Active Structures. *Journal of Structural Engineering*. Vol. 113. No. 11.
6. Păuleț-Crăiniceanu, F., *Earthquake Engineering*, Editura Cermi, Iași, 1999, ISBN 973-9378-81-1
7. Housner, G.W., Soong, T.T., Masri, S.F. 1994. Second Generation of Active Structural Control in Civil Engineering. *Proceedings of the First World Conference on Structural Control, Los Angeles, California, USA*. Vol. 1: Panel 3-18
8. Păuleț-Crăiniceanu, F. 1997. *Active Control Approach for Long Span Bridge Responses to Strong Earthquakes. Doctoral Thesis*. Yokohama: Yokohama National University
9. Păuleț-Crăiniceanu, F. 1999. Seismic Response Control of Long Cable-stayed Bridges. *Proceedings of the Second World Conference on Structural Control, Kyoto, Japan*. Vol. 2: pp. 959-964. Chichester: John Willey & Sons

10. Păuleț-Crăiniceanu, F., Atanasiu, G.M. 1998. Optimal active control for large three-dimensional fem models. *11th European Conference on Earthquake Engineering, Paris, France*: CD-ROM. Rotterdam: Balkema
11. L. Bakule, F. Paulet-Crainiceanu, J. Rodellar,: Mitigation of seismic vibrations of a benchmark cable bridge using structural active control, *Computational Civil Engineering 2004*, Editura Soc. Acad. "M.T. Botez", Iasi 2005, pp. 45-54 ISBN 973-7962-50-8

Considerations concerning the optimization of reinforced concrete bridge design

Constantin Ionescu¹

¹ Technical University "Gheorghe Asachi" Iasi, Romania

Summary

The paper suggests a procedure for optimal design of a bridge using computation software, which exists in the literature, and a special subroutine added in order to be applicable for reinforced concrete bridges.

The optimal solution results from combination of three main processes: bridge design going through classical stages according to present regulations; application of optimal design by automated computation software, based on finite element method; and finally selection of the optimal structure from more partially optimal structures, each in I own class, through multicriterial decision.

KEYWORDS: bridge, design, optimization, computer aided design, optimal solutions, objective function, restrictions and optimization variables, structural model and mathematical model.

1. INTRODUCTION

The optimization process, meaning the identification of the optimal solution, might be found equivalent with a research activity in the domain of admissible solutions. Reviewing the literature, one might find that different typical optimization methods differ mainly in the way of processing the succession of steps in admissible domain and by procedures to accelerate the convergence of the desired solution.

Development of the mathematical procedures (through selection of the directions and initial solution) represents the highest difficulty in application of mathematical programming methods to optimal design of structures. Hence, optimality criteria become more important because they imply, essentially, derivation of the necessary and sufficient conditions to apply for obtaining the optimum with regard to specific requirements of design. So far, discrete optimization criteria for a number of design condition was described implying resistance, static stiffness, dynamic stiffness, static stability etc. Several software like OPTSTAR, OPCOM, OPTIM, SESAT ETC. were developed to use discrete optimality criteria as basis of structures optimization. All these programs are based on finite element method.

2. CONSIDERATIONS ON OPTIMIZATION OF STRUCTURES USING COMPUTATION SOFTWARE - OPTSTAR

The COSMOS/M software includes an optimization procedure named OPTSTAR. This software is based on finite element method. The method consists in developing a structural model using three types of elements: one-dimensional (rods), bi-dimensional (slabs) and three-dimensional (solids). The software works mainly on PC compatible computers, integration also Fast Finite Element, an equation systems solving procedure developed by Structural Research and Analysis Corporation.

Structural optimization reached with this procedure (OPTSTAR) offers the possibility to define a structure which is optimal in geometry as well as in section, considering the conditions imposed while defining the specific elements of any optimization process: objective function, restrictions, and optimization variables.

Operation s steps into a structural analysis process are:

- **Construction of the geometrical model.** Classical entities are used: points, lines, curves (conics, splines etc.), surfaces (planes, curved, generated by rotation), volumes, regions.
- **Physical modeling.** This step consists in introducing the physical constants which define the material we are working with and, in the case of uni and bi-dimensional structures the geometric-inertial characteristics of the beams and slabs are introduced. Data on material enclose: elasticity moduli (E and G), density, linear dilatation coefficients etc.
- **Structure discretization.** It is the most complex operation necessitating a certain efficiency related to: knowledge about the finite element library experience concerning discretization to obtain the balance between the desired precision and rapidity in solving the problem.
- **Modeling the bearing and actions.** Bearings cancel a number of degrees of liberty of the elements. Actions might be imposed displacements, forces, pressure, torsions, linear or centrifugal accelerations, etc.
- **Analysis of the structure.** This stage consists in: obtaining, representation and verification of the results.

Computation software relies on an iterative process of transforming the physical model of the structure until the assessment criteria are fulfilled. The accepted criteria are selected by the designer. The two versions of the software (COSMOS/M and COSMOS/FFE) will modify the dimensions and the shapes in order to find the optimal model of the structure (feasible model). The software can optimize simple (plane) or tri-dimensional structures.

In modeling process the following sets of entities are defined: objective function (target, performance), variables and restrictions. These entities lead to formulation of the mathematical model.

The variables represent those independent parameters which describe certain specific aspects of the problem, such as: structural configuration and dimensions used to define the model of the structure.

There is a clear hierarchy between different classes of variables. As an example, for the bridge resistance structures the simplest class consists from the variables defining the geometric and technical characteristics of the elements.

The higher category encloses the variables which refer to the configuration of the structure (number and measure of the apertures, proportion between height and opening etc.).

Objective function is a mathematical function with real values that express a linear or non-linear relation between the chosen variables. It describes the criterion from quantitative point of view and it provides a modality of decision between the existent solutions.

Objective functions might be defined through the following factors: volume, weight, stress, tension, displacement, specific deformation, cross-section, velocity, acceleration, characteristic frequencies, temperature variations, and energy flows etc.

Admissible solutions, from which the optimal variant is selected identifying the variables that lead to the extreme value of the objective function, must satisfy certain conditions. Analytically they are expressed by mathematical equalities and inequalities imposing limits to variables or groups of variables. These are the constraints of the problem. The constraints are set according to operation behavior analysis of a bridge structure and they refer to: volume, weight, stress, tension, displacement, specific deformation, cross-section area, velocity, acceleration, proper (natural) frequency, temperature variation, energy flows etc.

Other restrictions refer to geometric configuration of the elements, i.e. height of the transversal section might fluctuate within a range (superior and inferior limit) or they are imposed directly to the variables: to be non-negative or integer numbers; to respect some condition of standardization etc.

3. THE CONCEPT OF OPTIMAL DESIGN OF A BRIDGE

The inconveniences of an optimal structural computation software are highlighted by the ways to determine the working stages of the reinforced concrete and limit states of bridge calculation or verification: normal and ultimate operation.

As an example, when using the OPTSTAR software, in the optimization of a reinforced concrete structure, the following inconveniences occur:

- Stiffness modulus, used for assessment of the tension and deformation state, is constant all along the optimization process progress and equal to that of the cement concrete according to the class of concrete. As a result, the reinforcement bars has no function in this process. Practically, it is like optimizing plain concrete structures.
- As demonstrated in the literature, stiffness modulus varies as a function of stress condition of the element, as well as along the element function of the initiation and development of fissures.
- Restrictions used in optimization process and imputed in OPTSTAR software (i.e. tensions, displacements, specific deformations etc.) cannot be used, due to the variety of computation hypothesizes for reinforced concrete (i.e. working stages); tensions are determined in stage I, displacements in stage II, and the stiffness modulus implies dimensioning of the cross-sections, meaning stage III.

Generally, the logic of the design process reveals the existence of six phases: problem definition, selection of the system parameters value, creation of the design structure, bridge structure evaluation, selection between the solutions, and technical verification. In this rational mode, each phase generates a clear and correct perspective and feedback might appear between phases due to problem refining effort and a partial overlaying or a fusion might exist between successive phases.

For the optimal design process of a bridge a logical sequence of the major stages is advised, as presented in Figure 1. Search for the optimal solution is done unifying, through continuity, three larger processes: classical design concept (which includes the six phases presented above), optimal design based on finite element computational software, and optimal structure selection from more optimal structures (each within its class) using multi-criteria decision.

4. CONCLUSIONS

1. Methods for design of bridge structures are iterative in nature, but iterations emerge mainly in the analysis of the design problem and they are not inherent to the design itself.
2. Through proper definition of the design problem, it can be seen that many of the iterative procedures of the design process might be eliminated if the systemic approach is used.

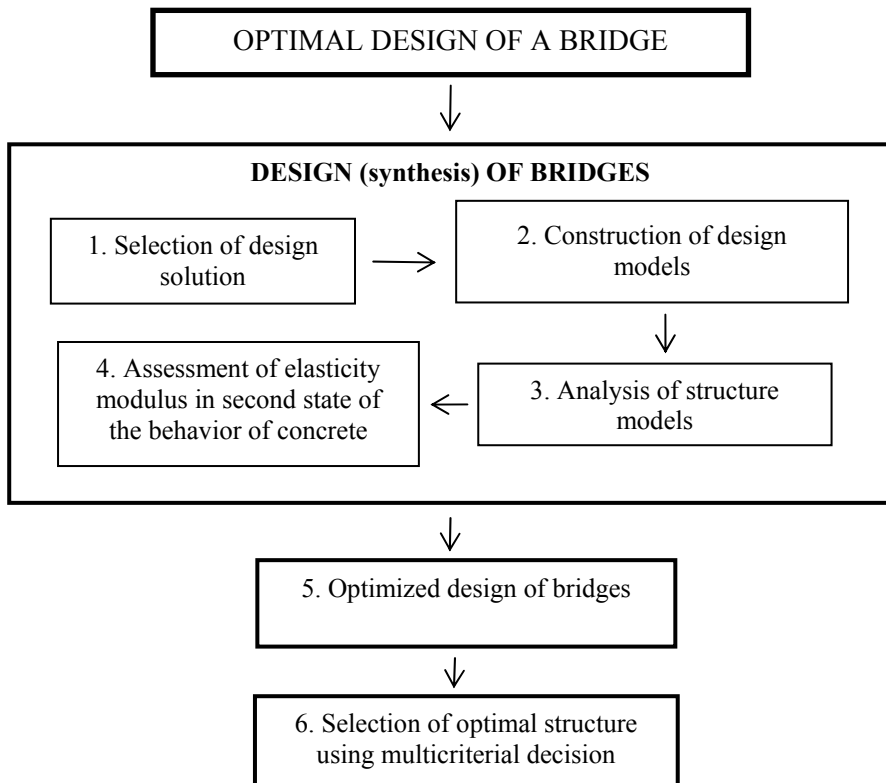


Fig.1 Proposal for design of frame bridges using the concept of optimization

References

1. Andrașiu, M. et al., Metode de decizii multicriteriale (Multicriterial decision methods). Editura Tehnică, București, 1986.
2. Capatu, C., Poterașu, V.F., Asupra optimizării structurilor de poduri (On bridge structure optimization). Conferința jubiliară a Facultății de Construcții, Institutul Politehnic Iași, sec. D. 320-324, 1981.
3. Dobre, D., FEA – Analiză cu elemente finite (Analysis with finite elements), CAD report, nr. 4., august 1997.
4. Florea, N., Patraș, M., Un procedeu de dimensionare optimă a elementelor încovoiate din beton precomprimat (A procedure of optimal dimensioning of the flexure prestressed concrete elements). Sesiunea Șt., Facultatea de Hidrotehnică Iași, 232-237, oct.1978.
5. Florea, N., Contribuții la proiectarea optimă a secțiunilor încovoiate din beton comprimat (Contributions to optimal design of cross-section of flexure prestressed concrete elements). Teză de doctorat, Institutul Politehnic Cluj-Napoca, 1980.
6. Poterașu, V.F., Florea, N., Practica optimizării structurilor (Structure optimization practice). Editura Junimea, Iași, 1984.
7. Reitman, M.I., Sapiro, G.S., Metode de proiectare optimă a corpurilor deformabile (optimal design methods for deformable bodies). Editura Tehnică, București, 1981.

A new type of joint assemblage for the thin-walled steel profiles

Mihai Budescu¹, Ioan Ciongradi², Octavian Roșca³

¹Sen. Lect., Technical University of Iasi, Romania, e-mail: victor_rosca@yahoo.com

²Prof., Technical University of Iasi, Romania, e-mail: vesper@telebit.ro

³Prof., Technical University of Iasi, Romania, e-mail: vesper@telebit.ro

Abstract

This paperwork presents the results of the study concerning the optimization of the KONTI type element joints.

The tests carried out on the joints connected with HSFG bolts demonstrated a decrease of the bearing capacity as a consequence of the painting layer used for the protection of the gussets. Under these circumstances it was advocated a new type of joint connected with normal bolts, based on the bolt strength when working in shear and compression on the hole.

The proposed box joint is capable to carry on the efforts from the node area without being necessary the HSFG bolts. A better behavior of the rotation of the KB profile in the box might be obtained in case of a better manufacturing process.

The experimental results obtained in the case of the 5mm thick profiles should be extended to other thicknesses (such as 3.0, 3.5 and 4 mm) used in several types of structures.

The actually accumulated experience during the tests allowed us to consider that the hardening of the KB profiles into the joint box might be better exploited, with significant economies in metal consumptions for joints.

1. INTRODUCTION

This paperwork presents the results of the study concerning the optimization of the KONTI type element joints. The justification of the present study is due to the existence of several lacks noticed at the joints connecting the KB elements used for beams and columns in structures with several destinations. These joints are made by the means of gussets assembled of welded steel plates. The effective connection of the KB profiles to the joints is currently performed by the means of the high strength pre-stressed (HSFG) bolts (see Fig. No.1).

The tests carried out on the joints connected with HSFG bolts demonstrated a decrease of the bearing capacity as a consequence of the painting layer used for the protection of the gussets.

Under these circumstances it was advocated a new type of joint connected with normal bolts, based on the bolt strength when working in shear and compression on the hole.



Fig.1 Classic joint connected with HSF bolts

The carbon steel strip of the profiles is protected by immersion into a zinc bath and is made of FeE 320 G as stated in the EN 10147 Product Norm (Euro Norm).

The mechanical properties of material (base - steel) are:

- The yielding strength of the basic material $f_{yb} = f_y = 320 \text{ N/mm}^2$,
- The ultimate strength of the basic material $f_u = 390 \text{ N/mm}^2$.

Ratio $f_u / f_y = 390/320 = 1,22 > 1,2$.

2 THE PHILOSOPHY OF THE JOINT

The design of such a joint is performed in order to undertake the maximum stresses that occur when subjected to load combinations, (N – axial force; Q – shear; M – bending moment).

The HSF bolts of a usual assemblage (Fig. No.1) are designed to carry on simultaneously all these efforts (N, Q, M).

- By analyzing the different kinds of elements that are connected and the loads acting on them it was thought a system that carries on the three efforts separately, each at the level of a separate element of the new joint, not only the bolts, which in turn are acting like usual bolts.

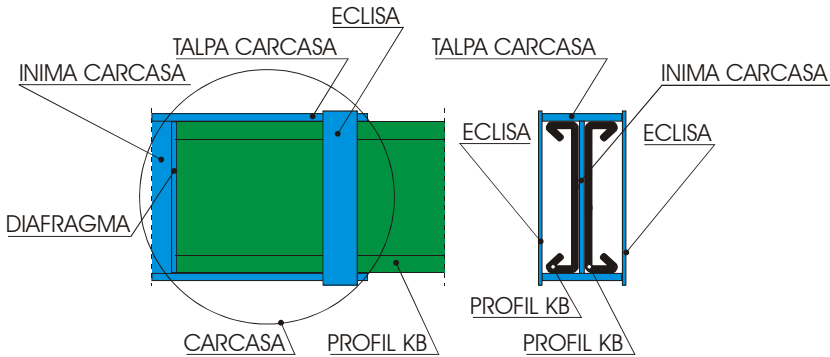


Fig. 2 Box-type joint

Thus it is advocated the construction of the joint as a box, Fig. No.2 where:

- The axial efforts, which are usually of compression, are supported by a steel plate placed at lower part (inside) of the box, Fig. No. 3;

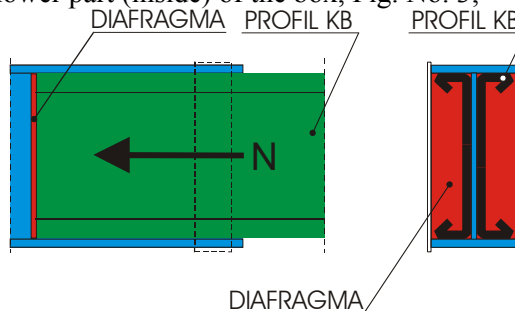


Fig. 3 Steel plate that undertakes the axial force

- The shear is carried on by the box using some plates to connect the bottom parts (flanges), Fig. No. 4;
- The bending moment is undertaken both by the bolts placed on the contour of the KB flanges and a pair of bolt rows fixed on the web. Moreover, the KB profiles are mounted into the box, thus one may consider that the bending is carried on by the entire box, the bolts now having mainly a fixing purpose.

To check on the behavior of the new joint, in the first stage it was proposed the testing of a specimen consisting of 600mm height and 5mm thick KB thin-walled steel profiles (the commonly used elements in KONTIROM structures).

The simply supported beam with a central joint was selected for the experimental model. In order to compare the jointing systems, two specimens were constructed, the (G0) with HSFG bolts fixed as in the classical way and (GN) with the new joint system (see Fig. No. 6).

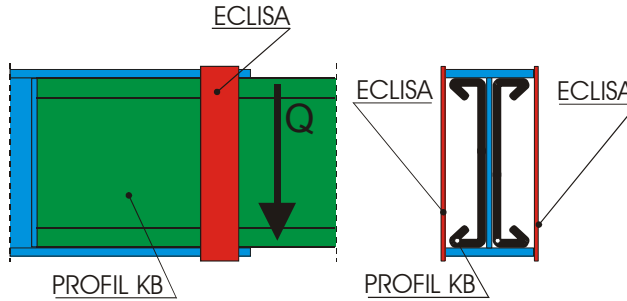


Fig. 4 Steel plate to undertake the shear

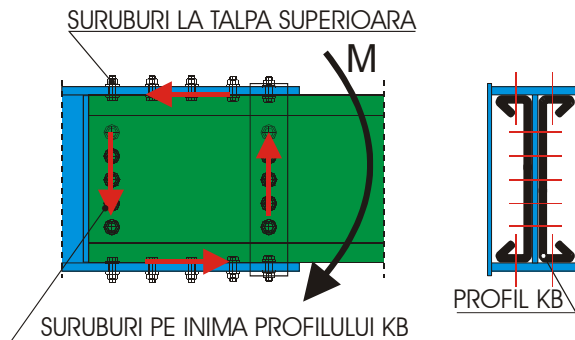


Fig. 5 The positions of the bolts that carry on the bending moment

3 THE TESTS

A 300.000daN hydraulic press was used for testing. In the Fig. No. 7 it is presented how the transducers are mounted on the specimens and the complementary elements used in the experiments. The beams were identically equipped (G0 – Fig. No. 7 and GN – Fig. No. 8). In order to avoid the lateral buckling of the beams a driving system was thought and mounted at each specimen edge.

At this testing stage it was proposed the following instrumentation of specimens:

- 2 displacement transducers mounted on the central joint from the midspan (D0, D1);
- 2 displacement transducers mounted at the joint edge (D2, D4 – D3, D5);

- 2 displacement transducers mounted on the KB profile at the joint vicinity (D6, D8 – D7, D9);
- One force transducer to accomplish the automatic load recording.

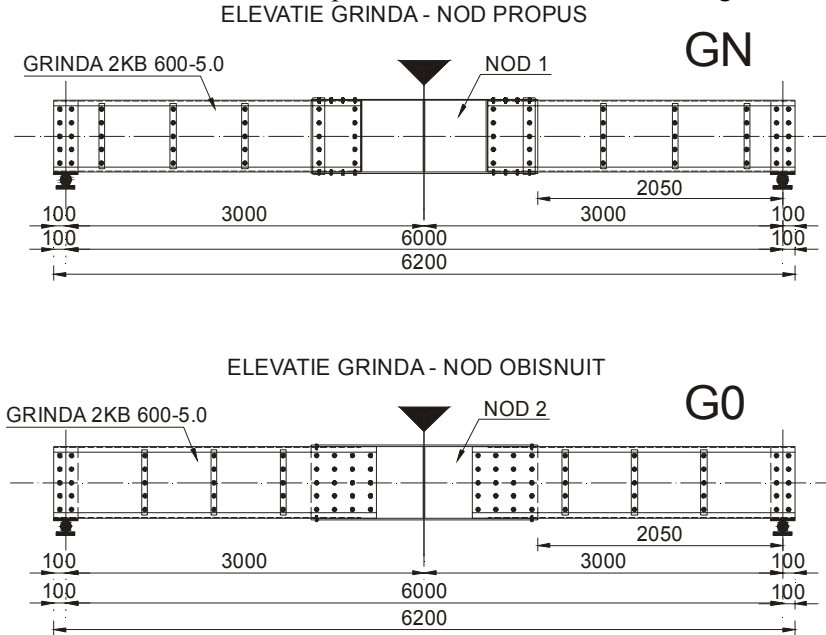


Fig. 6 The dimensions of the proposed specimens



Fig. 7 The G0 beam during the test

The tests were carried out in several loading – unloading steps up to 100 KN, 200 KN and 350 KN, the last value corresponding to the value of 2900 daN/cm² for the KB stress, i.e. the design strength.



Fig. 8 The GN beam during the test

3.1 Test results – G0 (joint with HSFG bolts)

In the figure No. 9 there is presented the force-displacement relationship for the G0 beam, corresponding to the transducers mounted on the both sides.

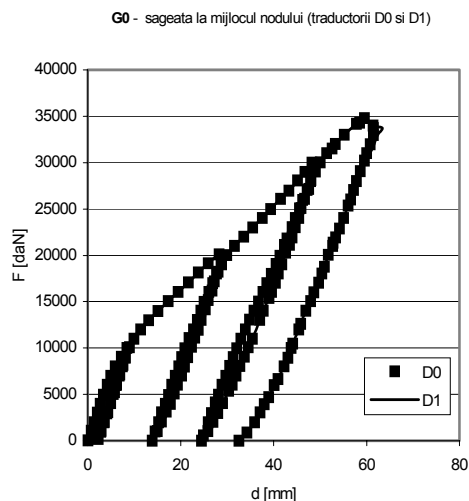


Fig. 9

The experiment shows the occurrence of some important permanent deflections for each loading-unloading cycle. These permanent deflections are caused by the KB element rotations in the central node as a consequence of the lack of adherence between the contact sides and fixed with HSFGB bolts.

During this test one may notice a shift between the KB profile and the central node, thus confirming the rotation of the KB element.

After the analysis of the results one may notice that the permanent deflections are decreasing as the load increases, thus means the KB profile is hardening inside the node, as an effect of the rotation.

3.2 Test results – GN (the new proposed joint)

In the figure No. 10 there is presented the force-displacement relationship for the GN beam recorded by the transducers mounted on both sides. For this beam type the tests were performed using the same loading steps.

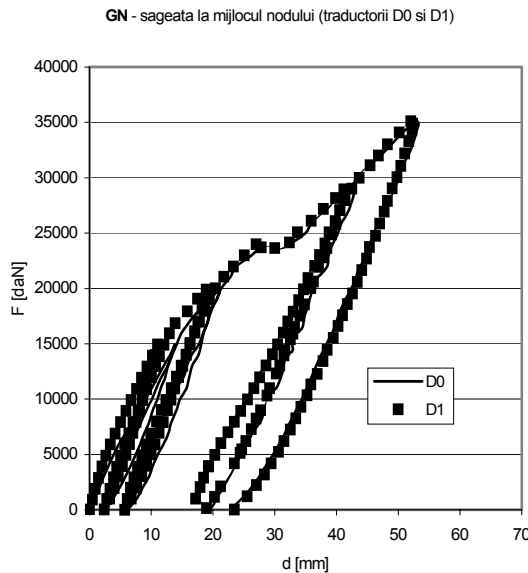


Fig. 10

After the test end the bolts from the flanges were eliminated and a second test was carried out with the profiles mounted inside the box and fixed with the bolts only in the web (a test denominated as GN-0). For this experiment a new loading cycle up to 400 KN was introduced, corresponding to the coverage of the yielding strength, see Figure No. 11.

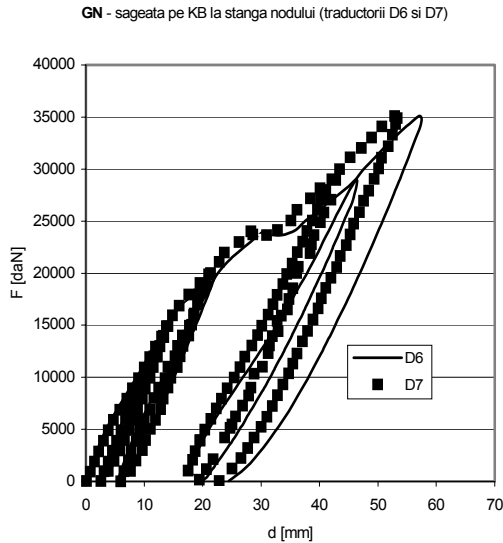


Fig. 11

It is important to underline that in all the cases the local buckling of flanges did not occur, even when the yielding strength was bypassed. Even though the GN beam was loaded to a level greater than that corresponding to the yielding stress, when reloading was performed for the GN-0 test a well behavior was observed, the maximum deflections were smaller than in previous tests. This was due to the rotation of the KB profile in the central node and the hardening.

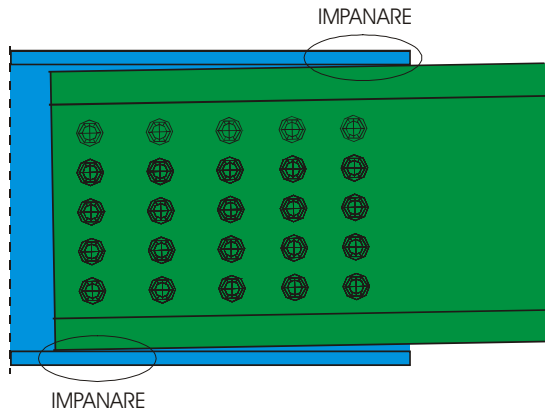


Fig. 12 The hardening of the profile into the joint of the G0 beam

A series of deficiencies in the GN behavior were caused by the manufacturing of the central node. The sinuous shape of the recorded deflections is caused by the rotations and re-positioning of the elements.

4 CONCLUSIONS

After the tests several conclusions were stated. The assemblage of the G0 beam with the HSFG bolts do not provide the expected stiffness, the painting layer do not allow the correct behavior – finally one must consider the hardening of the profile into the joint, thus the loads are carried on by the means of bolt shear and pressure on the hole, see Figure No. 12.

The joint of the GN beam had some manufacturing imperfections that led to the rotation of the KB profile in the box during the tests and the breaking in tension of some bolts from the flanges, Fig. 13.

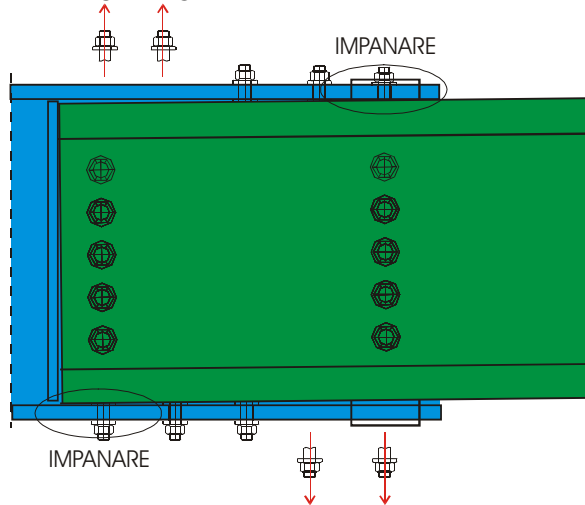


Fig. 13 The rotation of the KB profiles and the breaking of the bolts from flanges

The GN-0 beam showed the best behavior because it was produced the hardening in the box after loading over the yielding limit; the permanent deflections were insignificant in comparison to the other 2 cases. In the Figure No. 14 there are presented the load-displacement curves for the 3 beams at several loading steps/cycles.

Comparing the maximum displacements for the two types of beams (G0 and GN) it results an increase of 12% for the maximum displacement corresponding to the design strength (2900 daN/cm²) in the case of the beam fixed with HSFG bolts (G0) as the beam with normal bolts(GN), Fig. No.14.

The proposed box joint is capable to carry on the efforts from the node area without being necessary the HSFG bolts. A better behavior of the rotation of the KB profile in the box might be obtained in case of a better manufacturing process.

The experimental results obtained in the case of the 5mm thick profiles should be extended to other thicknesses (such as 3.0, 3.5 and 4 mm) used in several types of structures.

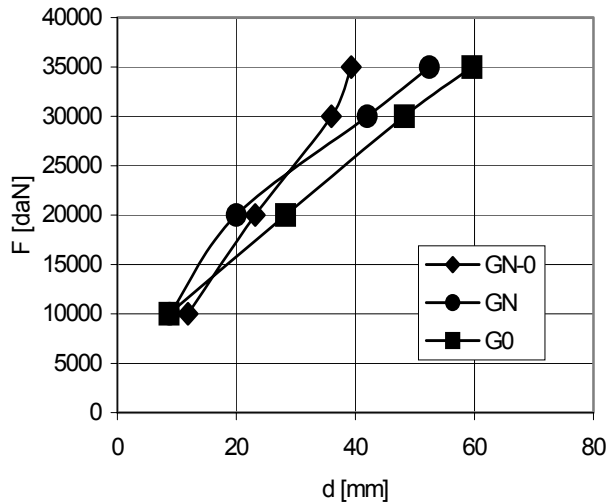


Fig. 14 the maximum displacements for the 3 tested beams

The actually accumulated experience during the tests allowed us to consider that the hardening of the KB profiles into the joint box might be better exploited, with significant economies in metal consumptions for joints.

References

1. VESPER SRL Iași, INCERC Iași, *Studiu privind îmbunătățirea îmbinărilor dintre elementele structurale tip KONTI*, contract: K077145/2005, pp. 1-35
2. Sinfex Comp Iași, INCERC Iași, *Încercări experimentale asupra panelor de acoperiș (Σ , C, Z) și a unui element KB450-3.5*, contract: K670/2002, pp. 1-74.
3. Sinfex Comp Iași, INCERC Iași, *Încercarea unei structuri tip Konti cu dimensiunile 9 x 5m pe platforma seismică de 10x10m a Filialei INCERC Iași*, contract: K1070/2002.
4. European Committee for Standardisation, Eurocode 3 Part 1.1: *Design of Steel Structures, General Rules and Rules for Buildings*, 1992.
5. AISI, *Cold Formed Steel Design Manual*, 1996, pp. 1-621.
6. ESDEP WG 9, *Thin-walled Construction, Lecture 9.1: Thin-walled Members and Sheeting*, 110pp.

Optimization of Booster Disinfection in Water Distribution Systems

Emanoil Bârsan¹, Anca Ignat²

¹*Department of Hydrotechnics Constructions and Sanitary Engineering, Technical University “Gh. Asachi”, B-dul D.Mangeron, nr. 63-65, Iași, 700.050, Romania, (E-mail ebarsan@hidro.tuiasi.ro)*

²*Department of Applied Informatics, University “Al.I.Cuza”, B-dul Carol I. Nr. 11, Iasi, 700506, Romania. (E-mail ignata@uaic.ro)*

Summary

In large water distribution networks and with tightening problems the introduction of some re-chlorination stations are a must in order to assure the necessary chlorine for the transported water biostability, with minimum chlorine consumption.

For a given network (configuration, demands etc) it is followed the minimization of total chlorine quantity injected in 24 hours for variable demands hour by hour (extended-period to 24 hours).

In order to realize the booster disinfection optimization a large number of nodes (but limited at 1/4 from total numbers of nodes)are chosen that may candidate to obtain the disinfection with minimum chlorine consumptions.

With a personal program the nodes that assure the minimization of total chlorine injection in the network are determined.

It is presented an example, the findings and conclusions for practical implementation

KEYWORDS: water supply; distribution network; disinfection; booster stations; optimization.

1. INTRODUCTION

Booster disinfection is the addition of disinfectant at locations distributed throughout a water distribution system with the goal to assure the transported water biostability, with a minimum chlorine consumption.

Chlorine introduction in distribution network may be realized by:

1. chlorine injection only in water supply nodes;
2. chlorine injection in more network nodes (inclusively in the supply ones)

The last procedure assures a more uniform distribution of chlorine concentration and permits chlorine consumption optimization by convenient choosing of booster injection locations, with a optimization model. Optimization models is formulated for a dynamic schedule of disinfectant injections and to minimize the total dose required for necessary chlorine assurance in limits required by Law 458/2002 and the avoidance of disinfection by-products formation (e.g.. trihalomethanes).

Even though the optimization problem is of unfinite-time horizon type, it is reduced to a finite-time problem by considering of periodicity for chlorine injections and network hydraulics (on a extended period to 24 hours).

The model is linear because it is shown that the disinfectant concentrations at control nodes come/result from more injection points may be applied them the linear superposition principle

Specialized literature presents the following possibilities (models) for the establishing of optimal (minimum) consuming chlorine dose and the locations of booster stations

1. Optimal scheduling of doses at booster stations as a linear programming problem (simplex method). It is established the minimum chlorine dose considering that they are known the locations of booster stations.
2. Optimal location and scheduling of booster-station dosing as a mixed-integer linear programming problem. It is applied the branch-and-bound technique combined with the simplex method.
3. Optimal location of booster stations as a maximum set-covering problem
4. Optimal location of booster stations with a genetic algorithm. It is established the location of booster stations and minimum chlorine dose

With a personal program, by the simulation, they are established the nodes that assure the minimization of total chlorine injection in the distribution network, from a set of nodes random proposed or imposed by a number of simulations that assure the chlorine consumption in required minimum and maximum limits

It is presented an example, the findings and conclusions for the utilization of proposed procedure

2. ADOPTED MODEL [1]

Chlorine, introduced in distribution network as disinfectant, is transported along a pipeline by advection with water average velocity from respective pipeline. Chlorine reaction is of first order (of type $C_{\text{downstream}} = C_{\text{upstream}} \exp(-kt)$) At junctions of two or more pipes, the water mixing is assumed to be complete and instantaneous. Chlorine concentration that leaves/goes out from junction is weighted average through the flow rates of concentrations that have entered the junction. For tanks, a complete mixing is considered (concentration in tank results from mixing of entered water, of the one from tank and of reactions that take place in tank volume). Chlorine introduction in the distribution network is done in a number of injection booster stations. The choosing of stations for chlorine injections may be done randomly or by imposing some nodes by modeler. With a number of imposed simulations it is established the minimum chlorine quantity necessary in 24 hours and the stations (nodes) from which it is managed so that at the water consuming nodes, the chlorine concentration to join in the limits specified by Law 458/2002 ($0.2 \text{ mg/L} < c < 0.5 \text{ mg/L}$). On the base of personal program concerning the hydraulic analysis and the chlorine concentration establishing at nodes and by means of some dialog windows there are introduced the necessary data and the obtained results are displayed tabular and/or graphically, that consist in the locations for chlorine injection booster stations, the necessary chlorine for the injection at each location and chlorine concentrations at nodes for minimum total chlorine consumption in 24 hours.

3. EXEMPLE

There is considered the network from fig.1. The network is supplied in the node 1 by a pumping station but in 11 node is supplied by 12 tank. The water consumptions in network on an extended period of 24 hours are given in table 1.

NODE/H	9	10	11	12	13	14	15	16
1	0.24	0.25	0.26	0.24	0.24	0.24	0.24	0.24
2	0.22	0.23	0.23	0.24	0.23	0.23	0.23	0.23
3	0.20	0.21	0.20	0.20	0.20	0.22	0.22	0.22
4	0.20	0.20	0.20	0.20	0.25	0.20	0.20	0.20
5	0.21	0.21	0.21	0.21	0.22	0.21	0.21	0.21
6	0.22	0.22	0.23	0.23	0.22	0.22	0.22	0.22
7	0.20	0.26	0.20	0.20	0.20	0.27	0.20	0.27
8	0.20	0.20	0.20	0.20	0.20	0.20	0.20	0.20
9	0.20	0.20	0.20	0.20	0.21	0.20	0.20	0.20
10	0.20	0.20	0.20	0.20	0.20	0.20	0.20	0.20
11	0.28	0.20	0.29	0.28	0.31	0.20	0.31	0.20
12	0.20	0.20	0.20	0.20	0.20	0.47	0.31	0.20

NODE/H	17	18	19	20	21	22	23	24
1	0.24	0.24	0.24	0.24	0.24	0.24	0.25	0.25
2	0.23	0.23	0.23	0.22	0.22	0.22	0.23	0.23
3	0.22	0.22	0.22	0.22	0.21	0.21	0.21	0.23
4	0.20	0.20	0.20	0.20	0.20	0.20	0.23	0.23
5	0.21	0.21	0.21	0.21	0.21	0.21	0.21	0.21
6	0.22	0.22	0.22	0.22	0.22	0.22	0.22	0.22
7	0.28	0.27	0.27	0.26	0.26	0.20	0.24	0.28
8	0.20	0.20	0.20	0.20	0.20	0.20	0.24	0.20
9	0.20	0.20	0.20	0.20	0.20	0.20	0.20	0.20
10	0.20	0.20	0.20	0.20	0.20	0.20	0.20	0.20
11	0.20	0.20	0.20	0.20	0.20	0.28	0.25	0.20
12	0.20	0.20	0.20	0.20	0.29	0.31	0.20	0.20

Table 3. The nodes with chlorine injections and injected quantity, in mg/L, corresponding to water flow rates transported in 24 hours

NODE/H	1	2	3	4	5	6	7	8
1	22.31	23.28	22.57	22.10	21.42	20.50	19.53	17.29
4	0.00	0.57	0.00	0.00	0.00	0.00	0.00	0.00
7	0.51	0.47	0.29	0.23	0.25	0.28	0.49	0.49
8	0.00	9.91	0.00	0.00	0.00	0.00	0.00	0.00
11	2.34	5.40	0.00	0.00	0.00	0.00	0.00	0.29
12	1.74	0.00	0.00	0.00	11.98	14.10	15.92	14.62

NODE/H	9	10	11	12	13	14	15	16
1	17.60	16.26	14.99	15.84	17.72	19.43	19.50	19.61
4	0.44	0.54	0.60	0.52	0.62	0.61	0.32	0.30
7	0.07	0.88	0.19	0.23	0.22	0.79	0.11	0.77
8	0.82	0.75	0.54	0.07	0.31	0.00	0.60	0.61
11	2.20	0.17	2.68	2.37	2.90	0.74	0.47	0.25

11	0.28	0.20	0.29	0.28	0.29	0.20	0.45	0.25
12	0.21	0.30	0.29	0.30	0.36	0.85	0.55	0.36
NODE/H	17	18	19	20	21	22	23	24
1	0.24	0.30	0.26	0.24	0.25	0.32	0.29	0.29
2	0.30	0.23	0.28	0.24	0.22	0.24	0.30	0.27
3	0.29	0.22	0.28	0.23	0.21	0.22	0.28	0.27
4	0.25	0.25	0.20	0.23	0.20	0.20	0.27	0.45
5	0.28	0.27	0.21	0.26	0.22	0.21	0.22	0.28
6	0.29	0.22	0.28	0.23	0.22	0.23	0.29	0.27
7	0.24	0.24	0.21	0.24	0.20	0.20	0.22	0.24
8	0.24	0.43	0.31	0.20	0.31	0.50	0.24	0.23
9	0.26	0.26	0.20	0.25	0.21	0.20	0.21	0.26
10	0.20	0.20	0.20	0.20	0.20	0.20	0.20	0.20
11	0.20	0.20	0.28	0.20	0.27	0.28	0.28	0.20
12	0.23	0.20	0.20	0.34	0.29	0.31	0.20	0.21

Table 5. Chlorine injection nodes and injected quantities in mg/L, corresponding to the water flow rates transported in 24 hours

NODE/H	1	2	3	4	5	6	7	8
1	24.70	25.07	24.60	24.28	25.03	20.50	19.79	21.22
4	0.00	0.00	0.00	0.00	0.00	0.00	0.00	0.00
8	0.00	8.81	0.00	0.00	0.00	0.00	3.22	0.00
12	1.65	3.20	0.00	0.00	11.62	13.59	15.84	33.49
NODE/H	9	10	11	12	13	14	15	16
1	17.60	16.26	17.27	21.99	18.87	23.18	25.62	25.41
4	0.43	0.29	0.58	0.38	0.57	0.00	0.10	0.00
8	2.62	1.77	2.18	0.07	0.31	0.00	0.19	0.61
12	3.51	26.16	13.11	11.49	16.84	57.46	0.00	0.00
NODE/H	17	18	19	20	21	22	23	24
1	19.61	24.43	20.61	19.01	20.19	25.55	23.65	23.39
4	0.00	0.00	0.21	0.00	0.24	0.50	1.33	5.07
8	1.08	4.78	1.78	0.60	1.59	2.89	1.02	0.00
12	0.00	3.65	4.72	10.82	1.97	1.16	0.00	0.00

3.3. Comparison between the choosing procedures of the injection booster- stations (BS) for nodes 2 and 5

For exemplification it is presented the chlorine concentration evolution for optimal solution (minimum total chlorine consumption in 24 hours) in nodes 2 and 5.

Blue line shows the evolution of chlorine concentration in 24 hours in nodes 2 and 5 for the case of the choosing of chlorine injection booster stations by a random procedure (nodes 1,4,7,8,11,12)

Black line shows the evolution of chlorine concentration in 24 ore in nodes 2 and 5 for the case of the imposing of chlorine injection booster–stations in 1,4,8,12 nodes.

It is ascertained that the random choosing procedure of chlorine injection booster stations conducts to a solution that confers a more reduced and more uniformity chlorine concentration at nodes.

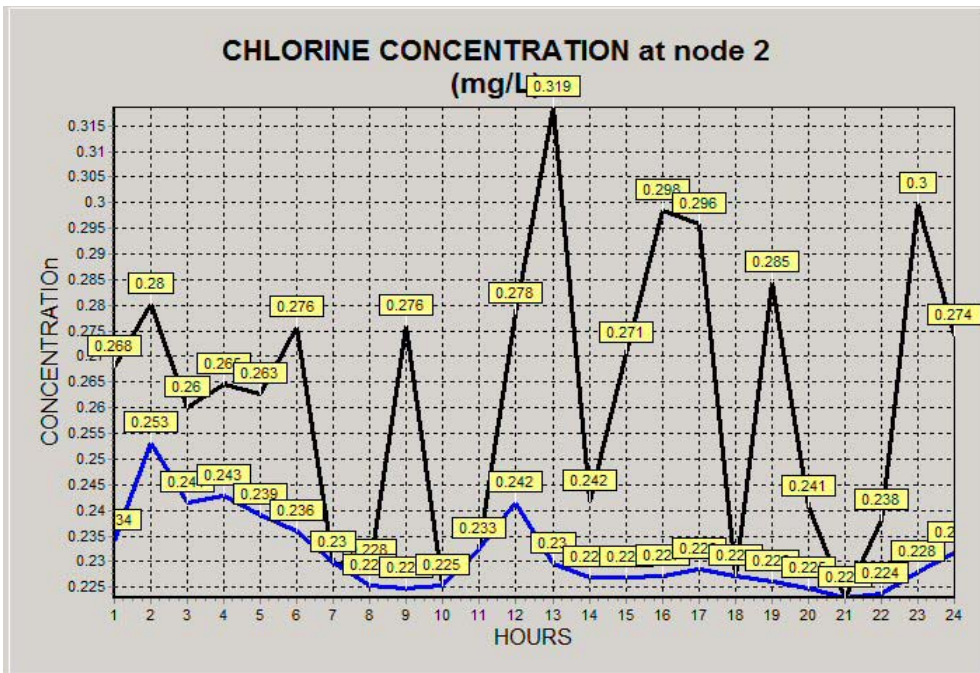


Figure 2. Legend: blue line – random choosing of BS; black line – imposing of BS

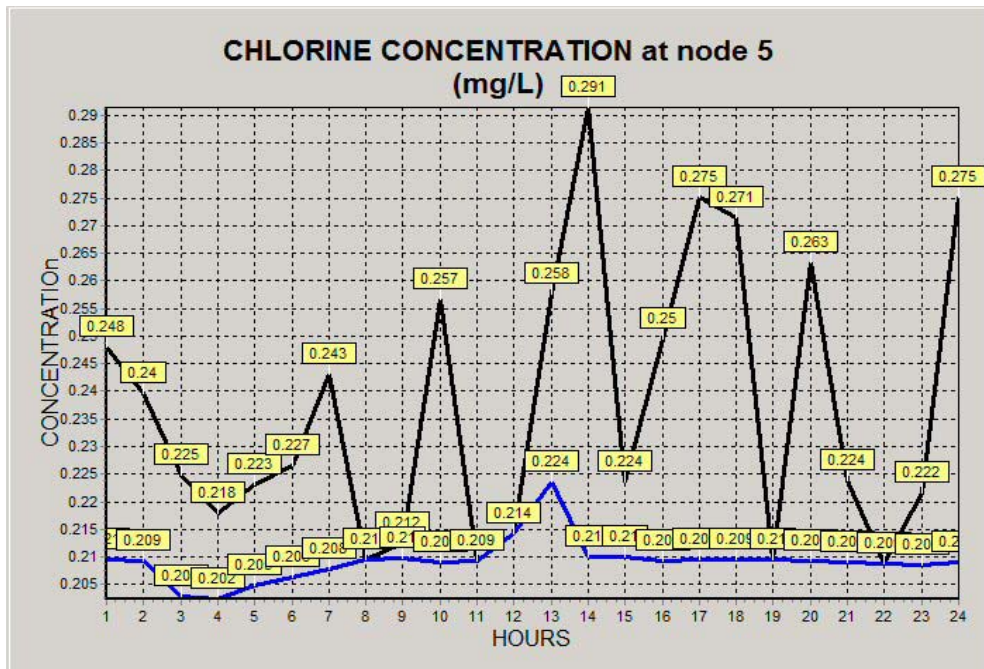


Figure 3. Legend: blue line – random choosing of BS; black line – imposing of BS

4. CONCLUSIONS

1. In large water distribution networks and with tightening problems the introduction of some re-chlorination /booster - stations are a must in order to assure the necessary chlorine for the transported water biostability, with minimum chlorine consumption.
2. For a given network (configuration, demands etc) it is followed the minimization of total chlorine quantity injected in 24 hours for variable demands hour by hour (extended-period to 24 hours).
3. In order to realize the booster disinfection optimization a large numbers of nodes (but limited at 1/4 from total numbers of nodes) are chosen that may candidate at obtaining the disinfection with minimum chlorine consumptions.
4. With a personal program the nodes that assure the minimization of total chlorine injection in the network are determined by a number of simulations using both a random procedure and imposed one.
5. It is presented an example from which results that the random procedure conducts at a location of booster stations with a reduction of the total chlorine consumption.

References

1. Bârsan, Em., Ignat, C., Evolution of Chlorine Concentration in Water Distribution Networks., *International Symposium "Computational Civil Engineering"*, Editors. C. Ionescu, F. Păuleț-Crăiniceanu, H. Bărbat, Ed Soc. Acad. Matei-Teiu Botez, Iași, 2003, 112-119,
2. Goldman, F.E., Burcu Altann Sakaria, A., Ormsbee, L.E., Uber, J.G., Mays L.W., *Optimization models for operations*, Chap 16 from *Water Distribution Systems Handbook*, McGraw-Hill, New York, 2000.
3. Bocelli, D.L., Tryby M.E., Uber J.G., Rossman L.A., Zierolf M.L., Polycarpu M.M., Optimal Scheduling of Booster Disinfection in Water Distribution Systems, *Journal of Water Resources Planning and Management*, March/April, 1998, 99-111.
4. Mukherjee, S., Laha, Sh., Genetic Algorithm to optimize disinfectant Booster Location, *1st World Water Congress of the International Water Association (IWA) Conference Preprint Book 2, Drinking Water Treatment*, Paris, 2000, 411- 417

Impact of failures from water distribution networks on booster disinfection

Emanoil Bârsan¹, Anca Ignat²

¹*Department of Hydrotechnics Constructions and Sanitary Engineering, Technical University “Gh. Asachi”, B-dul D.Mangeron, nr. 63-65, Iasi, 700.050, Romania, (E-mail ebarsan@hidro.tuiasi.ro)*

²*Department of Applied Informatics, University “Al.I.Cuza”, B-dul Carol I. Nr. 11, Iasi, 700506, Romania. (E-mail ignata@uaic.ro)*

Summary

The maintaining of water quality in distribution network is realized by preserving in the whole network some residual chlorine concentrations foreseen in Law 458/2002.

At a normal functioning, the necessary chlorine in network is assured by periodical injections in the existing booster disinfection stations, established for this state.

In the case of some failures (pipe breaking etc) the residual chlorine distribution it is perturbed.

In this paper the modifications that take place in this situation are simulated using an personal hydraulic program associated with pursuit of residual chlorine concentration evolution.

Having been taken an example, there are presented the findings and conclusions that result from this study.

KEYWORDS: water supply; distribution network; disinfection; booster stations; failure of pipelines.

1. INTRODUCTION

In normal operation conditions, the chlorine dosing established for booster stations are done after the methodology presented in [1]

In case of some failures (breaking of pipe lines) the chlorine distribution is perturbed.

The paper has as the a goal the establishing of chlorine concentration modifications that are produced when failures (breakings) takes place on pipes and the measures that must be taken for the framing of residual chlorine concentration in the limits required by the Law 458/2002 with a minimum total chlorine consumption at injection booster stations in network.

With a personal program are studied the modifications that are produced on a network for the cases: network without failures on pipelines and network with failures on the pipelines and the measures that must be taken in the case of failure.

2. ADOPTED MODEL

Chlorine, introduced in distribution network as disinfectant, is transported along a pipeline by advection with water average velocity from respective pipeline. Chlorine reaction is of first order (of type $C_{\text{downstream}} = C_{\text{upstream}} \exp(-kt)$). At junctions of two or more pipes, the water mixing is assumed to be complete and instantaneous. Chlorine concentration that leaves/goes out from junction is weighted average through the flow rates of concentrations that have entered the junction. For tanks, it is considered that takes place a complete mixing (concentration in tank results from mixing of entered water, of the one from tank and of reactions that take place in tank volume). Chlorine introduction in the distribution network is done in a number of injection booster stations. The choosing of stations for chlorine injections may be done randomly or by imposing of some nodes by modeler. With a number of imposed simulations it is established the minimum chlorine quantity necessary in 24 hours and the stations (nodes) from which is managed so that at the water consuming nodes, the chlorine concentration to join in the limits specified by Law 458/2002 ($0.2 \text{ mg/L} < c < 0.5 \text{ mg/L}$). On the base of personal program concerning the hydraulic analysis and the chlorine concentration establishing at nodes and by means of some dialog windows the necessary data are introduced and the obtained results are displayed tabular and/or graphically, that consist in the locations for chlorine injection booster stations, the necessary chlorine for the injection at each location and chlorine concentrations at nodes for minimum total chlorine consumption in 24 hours. For the study of influences of pipe failures on chlorine consumptions there will be compared the cases: network without and with failures on a pipeline (or pipelines).

3. EXEMPLE

There is considered the network from fig.1. The network is supplied in the node 1 by a pumping station but in node 11 is supplied by tank 12. The water consumptions in network on an extended period of 24 hours are given in table 1.

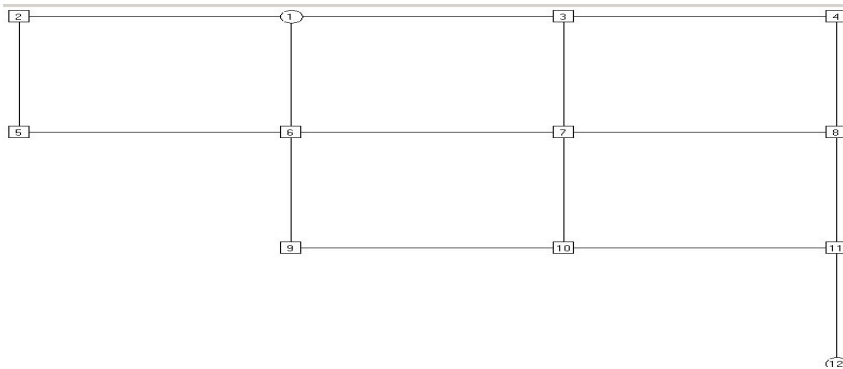


Figure 1. Example network

Table 1. Water consumption at nodes and supplying in nodes 1 and 12 (in L/s)

NODE/H	1	2	3	4	5	6	7	8
1	-	-	-	-	-	-	-	-
2	80.34	80.34	80.34	80.34	80.34	80.34	80.34	72.54
3	2.37	1.20	1.50	1.56	1.80	2.10	2.88	3.75
4	3.95	2.00	2.50	2.60	3.00	3.50	4.80	6.25
5	2.37	1.20	1.50	1.56	1.80	2.10	2.88	3.75
6	14.22	7.20	9.00	9.36	10.80	12.60	17.28	22.50
7	4.74	2.40	3.00	3.12	3.60	4.20	5.76	7.50
8	4.74	2.40	3.00	3.12	3.60	4.20	5.76	7.50
9	3.16	1.60	2.00	2.08	2.40	2.80	3.84	5.00
10	10.27	5.20	6.50	6.76	7.80	9.10	12.48	16.25
11	3.95	2.00	2.50	2.60	3.00	3.50	4.80	6.25
12	11.85	6.00	7.50	7.80	9.00	10.50	14.40	18.75
	18.72	49.14	41.34	39.78	33.54	25.74	5.46	-
								24.96

NODE/H	9	10	11	12	13	14	15	16
1	-	-	-	-	-	-	-	-
2	73.58	65.78	57.98	64.74	72.54	80.34	80.34	80.34
3	3.69	3.60	3.24	3.45	3.00	3.45	3.30	3.30
4	6.15	6.00	5.40	5.75	5.00	5.75	5.50	5.50
5	3.69	3.60	3.24	3.45	3.00	3.45	3.30	3.30
6	22.14	21.60	19.44	20.70	18.00	20.70	19.80	19.80
7	7.38	7.20	6.48	6.90	6.00	6.90	6.60	6.60
8	7.38	7.20	6.48	6.90	6.00	6.90	6.60	6.60

11	0.20	0.20	0.44	0.21	0.23	0.23	0.22	0.28
12	0.20	0.20	0.20	0.20	0.20	0.20	0.20	0.29
NODE/H	9	10	11	12	13	14	15	16
1	0.24	0.25	0.30	0.34	0.26	0.29	0.32	0.32
2	0.28	0.23	0.23	0.28	0.32	0.24	0.27	0.30
3	0.25	0.21	0.20	0.23	0.28	0.23	0.26	0.29
4	0.20	0.20	0.20	0.20	0.25	0.23	0.20	0.22
5	0.21	0.26	0.21	0.21	0.26	0.29	0.22	0.25
6	0.27	0.22	0.23	0.27	0.31	0.23	0.26	0.29
7	0.20	0.25	0.20	0.20	0.20	0.23	0.20	0.22
8	0.50	0.36	0.41	0.20	0.20	0.20	0.20	0.20
9	0.20	0.25	0.20	0.20	0.24	0.28	0.21	0.24
10	0.20	0.20	0.20	0.20	0.20	0.20	0.20	0.24
11	0.28	0.20	0.29	0.28	0.29	0.20	0.45	0.25
12	0.21	0.30	0.29	0.30	0.36	0.85	0.55	0.36
NODE/H	17	18	19	20	21	22	23	24
1	0.24	0.30	0.26	0.24	0.25	0.32	0.29	0.29
2	0.30	0.23	0.28	0.24	0.22	0.24	0.30	0.27
3	0.29	0.22	0.28	0.23	0.21	0.22	0.28	0.27
4	0.25	0.25	0.20	0.23	0.20	0.20	0.27	0.25
5	0.28	0.27	0.21	0.26	0.22	0.21	0.22	0.28
6	0.29	0.22	0.28	0.23	0.22	0.23	0.29	0.27
7	0.24	0.24	0.21	0.24	0.20	0.20	0.22	0.24
8	0.24	0.43	0.31	0.20	0.31	0.50	0.24	0.23
9	0.26	0.26	0.20	0.25	0.21	0.20	0.21	0.26
10	0.20	0.20	0.20	0.20	0.20	0.23	0.20	0.20
11	0.20	0.20	0.28	0.20	0.35	0.28	0.28	0.20
12	0.23	0.20	0.20	0.45	0.29	0.31	0.20	0.21

Tabelul 3. The nodes with the chlorine injection and injected quantities, in mg/L, corresponding to the water flow rates transported in 24 hours

NODE/H	1	2	3	4	5	6	7	8
1	24.70	25.07	24.60	24.28	25.03	20.50	19.79	21.22
4	0.00	0.00	0.00	0.00	0.00	0.00	0.00	0.00
8	0.00	8.81	0.00	0.00	0.00	0.00	3.22	0.00
12	1.65	3.20	6.33	0.00	11.62	13.59	15.84	33.49
NODE/H	9	10	11	12	13	14	15	16
1	17.60	16.26	17.27	21.99	18.87	23.18	25.62	25.41
4	0.43	0.29	0.58	0.38	0.57	0.00	0.10	0.00
8	2.62	1.77	2.18	0.07	0.31	0.00	0.19	0.61
12	3.51	26.16	13.11	11.49	16.84	57.46	0.00	0.00
NODE/H	17	18	19	20	21	22	23	24
1	19.61	24.43	20.61	19.01	20.19	25.55	23.65	23.39
4	0.00	0.00	0.21	0.00	0.24	0.50	1.33	0.16

5	0.30	0.22	0.22	0.23	0.23	0.29	0.22	0.30
6	0.22	0.22	0.23	0.23	0.29	0.22	0.30	0.29
7	0.25	0.20	0.21	0.20	0.20	0.24	0.22	0.25
8	0.34	0.38	0.20	0.20	0.20	0.44	0.24	0.23
9	0.27	0.20	0.20	0.21	0.21	0.27	0.20	0.27
10	0.20	0.20	0.20	0.20	0.20	0.20	0.20	0.20
11	0.20	0.28	0.26	0.26	0.25	0.20	0.27	0.20
12	0.23	0.20	0.43	0.32	0.21	0.31	0.20	0.21

Table 5. Nodes for chlorine injection and injected quantities, in mg/L, corresponding to the water flow rates transported in 24 hours

NODE/H	1	2	3	4	5	6	7	8
1	23.86	23.90	23.61	23.45	24.71	24.61	18.86	16.74
2	0.08	0.11	0.15	0.15	0.16	0.15	0.15	0.10
4	0.00	0.00	0.00	0.00	0.00	0.00	0.00	0.00
8	0.00	8.38	0.00	0.00	0.00	0.00	0.10	0.00
12	1.67	3.20	0.00	0.00	11.78	13.77	15.89	58.29
NODE/H	9	10	11	12	13	14	15	16
1	17.09	15.74	14.37	17.54	20.01	25.20	25.67	18.91
2	0.04	0.20	0.20	0.20	0.19	0.18	0.12	0.12
4	0.46	0.56	0.52	0.53	0.68	0.15	0.00	0.00
8	1.68	1.47	1.33	1.29	0.00	0.00	1.35	0.46
12	0.00	15.26	39.81	0.00	42.67	0.00	0.00	15.67
NODE/H	17	18	19	20	21	22	23	24
1	18.87	19.78	19.72	24.78	18.48	25.55	25.11	22.75
2	0.04	0.05	0.20	0.20	0.17	0.16	0.02	0.20
4	0.00	0.30	0.33	0.21	0.32	0.04	1.52	4.98
8	2.55	3.75	0.62	0.61	0.59	2.58	1.05	0.00
12	0.00	3.63	20.54	2.08	0.00	1.70	0.00	0.00

3.3. Comparison between the cases :network without failures and the network withthe failure on (1-2) pipeline

For the situation from fig. 1, witout failures on pipelines, the unknowns in simplex problem are the chlorine concentrations at nodes and the chlorine quantities introduced in injection points with the condition as $0.2 \text{ mg/L} \leq \text{concentration at node} \leq 0.5 \text{ mg/L}$, but the optimum is obtained by minimization the sum of chlorine quantities introduced in injecting nodes. In fig. 2, 3, 4, 5, blue line presents the evolution of chlorine concentrations at nodes established in specified conditions above, for 2 and 5 nodes in 24 hours. In fig. 2 and 3 black line presents the concentration calculated at 2 and 5 nodes by elimation of pipeline (1-2), with the same total chlorine quantities injected in network, the unknown being only the chlorine concentrations at nodes. In fig.3 and 4, black line shows the evolution of chlorine in 24 hours for nodes 2 and 5 when the pipeline (1-2) is eliminated and a suplementary injection is introduced in node 2 to have an optimal solution.

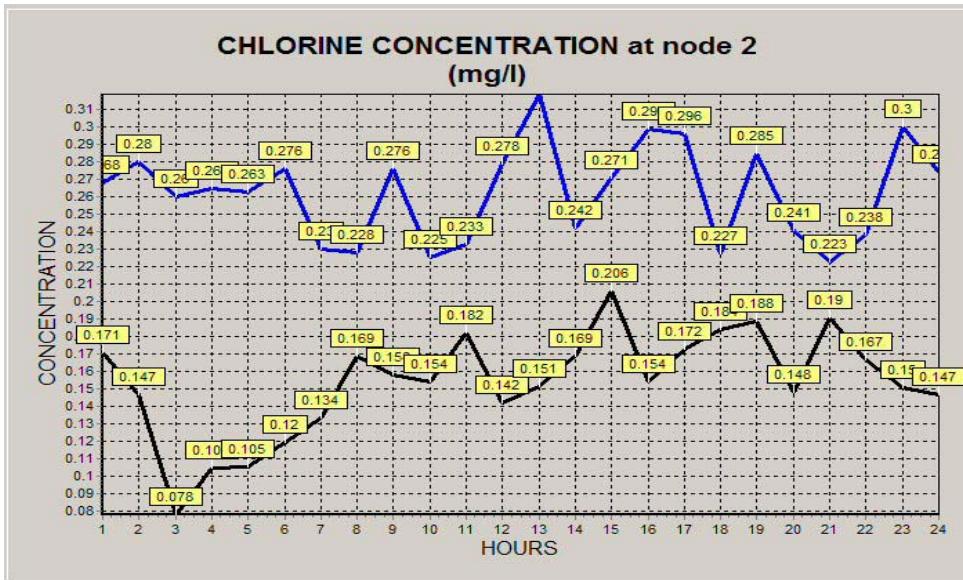


Figure 2. Legend: blue line – network without the failures; black line – failure on pipeline (1-2), keeping the injection nodes and chlorine quantities introduced in the network without failure

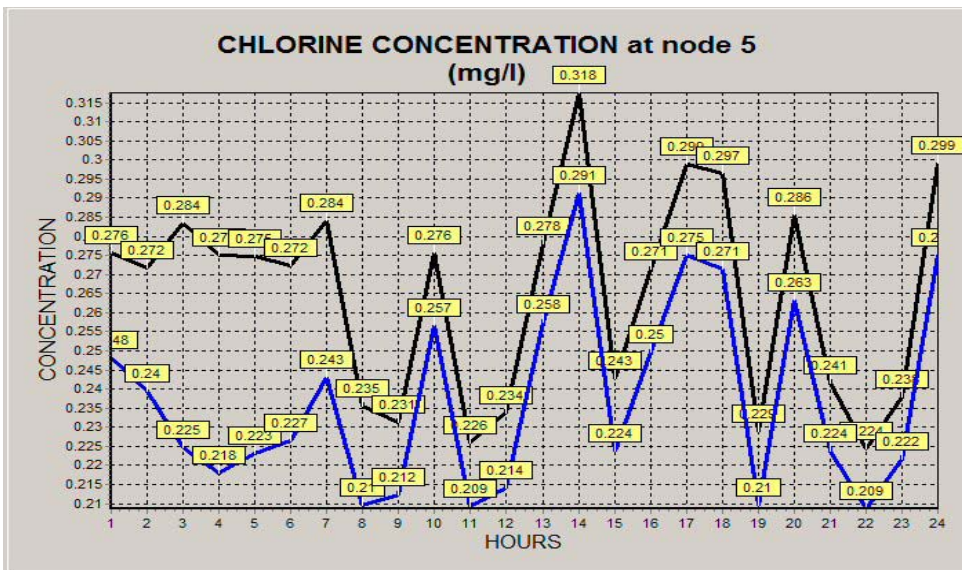


Figure 3. Legend: blue line – network without the failure; black line – failure on pipeline, (1-2) keeping the injection nodes and chlorine quantities introduced in the network without failure

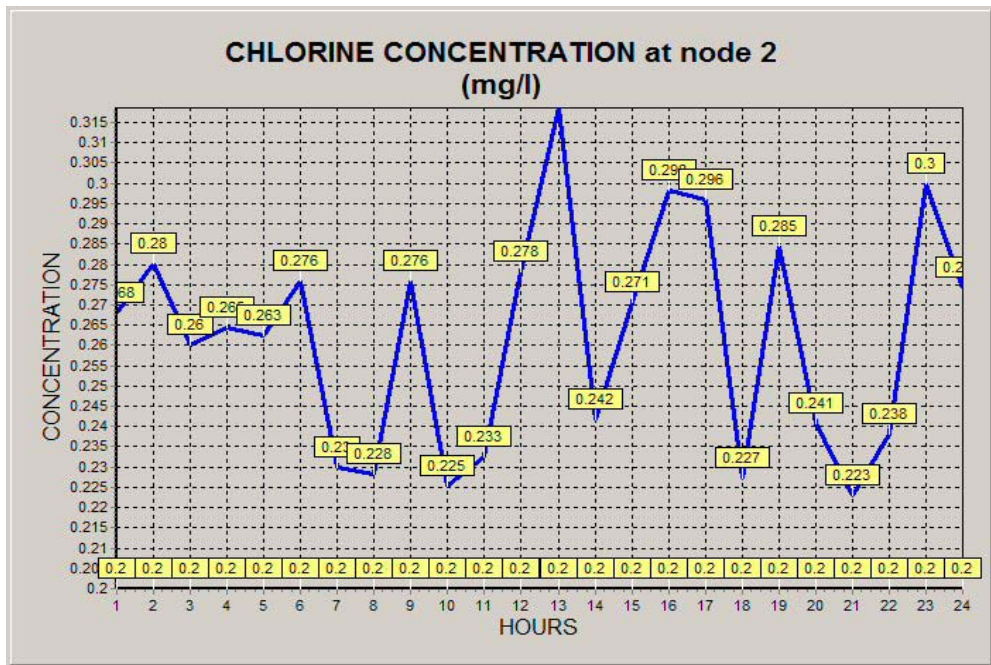


Fig. 4. Legend: blue line – chlorine concentration in node 2 (the same as fig.2) at which is added a supplementary injection in node 2 of 0.2 mg/L,

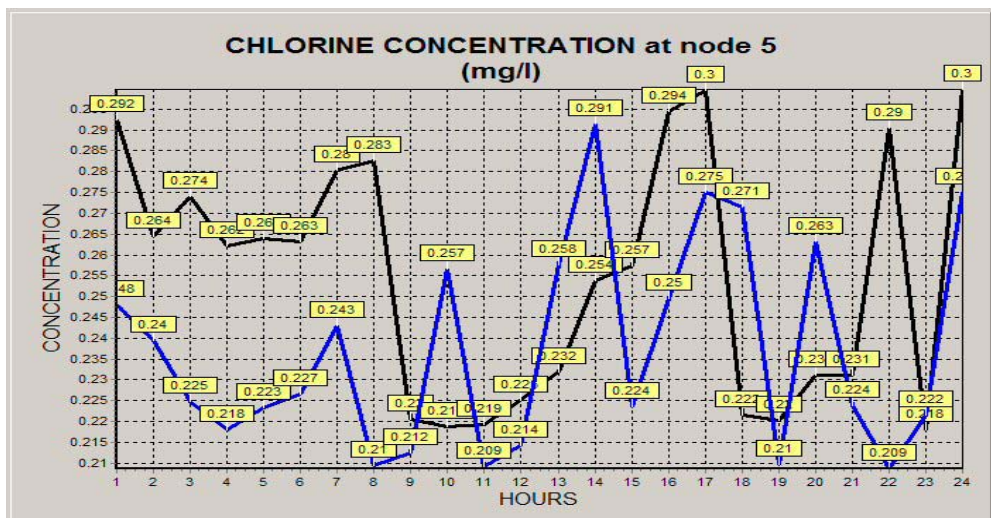


Figure 5. Legend: blue line – network without failure; black line – network with failure on pipeline (1-2) and supplementary chlorine injection in node 2.

4. CONCLUSIONS

1. The maintaining of water quality in distribution network is realized by preserving in the whole network some residual chlorine concentrations forecast in Law 458/2002.
2. At a normal functioning, the necessary chlorine in network is assured by periodical injections in the existing booster disinfection stations, established for this state.
3. In the case of some failures (pipe breaking etc) the residual chlorine distribution it is perturbed.
4. With a personal program it is made evident the chlorine evolution in nodes of a distribution network for cases: network without the failures and network with the failures on pipelines and the necessity to have the stand-by booster stations for chlorine injections in the cases of failures.
5. The procedure may be applied for the elimination of pipelines, excepting the cases when appear the isolated nodes (situation that affects the graph connexion).

References

1. Goldman, F.E., Burcu Altann Sakaria, A., Orsmbec, L.E., Uber, J.G., Mays L.W., *Optimization models for operations*, Chap 16 from Water Distribution Systems Handbook, McGraw-Hill, New York, 2000.
2. Bârsan, Em., Ignat, C., Evolution of Chlorine Concentration in Water Distribution Networks., *International Symposium "Computational Civil Engineering"*, Editors. C. Ionescu, F.Păuleț-Crăiniceanu, H. Bărbat, Ed Soc.Acad. Matei-Teiu Botez, Iași, 2003, 112-119,
3. Bârsan, Em., Ignat, C., Development of a Existed Water Supply Network, *Proceedings of VII International Symposium on Water Management and Hydraulic Engineering*, 10-12.09 .2001, Gdansk (Miedzybrodzie zywieckie), Poland, 397 - 404
4. Bocelli, D.L., Tryby M.E., Uber J.G., Rossman L.A., Zierolf M.L., Polycarpu M.M., Optimal Scheduling of Booster Disinfection in Water Distribution Systems, *Journal of Water Resources Planning and Management*, March/April, 1998, 99-111.
5. Mukherjee, S., Laha, Sh., Genetic Algorithm to optimize disinfectant Booster Location, *1st World Water Congress of the International Water Association (IWA) Conference Preprint Book 2, Drinking Water Treatment*, Paris, 2000, 411- 417

Finite element model for obtaining the structural response considering soil-structure interaction

Țepeș Onea Florin

University Ovidius of Constanța, Faculty of Construction, Constanța, România

Summary

This paper aims to emphasize the influence of local conditions of the location on the structural response by using advanced calculation methods able to reflect as precisely as possible the structure's reaction, emphasizing the evolution of the stages of solicitation during an earthquake.

According to the norms of design we can use: a) methods of usual design; b) methods of design based upon considering the nonlinear deformation of the structure.

It will be take into consideration a structure type P+5, in frame, namely a hotel, build at the seaside.

It is interested analyzing the results obtained by the method of design “a” and those obtained by method “b” aiming to find out in what measure the use of method “b” is necessary at structures which do not belong to the class of importance structures.

The method “b” will be a nonlinear calculus taking into consideration the soil structure interaction. The respective calculus will give results regarding the history of the efforts in beams, spectral response.

The results will offer useful information for a future design of same similar structures in frame.

KEYWORDS: usual design, nonlinear, deformation, soil, structure, interaction, beams, efforts

1. STRUCTURAL ANALYSIS

The calculation made for a plane elevation in the P+5 structure, using soil-structure interaction program (FLUSH) have emphasized a structural response offering from a calculation made on the same structure using seismic forces that are static equivalent.

Firstly we emphasize the influence of the deformability of the soil on the structural response displacements.

In this way the response in displacements considering the ground deformable is evidently grown as opposed to the hypothesis of fixing the structure at the basis.

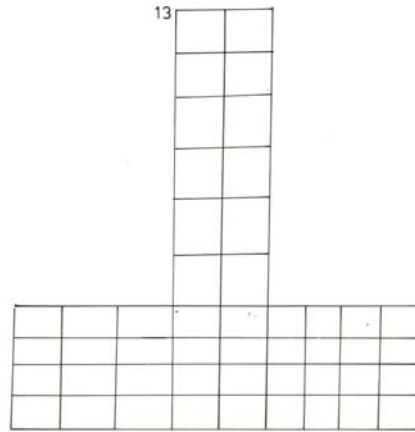


Figure 1 Discretization for soil-structure interaction

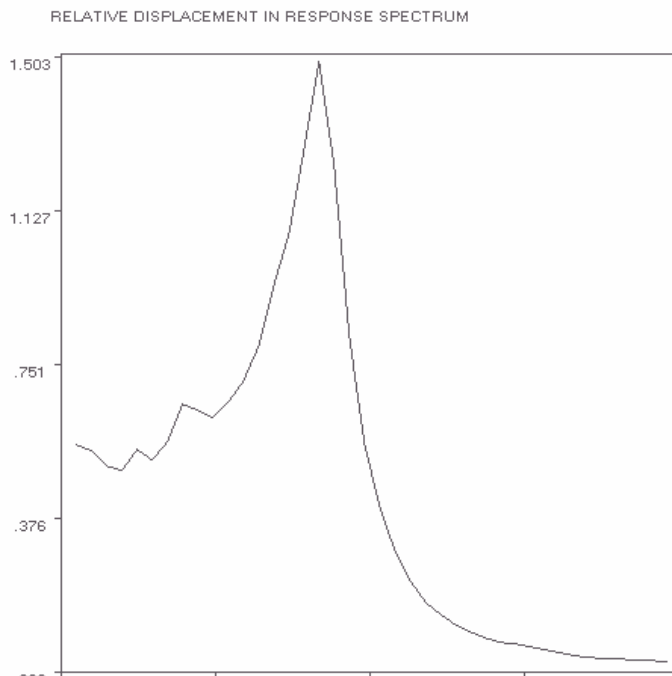


Figure 2 Relative displacement in response spectrum. Nodal point 13, damping 10%.
Maximum displacement=1,5ft

On the other hand the fundamental period is slightly modified. Thus for a dynamic analysis considering the structure fixed at the basis (spatial calculation) the fundamental period was of 0,69s and speaking of an analysis in frequency for the plane elevation a maximum response of 0,51s is obtained.

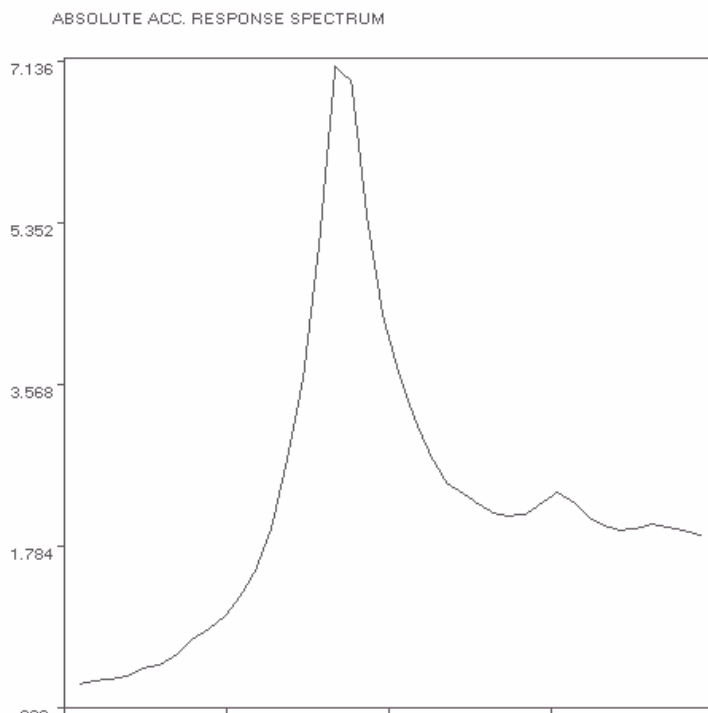


Figure 3 Absolute acceleration in response spectrum. Nodal point 13, damping 10%. Maximum acceleration =7,13g at frequencies 1,94Hz

Another phenomenon observed analyzing the spectral response in displacements, velocities and accelerations is that of resonance around the value of 1,94Hz, as we can see in figures 2,3.

Unfortunately the resonance phenomenon cannot be emphasized through a pseudo-static calculation. As we know making such a calculation the structure’s response depends on the level of the seismic forces, calculated by the help of some norm coefficients: $k_s, \beta, \psi, \epsilon, \eta$.

Depending on the type of the structure and of the seismic zone we obtain a seismic coefficient of a fixed numerical value multiplied by a coefficient (η) that takes into account its own vectors.

The former calculations we had demonstrated in other cases the precision of these coefficients.

It is compared the response of a diaphragm made of brick and calculated by means of the pseudo-static comparative method with integration in time. The respective calculations were made in the linear domain without considering the damping.

The conclusion is that in some cases, a number of advanced calculations: the analysis in frequency, the taking into consideration of the nonlinear reaction of the foundation ground, the damping, can emphasize a totally different reaction as opposed so the one obtained through the usual methods.

Speaking of this case, the analysis was made for an accelerogram on the scale of 0,2g, for different damping as we can observe in Table 1.

Tabel 1 Maximum spectral values at 13 node.

Maximum spectral values	Damping ratio	2%	5%	10%
Displacement (FT)	0.5%	4.11	2.47	1.5
Acceleration (g)	6.5	19.19	11.6	7.13

Thus from this table we can observe that for a damping of 5%, at the superior end of the structure we obtain a maximum spectral in displacements of 2,4ft.

Even for a damping of 10% the spectral response in displacements remains elevated around the frequencies of the resonance.

In the case of the pseudo-static calculation we obtained a maximum displacement of 0,012m and a moment on the basis of the structure is 6,7tfm.

Even for a damping of 10% the spectral response in displacements remains elevated around the frequencies of the resonance.

In the case of the calculation of soil-structure interaction was obtained for 10% damping maximum displacement is 1.5ft.

2. CONCLUSION

The conclusion is that a pseudo-static calculation does not always give us a response according to reality.

Thus for the structures that we cannot introduce in the category of very important structures it is sometimes necessary an nonlinear calculus in parallel with a pseudo-static calculation.

References

1. John Lysmer, Takekazu Udaka, Chan-Feng Tsai, *A Computer Program for Approximate 3-D Analysis of Soil-Structure Interaction Problems*, Berkeley, California, 1979
2. M. Ieremia, Țepeș Florin, , WCEE, *Earthquake response analysis of a concrete barrage in interaction with the soil*.
3. Stefan Balan, March 4MARTIE, 1977 *earthquake*, Editura Tehnică București, 1982.

ISBN 973-7962-65-6



MANIFESTARI STIINTIFICE